

LITHO-STRUCTURAL AND GEOCHEMICAL  
CHARACTERISTICS OF URANIFEROUS BASEMENT  
ROCKS AND GULCHERU QUARTZITE IN AND AROUND  
VELDURTHI AREA ALONG WESTERN MARGIN OF THE  
CUDDAPAH BASIN, KURNOOL DISTRICT, A.P.

*by*

SACHIN AGGARWAL

ENGG1G201801012

**Bhabha Atomic Research Centre, Mumbai**

*A thesis submitted to the  
Board of Studies in Engineering Sciences*

*In partial fulfillment of requirements*

*for the Degree of*

MASTER OF TECHNOLOGY

*of*

**HOMI BHABHA NATIONAL INSTITUTE**

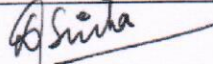
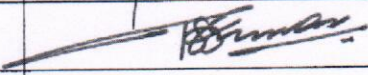
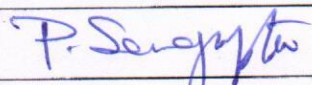
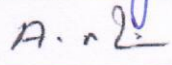
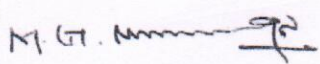
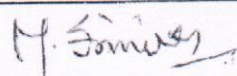
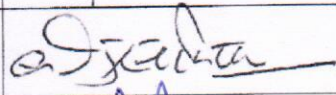
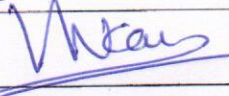


**February, 2021**

# Homi Bhabha National Institute

## Recommendations of the Thesis Examining Committee

As members of the Thesis examining Committee, we recommend that the thesis prepared by SACHIN AGGARWAL entitled "LITHO-STRUCTURAL AND GEOCHEMICAL CHARACTERISTICS OF URANIFEROUS BASEMENT ROCKS AND GULCHERU QUARTZITE IN AND AROUND VELDURTHI AREA ALONG WESTERN MARGIN OF THE CUDDAPAH BASIN, KURNOOL DISTRICT, A.P. " be accepted as fulfilling the thesis requirement for the Degree of Master of Technology.

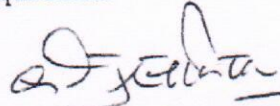
	Name	Signature
Member-1	Dr. D. K. Sinha	
Member-2	Dr. T. S. Sunil Kumar	
Member-3	Dr. Navin Goyal	
Member-4	Dr. Pranesh Sengupta	
Member-5	Dr. A. Rama Raju	
Technical advisor	M. G. Murugan	
Examiner	Prof. M. Srinivas	
Guide & Convener	Dr. B. S. Bisht	
Chairman	Prof. Vivekanand Kain	

Final approval and acceptance of this thesis is contingent upon the candidate's submission of the final copies of the thesis to HBNI.

I hereby certify that I have read this thesis prepared under my direction and recommend that it may be accepted as fulfilling the thesis requirement.

Date: 11-02-2021

Place: Hyderabad

  
(Dr. B. S. Bisht)  
Guide

## **DECLARATION**

I, hereby declare that the investigation presented in the thesis has been carried out by me. The work is original and has not been submitted earlier as a whole or in part for a degree / diploma at this or any other Institution / University.

  
(Sachin Aggarwal)

## ACKNOWLEDGEMENTS

I express my sincere gratitude to my Guide Dr. B. S. Bisht, SO/H, AMD, Western Region, Jaipur for his valuable guidance, advice and encouragement throughout the course of this work. I also wish to convey my sincere gratitude to Technical Advisor, Shri. M.G. Murugan, SO/G, AMD, South Central Region, Hyderabad for technical support throughout the duration of the work.

I am extremely thankful to the HBNI for providing the opportunity to pursue the M. Tech. degree. I am highly indebted to Shri D.K Sinha, Director, Atomic Minerals Directorate for Exploration and Research for providing kind permission to pursue the M. Tech. course. I express sincere gratitude to Additional Director (OP-III) and Regional Director, AMD, South Central Region, for their constant encouragement and motivation.

I extend my sincere thanks to Incharge, BARCTS, AMD Campus, Hyderabad for technical guidance and administrative support to during the M. Tech programme.

I thank Dr. Neeru Rawal, SO-G, Shartendu Saurabh, SO-D for their support in the work. I also extend sincere thanks to officers and staff of Petrology, XRF, XRD, Chemistry laboratory and ASRS Group, AMD, Hyderabad for their constant co-operation.

  
**SACHIN AGGARWAL**

## CONTENTS

<b>SYNOPSIS</b>	i-ii
<b>LIST OF FIGURES</b>	iii-ix
<b>LIST OF TABLES</b>	x-xiii
<b>Chapter 1 INTRODUCTION</b>	<b>1-7</b>
1.1 Previous Work	2-3
1.2 Present Work	4
1.3 Approachability and Accessibility	5
1.4 Climate and Rainfall	5-6
1.5 Organization of Thesis	6-7
<b>Chapter 2 METHODOLOGY</b>	<b>8-18</b>
2.1 Literature survey	8
2.2 Study of toposheets and satellite imagery	8
2.3 Geological and lithostructural mapping	8-11
2.4 Laboratory/analytical studies	11-18
<b>Chapter 3 REGIONAL GEOLOGY</b>	<b>19-29</b>
3.1 Geological and tectonic setting of Cuddapah Basin	19-21
3.2 Lithostratigraphy of Cuddapah Basin	22-24
3.3 Regional structural Framework	25-28
3.4 Structural features in the western part of Cuddapah Basin	28-29
<b>Chapter 4 LITHO-STRUCTURAL MAPPING</b>	<b>30-45</b>
4.1 Local Geology of the Govardhanagiri-L.Banda area	30-31
4.2 Remote Sensing studies: Lineament mapping/geomorphological feature extraction	32-33
4.3 Litho-structural mapping of the area	34-42

4.4	Structural analysis	42-43
4.5	Radioactive anomalies	44-45
<b>Chapter 5</b>	<b>RADIOELEMENTAL CHARACTERIZATION</b>	<b>46-53</b>
5.1	Radioelemental Studies of granites	46
5.2	U, Th and K in granites	46-47
5.3	Radioelemental distribution in the study area	47-49
5.4	Characterization based on radioelements	49-51
5.5	Classification of Govardhanagiri-L.Banda granitoids	52
5.6	Alteration	52
5.7	Uranium enrichment/depletion and migration	53
<b>Chapter 6</b>	<b>SEDIMENTOLOGICAL STUDIES</b>	<b>54-68</b>
6.1	Paleohydraulic reconstruction using cross-bed set thickness	54-61
6.2	Pebble morphometric studies	61-68
<b>Chapter 7</b>	<b>PETROGRAPHY</b>	<b>69-90</b>
7.1	Petrographic studies	69
7.2	Petro-mineralogy of Govardhanagiri-Lanjabanda granites	69-75
7.3	Petro-mineralogy of basic dyke	75-76
7.4	Petro-mineralogy of Govardhanagiri-L.Banda Quartzites	77-82
7.5	U mineralization	82-84
7.6	Radioactive Minerals	84-87
7.7	Hydrothermal Alterations	87-88
7.8	XRD analysis	88-89
7.9	Mineral Paragenesis	89-90
<b>Chapter 8</b>	<b>GEOCHEMISTRY</b>	<b>91-130</b>
8.1	Introduction	91

8.2	Geochemistry of granite	91-106
8.3	Geochemistry of Dolerite dykes from Govardhanagiri area	107-111
8.4	Geochemistry of Gulcheru Quartzite	112-120
8.5	Geochemistry of Gulcheru Shale	120-130
<b>Chapter 9</b>	<b>INTEGRATED GEOPHYSICAL AND GEOLOGICAL STUDIES</b>	<b>131-148</b>
9.1	Integration of airborne geophysical and geological data	131
9.2	Ratio Radioelemental Maps	132
9.3	Airborne Gamma Ray Spectrometric Survey	132
9.4	Qualitative interpretation	133-137
9.5	Comparative geochemical studies of Kappatralla and Lanjabanda basement granites	138-142
9.6	Comparison of Gulcheru Quartzite of Govardhanagiri-Lanjabanda area and Kappatralla area	143-148
<b>Chapter10</b>	<b>DISCUSSIONS AND CONCLUSIONS</b>	<b>149-153</b>
	<b>REFERENCES</b>	<b>154-165</b>

## SYNOPSIS

The Govardhanagiri-Lanjabanda area lies in the western margin of Cuddapah basin where Palaeo-Mesoproterozoic Papaghni Group comprising of Gulcheru and the Vempalle Formation non-conformably overlies the Archaean basement. The basement crystallines comprises peninsular gneisses, different types of intrusive granites, basic dykes and quartz reefs. The basement gneisses and intrusive granite are unconformably overlain by 10-20° easterly and southeasterly dipping basal conglomerate and quartzite sequence of Gulcheru Formation.

Detailed geological and litho-structural mapping (1:5000) over 10 sq. km carried out in Govardhanagiri-Lanjabanda area shows that the basement granites and overlying Gulcheru sediments are affected by vertical to steeply dipping fractures of E-W, N80°E-S80°W, N60- 80°W-S60-80°E and N-S trends. A number of doleritic dykes, pegmatite and quartz veins are intruding in basement granite along ENE-WSW and WNW-ESE trending fracture planes. The entire basement-sediment sequence is affected by E-W trending sinistral Veldurthi-Kalva-Gani (VKG) strike slip fault systems and associated cross faults with prominent E-W displacements.

The study area poses geological setup similar to that of Kappatralla where Unconformity- proximal uranium mineralisation has been recorded in the outlier of the Gulcheru Formation, Kurnool district, A.P. The present study aims to understand the nature of both basement granitoids and Gulcheru sediments and controls of mineralisation by using integrated structural, sedimentological and petro-mineralogical data.

Fracture data collected(n=75) using joints(n=65), dykes(n=4) and veins(n=6) in Lanjabanda area from basement and Gulcheru Quartzite delineates NW-SE and NE-SW as most prominent trends. Deductive palaeohydraulic reconstructions using cross-bed set thickness of Gulcheru quartzite and pebble morphometric analysis of Gulcheru conglomerate suggest fluvial environment of deposition for Gulcheru sediments. Petro-mineralogical studies of basement granites and Gulcheru quartzite reveals sub-arkosic to arkosic nature, texturally sub-mature to immature sediments derived from deformed granitic source.

Analytical results of Gulcheru sediments, major element distribution pattern and bivariate plots of  $Al_2O_3$  Vs  $TiO_2$ ,  $(Fe_2O_3+MgO)$  % Vs  $TiO_2$  suggests alkali granite to granitic source and passive margin setting. Weathering indices calculation (CIA, CIW, PIA) and plotting suggests moderate chemical weathering in the provenance with effects of K-metasomatism. Analytical results of basement granite suggest peraluminous, S type, alkali-calcic nature of granites related to syn-post orogenic origin. Additionally, the ASRS survey over Kurnool-Dhone block reveals the occurrence of high K bearing younger basement granites and their continuity towards basin margin. So, the integrated study using ground geology, satellite data, airborne geophysical study, petro-mineralogical and geochemistry suggests that basement and overlying Gulcheru sediments are favourable for hosting unconformity related uranium mineralisation.

## LIST OF FIGURES

Figure No.	Description of figures	Pg. No.
1.1	Route map from Hyderabad to the study area	5
2.1	Ultima 2 inductively coupled plasma optical emission spectrometer	18
3.1	Regional geological map of Cuddapah basin	20
3.2	Regional tectonic map of Cuddapah Basin showing regional structures	26
4.1	Regional geological map of Chinnakolumulapalle-L.Banda-Govardhanagiri area	31
4.2	Lineament map using FCC image (421) of Dupadu-Veldurti-Dhone area, Kurnool district, Andhra Pradesh.	33
4.3	Detailed geological map (1:5000) of Govardhanagiri-L.Banda area, Kurnool district, A.P.	34
4.4	Schematic geological cross-section along profile line A-B.	35
4.5	Schematic geological cross-section along profile line C-D.	35
4.6	a) Enclaves of metabasics in pink biotite granite b) Migmatitic banding within PGC	36
4.7	a) Intrusive contact (N330°) between younger and older grey biotite granite with older phase showing foliation along N30°E trend b) Right lateral displacement of pegmatitic vein by N70°E and E-W fractures, L.Banda area c) Emplacement of quartz reef trending N60°E.	37
4.8	a) Silicification along NE-SW(N40°E) trending fracture b) Ferruginization along N320°(NW-SE) trending fracture c) Tourmaline	38

	veins along N40°W trending fracture d) Displacement of tourmaline vein by NE-SW fracture.	
4.9	a) N70°E trending basic dyke in granite b) Large actinolite crystals in fractured granite	39
4.10	a) Non-conformity contact(sharp) between basement granite and Gulcheru Quartzite b) Paleosol development over unconformity surface c) Clast supported polymictic conglomerate having clasts of qtz, jasper and BIF d) NE-SW and E-W fractures cutting through the pebbles of conglomerate e) Gradational contact between Gulcheru Quartzite and shale f) Quartz veination along N205° trending fracture	40
4.11	a) Silicification in Gulcheru Quartzite along N205° fracture b) Ferruginization along N300° fracture c) Asymmetrical ripple marks in GQ d) Mudcracks in Gulcheru shale	41
4.12	Litholog showing different facies of Gulcheru Formation exposed in Lanjabanda area.	42
4.13	a) Rose diagram of fracture sets North of Lanjabanda showing NE-SW as dominant structural trend b) South of Lanjabanda showing NW-SE as dominant structural trend. c) Stereoplot of joint planes with their poles, North of Lanjabanda area d) Stereoplot of joint planes with their poles, south of Lanjabanda area e) NW-SE trending fault causing displacement of Gulcheru shale.	43
5.1	Radioactive ferruginized pink granite showing 100ppm activity (PGRS), Govardhanagiri area.	48
5.2	Secondary U mineral on the exfoliation plane of pink granite	48
5.3	Comparative U-Th plot for Closepet Granite and granites of study area	50
5.4	Log Th-K plot for granites of study area	50

5.5	Kx(U/Th) vs U/K plot for granites of study area	51
6.1	Binary plot paleoslope (S) and mean annual bankful discharge values (Q <sub>b</sub> ) calculated for the Lanjabanda section.	57
6.2	a) Fractured oligomictic Gulcheru conglomerate, Lanjabanda area b) Trough cross-stratified quartzite	62
6.3	Concept and measurement of pebble diameter	63
6.4	a) Coefficient of Flatness vs. Sphericity plot b) Sphericity vs. Oblate-Prolate Index plot	65
6.5	Classification of pebble shapes	66
7.1	Photomicrographs of Govardhanagiri-Lanjabanda granites showing <b>a)</b> Biotite in pulverised matrix <b>b)</b> Chlorite in altered granite <b>c)</b> Myremekitic texture <b>d)</b> Pokilitic texture <b>e)</b> Coarse microcline crystal <b>f)</b> Bent secondary muscovite in sericitized matrix <b>g)</b> Titanium bleeding in chloritized biotite <b>h)</b> Sericitized plagioclase <b>i)</b> Fracture orthoclase and quartz <b>j)</b> Sericitization along quartz vein <b>k)</b> Accessory sphene as inclusion <b>l)</b> Pyrite crystal <b>m)</b> Altered zoned plagioclase <b>n)</b> Brecciated quartz in sericitized matrix <b>o)</b> Biotite and muscovite in fractured microcline <b>p)</b> Microperthite <b>q)</b> Epidote as fine size aggregate <b>r)</b> Primary muscovite intergrown with quartz <b>s)</b> Medium grained hypidiomorphic granular texture <b>t)</b> Biotite in fractured feldspar <b>u)</b> Magnetite-pyrite association in granite <b>v)</b> Tourmaline bearing granite	74
7.2	a) Ophitic texture in dolerite b) Intergranular texture in dolerite c) Quartz vein in dolerite d) Large actinolite crystal e) Intense chloritization in dolerite f) Altered dolerite	76
7.3	Photo- micrographs of quartzites of Gulcheru Formation showing <b>(a)</b> Poorly sorted quartzite with sericite matrix <b>(b)</b> Fresh K-feldspar (microcline) dominance over plagioclase <b>(c)</b> Textural immaturity shown	81

by sub-angular to sub-rounded grains **(d)** Rock fragment of granite in quartzite **(e)** Accessory heavy minerals (Apatite and zircon) as inclusions in quartz **(f)** Detrital zircon in matrix of quartzite **(g)** Intensely fractured quartz and feldspar **(h)** Strained quartz as indicator of source rock deformation **(i)** Authigenic silica as cement forming quartz overgrowth **(j)** Floating texture in fine grained sericite matrix and altered muscovite **(k)** Two distinct types of Polycrystalline quartz **(l)** Straight and concavo-convex contact in quartzite **(m)** Rutile occurring as needle shaped inclusion in monocrystalline quartz **(n)** Rock fragment of chert **(o)** Intensely sericitized K-feldspar **(p)** Qtz vein in pebble of conglomerate **(q)** Medium grained quartzite **(r)** Monazite as a inclusion in quartz **(s)** Xenotime in quartzite **(t)** Quartzite-shale intercalation.

7.4	Positive spots indicated in the form of brown colour in these samples.	82
7.5	<b>a)</b> Intense brecciation around grain boundary <b>b)</b> Plagioclase identified as albite <b>c)</b> Microcline showing cross-hatched twinning <b>d)</b> Muscovite in intergranular space in quartzite	84
7.6	<b>e)</b> Quartzo-feldspathic vein in quartzite <b>f)</b> Sericitization of feldspars in vein <b>g)</b> High density $\alpha$ -tracks due to coffinite <b>h)</b> Fractured quartzite <b>i)</b> Ultrafine disseminated pyrite in quartz vein <b>j)</b> Coffinite associated with pyrite	85
7.7	<b>a)</b> Poorly sorted quartzite <b>b)</b> Fractured and brecciated quartz <b>c)</b> Detrital zircon in quartzite <b>d)</b> Ferruginous matrix and cement <b>e)</b> Microcline <b>f)</b> Plagioclase <b>g)</b> Monocrystalline and polycrystalline qtz <b>h)</b> Sericitization along grain boundaries <b>i)</b> Goethitisation along fractures <b>j)</b> U adsorbed on goethite	87
8.1	Harker variation diagrams of major oxides w.r.t SiO <sub>2</sub> of granites of study area.	94

8.2	a) Total alkali vs. silica classification of granites of study area (after Middlemost, 1985) b) AFM ternary plot for granites of the study area (after Irvine and Barager, 1971).	95
8.3	a) TAS classification of granites of study area (after Cox et al., 1979) b) Ab-An-Or diagram (Baraker, 1979 and O' Conner 1965)	96
8.4	K <sub>2</sub> O-Na <sub>2</sub> O binary plot for granites of study area (after Harpum 1963)	96
8.5	a) K <sub>2</sub> O-SiO <sub>2</sub> binary plot for granites of study area (after Peccerillo and Taylor, 1976) b) MALI vs. SiO <sub>2</sub> plot for granites of study area (after Frost et al., 2001).	97
8.6	A/NK vs. A/CNK plot for granites of study area (after Shand, 1943)	98
8.7	a) B-A binary plot for granites of study area (modified after Villaseca et al., 1998) b) B-A binary plot for granites of study area (after Debon and Le Fort, 1983)	98
8.8	Rb-Ba-Sr ternary plot for granites of study area	102
8.9	a) Na <sub>2</sub> O-K <sub>2</sub> O binary plot for granites of study area (after Chappell and White, 2001) b) CaO-FeO <sub>t</sub> binary plot for granites of study area (after Chappell and White, 2001)	102
8.10	a) Discrimination diagram for partial melt source for granites of study area (after Sylvester 1998) b) Rb-Sr plot for depth of generation for granites of study area (after Condie, 1986).	103
8.11	Geo-tectonic discrimination diagram for granites of study area (after Batchelor and Bowden, 1985)	104
8.12	Chondrite normalized REE plot of Govardhanagiri-L.Banda granites	106
8.13	CaO/Al <sub>2</sub> O <sub>3</sub> -MgO/10-SiO <sub>2</sub> /100 ternary diagram (Schweitzer and Kroner (1985)	107

8.14	Total alkali Silica plot (TAS) (Le Bas et.al., 1986)	110
8.15	Y (Zr + Y) – T (TiO <sub>2</sub> ×100) –C (Cr) ternary plot (after Davis et al. 1979).	111
8.16	AFM classification Scheme (Irvine and Baragar, 1971).	111
8.17	a) Al <sub>2</sub> O <sub>3</sub> versus TiO <sub>2</sub> bivariate discrimination diagram (McLennan SM et al., 1990) b) TiO <sub>2</sub> versus Ni (ppm) bivariate diagram (Floyd PA et al.,1989) c) TiO <sub>2</sub> versus (Fe <sub>2</sub> O <sub>3</sub> +MgO) diagram (after Bhatia, 1983) d) Zr vs. TiO <sub>2</sub> plot (after Hayashi et al., 1997)	116
8.18	SiO <sub>2</sub> and (Al <sub>2</sub> O <sub>3</sub> +K <sub>2</sub> O+Na <sub>2</sub> O) (after Suttner and Dutta, 1986).	116
8.19	<b>(a)</b> Sandstone classification diagram using log(Na <sub>2</sub> O/K <sub>2</sub> O) vs. log(SiO <sub>2</sub> /Al <sub>2</sub> O <sub>3</sub> ) (after Pettijohn et al. 1987), <b>(b)</b> Two weathering indicators, Index of Chemical Variation (ICV) vs. Chemical Index of Alteration (CIA; fields after Potter et al. 2005), <b>(c)</b> A–CN–K ternary diagram of molecular proportions of Al <sub>2</sub> O <sub>3</sub> –(CaO+Na <sub>2</sub> O)–K <sub>2</sub> O for Gulcheru Quartzite (after Nesbitt and Young 1984).	120
8.20	Bivariate plot of log (SiO <sub>2</sub> / Al <sub>2</sub> O <sub>3</sub> ) versus log (Fe <sub>2</sub> O <sub>3</sub> / K <sub>2</sub> O) (Herron 1988).	123
8.21	Major element distribution in the Gulcheru shales in Fe <sub>2</sub> O <sub>3</sub> – K <sub>2</sub> O–Al <sub>2</sub> O <sub>3</sub> compositional space	124
8.22	Distribution of PAAS normalized trace elements of Gulcheru shale.	125
8.23	A-CN-K diagram for the Gulcheru shales.	126
8.24	Scatter plots of a) Al <sub>2</sub> O <sub>3</sub> versus TiO <sub>2</sub> ; b) Ni versus TiO <sub>2</sub>	127
8.25	Binary plot of SiO <sub>2</sub> versus (Al <sub>2</sub> O <sub>3</sub> + Na <sub>2</sub> O + K <sub>2</sub> O).	128
8.26	Chondrite normalized REE plot of Gulcheru sandstones, Govardhanagiri-L.Banda area.	130

9.1	Geological map (1:50,000) of Kurnool- Dhone Block (Bhukosh) with ASRS anomalies and major lineaments.	133
9.2	Ternary radiometric map of Kurnool-Dhone block showing different radioelement concentration zones.	134
9.3	Pseudo geological map prepared on the basis of different radioelemental zones.	135
9.4	Geological map as a base map for geophysical interpretation.	135
9.5	a) U/Th map of the area b) Thorium map c) Uranium map d) Potassium map	136
9.6	a) Ternary radiometric map b) Total counts c) RTP map of the area	137
9.7	<b>a)</b> Total alkali-silica diagram (Middlemost, 1994) <b>b)</b> AFM ( $\text{Na}_2\text{O}+\text{K}_2\text{O}-\text{FeO}^{\text{t}}-\text{MgO}$ ) diagram (Irvine and Baragar, 1971) <b>c)</b> Ab-An-Or diagram (Barker, 1979 and O'Conner 1965) <b>d)</b> Ba-Rb-Sr ternary plot	140
9.8	<b>a)</b> A/CNK-A/NK plot (Shand 1943) <b>b)</b> $R_1-R_2$ geo-tectonic discrimination diagram Batchelor and Bowden (1985) <b>c)</b> ( $\text{Fe}^*=\text{FeO}^{\text{t}}/\text{FeO}^{\text{t}}+\text{MgO}$ ) vs $\text{SiO}_2$ diagram (Frost et al.,2001) <b>d)</b> MALI vs. $\text{SiO}_2$ diagram (Frost et al., 2001).	142
9.9	Geochemical classification of sandstone (a) Bivariate plot $\text{Log}(\text{SiO}_2/\text{Al}_2\text{O}_3)$ vs. $\text{Log}(\text{Na}_2\text{O}/\text{K}_2\text{O})$ (b) Bivariate plot $\text{Log}(\text{SiO}_2/\text{Al}_2\text{O}_3)$ vs. $\text{Log}(\text{Fe}_2\text{O}_3/\text{K}_2\text{O})$ .	144
9.10	Bivariate Plot <b>(a)</b> $\text{Al}_2\text{O}_3$ versus $\text{TiO}_2$ plot (McLennan SM et al., 1990) <b>(b)</b> Ni (ppm) versus $\text{TiO}_2$ plot (Floyd PA et al.,1989). <b>(c)</b> Zr vs. $\text{TiO}_2$ plot (after Hayashi et al., 1997) <b>(d)</b> $(\text{Al}_2\text{O}_3 +\text{K}_2\text{O}+\text{Na}_2\text{O})$ versus $\text{SiO}_2$ (after Suttner and Dutta, 1986). <b>(e)</b> Index of Chemical Variability (ICV) vs. Chemical Index of Alteration (CIA) plot (after Potter et al. 2005) <b>(f)</b> $(\text{Fe}_2\text{O}_3 + \text{MgO})$ versus $\text{TiO}_2$ bivariate diagram (Bhatia MR, 1983).	145

9.11	A–CN–K ternary diagram of molecular proportions of $\text{Al}_2\text{O}_3$ – ( $\text{CaO}+\text{Na}_2\text{O}$ )– $\text{K}_2\text{O}$ for Gulcheru Quartzite (after Nesbitt and Young 1984).	148
9.12	$\text{K}_2\text{O}/\text{Al}_2\text{O}_3$ vs $\text{MgO}/\text{Al}_2\text{O}_3$ diagram (Sopuck et al., 1983).	148

## LIST OF TABLES

Table No.	Description of tables	Pg. No.
2.1	Details of the ICP-OES instrument used for analysis	18
3.1	Stratigraphy of Cuddapah Basin (Nagaraja Rao et al. 1987)	21
4.1	Stratigraphy of the study area	30
4.2	Radiometric result of anomalies of Govardhanagiri – Lanjabanda area	44
4.3	Radio-elemental distribution in various litho-units exposed at Govardhanagiri-L.Banda area	45
5.1	Radioelemental abundance and ratios of Govardhanagiri-L.Banda granites	47
5.2	Radioelemental abundance and ratios of granites of study area	49
5.3	Radioelemental abundance and ratios of Closepet granites	51
5.4	Uranium migration studies of granites of study area	53
6.1	Palaeohydraulic data estimated for the Gulcheru Formation based on set thickness of trough cross-beds, Lanjabanda area	58-59
6.2	Morphometric indices with their formulae used during calculations	63
6.3	Morphometric indices of Gulcheru sediments from study area	64-65
6.4	Summary of pebble morphometric analysis	66-67
7.1	XRD result of samples from Govardhanagiri- L. Banda area	89
7.2	Paragenetic sequence for different rock forming and ore minerals.	91

8.1	Major oxide (wt%) data of granites(n=11) in study area	93
8.2	CIPW Norms of the granites (n=11) of study area	93
8.3	Pearson correlation coefficients of major elements in Govardhanagiri granites	94
8.4	Trace element data(ppm) of the granites of study area	101
8.5	Pearson correlation coefficients of trace elements in Govardhanagiri-L.Banda granites	102
8.6	REE data of Govardhanagiri- Lanjabanda granites.	106
8.7	Major oxide compositions of the basic rock of Govardhanagiri area (values in wt.%)	110
8.8	CIPW norm obtained by standard GCD kit software	111
8.9	Major element oxide data (%) of Gulcheru quartzite samples	113
8.10	Trace element (ppm) data of Gulcheru quartzite samples.	114
8.11	Correlation coefficient of major oxides and selective trace elements.	114
8.12	Major elements (in wt%) and trace elements (in ppm) concentrations in the Gulcheru shale	122
8.13	Pearson correlation coefficient for major oxides in shale	123
8.14	Pearson correlation coefficient for trace elements in shale	123
8.15	REE data of Gulcheru sandstones (n=6), Govardhanagiri-Lanjabanda area.	130
9.1	Radioelemental concentration in different classes of rocks and soil (after Dickson and Scott, 1997).	133
9.2	Major, minor and trace elements of Biotite granite, Kappatralla area	139

9.3	Major, minor and trace elements of Biotite granite, Lanjabanda area	140
9.4	Major oxide (wt%) and trace elements (ppm) data of Gulcheru Quartzite of Govardhanagiri – Lanjabanda and Kappatralla area.	144-145

## CHAPTER 1

### INTRODUCTION

Middle to upper Proterozoic Cuddapah Basin has been extensively explored by AMD since early 1950s and successfully established as one of the major U-Province in India. In Cuddapah Basin and its environs, uranium mineralization is hosted in fracture controlled granitoids in the southwest, strata bound dolostone in southern part and unconformity proximal at the Srisailam and Palnad sub basins in the northern parts. Uranium mineralisation in Cuddapah Basin was located in

(1) In the basement granitoids in the southern part of Cuddapah Basin i.e. Kamaguntapalle, Kamapalle, Lakkireddipalle (**fracture-controlled uranium mineralisation**) (Srivastava and Rajasekharan., 2001, Dhana Raju et al., 2002, Rai et al., 2002).

(2) In the grey quartzites of Gulcheru Formation i.e. Gandi-Madiyalabodu (**Hydrothermal vein-type mineralisation**) (K.Umamaheshwar et al.,2001, S.Zakaulla et al., 2004).

(3) Phosphatic dolostone of Vempalle Formation of Papaghni Group i.e. Tumulapalle (**Stratabound carbonate hosted uranium mineralisation**) (M. Roy et al.,1990, R.Dhana Raju et al.,1997).

(4) In the Nellore Schist belt to the east of Nallamalai Sub-basin (**Shear-controlled mineralisation**) (M. Thimmaiah et al., 1986, D.Veerabhaskar et al.,1991).

(5) Along the unconformity contact of the basement Mahaboobnagar granite and overlying Srisailam / Banganapalle Formation i.e, Lambapur, Peddagattu, Chitrial, Koppunuru and Sarangipalli (**Unconformity related Uranium mineralization**) (B.S. Bisht et al., 2001, A.V Jeyagopal et al., 2011, R.M Sinha et al., 1995, V.K Srivastava et al., 1992).

Recently Unconformity-related uranium mineralisation has been recorded in the outlier of the Gulcheru Formation near Kappatralla (Rajaraman et al.,2019), Kurnool district, A.P.

Of these five geological settings, unconformity related type of utmost importance for uranium exploration considering

- (i) Fertile nature of the EDC which hosts younger K-rich granitoids.
- (ii) Highly fractured nature of the basement granitoids in the immediate vicinity of the basin, which are often occupied by the dyke swarms.
- (iii) Multi-phase deformational events, which are one of the causes for initiation of sub-basins and relocation of depocenters throughout the history of Cuddapah Basin.

The present study area (N15°28'45", E77°58'45") is located in the western margin of Cuddapah Basin in Papaghni sub-basin and focuses on the basal lithounit of the Papaghni group of sediments (Gulcheru Quartzite) resting non-conformably over basement crystallines. The Paleo-Proterozoic Papaghni Group, comprising the Gulcheru and the Vempalle Formations, non-conformably overlies the Archaean basement granites. The gently dipping Gulcheru Formation mainly comprises of rudaceous and arenaceous sediments is frequently offset by a number of mainly ESE-WNW trending diagonal faults. The overlying Vempalle Formation comprises mainly calcareous sediments with subordinate amount of argillaceous and arenaceous sediments. The present study aims to understand the nature of both basement granitoids and Gulcheru sediments and the controls of uranium mineralisation by using integrated structural, sedimentological and petro-mineralogical data.

### **1.1 Previous work**

The investigations for uranium mineralisation in the Gulcheru Quartzite immediately overlying the fertile basement granitoids led to important discoveries of uranium mineralisation in the sedimentary units along the southern margin of the Cuddapah basin (Gangadharan et al. 2000; Umamaheswar et al. 2001; Zakaula et al. 2004; Dwivedi et al.2006; and Sharma et al. 2006).

During the course of radiometric surveys carried out by AMD since 1999 in the Gulcheru Formation many uranium occurrences have been located and they are divided into

two sub-types based on the controls of mineralisation, namely, (a) Lithologically-controlled mineralisation and (b) Structurally controlled hydrothermal type of mineralisation driven by E-W dykes in the area. The occurrences are located along a 45 km stretch from Ambakapalle in the west to Mamidigundam in the east. Grab samples analysed upto 2.42%  $U_3O_8$ .

Uranium mineralisation occurs over a 35 km long belt and a total of more than 50 anomalies noted, important occurrences being Gandhi, Chintalamadugupalle, Bolaguntacheruvu and Rachakuntapalle. Analysis of the samples indicated values up to 2.112%  $U_3O_8$  with negligible thorium.

Field investigations carried out during the field season 1998-99 in the Gulcheru Quartzite Formation of Papaghni sub-basin have revealed significant concentration of uranium (with values up to 1.441%  $U_3O_8$  and negligible thorium) in quartzite exposed along stream section about 2 km east of the Lord Anjaneya temple at Gandhi ( $14^{\circ}19'30''N$ ;  $78^{\circ}30'30''E$ , Survey of India toposheet no.57 J/11) near the Vempalle town in Cuddapah District, Andhra Pradesh.

During F.S. 2001-02, radioactive anomalies were primarily located in basement granite at few places e.g. Chinnakolumulapalli (0.042avg% $U_3O_8$ ), Lakshmipalli(0.046avg% $U_3O_8$ ), Govardhanagiri (0.046 avg% $U_3O_8$ ) and Dhone (0.034 av% $U_3O_8$ ) etc. These anomalies though spotty are confined along certain fractures with close proximity to unconformity contact.

During F.S. 2002-03, radioactive anomalies recorded in Gulcheru conglomerate and quartzite were found to be thoriferous while those associated with granite cataclasite were uraniferous. Also, gamma ray logging of one private borewell (CKP-1) located west of Chinnakolumulapalli village recorded radioactivity over 50cm thickness from 18.20m depth with an average grade of 0.014%  $eU_3O_8$ .

## **1.2 Present work**

### **Principal Objectives**

- Detailed geological mapping over 10 sq km area (1:5000) to delineate the litho-units and their contact-relationship.
- Detailed analysis of structural elements (fractures, veins and dykes).
- Detailed study of alteration patterns.
- Preparation of lithocolumn and structural plots (Stereoplots, Rose diagram).
- Sedimentological and geochemical characterization of Gulcheru sediments and basement granitoids.
- Integration of structural data with available satellite and airborne geophysical data.
- Understanding the controls of U mineralisation.

### **Research Plan/Methodology**

#### **a) Field Work:**

- Litho-structural and radiometric mapping of the area (10 sq km) on 1:5000 scale.
- Systematic sampling from the basement rocks and Gulcheru sediments for petro-mineralogical and geochemical studies.

#### **b) Lab Work:**

- Petro-mineralogical study to characterize different litho-units.
- Geochemical characterization of the different litho-units for major, trace and REE's by XRF and ICP-OES.

### **Deliverables**

- Detailed litho-structural and radiometric map of the study area (10 sq km) on 1:5000 scale.
- Analysis of structural deformations in the area.

- Petro-mineralogical and geochemical characterization of the host rock for alteration and mode of occurrence of various mineral phases.
- Understanding the controls of U mineralisation using field and lab data.
- Publication of scientific papers based on the research.

### 1.3 Approachability and accessibility

The study area lies 257km south of Hyderabad and can be approached directly by road via NH-44(Figure1.1). The nearest railway station is Kurnool city which is about 35 km north from Veldurthi village. The Govardhanagiri, Lanjabanda area lies approx. 12 km from Veldurthi where our base camp was established. The study area falls under dense Lanjabanda Reserve Forest.

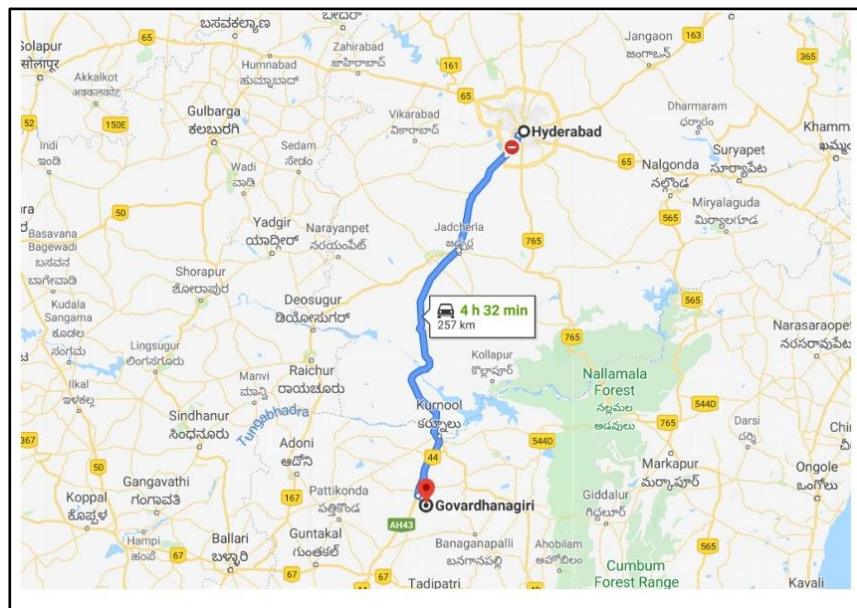


Figure 1.1 Route map from Hyderabad to the study area

### 1.4 Climate and Rainfall

The study area falls under semi-arid tropical zone. The area is having dry climate. The average annual rainfall of the area is 659 mm. The temperatures recorded in this area 27°C in winter and about 43°C in summer season. The general wind direction is SW to NE. January, February and March months are usually pleasant with moderate winds from South-East. April and May

are the hottest months of the year, during these months the wind shifts to Southwest with increased force and brings welcome showers by the end of May. By the end of September, the wind is light and pleasant forecasting the onset of Northeast monsoon. In November and December, the weather is fine, Rainfall is rare and wind is light with occurrence of heavy dew. The rainy season commences with the onset of the South-west monsoon in the part of June.

### **1.5 Organization of Thesis**

**Chapter 1** deals with the brief introduction of Cuddapah Basin and its environs which are hosting different types of U-mineralisation, previous work in and around study area, location and accessibility, climate and rainfall, objectives, methodology, deliverables of the present work.

**Chapter 2** deals with the methodology adopted including the field and lab work to fulfil the objectives.

**Chapter 3** focuses on the regional geology of the Cuddapah Basin with emphasis on western margin.

**Chapter 4** covers the local geology of the study area including detailed geological mapping, structural evaluation using fracture analysis and details of radioactive anomalies.

**Chapter 5** covers the radioelemental characterization of Govardhanagiri-L.Banda granites using various cross plots of elemental ratios as well as uranium migration studies.

**Chapter 6** incorporates the field based sedimentological studies using paleohydraulics and pebble morphometric analysis to decipher the environmental conditions of deposition of Gulcheru sediments.

**Chapter 7** covers detailed petro-mineralogical studies of uranium mineralized and non-mineralized lithounits, their characterization, radioactive minerals identification and their characterization, alteration studies and building paragenetic sequence.

**Chapter 8** covers the geochemical characterization of different lithounits using major, minor, trace elements and REE data with their interpretation.

**Chapter 9** focuses on the integrated geological and geophysical study of the area.

**Chapter 10** outlines the discussion and conclusion using integrated dataset as dealt in previous chapters.

## CHAPTER 2

### METHODOLOGY

The methodology adopted in the present work is dealt under (a) Field investigations and b) Laboratory investigations.

**2.1 Literature survey-** Published research papers in national /international journals related to uranium geology/geochemistry, genetic types of Uranium mineralization and available AMD exploration reports on the exploration outputs in and around the study area was referred.

**2.2 Study of toposheets and satellite imagery-** Toposheets of the study area and satellite imagery was studied to extract information on topography/geomorphology of the area and major structural attributes/features. Toposheets used as base map shows surface features on a sufficiently large scale to enable the individual feature to be identified on the ground by their shape and position. These maps are generally prepared on scales of 1:50,000. Toposheets provide basic information to commence mapping such as vegetation, plains, rock outcrop, broken ground, lowland features, irrigation areas, settlements, transport (Roads and Railway lines) and geomorphological landforms. For study of relief on topographic scale study of contours in toposheets are very important. Contour is an imaginary line on the ground joining all contiguous points at the same elevation from a reference surface. The shape of the contours indicates the shape of the ground. Wide spaced contour lines indicate gentle slopes, closely spaced contour lines indicate steep slopes and uniformly spaced contour lines indicate a uniform slope. Contour intervals also differ according to the scale and nature of terrain. On a 1:50,000 map the interval is 10 m, 20m, 40m depending on steepness and flat nature of ground.

#### **2.3 Geological and lithostructural mapping**

Geological and detailed structural mapping is carried out in Govardhanagiri-Lanjabanda area. Before planning of geological mapping some preparations were done such as

consultations of old literature on different aspects like physiography, drainage pattern, accessibility, geology of the area as well as of adjacent areas or areas having supposedly similar geological set up and collection and study of toposheets (57E/14, 57E/15 and 57I/2) and Satellite images of the area to get acquainted with approach, accessibility, surface features of the area etc. Accordingly, it has been found that, along the whole stretch from Kurnool to Dhone through VKG fault system (more than 200 sq. Km), the nature of basement varies from Gadwal Schist Belt to younger basement granites in the north and south of VKG respectively. The whole stretch is partly soil covered and cultivated. For proper lithological and structural observations of the area, Govardhanagiri-L.Banda area (10 sq. Km) south of VKG taken up for geological and structural mapping due to presence of geological setup of unconformity related mineralization.

#### **a) Work outlay**

1. Mapping of the outcrops and observations of different lithological and structural features.
2. The examination of outcrops, rock identification and attitude, topographic forms etc.
3. Recording field data comprising bedding, joints, sedimentary structures in detail in field note book.
4. Plotting of bedding, joints with geological data on a map.
5. Prepared transverse section and rose diagrams, stereoplots with field photography of important geological features.

#### **b) Field equipments used**

Field equipment used to carry out mapping of the area are field note book, brunton compass, geological hammer, field notebook, handheld GPS, chisel, streak plate, magnet, hand lens, pencil/marker, scale, acid bottle, haversack and sample bags.

### **c) Traverse planning**

For geological mapping on a scale of 1:5000 some regional traverses/orientation survey taken up to understand the ground condition of the study area. In the area where outcrop/exposures are rare and scanty, traverses taken through some selected accessible routes preferably in a direction across the regional strike like roads, nallas etc. Traverses for the geological mapping planned along E-W profiles across the Papaghni group of sediment in Govardhanagiri-Lanjabanda area. Uniform spacing between the different profiles could not be maintained due of inaccessibility to the area at places. Along the profiles, observations are recorded at every 50m spacing. Traverse lines data projected to infer the geology of in between areas. At every location observation recorded properly with the detail of types of lithology and their variants, location (Lat/ Long), structures (sedimentary and tectonic), attitude of the strata (strike/dip, dip direction), elevation, proper photographs of the features etc. To observe the presence of major lineaments in the area study of satellite images was carried out.

### **d) Field data collection, structural analysis and preparation of geological map**

Geological observations and inferences made during field work plotted on the base map to prepare a complete geological map of the area. The data plotted on the map generally are i). Outcrop / projected outcrop pattern of different mappable rock units ii) their contacts iii) attitudes of primary structures like bedding, cross bedding etc. iv) attitudes of secondary structures like fold, fault, and joint etc. (v) attitude of linear features. All these features are plotted on the map using standard symbols. Different mappable rock units were traced and mapped. Continuity of geology concealed under soil cover are indicated as inferred contacts. After plotting of the map, it was digitized using CAD based software. In the present study various structural plots have been prepared. The techniques utilised in the field are presented here in the following section and the interpretation part is dealt in chapter 4. Stereographic

plotting is used to represent the orientations of planar and linear structures of an area and to find out the angular relations among them. Rose diagrams are used to plot the orientation of joints and dykes.

#### **2.4 Laboratory/analytical studies:**

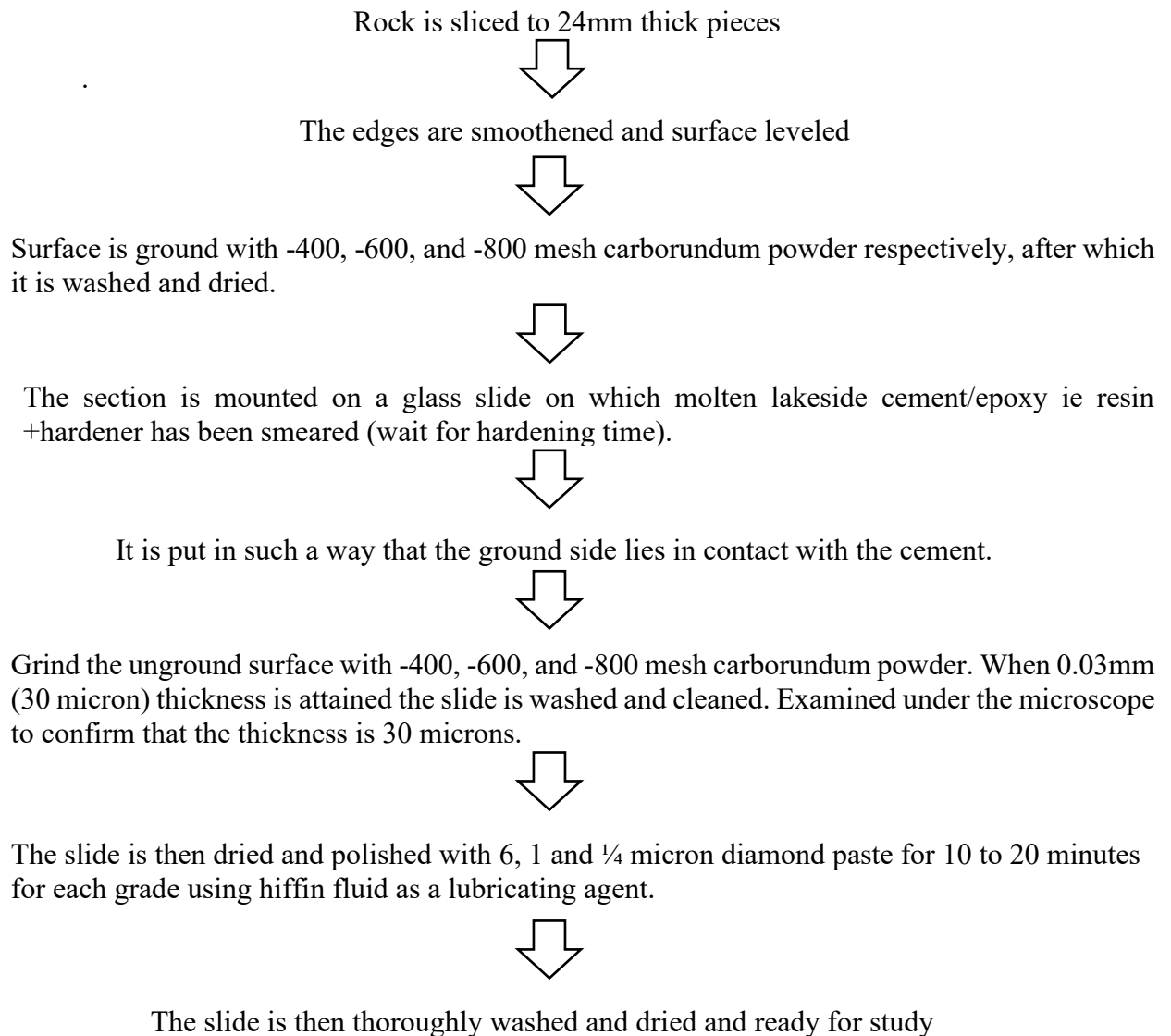
**Petro-mineralogical study:** Transmitted Light Microscopy of 46 samples including granite(n=14), dolerite(n=8), quartzite(n=18), shale(n=3), and conglomerate(n=3) have been studied for petro-mineralogical characterization using orthoplan microscope by Leica systems at Petrology Lab, AMD, SCR to identify rock forming minerals, textural relationship and alteration assemblages/pattern. Reflected light microscopy is used to identify ore minerals.

#### **Sample Preparation**

Various samples preparation techniques are used in preparing samples of rocks and radioactive specimens for examination under the polarizing microscope. Ultrasonic cleaner is used to remove the dust particles from the surface of the sample and the samples examined under the ultraviolet lamp for detection and removal of soft and fluorescent secondary uranyl minerals. Friable and unconsolidated materials were firmly cemented with a penetrating binding substance like Canada balsam before slicing. In case of radioactive samples, radioactive portion was first selected using scintillometer and representative portion slabbed/sliced. The selected slabs/slices were subjected to chromogram test for locating concentration of uranium minerals with easily soluble uranium. The representative thin slice of the sample was mounted on thin glass slide by colourless transparent cement (Canada balsam, thermoplastic cement, epoxy etc.) having refractive index closer to the glass and ground to a thickness of 0.03mm. Both the cut slab and the glass slide mounted thin section were polished with diamond pastes of different grades until a brilliantly reflecting surface was developed. Polished thin section has the advantage that it can be subjected to both transmitted and incident light microscopic studies for better understanding textural relationship of ore and radioactive minerals with other mineral

species. Mineral grains and smaller rock chips were mounted in bakelite, thermosetting powder, epoxy and araldite moulds and polished using both silicon-carbide and diamond polishing compounds. The polished mounts and thin sections are suitable for incident light microscopic observation and alpha particle autoradiography.

### Method



While commencing the petrographic study it was confirmed that the thin sections of standard thickness 30µm or 0.03mm of quartz and feldspar grains show first-order grey-white interference colours. Such observations confirm perfect alignment of the optical settings of the microscope for good petrographic observations.

## **Supportive Aids used for Identification of Radioactive Minerals in Petrology Lab**

All the economically important radioactive minerals have optical properties overlapping with common ore minerals. Only on the basis of optical properties, it may not be appropriate to characterize specific radioactive mineral.

Common aids used in petrology lab related to alpha particle autoradiography:

I). Cellulose Nitrate films

II). Chromogram test

**CN Film Autoradiography (SSNTD):** Cellulose Nitrate films are in the form of flexible sheets, available in two types.

a) CN-85 Film: Transparent in nature of colourless, and consists of 85 ( $\mu$ ) micron thick layer of cellulose nitrate on an inert polyester substrate.

b) LR-115 Film: It is deep red in colour and consists of 12-micron thick layer of Cellulose Nitrate.

Both the films are alpha sensitive with energies below 4 Mev and are insensitive to beta ( $\beta$ ), gamma ( $\gamma$ ) and light radiations.

### **Methodology adopted in using alpha-sensitive films**

These films were put in direct and even contact with the polished surface of the radioactive mineral for period ranging from 24 hours to upto 5 or 7 days depending on the nature of radioactive minerals. Before putting the film on a thin polished section, indicator marks were put on the glass slide, which will help for matching the film after the etching of the film. (Indicator means alpha emitting indicator as reference points).

**Indicator materials-** Powder of uraninite, uranyl nitrate or MDU (yellowcake) mixed with nail polish. After due time, the film was removed and etched in 10% aqueous solution of NaOH in case of CN-85 and 20% aqueous solution of NaOH in case of LR-115 film. Generally, the time allocated for etching in present case was 2-3 hours at 35°C to 40°C. But to be on safer side

films were kept in the solution for overnight etching at normal room temperature to enhance the size of alpha tracks. The alpha bombardment on the alpha sensitive films causes damage the structure of the film. So, when etched in alkali solution these phases will be more reactive compared to rest of the film. This will leave the tiny black marks on the film called as tracks; as these are due to alpha bombardment, therefore called as alpha tracks. These can be easily observed under the microscope. The pattern and density of the alpha ( $\alpha$ ) tracks, when combined with other optical properties give fairly good idea about the radioactive mineral(s) present.

1) Possible nature of the radioactive mineral- If uranium and thorium occur as essential element in minerals it will give high-density tracks. But if they occur as non-essential elements the track density will be low. Thus, Uraninite would always produce very high-density alpha tracks, whereas zircon would normally produce very low-density tracks.

2) Mode of occurrence- The occurrence of radioactive mineral source can be understood by examination of patterns formed by the alpha tracks. The trail of tracks may suggest that the radioactive minerals a vein like structure or occur along a fissure or weak plane whereas cluster of alpha tracks indicate that the radioactive minerals occur as discrete disseminated grains. The relative density of the tracks can only be matched keeping exposure time and etching conditions same. The density of the tracks depends on

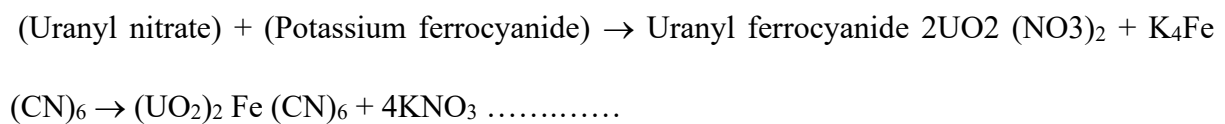
- a) Nature and composition of radioactive minerals
- b) Size-the difference in the size of the same mineral will give different density tracks
- c) Age of radioactive minerals

Two grains of the same size and minerals may give different density tracks, if they differ in the age. The grain older in age will give lesser density tracks in comparison to the grain of same mineral of the younger age.

**Advantage:** a) Easy to match with the radioactive sources.

b) Track contrast is good and can be enhanced by giving longer time for etching in case of CN - 85 films.

**Chromogram:** It is a chemical method and used to locate the presence/absence of easily soluble / leachable uranium rich source. This method involves: a) Taking a dried photo printing paper soaked in photographic fixer (called as hypo, chemically named as sodium thiosulfate) b) Wetting this photo printing paper with 1:1 Nitric acid solution c) The surface of the polished slab or thin / polished section is pressed against it for a minute. d) Removing the slab and treating the paper in potassium ferro cyanide solution. One may get brown spots, rose-red spots, and these may correspond with presence of leachable uranium (U), copper (Cu) and Iron (Fe) in the samples respectively. e) For confirmation put a drop of NaOH solution on brown spots, if it get disappeared confirm presence of mineral phase with leachable uranium, e.g. Uraninite, Pitchblende, Coffinite, and secondary uranium minerals respond positive (+ve) to this test (viz. Brown spots) and refractory minerals like Brannerite and Davidite respond negative (-ve). Uranium (VI) oxide reacts with nitric acid  $U_3O_8 + 6HNO_3 \rightarrow 3UO_2(NO_3)_2 + 5H_2O$  ..... Uranium (IV) oxide reacts with nitric acid  $3UO_2 + 8HNO_3 \rightarrow 3UO_2(NO_3)_2 + 2NO + 4H_2O$  .....



**X-ray Powder Diffraction (XRD) studies:** Two samples (n=2), one radioactive sample of granite and one non-radioactive sample of quartzite from Govardhanagiri-L.Banda area were analysed at XRD laboratory, AMD, Hyderabad for radioactive phase determination and clay mineral studies. Radioactive sample were first examined under the ultraviolet lamp. Fluorescent minerals at place were scrapped with the help of knife/blade. Subsequently the radioactive sample were crushed to minus 80 mesh. These were then taken up for sequentially heavy liquid separation using bromoform (specific gravity, SG 2.88), methylene iodide (SG,

3.31), and Clerici solution (SG, 4.20). The Clerici heavy (CH) fraction were further subjected to the magnetic separation using a Frantz isodynamic magnetic separator at different amperes. The X ray diffraction (XRD) study was carried out in a Siemens D-500 diffractometer. The accelerating voltage was maintained at 35 kV and the tube current at 20mA. CuK $\alpha$  radiation (1.5418Å), monochromatised using curved graphite monochromatized, was used for diffraction. For identification, a scanning speed of 0.03-degree 2 $\theta$ /second, over a long angular range (4-90degree 2 $\theta$ ), with a sampling time of 2 second was selected. The respective 2 $\theta$  value of the reflection and the value of their interplanar spacing were obtained directly by using Wassermann ADM software. Mineral identification was done from the powder diffraction data so obtained by comparing the same with the international center for Diffraction Data card.

#### **X-RAY Fluorescence (XRF) studies**

**Principle:** X-ray fluorescence analysis is a widely accepted technique for obtaining rapid chemical analyses of geological samples. It is the fastest and non-destructive analytical tool to study the different types of geological samples having different concentration range of various elements present, usually requires minimum of sample preparation. XRF is the only analytical technique for elemental analysis that allows the direct measurement of a sample without vaporization and prior digestion. The precision and reproducibility of XRF is very high. According to the detection limits attained for elemental analysis in XRF, the elements analysed for the study include Si, Ti, Al, Fe, Mg, Mn, Ca, Na, K, P, Cr, Ni, Cu, Zn, Rb, Sr, Y, Zr, Nb, Pb, Ba, Ce, Th, and U (24 elements). The sample specimen is prepared as pressed powdered pellet on a boric acid backing.

**Sample preparation:** This is the most crucial part of the analytical work of production meaningful data. The success of analytical results depends on production of fineness of the powdered samples (200 mesh particle size) by suitable means before attempting chemical

processing otherwise errors may be introduced in the final results which may not bear with the objectives of the studies.

Each sample (500 gm) have been collected from the field are finely powdered to 200 mesh size in a suitable high-speed planetary ball mill which could take up 500 gm sample in 4-agate mortars (125-ml capacity) with assorted size agate balls for grinding.

During the M. Tech work rock samples from different lithounits (n=43) have been analysed using Wavelength dispersive spectrometer (WDXRF). Quantitative analyses of major and trace elements were made on Philips MAGIXPRO (4kW, 60kV, 125mA; super sharp, end window tube) – WDXRFS at XRF laboratory, AMD, HQ. WDXRFS spectrometer equipment at AMD, Hyderabad consist of the following (1) 60kV, 125mA generator, (2) End window super sharp (4kW) X-ray tube, (3) Primary and secondary collimators, (4) analyzing crystals, (5) Gas (P-10, 90% Ar and 10% methane) flow proportional counter, sealed xenon and scintillation detector systems, (6) Measuring electronics, (7) Microprocessor, (8) Terminal computer.

In order to get maximum counts vacuum path was used and controlled by computer with Super Q software. The sample pellets were subjected to different operating conditions for determination of major and trace elements i.e.30 kV accelerating potential and 100 mA beam current for major elements while 60 kV accelerating potential and 40-60 mA beam current for trace elements. Suites of well-characterized natural International Rock Standards (IRS) were used as calibration standard using similar matrix composition. The calibration and validation material standards of similar composition range to that of analyzed samples were chosen viz. GS-N, SG-3, G-2, JG-2, JG-3, JG-1A, ASK-1, AC-E, MA-N, NIM-G, Ga for acidic rocks (Granites and granodiorite), and JA-1, JA-2, AGV-1, AGV-2, ST-2, JB-2, BCR-2, BR for basic rocks (basalt and dolerite etc).

**ICP- Optical Emission Spectrometry:** A total of 14 samples consisting of granite(n=8) and quartzite(n=6) were analysed for trace and REE analysis using Ultima 2 Inductively coupled Plasma- optical emission spectrometer at Chemistry Lab, AMD, Hyderabad (Figure 2.1). The details of the instrument with its working principle is mentioned and tabulated below (Table 2.1).

**Working Principle:** ICP-OES is an instrument which measures the intensity of atomic / ionic emission lines emanating from plasma when the sample solution is introduced to it. The intensity of emission line is directly proportional to the concentration of the analyte (element) present in sample solution. ICP-OES is suitable for analysis of refractory elements like REEs, Mo, V, Zr, Hf, Nb, Ta etc. Although the technique is very sensitive, spectral interference from matrix elements needs to be considered for generation of accurate results. Hence, separation techniques are used prior to analysis of ultra-trace elements like REEs in geological samples.

Table 2.1 Details of the ICP-OES instrument used for analysis.

Parameter	Setting	Parameter	Setting
Mounting	Czerny-Turner	Frequency of generator	40.68 MHz
Focal length	1m	Power	1000W
Grating	4320 & 2400 grooves mm <sup>-1</sup>	Plasma gas flow rate	12 L min <sup>-1</sup>
Order of measurement	1 <sup>st</sup>	Nebulizer gas flow rate	0.8 L min <sup>-1</sup>
1 <sup>st</sup> order resolution	0.005nm	Nebulizer type	Meinhard
Type of generator	Solid state	Type of spray chamber	Cyclonic
Observation	Radial View	Injector tube diameter	1.8 mm



Figure 2.1 Ultima 2 inductively coupled plasma optical emission spectrometer

## CHAPTER 3

### REGIONAL GEOLOGY

#### **3.1 Geological and tectonic setting of Cuddapah Basin**

The Proterozoic Cuddapah basin in southern India with an outcrop area of 44,500 square km and >12 km of cumulative sedimentary thickness is the second largest Proterozoic basin in India. The poly history basin is traditionally subdivided into a number of sub-basins (Nagaraja Rao et al., 1987). The Papaghni and Kurnool sub-basins with fluvial to shallow marine depositional environment in the western part of the Cuddapah basin host sedimentary sequences with major internal unconformities (Figure 3.1; Nagaraja Rao et al., 1987; Saha and Tripathy, 2012a; Patranabis-Deb et al., 2012). These were deposited over a time span exceeding 1000 Ma beginning from ~1900 Ma (Bhaskar Rao et al., 1995; Ramam and Murty, 1997; Chaudhuri et al., 2002; Anand et al., 2003). The sedimentary successions of the Paleoproterozoic Papaghni Group in the western part unconformably overlie the c. 2.5 Ga old Peninsular Gneiss and greenschist belts. The Papaghni Group and the unconformably overlying Chitravati Group constitute the Papaghni sub-basin which is overshadowed by a younger sub-basin which hosts the unconformably overlying Neoproterozoic Kurnool Group (Table 3.1 and Figure 3.1). In contrast, the deformed sedimentary succession in the eastern half of the Cuddapah basin constitute a N–S trending 400 km long arcuate fold-and-thrust belt, named as the Nallamalai fold belt (NFB) which has suffered the main deformation prior to 1.5 Ga.

Lying over the Eastern Dharwar craton which was stabilized by c. 2.6–2.5 Ga, the Cuddapah basin at the eastern margin of the craton evolved over a prolonged period of time in the Proterozoic as evidenced by several unconformity bound sequences. The occurrence of extensive mafic dykes and sills in the lower Cuddapah sequences and the western basin margin has been posited as signatures of a large igneous province affecting India around 1.9 Ga (French et al., 2008). Recent recognition of the late Paleoproterozoic/early Mesoproterozoic NFB as an

allochthonous unit thrust over the Neoproterozoic Kurnool sub-basin add to the complexity of the regional tectonic build up involving multiple crustal convergences.

Three cycles of siliciclastic to carbonate sedimentary rocks with alkaline to sub-alkaline basaltic flows, mafic to ultramafic sills/dykes and ash fall tuffs have been recognized within the Cuddapah basin (King, 1872; Nagaraja Rao et al., 1987; Ramam and Murty, 1997; Anand et al., 2003; Saha and Tripathy, 2012a). The lower Cuddapah rocks (the Papaghni and the Chitravati groups with a composite thickness of ~7 km) are restricted to the western and

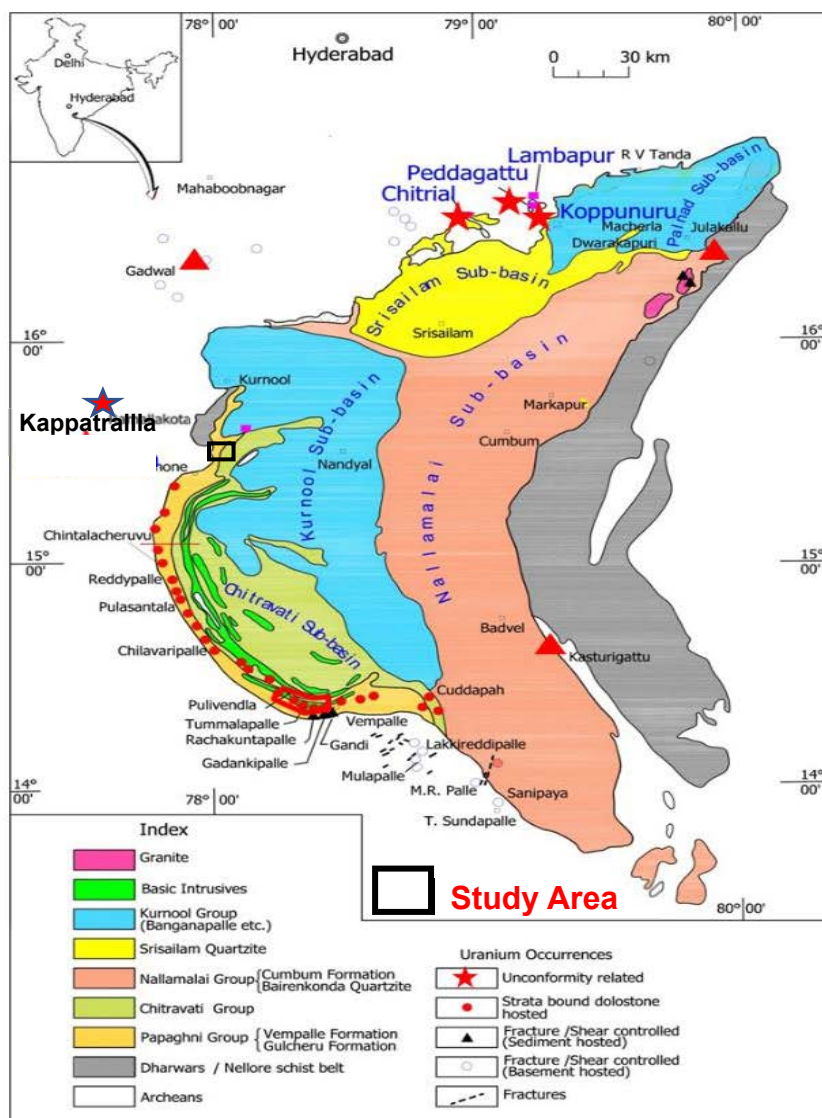


Figure 3.1 Regional geological map of Cuddapah basin (Modified after Nagaraja Rao, 1987).

southwestern part of the basin while the deformed Nallamalai Group constitutes NFB in the eastern part of the basin. The presence of mafic sills, dykes and flows in the Papaghni and the Chitravati groups is in contrast to the younger and relatively thinner Kurnool Group (450 m) which is devoid of mafic igneous rocks suggesting a major shift in tectono thermal environment.

Table 3.1 Stratigraphy of Cuddapah Basin (Nagaraja Rao et al. 1987)

Super Group/ Group /Sub Group	Formation	Thickness in m	
Kurnool Group	Kundair Sub-Group	Nandyal Shale	50 - 100
		Koilkuntla Limestone	15 - 50
		Paniam Quartzite	10 - 35
	~~~~~Para conformity~~~~~		
	Jammalamadgu Sub-Group	Owk Shale	10 - 15
		Narji Limestone	50 - 100
		Banganapalle quartzite	10 - 50
	~~~~~Unconformity~~~~~		
	Cuddapah Supergroup	Srisaliam	Srisaliam Quartzite
~~~~~Unconformity~~~~~			
Nallamalai Group		Cumbum Formation	2000
		Bairenkonda Quartzite	1500 - 4000
~~~~~Angular Unconformity~~~~~			
Chitravati Group		Gandikota Quartzite	300
		Tadpatri Shale	4600
		Pulivendla Quartzite	1 - 75
~~~~~Disconformity~~~~~			
Papaghni Group		Vempalle Limestone	1900
		Gulcheru Quartzite	28 - 210
~~~~~Nonconformity~~~~~			
Archaean and Dharwars	Intrusive grey medium grained chloritized biotite granite, gneisses/ greenstones		

### 3.2 Lithostratigraphy of Cuddapah Basin

The Cuddapah Basin-fill, the Cuddapah Supergroup, is composed dominantly of argillaceous and arenaceous sedimentary rocks with subordinate calcareous deposits, and is unconformably overlain by the Kurnool Group (a 500 m thick orthoquartzite–carbonate–shale association with a basal conglomerate).

**Papaghni Group:** The basal Papaghni Group in the Papaghni sub-basin (which is much older than the Nallamalai sub-basin fill) is exposed in a narrow, arcuate strip along the western and southwestern margin of the basin and comprises the lowermost Gulcheru Quartzite (30–201 m thick) overlain conformably by the Vempalle Formation (up to 1900 m thick; mainly carbonates, lesser clastic sedimentary rocks, mafic sills and volcanics; Ramakrishnan & Vaidyanadhan 2008).

**(i) Gulcheru Quartzite:** The Gulcheru Quartzite is widespread along the west of the preserved basin margin, where it overlies a variety of Peninsular gneisses and Dharwar schists of Archaean age above a distinct unconformity. The lowermost unit Gulcheru conglomerate and quartzite with intercalations of shales and ferruginous bands overlies the Archaean basement unconformably in the northern half of the sub-basin, but in the southern half there is little trace of the conglomerate (e.g. Saha & Tripathy 2012). The thickness of the quartzite member is not uniform, but increases towards the southern end of the preserved sub-basin.

**(ii) Vempalle Formation:** The Vempalle Formation comprising essentially mudrocks, magnesian limestones, dolomites and cherts (Jhanwar et al. 1964), also crops out along the western and southwestern margins of the basin. The lower part of the formation consists of thin-bedded ripple-laminated calcareous sandstone with the local occurrence of herringbone cross-beds, thin gritty units with clasts of lime mud (intraformational flat pebbles) and desiccation cracks in silty units. Further up-plane laminated to rippled impure dolomites are intercalated with thin calcareous rippled sandstone beds. Biosedimentary structures include

algal laminites–stromatolites with isolated stacked hemispheroids to laterally linked hemispheroidal forms (SH/LLH: Logan et al. 1964) in the thinly laminated dolomitic units. The lithological association, and the sedimentary and common bio-sedimentary structures suggest an intertidal–subtidal origin for the carbonates of the Vempalle Formation.

**Chitravati Group:** The Chitravati Group, having a similar distribution along the preserved western Cuddapah Basin margin to the basal Papaghni Group overlies the latter disconformably. It starts with lower Pulivendla Formation consisting of quartzites, conglomerates, sandstones and flagstones which is overlain by Tadpatri Formation consisting of slaty shales with thin beds of siliceous limestone, chert, jasper and intrusive basic sills. The Gandikota Quartzite (shale, glauconite-bearing quartzite and an alternate sequence of quartzite and shale) overlies the Tadpatri Formation with a conformable and gradational contact.

**Nallamalai Group:** The Nallamalai Group occupies a large area and stratigraphically unconformably overlies the Chitravati Group, and is well developed in the eastern part of the Cuddapah Basin. The discordant relationship between the Chitravati Group and the Nallamalai Group may be explained as being due to a thrust contact and hence, the Nallamalai Group may be allochthonous in origin (Saha and Tripathy 2012). The lowest unit, the Bairenkonda Quartzite (an essentially arenaceous unit with volcanic flows, sills and other intrusives; Nagaraja Rao et al. 1987) has been extensively deformed into the Nallamalai fold belt. The succeeding Cumbam Formation is preserved within the synclinal troughs of the Nallamalai fold belt and is an argillaceous unit with intercalations of quartzite and dolomite at various levels. The arenaceous Srisailam Quartzite overlies the Nallamalai Group and is a glauconite-bearing ferruginous quartzite occurring geomorphologically in the form of a plateau.

## **Kurnool Group**

**(i) Banganapalle quartzite:** Basal most unit with a lower conglomerate bed followed successively by grit, quartzite and shale. Conglomerate is oligomictic, consisting of subrounded pebble of chert and quartzite.

**(ii) Narji Limestone:** Narji Limestone rests over the Banganapalle Quartzite conformably and contact between two is gradational. The limestone is divisible into lower flaggy, middle massive and upper flaggy units. The limestone is bluish grey to dark grey in colour, hard and compact in the middle horizon and breaks with conchoidal fracture. Thickness ranging from 120m to 180m.

**(iii) Owk shale:** Owk shale in most of the cases is ochreous and characterised by the presence of yellow and white ochre. This is well laminated thin bedded unit consisting of silty claystone with thin beds of fine-grained quartzite (Richards et. al ,1968). Thickness range from few meters to 35 m.

**(iv) Paniam Quartzite:** this is essentially quartz arenite, but Dutt (1962) recorded siliceous shale in the upper part and identified thin conglomerate and grit beds at the base. The upper horizon of the Paniam quartzite exhibits typical pinnacle nature, a feature which distinguishes the Paniam Quartzite from the rest of the quartzite of the Kurnool Group.

**(v) Koilkuntla Limestone:** This is basically a calcareous unit, but is more siliceous and argillaceous when compared with Narji Limestone of Kurnool Group. The limestone is light grey to dark grey in color and flaggy with occasional massive bands. Thickness Koilkuntla Limestone is nearly about 15m - 50m.

**(vi) Nandyal Shale:** This unit basically argillaceous unit, has calcareous intercalations and shows lower shaly and calcareous flaggy unit and an upper shaly limestone. The shaly flag is a purple calcareous shale which is soft and weathers into pencil like fragments. The shaly

limestone is dark grey and greenish grey and breaks with sharp edges. The thickness of Nandyal shale varies from 50-100 m.

### **3.3 Regional structural Framework**

Cuddapah basin has an undeformed western half and a deformed eastern half called the Nallamalai fold belt (NFB). NFB is a unique morpho-tectonic element of the Proterozoic Cuddapah Basin of Southern India. NFB is an arcuate belt of intense folding, faulting and thrusting in the eastern half of the Proterozoic Cuddapah Basin (Narayanaswami, 1966; Meijerink et al., 1984; Nagaraja Rao et al., 1987; Venkatakrishnan and Dotiwalla, 1987). Meijerink et al. (1984) put forward a distinct and elaborate tectonic model of the basin. They interpreted the boundary between the undeformed gently dipping western half and the highly deformed eastern half as a fault and termed it 'Rudravaram line'. Rudravaram line to the west and the Velikonda thrust to the east defines the tectonic limit of the Nallamalai Fold Belt. Within this belt rocks of the Nallamalai Group have been folded into a series of doubly plunging anticlines/synclines interspersed by oblique and cross faults (Nagaraja Rao et al., 1987). The western margin of the NFB is referred to as the Rudravaram line suggests westward tectonic transport of the Nallamalai rocks and presence of a major thrust (Maidukuru thrust) between the Paleo-Mesoproterozoic Nallamalai rocks and the Neoproterozoic Kurnool rocks (Saha et al. 2009). Folding increases in intensity from west to east in the Nallamalai fold belt with low amplitude open folds progressively becoming tight isoclinal folds. The fold belt commences where cleavage is noticed in the slates in the middle of the Cuddapah basin. Curvature being probably related to compression from the east. The folds in most of the cases are doubly plunging resulting in numerous culmination and depression.

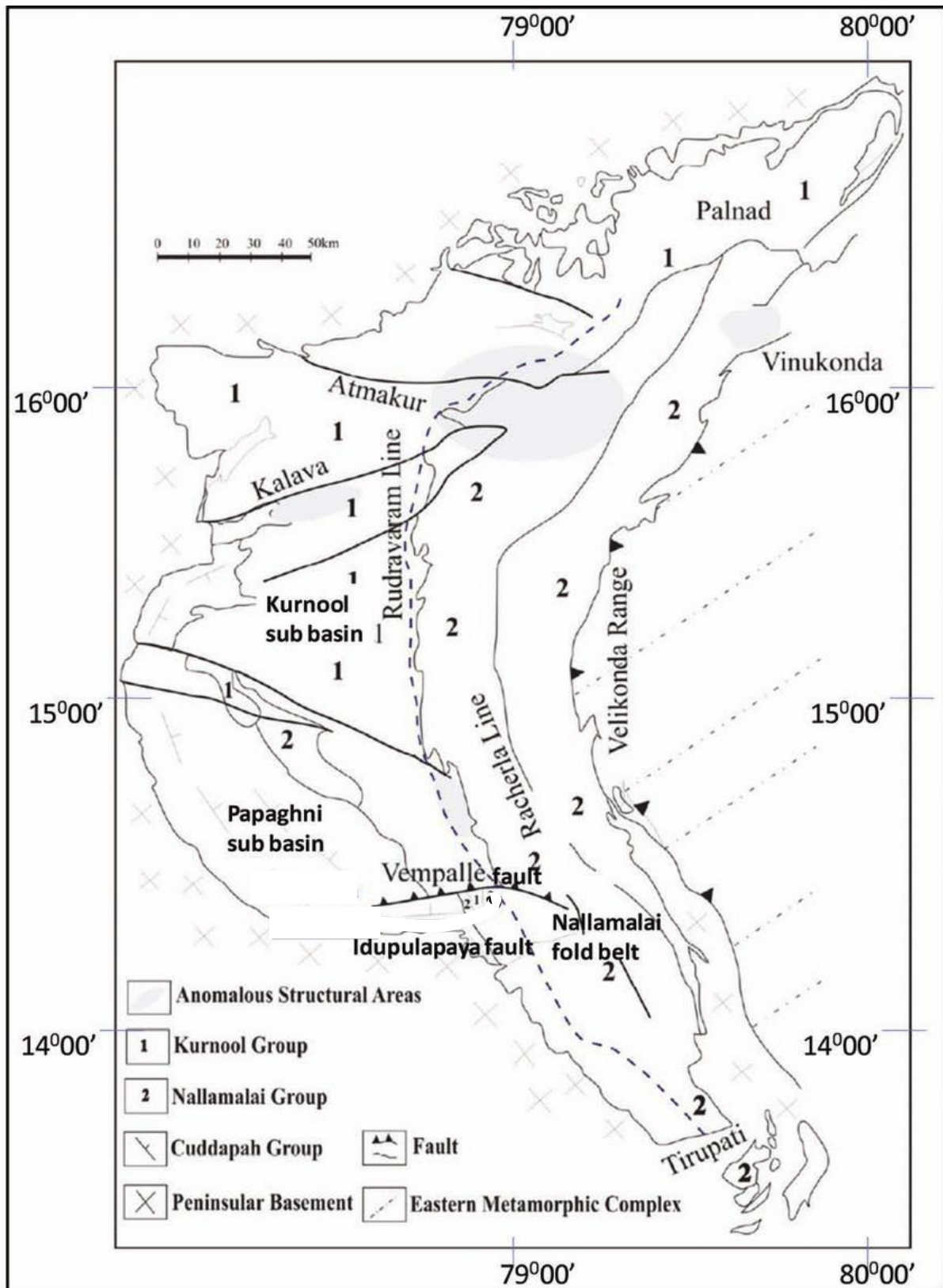


Figure 3.2 Regional tectonic map of Cuddapah Basin showing regional structures (after, Meijerink et al., 1984)

On the basis of the structural geometry of the rocks Matin and Guha (1996) identified two phases of deformation in the extreme southern part of the NFB. However, Mukherjee (2001) opined that mutual relationships of structural elements in a part of the southern NFB indicated a combination of bulk inhomogeneous shortening across the belt and top-to-west variable simple shear under a progressive contractional deformation. From the occurrence of small-scale refolded folds, deformed lineations and overprinting of foliation three phases of deformation were suggested in the northern part of the NFB (Saha, 2002).

Venkatakrishnan and Dotiwalla (1987) put forward a kinematic model wherein the arcuate geometry of the NFB was interpreted as the result of differential buttressing of the advancing west-verging thrust sheets, its transpression and refolding. According to several researcher's deformation in the NFB took place in several episodes with overall E-W shortening in association with westerly thrust transport (Meijerink et al., 1984; Saha, 2002, Saha et al., 2010). From west to east across this belt an increasing complexity and intensity of folding can be observed (Meijerink et al., 1984; Nagaraja Rao et al., 1987). Harmonic folds to the east of the Rudravaram ine gradually pass into disharmonic folds, isoclinal folds, thrusts and imbricate thrusts towards east (Meijerink et al., 1984; Nagaraja Rao et al., 1987). The axial trend of the folds varies from NW-SE in the southern part to N-S in the middle to NE-SW in the northern part of the NFB (Nagaraja Rao et al., 1987; Matin and Guha, 1996).

Within the Nallamalai sub-basin five distinct tectonic zones were identified and their mutual boundaries were interpreted to be defined by deep faults or thrusts (Meijerink et al., 1984). Proceeding from west to east, an increasing complexity and intensity of folding observed, as well as increase of metamorphism.

**Zone1:** All along the western part of Nallamalai basin, near horizontal to gently monoclonal dipping beds prevail, indicating gently tilted crustal blocks.

**Zone 2:** The border line between Zone 1 and Zone 2, the latter containing harmonic folds without great amplitude can be traced through the basin from the extreme south to the extreme north. The line is covered by the rocks of Kundair formation west of the Nallamalai rocks. This line termed the Rudravaram line.

**Zone 3:** Marked by tight folding, occurring in the slates and phyllites of the Cumbum Formation. Zone 3 contains close disharmonic folding, isoclinal folding & thrusting.

**Zone 4:** Isoclinal overturning is more common and the amplitude of the folds is larger. Boundary between zone 3 and zone 4 formed by deep seated high angle reverse fault.

**Zone 5:** Imbricated thrust, eastern metamorphism occurs and folded Nallamalai rocks.

### **3.4 Structural features in the western part of Cuddapah Basin**

A number of E–W trending faults (e.g. Gani–Kalva fault, Kona fault, Atmakuru fault) occur in the western part of the Cuddapah basin (Figure 3.2). The ~60 km long steep ENE-WSW trending Gani–Kalva fault offsets the outcrop of Archean Peninsular gneiss and overlying Proterozoic sequences (Nagaraja Rao et al., 1987; refer to Tripathy, 2010). Similarly, the NW-SE trending ~50 km long Kona fault cuts through the western part of the basin. The sedimentary sequences in the western part of the basin usually show gentle dips except along these fault lines. These large faults, running at a high angle to the N–S trending NFB, likely suffered reactivations during the prolonged tectono sedimentary evolution of the Cuddapah basin beginning from the Paleoproterozoic till the Neoproterozoic (Coulson, 1933; Nagaraja Rao et al., 1987; Meijerink et al., 1984; Tripathy and Saha, 2008, 2009).

Veldurti-Kalva-Gani (VKG) fault in the northern part of CB is of complex type and strikes mainly along NE-SW direction. Narayanaswami (1966) recognised the strike-slip character of this fault. The complexity of VKG fault in the basement in the west is exhibited in the form of series of arcuate structures in the Kurnool strata and the westerly shifting of beds, which are analogous to the flower structures, typical of strike-slip faults (Milani and Davison, 1988). The

Gani-Kalva anticline shows drag folded nature at intervals in sinistral as well as dextral pattern and marked by WSW-ENE trending en-echelon shear faults (Narayanaswami, 1959). It also displays a long history of repeated movements associated with both down thrown and uplifted movements.

Dextral movements along the VKG-fault can be inferred from displacement observed at the western boundary of CB as well as the displacement pattern of the mafic dykes in the basement. However, differential strike-slip movements at different places were reported along the fault that caused a steep monocline “Kalva Wall” (Nagaraja Rao et al. 1987). The VKG fault system has been reactivated time and again, giving rise to both strike- slip as well as oblique-slip sinistral and dextral movement patterns.

All the characteristics of the VKG-fault system described above are typical of transfer faults (Gibbs, 1984). Therefore, VKG-fault system should not be confused with strike-slip or rotational faults of “Anderson type” (Anderson, 1951) and is re-interpreted here as transfer fault that forms a part of the extensional tectonic regime.

## CHAPTER 4

### LITHO-STRUCTURAL MAPPING

#### 4.1 Local Geology of the Govardhanagiri-L.Banda area

The study area is located along the western margin of Cuddapah basin at about 35km south of Kurnool where the Neo-archean to Paleoproterozoic Peninsular Gneissic Complex intruded by younger fertile closepet equivalent granite are unconformably overlain by Paleoproterozoic Papaghni group of rocks represented by Gulcheru (arenaceous) and Vempalle(carbonaceous with subordinate argillaceous units) of Cuddapah Supergroup are exposed(Figure 4.1). Local stratigraphy of the area is tabulated below (Table 4.1) followed by description of individual lithounits.

Table 4.1 Stratigraphy of the study area

Age	Group	Formation	Lithology
Mesoproterozoic	Papaghni Group	Vempalle Fm.  Gulcheru Fm.	Dolostone, siltstone, shale  Conglomerate, pebbly-gritty quartzite, siltstone
----- <b>Unconformity</b> -----			
Neoarchean- Paleoproterozoic	Basement	Basic intrusives  Younger granites  Peninsular Gneissic Complex (PGC)	Doleritic dykes  Younger granitic/ pegmatitic intrusions (Closepet equivalent) <b>PGC-</b> Granite gneiss, granodiorite and tonalite

## REGIONAL GEOLOGICAL MAP OF CHINNAKOLUMULAPALLE-L.BANDA-GOVARDHANAGIRI AREA

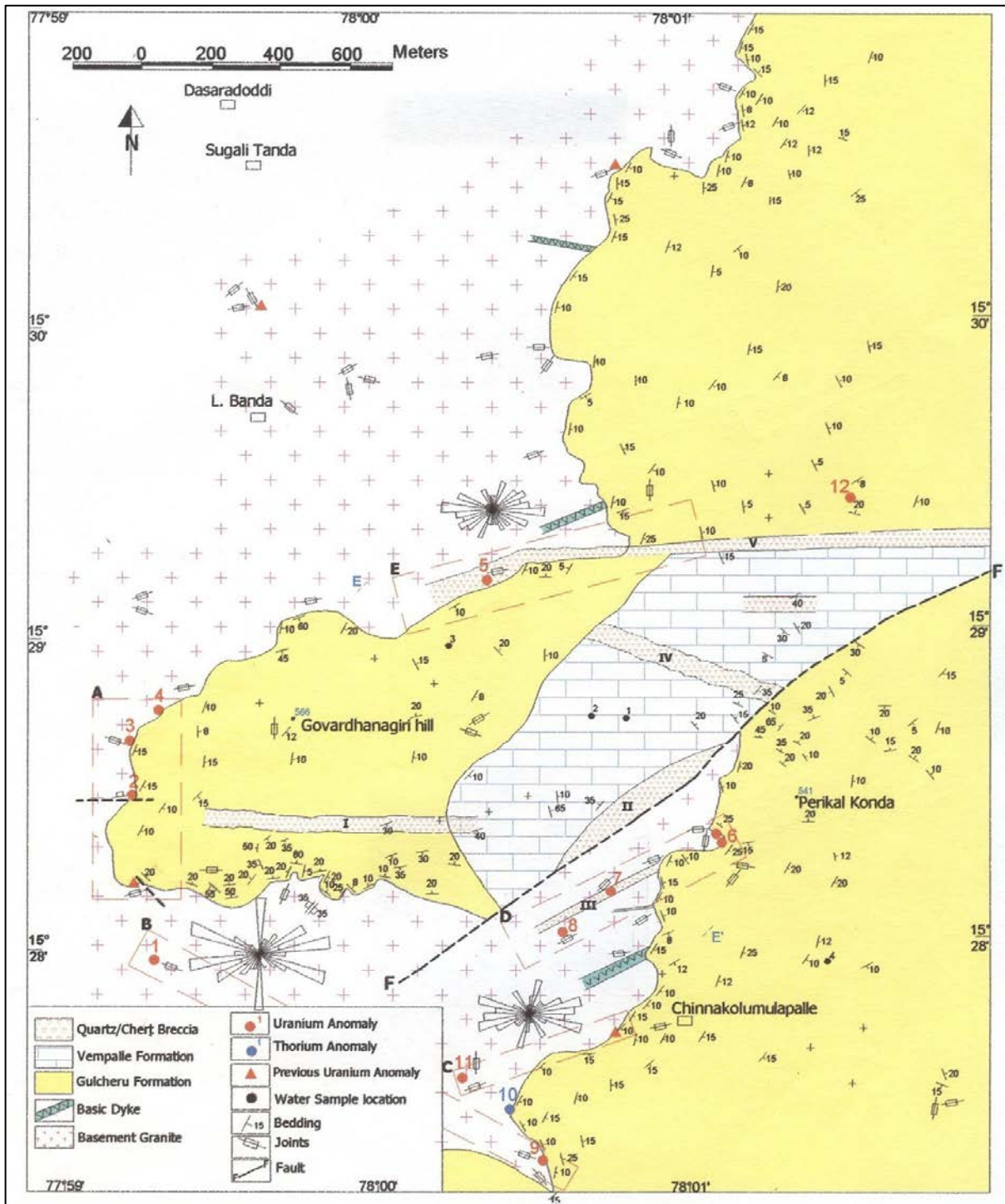


Figure 4.1 Regional geological map of Chinnakolumulapalle-L.Banda-Govardhanagiri area (T.S. Sunil Kumar and R. Sarvanan, Brief annual report, F.S 2004-05).

#### **4.2 Remote Sensing studies: Lineament mapping/geomorphological feature extraction**

The present work includes analysis of satellite images and interpretation of lithostructural elements in the western margin of Cuddapah Basin. To fulfil this objective open source satellite data of Landsat 7 ETM<sup>+</sup> has been downloaded through USGS portal and processed using Arc GIS 10.3. Based on the feature morphology, tonal contrast and texture, lineaments have been marked (Figure 4.2). The resultant product is being made into False Color Composites (FCC) for better visual interpretation thereby discriminate different rock types and delineate structural elements. The FCC 421 (Figure 4.2) indicate vast area appear in light pinkish tone in the south West of VKG fault suggesting granitic soil whereas, in the western side above VKG fault, the area is covered by mostly black soil of Gadwal Schist belt. Lithological units were demarcated based on the tonal-textural variation. The escarpment faces have the unconformity contact of Gulcheru Formation with different lithounits of Gadwal schist belt, Basement granite (PGC), and Younger granite. Further east of the Gulcheru formation lies Vempalle Dolomite followed by Kurnool Group of rocks.

Similar spectral signatures are grouped to single litho-unit and structural features are marked as the lineaments. NW-SE trending structural elements are prominent in the area as represented by dykes, quartz reefs and fracture, minor E-W and ENE-WSW elements are also noted (Figure 4.2).

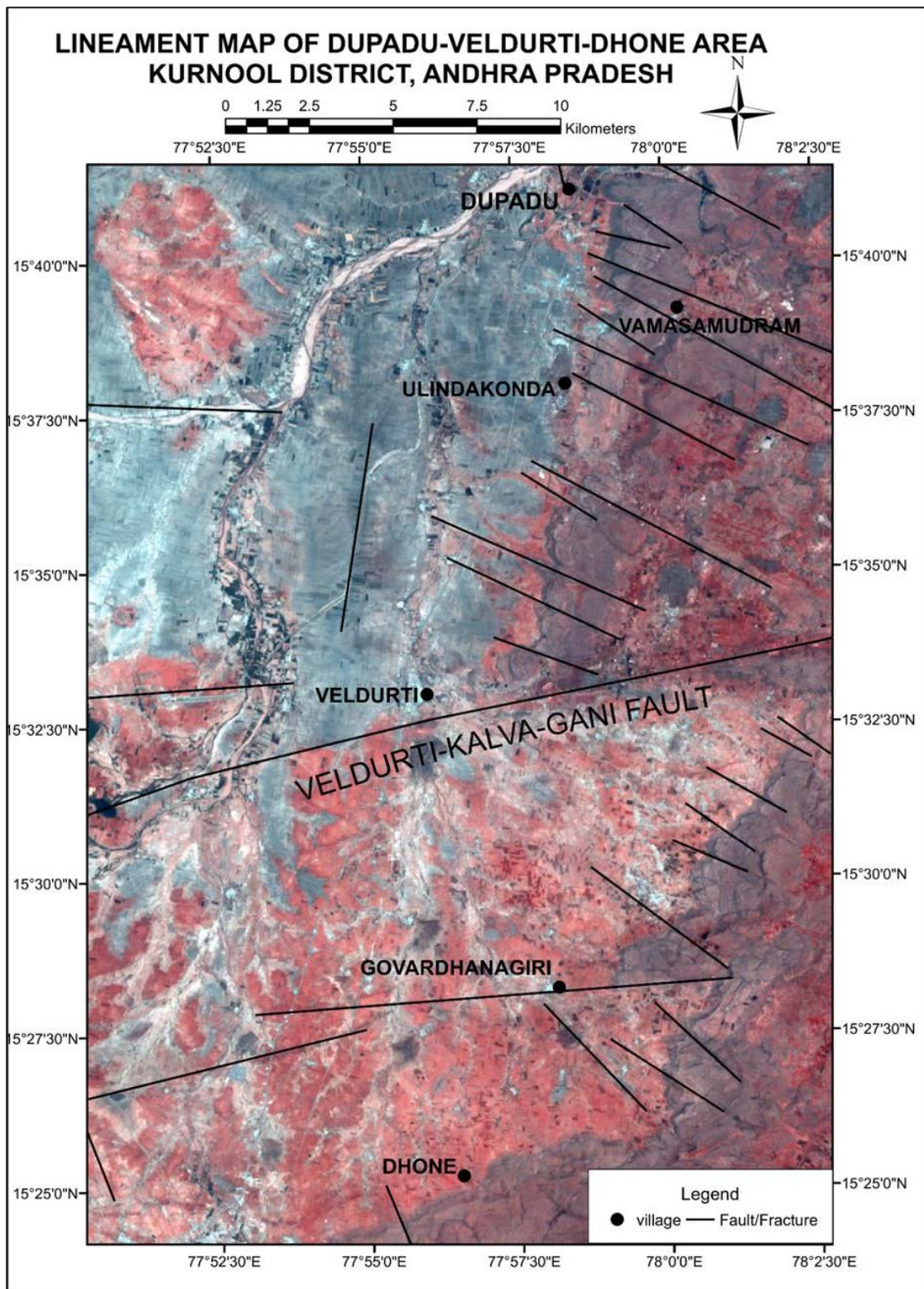


Figure 4.2 Lineament map using FCC image (421) of Dupadu-Veldurti-Dhone area, Kurnool district, Andhra Pradesh.

**4.3 Litho-structural mapping of the area:** Detailed geological mapping (1:5000) over 10 sq km was carried out in Govardhanagiri-L.Banda area. The different lithounits and structures encountered during the mapping are described below and a detailed map was prepared (Figure 4.3). Schematic geological cross-sections were also prepared along profile line A-B (Figure 4.4) and C-D (Figure 4.5) to understand the variation in lithology and structures along E-W and N-S directions.

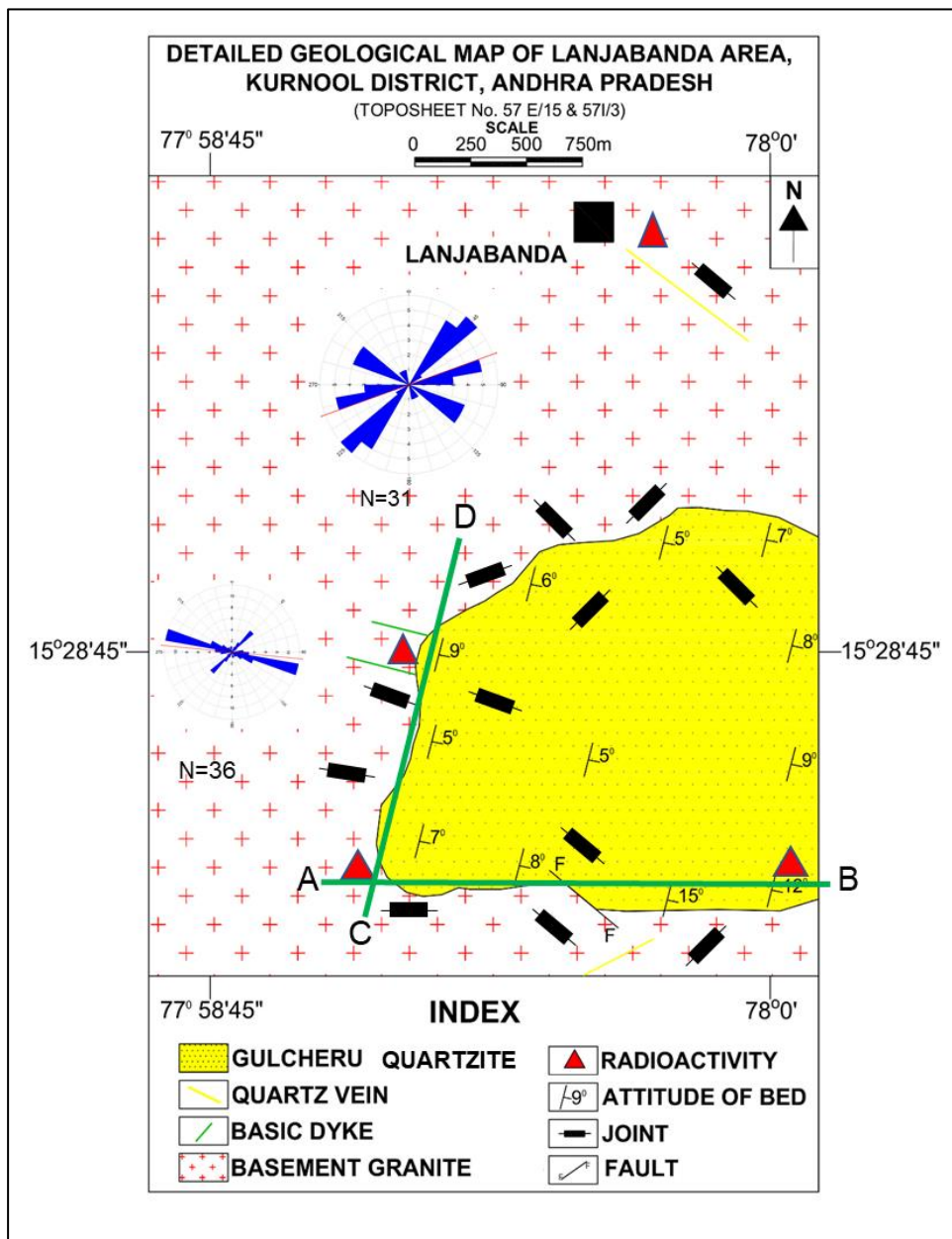


Figure 4.3 Detailed geological map (1:5000) of Govardhanagiri-L.Banda area, Kurnool district, A.P.

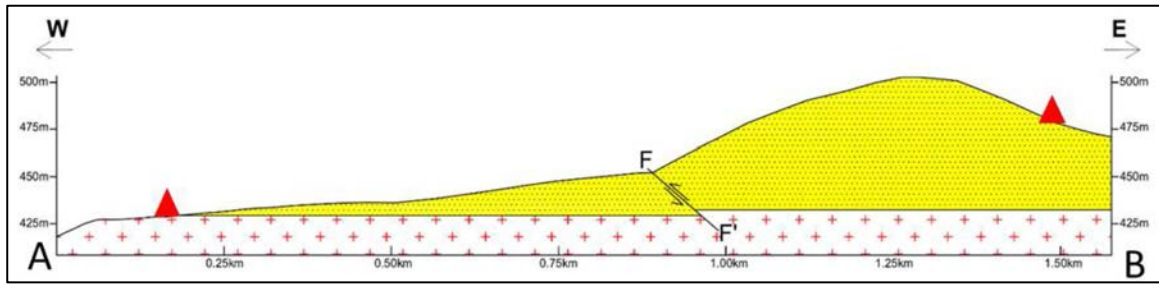


Figure 4.4 Schematic geological cross-section along profile line A-B.

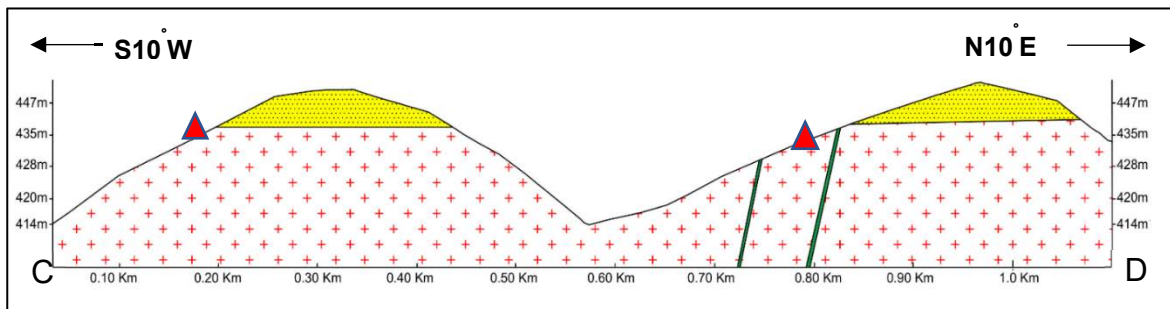


Figure 4.5 Schematic geological cross-section along profile line C-D.

**Basement:** The basement crystallines comprises peninsular gneisses, different types of granites, basic dykes and quartz reefs (Figure 4.3). The peninsular gneisses are exposed in the southern part of the surveyed area whereas in the northern part of the area younger closepet equivalent intrusive granites of pink and grey varieties showing are exposed. These are intruded by basic dykes of varied dimensions mainly trending along E-W direction and abutting against the unconformity (Figure 4.3).

**Peninsular gneissic complex (PGC):** The PGC group of rocks are represented by grey/pink alkali feldspar granite which forms the major rock type. The alkali feldspar granite is homogenous, at places migmatitic (Figure 4.6b) and contains metabasic enclaves (Figure 4.6a).



Figure 4.6 a) Enclaves of metabasics in pink biotite granite b) Migmatitic banding within PGC

**Younger granites:** The area exposes medium to fine grained grey biotite granite (both older and younger phases) (Figure 4.7a). Older phase shows foliation along N30°E trend (Figure 4.7a, inset) while younger phase shows no foliation. The intrusive contact between these two phases lies along N330° direction (Figure 4.7a). There are several pegmatitic intrusions within grey granite NW-SE(N320°) trend. These pegmatitic bodies shows right lateral(dextral) displacement by later generation N70°E and E-W trending fractures which are sympathetic to that of Veldurthi-Kalva-Gani(VKG) fault system(Figure 4.7b). Epidote veins have been observed along these fracture fills (Figure 4.7b). Quartz reef trending N60°E have been emplaced in the granite in this area (Figure 4.7c).

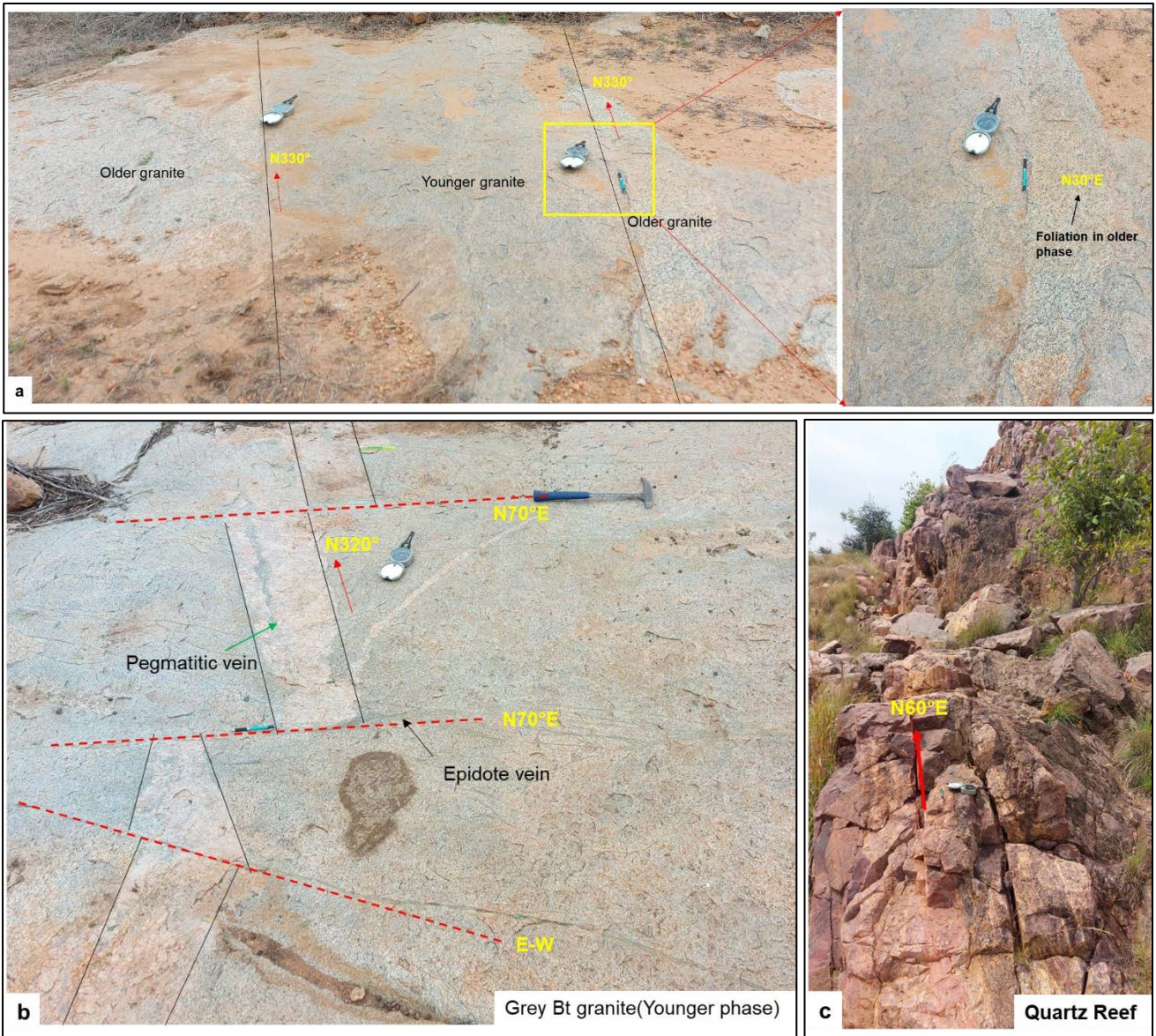


Figure 4.7 a) Intrusive contact (N330°) between younger and older grey biotite granite with older phase showing foliation along N30°E trend. b) Right lateral displacement of pegmatitic vein by N70°E and E-W fractures, L.Banda area c) Emplacement of quartz reef trending N60°E.

Silicification, sericitization, ferruginization (Figure 4.8 a&b) and epidotization is observed along E-W and NE-SW fractures. Tourmaline bearing veins are emplaced along NW-SE fracture (Figure 4.8c). They also show displacement by later NE-SW fracture (Figure 4.8d). Granitic body is also traversed by quartzo-feldspathic veins along N-S, NNE-SSW trending fractures. Pegmatite and vein quartz are seen along ENE-WSW and WNW-ESE trending fracture planes (Figure 4.8d). Intense fracturing in these trends also has resulted in varying degrees of alteration and formation of cataclastic bands and ferruginous quartz breccia.

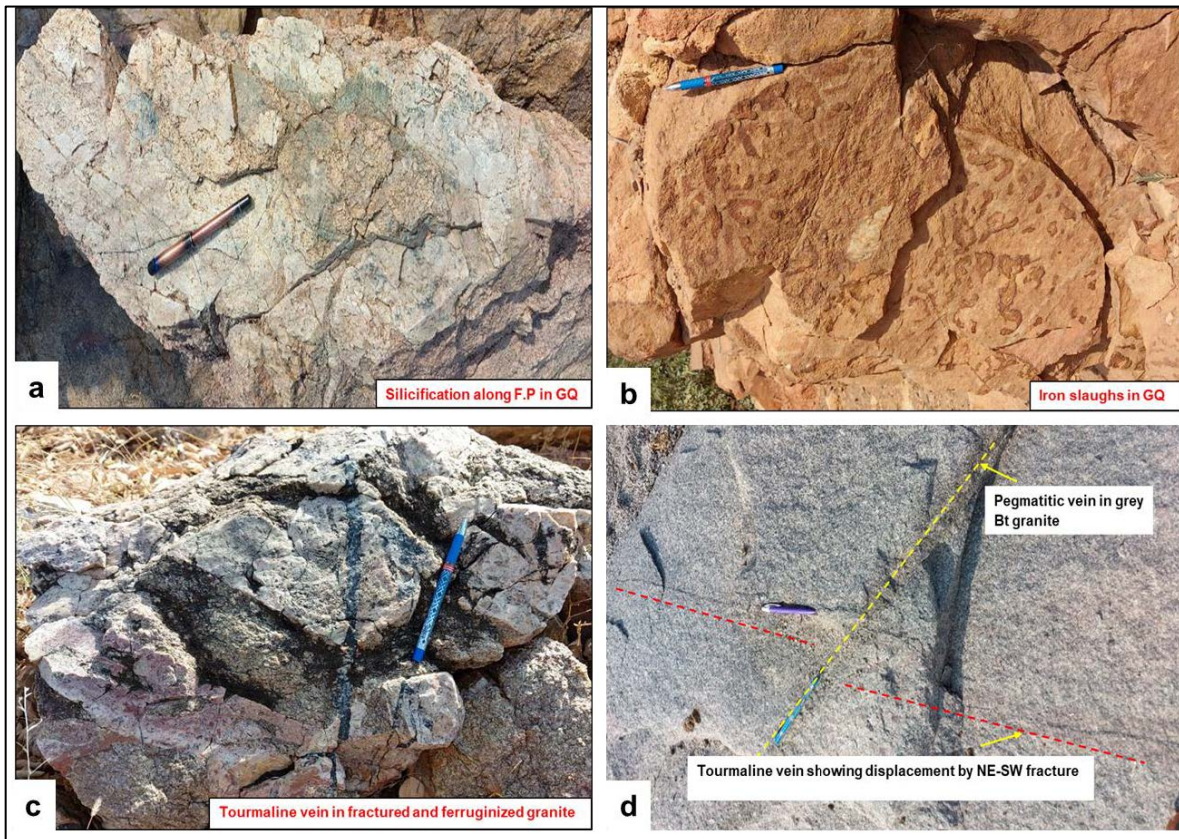


Figure 4.8 a) Silicification along NE-SW(N40°E) trending fracture b) Ferruginization along N320°(NW-SE) trending fracture c) Tourmaline veins along N40°W trending fracture d) Displacement of tourmaline vein by NE-SW fracture.

**Basic dykes:** A number of basic dykes trending NW-SE are seen intruding in basement granite in both Lanjabanda and Kottapalli areas. Basic dyke (30m width) is seen intruding the granite having N70°E trend and subvertical dipping (Figure 4.9a). Large crystals of actinolite are seen along the fractures in granite in close vicinity to basic dyke (Figure 4.9b).

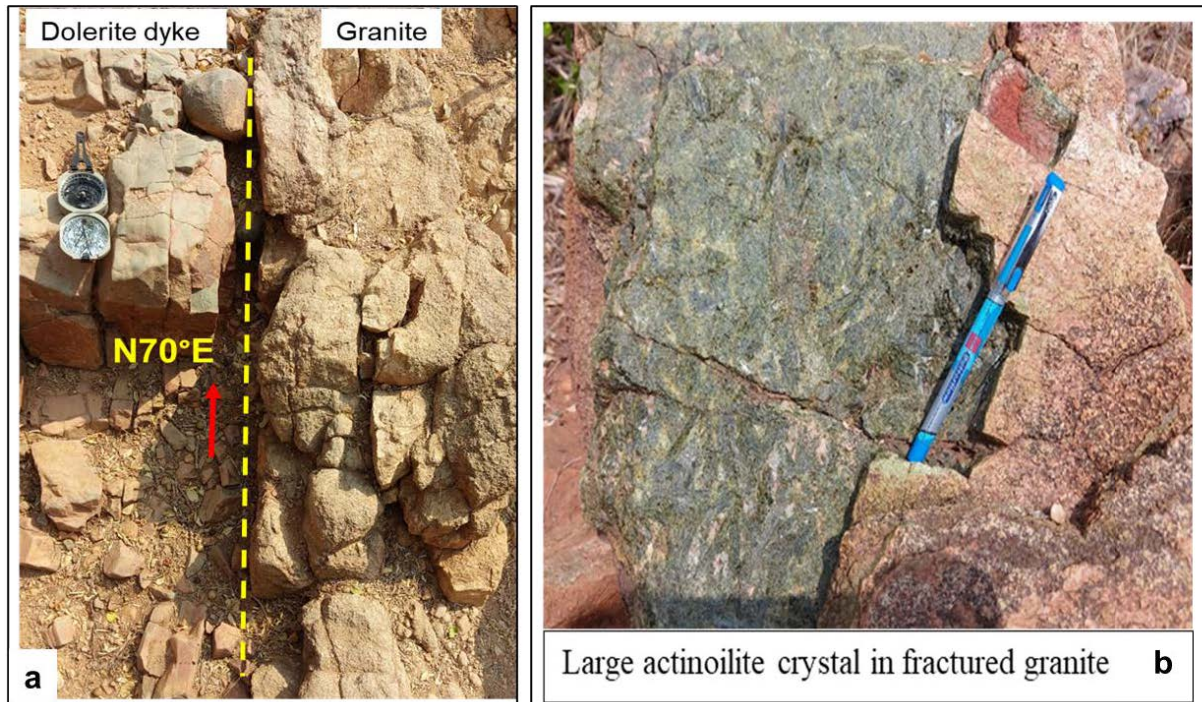


Figure 4.9 a) N70°E trending basic dyke in granite b) Large actinolite crystals in fractured granite

**Gulcheru formation:** Granite is unconformably overlain by 10-20° easterly and southeasterly dipping basal conglomerate and quartzite sequence of Gulcheru Formation. The unconformity is clearly exposed at many places with occasional thin layer of (about 5-10cm) paleosol between the Gulcheru conglomerate and basement granite (Figure 4.10 a and b). Above the unconformity, the Gulcheru sequence starts with conglomerate followed successively by Gulcheru Quartzite and shale. Conglomerate is polymictic and clast supported having sub-rounded to rounded clasts of quartz(predominantly), chert, jasper, BIF(?) and mafic set in arenaceous matrix (Figure 4.10c). NW-SE(N300°), NE-SW(N230°) and E-W fractures are seen cutting through the pebbles of conglomerate (Figure 4.10d).

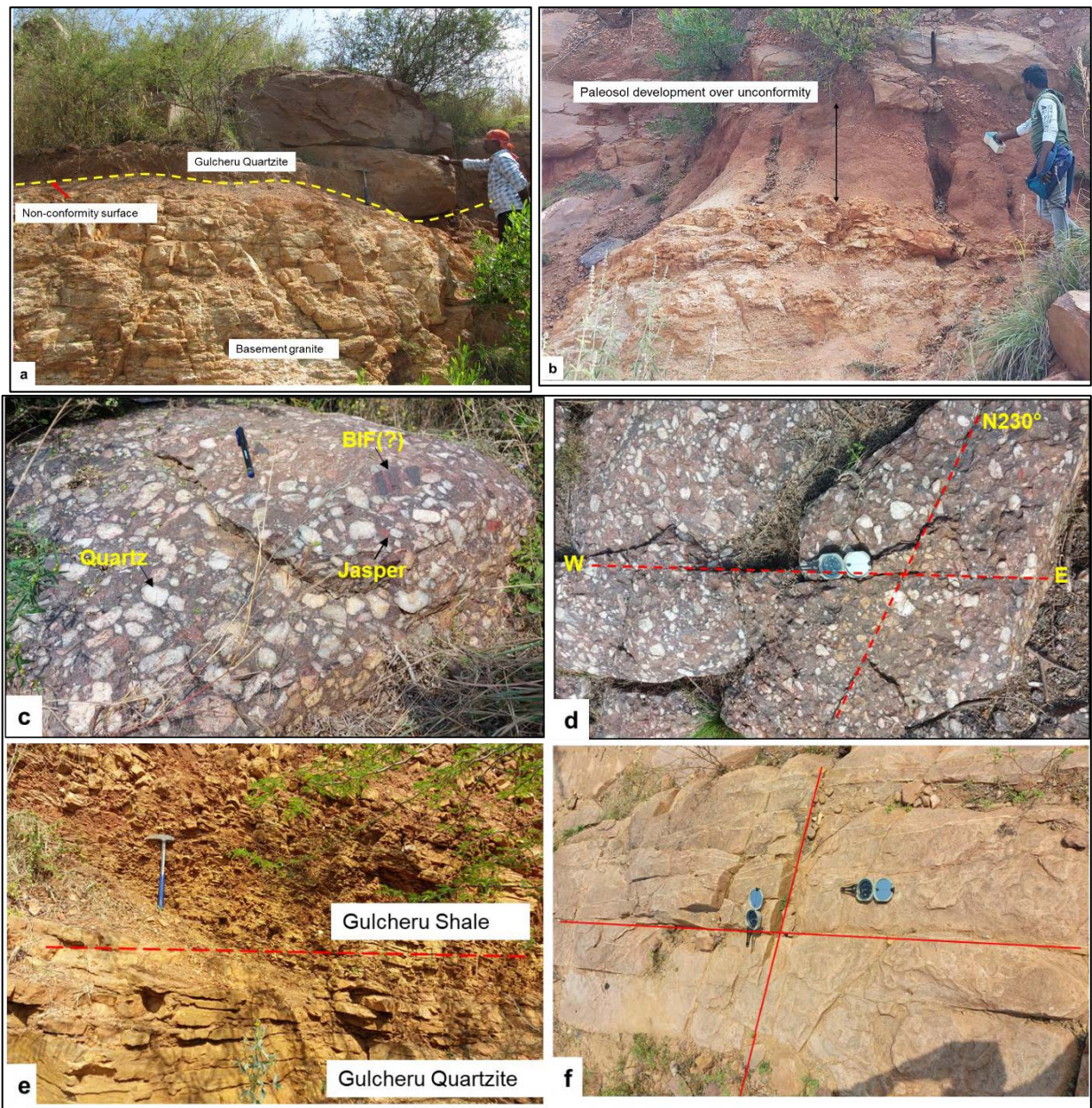
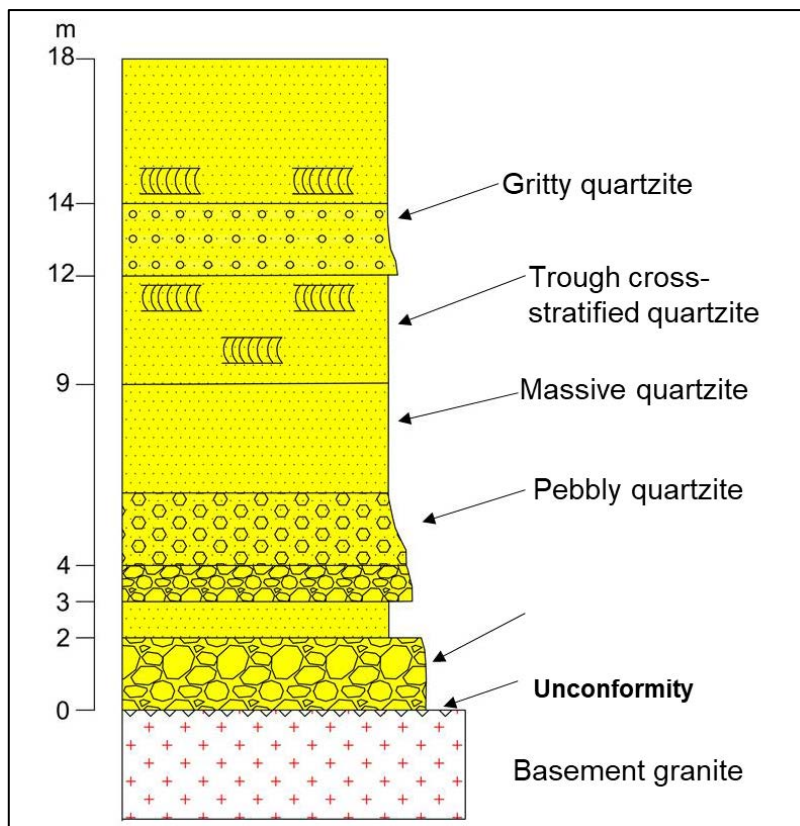


Figure 4.10 a) Non-conformity contact(sharp) between basement granite and Gulcheru Quartzite b) Paleosol development over unconformity surface c) Clast supported polymictic conglomerate having clasts of qtz, jasper and BIF d) NE-SW and E-W fractures cutting through the pebbles of conglomerate e) Gradational contact between Gulcheru Quartzite and shale f) Quartz veination along N205° trending fracture.

The overlying Gulcheru Quartzite is medium to coarse grained buff brown to reddish brown coloured, gritty, massive as well as trough cross-stratified, sub-feldspathic in nature with thin lenses of grey shale intermittently. Intercalated quartzite-shale sequence grades in argillaceous dominant sequence to top of sequence (Figure 4.10e). The strike of the bedding is N45-55°E dipping 12-14° due SE direction. Quartz veination is prominent along N205° trending fracture (Figure 4.10f). Silicification and ferruginization (Figure 4.11 a and b) in Gulcheru Quartzite is observed along NE-SW(N205°) and NW-SE(N300°) trending fractures. Asymmetrical ripple marks (Figure 4.11c) and mudcracks filled with arenaceous material (Figure 4.11d) were seen within the intercalation of shale and medium-fine grained quartzite.



Figure 4.11 a) Silicification in Gulcheru Quartzite along N205° fracture b) Ferruginization along N300° fracture c) Asymmetrical ripple marks in GQ d) Mudcracks in Gulcheru shale



A graphic sedimentary log showing all the lithofacies described above is prepared and presented here to have better visualization of Gulcheru sequence in the area (Figure 4.12).

Figure 4.12 Litholog showing different facies of Gulcheru Formation exposed in Lanjabanda area.

**4.4 Structural analysis:** The major structure present in the area is represented by the ENE-WSW trending Veldurthi-Ramallakota – Kalva – Gani basement fault. It is the most prominent structural lineament in the area. Other trends are WNW-ESE trending lineaments at the peripheral part of the Cuddapah basin and NE-SW trending lineament to the south east of Kurnool town. The ENE-WSW and NE-SW faults have affected basement and the overlying sediments. A number of sympathetic fractures on either side of VKG fault indicates that this fracture was reactivated during different periods.

Prominent sets of fractures in the surveyed area are NW-SE (>60%) followed by E-W/ENE-WSW and NE-SW fractures. The NW-SE fractures are largely occupied by basic dykes. The younger granite emplacement is also in the NW-SE/NNW-SSE trend possibly controlled by two major lineaments in the area. The younger granites are itself fractured at places mostly in NE-SW and E-W directions. Major lineaments also trend parallel to the younger granites whereas the minor lineaments are parallel to the fractures within the younger granites. The fracture and joint trends in granite and sedimentary terrain in the area had been measured and Rose diagrams were prepared separately for two domains, viz. North of

Lanjabanda and South of Lanjabanda respectively. Major fracture trends in L.Banda north are N75°E-S75°W, N50°E-S50°W, E-W and N60°W-S60°E (Figure 4.13a) while that in L.Banda south are N85°W-S85°E and N45°E-SW(Figure 4.13b). Also, the fracture and joint plane data were plotted on the stereonet with their poles which reveals the NE-SW, NW-SE, ENE-WSW and WNW-ESE as dominant trends of brittle fracturing (Figure 4.13c & d). NW-SE(N310°) trending fault causing displacement of Gulcheru shale was also observed in the area (Figure 4.13e).

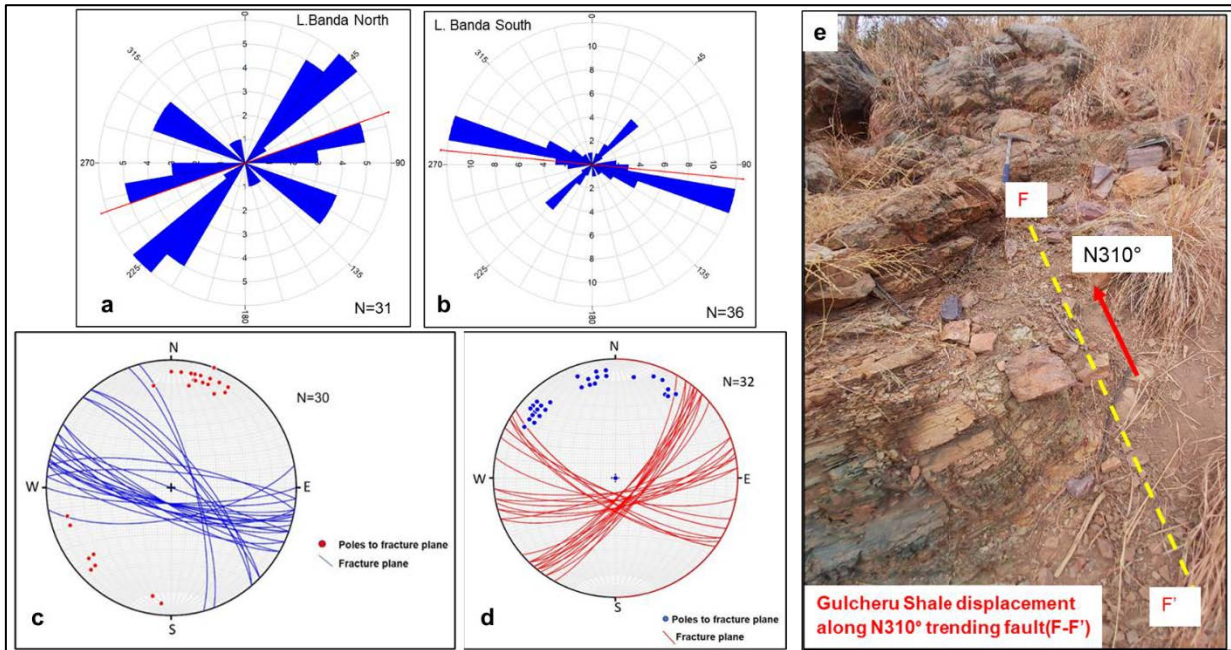


Figure 4.13 a) Rose diagram of fracture sets North of Lanjabanda showing NE-SW as dominant structural trend b) South of Lanjabanda showing NW-SE as dominant structural trend. c) Stereoplot of joint planes with their poles, North of Lanjabanda area d) Stereoplot of joint planes with their poles, south of Lanjabanda area e) NW-SE trending fault causing displacement of Gulcheru shale

**Vempalle formation:** The Vempalle Formation is dominated by carbonate facies, comprised mostly of dolostones with subordinate limestones / arenaceous / argillaceous sediments. The Vempalle Formation is capped by basic extrusive volcanics. Although the individual lithounits may vary from place to place, the Vempalle Formation can be broadly classified into three divisions. They are the lower Massive dolostone/limestone, the intermediate silicious phosphatic dolostone and the upper Cherty dolostone/ limestone. Of these the lower massive limestone unit having a maximum thickness of ~100m and the intermediate siliceous

phosphatic dolostone has thickness of 20-40m and the upper Cherty limestones have thickness of ~1700m. In the present survey area, Gulcheru Formation is overlain by cherty limestone and stromatolitic limestone of Vempalle Formation showing undulations in bedding plane from N75°E-S75°W with 30°SE dip. Cherty limestone/dolostone is characterized by chert breccia, silicious oolite, intercalation of purple shale and minor quartzite.

**4.5 Radioactive anomalies:** In course of radiometric survey in Govardhanagiri-L.Banda area, four radioactive anomalies were recorded in both the basement granite(n=3) and Gulcheru quartzite(n=1). Anomalies in the altered fractured basement granite close to the unconformity contact are uraniferous (Table 4.2) while those in Gulcheru sediments are thoriferous in nature (Table 4.3).

Table 4.2 Radiometric result of anomalies of Govardhanagiri – Lanjabanda area

A. Id	Coordinate	Rock Type	Dimension	%eU <sub>3</sub> O <sub>8</sub>	%U <sub>3</sub> O <sub>8</sub>	%ThO <sub>2</sub>	%Ra (eU <sub>3</sub> O <sub>8</sub> )
1	N15°28'14.1", E77°59'12.2"	Granite (n=2)	3 x 1.5m	0.01 – 0.025	0.007 – 0.022	<0.005	0.007 – 0.022
2	N15°28'43.6", E077°59'07.6"	Granite	Spotty	60ppm	-	<5	59
3	N15°29'38.3", E077°59'53.1"	Granite	Spotty	50 ppm	-	15	35
4	N15°28'22.1", E077°59'58.8"	Quartzite (n=7)	3m x 0.5 to 1m	67ppm– 0.026	-	0.013– 0.055	<0.005

Table 4.3 Radio-elemental distribution in various litho-units exposed at Govardhanagiri-L.Banda area

S.No.	Lithology	eU <sub>3</sub> O <sub>8</sub> (ppm)	ThO <sub>2</sub> (ppm)	Ra(eU <sub>3</sub> O <sub>8</sub> ) (ppm)	%K
1	Granite (n=16)	8 – 62 Av. 35.93	<5 – 53 Av. 32.5	<5 – 59 Av. 20.25	0.6 - 7.1 Av. 3.63
2	Quartzite (n=10)	9 – 31 Av. 16.6	5 – 50 Av. 21.87	<5	1.4 – 4.2 Av. 2.57
3	Conglomerate (n=3)	6-23 Av. 13.67	<5 – 38 Av. 27.5	<5	0.7 – 1.9 Av. 1.47
4	Shale (n=6)	29-58 Av. 40.66	12-17 Av. 13.2	8-34 Av. 17.33	6.9-7.4 Av. 7.12
5	Basic body (n=4)	<5 – 7	<5	<5	0.5

## CHAPTER 5

### RADIOELEMENTAL CHARACTERIZATION

#### **5.1 Radioelemental Studies of granites**

Radioelemental characterization of granitoids in known uranium provinces are vital to uranium exploration, because such studies may lead to the discovery of new uranium deposits through the recognition of similar source rocks (Stuckless and Ferreira, 1985). Main source of uranium for many uranium deposits is attributed to the granitoids occurring in the respective provinces.

Enrichment of uranium commenced since the formation of the early crust by the upward migration of uranium and associated large ion lithophile elements from the mantle to the crust, followed by later mantle magmatism leading to granite formation and cratonisation (Sinha, 1997).

Granitic magmas tend to naturally concentrate the incompatible radioactive elements such as U, Th and alkali element K as it is formed at the later stages of magmatic crystallization process. The incompatible elements and alkali element proportion varies within granitoids as the melt undergoes further differentiation processes. The later immiscible fractions of such differentiation process rich in volatile phases/ligands favour the migration of these elements as they form strong bonds with the incompatible phases. The relative concentration of these elements varies among same suit of rocks. Much evolved younger granite will be having higher relative proportion of incompatible elements than its less evolved counterparts.

#### **5.2 U, Th and K in granites**

Granites and related younger intrusive/extrusive rocks are known to contain U and Th greater than the average content of the earth crust. The uranium content of the earth's crust varies from 2.2-2.8ppm while that of thorium ranges from 6-9ppm (Condie, 1993). The relative

concentrations of these elements in granites range from 3.3-4ppm and 17.5-18ppm (Cuney, 2014) respectively. The content of potassium also varies 2.1-2.8% while in granite it goes up to 2.6% - >6% (Wedepohl, 1978).

### 5.3 Radioelemental distribution in the study area

U, Th and K content of the granitoids in the western margin of Cuddapah Basin is high and these granitoids show hyper-acidic to acidic composition with characteristic calc-alkaline affinity (Rajaraman et al., 2018). To understand the radioelemental concentration and distribution, radiometric survey using scintillometer and radiation survey meter has been carried out. Generally, the pinkish varieties of granite have recorded high background than the corresponding grey varieties (Figure 5.1). Surface encrustations of secondary uranium phases have also observed at many places (Figure 5.2). Rock exposures showing 2xBG values or >30 ppm have collected for radiometric assay. Those recorded >100ppm are considered as anomalous samples. The samples(n=15) have been studied by physical assay for %U<sub>3</sub>O<sub>8</sub> by β/γ method (Acharyulu et al., 2004; Bhaumik et al., 2004) and analysed for equivalent U<sub>3</sub>O<sub>8</sub>(%eU<sub>3</sub>O<sub>8</sub>), radium equivalent U<sub>3</sub>O<sub>8</sub>(%Ra eU<sub>3</sub>O<sub>8</sub>), %ThO<sub>2</sub> and %K (Srivastava et al., 2015). Three radioactive anomalies have been located in the area in these granites out of which one is uraniferous and other two are thoriferous in nature.

Table 5.1 Radioelemental abundance and ratios of Govardhanagiri-L.Banda granites

Area and no. of samples		U ppm	Th ppm	K%	(Th/K) x10 <sup>-4</sup>	(U/K) x10 <sup>-4</sup>	U/Th	Kx (U/Th)
<b>Govardhanagiri-L.Banda(n=15) (This Study)</b>	Mean	32.27	15.83	2.96	5.33	10.87	2.04	6.05
	Range	8-62	2.5-53	0.6-5.7	0.51-26.15	3.06-100	0.67-24	0.87-70.68
	s.d	15.81	17.24	1.443	6.63	23.65	7.74	17.86
Kappatralla-Nelibanda(n=42) <b>Rajaraman et al. (2018)</b>	Mean	29.13	39.73	4.59	8.75	5.74	0.91	3.88
	Range	1-47	3-105	1.2-8	0.81-36.21	0.01-20.64	0.01-9.67	0.01-35.77
	s.d	24.37	23.68	1.31	5.96	5.60	1.54	6.04
	rsd.	0.84	0.60	0.29	0.68	0.98	1.70	1.56
Closepet granite(n=16) <b>Divakarrao et al. (1972)</b>	Mean	3.5	18.2	3.8	5.03	0.80	0.22	0.82
	Range	1.4-5.3	3.9-52.5	2.5-4.7	1.44-12.64	0.39-1.26	0.06-0.44	0.24-1.89



Figure 5.1 Radioactive ferruginized pink granite showing 100ppm activity (PGRS), Govardhanagiri area.



Figure 5.2 Secondary U mineral on the exfoliation plane of pink granite

Table 5.2 Radioelemental abundance and ratios of granites of study area.

Sample Id	U ppm	Th ppm	%K	(Th/K) x10 <sup>4</sup>	(U/K) x10 <sup>4</sup>	U/Th	Th/U	Kx (U/Th)	logTh (ppm)
LNJB-1/Gr	33	33	4.1	8.04	8.04	1	1	4.1	1.52
LNJB-2/Gr	57	2.5	3.1	0.81	18.38	22.8	0.04	70.68	0.39
LNJB/Gr/4	62	53	3.2	16.56	19.37	1.17	0.85	3.74	1.72
GVD/Gr/1	42	50	4.4	11.36	9.54	0.84	1.19	3.69	1.70
GVD/Gr/2	35	28	4.4	6.36	7.95	1.25	0.8	5.5	1.44
LNJB/Gr/1	15	2.5	4.9	0.51	3.06	6	0.17	29.4	0.39
LNJB/Gr/2	8	2.5	1.3	1.92	6.15	3.2	0.31	4.16	0.39
LNJB/Gr/3	60	2.5	0.6	4.16	100	24	0.04	14.4	0.39
LNJV/Gr/1	50	15	3.5	4.28	14.28	3.33	0.3	11.67	1.17
LNJB/GRP/1	35	35	5.7	6.14	6.14	1	1	5.7	1.54
LNJB/UC/1	23	34	1.3	26.15	17.69	0.67	1.47	0.88	1.53
GVD/2	25	23	4	5.75	6.25	1.08	0.92	4.34	1.36
GVD/3	30	22	2.4	9.17	12.5	1.36	0.73	3.27	1.34
CKP/GR/2	32	26	4.3	6.05	7.44	1.23	0.81	5.29	1.41
CKP/GR/1	36	44	3.8	11.57	9.47	0.81	1.22	3.10	1.64
<b>Min</b>	<b>8</b>	<b>2.5</b>	<b>0.6</b>	<b>0.51</b>	<b>3.06</b>	<b>0.67</b>	<b>0.04</b>	<b>0.87</b>	<b>0.39</b>
<b>Max</b>	<b>62</b>	<b>53</b>	<b>5.7</b>	<b>26.15</b>	<b>100</b>	<b>24</b>	<b>1.47</b>	<b>70.68</b>	<b>1.72</b>
<b>Average</b>	<b>32.27</b>	<b>15.84</b>	<b>2.96</b>	<b>5.33</b>	<b>10.87</b>	<b>2.04</b>	<b>0.49</b>	<b>6.05</b>	<b>1.20</b>

#### 5.4 Characterization based on radioelements

The radioelemental concentration of the granitoid rocks of the study area varies from U (8-62ppm, avg. 32ppm), Th (2.5-53ppm, avg. 16ppm) and K (0.6%-5.7% avg. 2.96%) (n=15) (Table 5.2). The average concentration of these elements in Closepet granite is 3.5ppm of U,

18.2 ppm of Th and 3.8% of K (Rao et al., 1972). The Th/U ratio of granites of the study area with average value of 0.5 (Table 5.2 and Figure 5.3) indicate less evolved felsic magma than Closepet Granite (avg. Th/U ratio 6.4). It is observed that the grey and pink varieties of granite show differential degree of differentiation and the pink varieties appear to be more evolved than corresponding grey varieties.

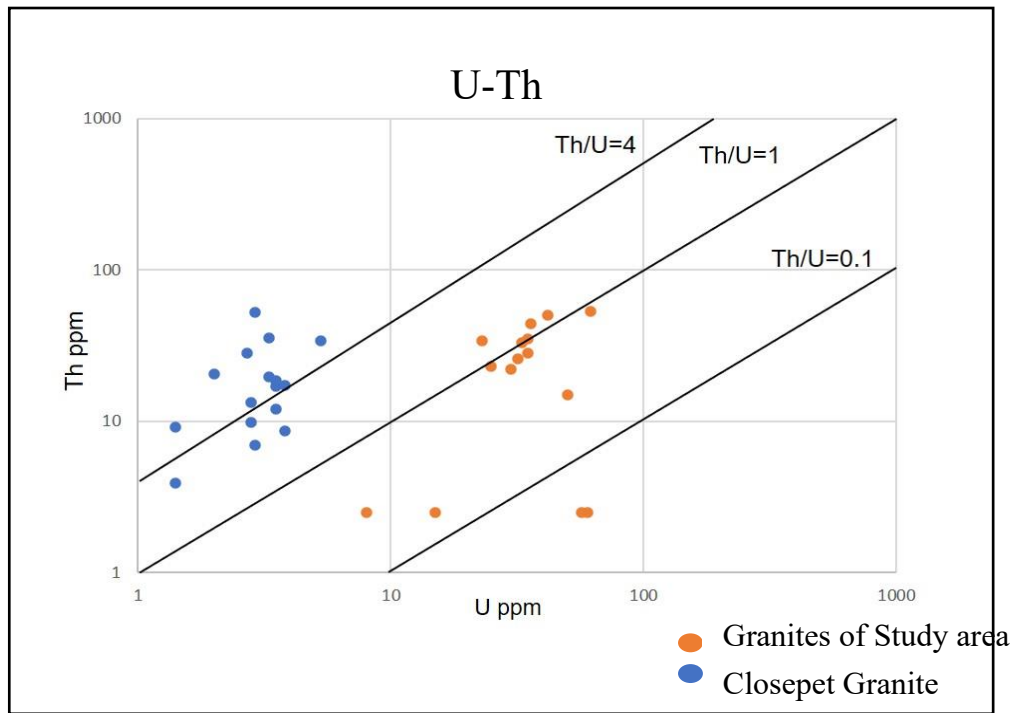


Figure 5.3 Comparative U-Th plot for Closepet Granite and granites of study area

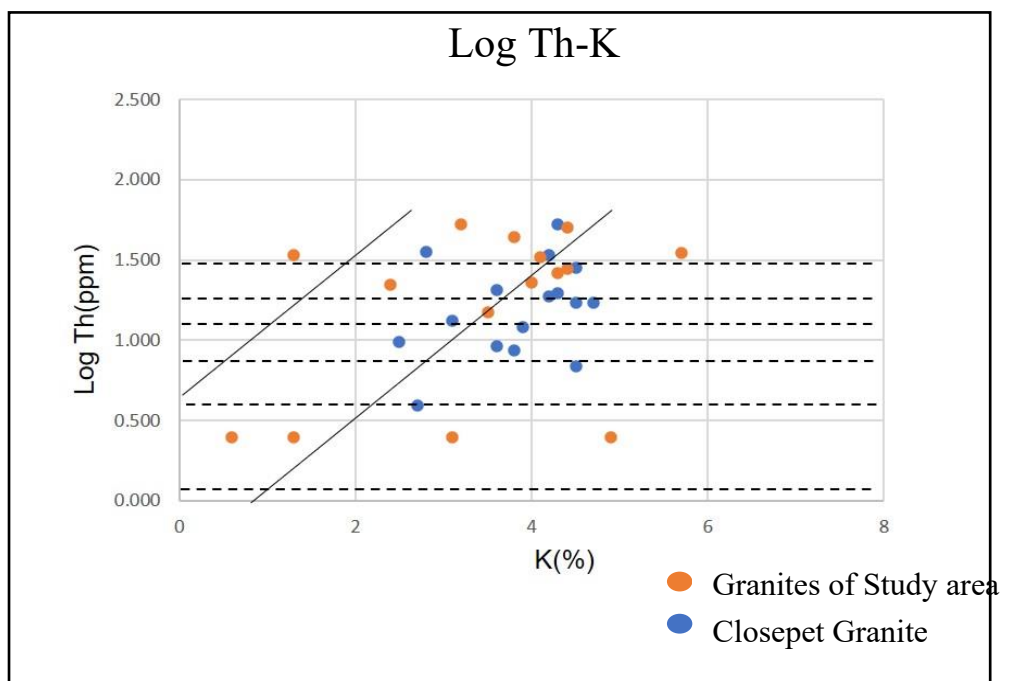


Figure 5.4 Log Th-K plot for granites of study area (Galbraith and Saunders, 1983)

Table 5.3 Radioelemental abundance and ratios of Closepet granites

Sample Id	U ppm	Th ppm	%K	(Th/K) x10 <sup>4</sup>	(U/K) x10 <sup>4</sup>	U/Th	Th/U	K x(U/Th)	log Th (ppm)	U/K
Closepet granite	5.3	34	4.2	8.09	1.26	0.15	6.41	0.65	1.53	1.26
	2.9	52.5	4.3	12.20	0.67	0.05	18.10	0.24	1.72	0.67
	2	20.4	3.6	5.66	0.56	0.09	10.20	0.35	1.31	0.55
	3.5	17	4.7	3.61	0.74	0.20	4.85	0.96	1.23	0.74
	3.8	17.2	4.5	3.82	0.84	0.22	4.52	0.99	1.24	0.84
	2.8	9.8	2.5	3.92	1.12	0.29	3.50	0.71	0.99	1.12
	3.5	12	3.9	3.07	0.89	0.29	3.43	1.14	1.08	0.89
	1.4	9.2	3.6	2.55	0.38	0.15	6.57	0.55	0.96	0.38
	2.7	28.3	4.5	6.28	0.60	0.09	10.48	0.43	1.45	0.6
	3.3	19.6	4.3	4.55	0.76	0.16	5.94	0.72	1.29	0.76
	2.8	13.3	3.1	4.29	0.90	0.21	4.75	0.65	1.12	0.90
	2.9	6.9	4.5	1.53	0.64	0.42	2.38	1.89	0.83	0.64
	1.4	3.9	2.7	1.44	0.52	0.36	2.79	0.97	0.59	0.52
	3.8	8.6	3.8	2.26	1.00	0.44	2.26	1.68	0.93	1
	3.5	18.6	4.2	4.42	0.83	0.18	5.31	0.79	1.27	0.83
3.3	35.4	2.8	12.64	1.18	0.09	10.72	0.26	1.55	1.17	
<b>min</b>	<b>1.4</b>	<b>3.9</b>	<b>2.5</b>	<b>1.44</b>	<b>0.38</b>	<b>0.05</b>	<b>2.26</b>	<b>0.23</b>	<b>0.59</b>	<b>0.38</b>
<b>max</b>	<b>5.3</b>	<b>52.5</b>	<b>4.7</b>	<b>12.64</b>	<b>1.26</b>	<b>0.44</b>	<b>18.10</b>	<b>1.89</b>	<b>1.72</b>	<b>1.26</b>
<b>average</b>	<b>3.05</b>	<b>19.17</b>	<b>3.8</b>	<b>5.02</b>	<b>0.81</b>	<b>0.21</b>	<b>6.39</b>	<b>0.81</b>	<b>1.20</b>	<b>0.81</b>

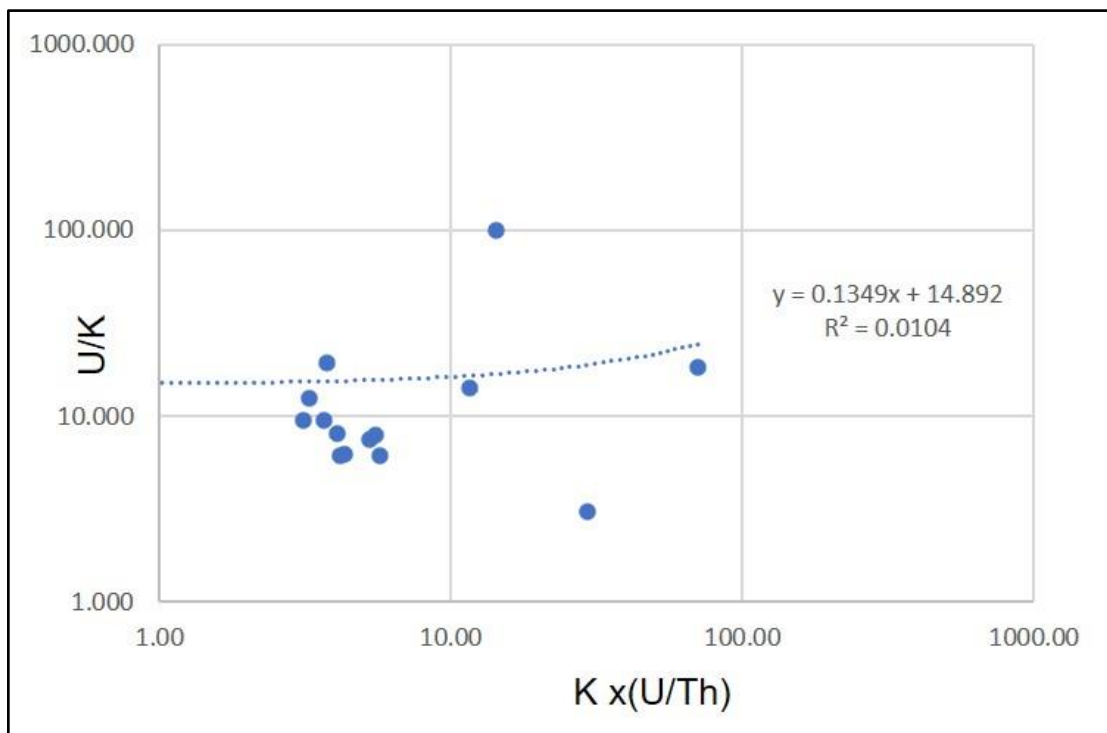


Figure 5.5  $K \times (U/Th)$  vs  $U/K$  plot for granites of study area

### **5.5 Classification of Govardhanagiri-L.Banda granitoids**

The granitoids of Govardhanagiri- L.Banda were classified on the basis of their Th and K contents, a classification scheme proposed by Galbraith and Saunders(1983). In the binary plot of Log Th vs %K (Figure 5.4), the granitoids of the study area falls in alkaline to calc-alkaline field and shows intermediate-acidic and hyperacidic nature. Most of the samples show Log Th values  $>1.5$  and  $K>3\%$ . This suggests that these granites are high potassic in composition. The Closepet Granite shows variation from intermediate to acidic nature with few on hyper acidic field signifying its variable composition from monzonite- quartz monzonite to granite.

### **5.6 Alteration**

The average radioelemental content of the magma increases as it undergoes differentiation. The Th/K, U/K and U/Th ratios also increase with differentiation (Darnley and Ford, 1989). These ratios are effective tools for demarcating zone of various alterations related to their later enrichment loci. As the radioelemental ratios has shown signatures of significant potassic enrichment of basement granite of Kappatralla outlier (Rajaraman et al., 2018) similar method is used here to find any such zones in the basement granite occurring in the study area. The Th/K ratio (Shives et al., 1997) and potassium alteration factor  $[Kx(U/Th)]$  (Gnojek and Prichystal, 1985) ratio can be effectively utilised to infer zones of potassium associated with alteration and anomalies (Figure 5.5). The Th/K ratio of granites of study area ranges from 1.44-12.64(avg.5.02) clearly indicate no signatures of potassic alteration as Th/K would be  $<3$  if the zone has any enrichment of K. Similarly, the  $Kx(U/Th)$  value of these granites ranges from 0.87-70.68(avg. 6.05) indicates no potassic alteration in majority of samples except one which shows very high  $Kx(U/Th)$  ratio. The restricted U/Th ratio 0.055-0.441(avg. 0.215) and

Th/U ratio 2.26-18.10(avg.6.39) of these granites indicate preponderance of thorium over uranium. This may be due to the remobilization of uranium from the system by later process.

### 5.7 Uranium enrichment/depletion and migration

The process of uranium migration can be quantified from calculated values of  $U_o$  and  $U_m$  from the existing U value ( $U_p$ ), Th value ( $Th_p$ ) in ppm and regional U/Th ratio( $(U/Th)_r$ )(average regional ratio in the geological domain(0.3 for the studied area)(Ali et al., 2002).

The  $U_o$  is obtained as  $U_o = Th_p \times (U/Th)_r$  and  $U_m$  as  $U_m = U_o - U_p$ . From this value rate of uranium migration  $U_{mr}$  is calculated as  $U_{mr} = (U_m/U_p) \times 100$ . The +ve  $U_{mr}$  value indicate inward migration of uranium while the -ve  $U_{mr}$  indicate outward migration of U from the system. The  $U_{mr}$  of the granites of the study area shows outward migration of U from the system (Table 5.4). The negative values of  $U_{mr}$  suggest remobilization of uranium by surficial processes.

Table 5.4 Uranium migration studies of granites of study area

Sample Id	$U_o$	$U_m$	$U_{mr}\%$
LNJB-1/Gr	9.9	-23.1	-70
LNJB-2/Gr	0.75	-56.25	-98.68
LNJB/Gr/4	15.9	-46.1	-74.35
GVD/Gr/1	15	-27	-64.28
GVD/Gr/2	8.4	-26.6	-76
LNJB/Gr/1	0.75	-14.25	-95
LNJB/Gr/2	0.75	-7.25	-90.62
LNJB/Gr/3	0.75	-59.25	-98.75
LNJV/Gr/1	4.5	-45.5	-91
LNJB/GRP/1	10.5	-24.5	-70
LNJB/UC/1	10.2	-12.8	-55.65
GVD/2	6.9	-18.1	-72.4
GVD/3	6.6	-23.4	-78
CKP/GR/2	7.8	-24.2	-75.62
CKP/GR/1	13.2	-22.8	-63.33
<b>Min</b>	<b>0.75</b>	<b>-59.25</b>	<b>-98.75</b>
<b>Max</b>	<b>15.9</b>	<b>-7.25</b>	<b>-55.65</b>
<b>Average</b>	<b>7.46</b>	<b>-28.74</b>	<b>-78.24</b>

## CHAPTER 6

### SEDIMENTOLOGICAL STUDIES

#### **6.1 Paleohydraulic reconstruction using cross-bed set thickness**

Paleohydraulics concerns with the study of quantitative relationship between hydraulic parameters of rivers (depth, width, slope, discharge, sediment type, etc.) and preserved deposit of river system. Established formulae for such reconstruction are built up from observations in modern systems (Allen, 1968; Leclair and Bridge, 2001; Ito et al., 2006) and extended in ancient river systems (Vander Neut and Eriksson, 1999; Eriksson et al., 2006, 2008; Sarkar et al., 2012). In stratigraphic record, characteristic of any ancient river system can be reconstructed from width and depth of preserved channel forms or in their absence from the decompacted thickness of preserved macroforms e.g. mid-channel bar, point bar etc. However, incomplete preservation of macroforms in rock record and rare availability of lenticular, concave-up channel geometry in vegetation-free, soil-poor Precambrian systems often do not allow direct measurements of channel depth or width in field and therefore indirect method needs to be applied. Data commonly collected from stratigraphic sections for use of such indirect methodologies are based largely on sandstone grain-size analysis, clast sizes in channel conglomerates or set thickness of in-channel dune bedforms. Despite unavoidable errors (often as high as 50%; Eriksson et al., 2006) associated with such estimations, researchers (Miall, 1976; Eriksson et al., 2008) have unanimously agreed upon using the estimations done in ancient fluvial systems, especially when used on a comparative basis. We relied on field measurements of cross-bedding set thickness for undertaking palaeohydraulic estimations (cf. Sarkar et al., 2012). Measurements were carried out separately for the fluvial systems present in Gulcheru formation exposed in Lanjabanda area, Kurnool district, A.P. Original stratal thickness data was collected taking into account a 10% compaction factor (Lorenz et al., 1985). A total of 50 readings were collected from Gulcheru Quartzite exposed in Lanjabanda area.

The following sets of formulae were used to estimate the parameters:

Estimation from cross-bed set thickness:

The mean water depth is calculated by:

$$h = 0.086(dm)^{1.19} \quad (1)$$

where,  $h$  is the mean set thickness of cross-beds in metres (Allen,1968).

The ratio between channel width and channel depth is given by:

$$F = 225M^{-1.08} \quad (2)$$

Where  $F$  is the ratio between channel width and depth,  $M$  and is the sediment load variable, *i.e.* the percentage of silt and clay in the channel margins, which can be assumed to be a constant of 5% for coarse bedload channels (cf. Schumm, 1968; Van der Neut and Eriksson, 1999), as also inferred in case of Par fluvial system. This gives a fixed channel width to depth ratio *i.e.*  $F=40$ .

The estimation of the width of channel,  $w$ , is given by:

$$w = F dm \quad (3)$$

(Schumm, 1968)

Average daily discharge (also called the mean annual discharge by some workers) is estimated by

$$Q_m = vA \quad (4)$$

$Q_m$  is average daily discharge, measured in  $m^3s^{-1}$ , and  $A$  is the mean cross-sectional surface area (approximated by  $dm \times w$ ) in  $m^2$ ;  $v$  is the velocity of water in  $ms^{-1}$ , and range between 0.5 and 1  $ms^{-1}$  in conditions where large subaqueous dune bedforms migrate (*i.e.* when cross-bedding is formed) (Leopold et al., 1964). For the purposes of present study, an intermediate velocity of 0.75  $ms^{-1}$  is assumed (cf. Eriksson et al., 2006).

On getting  $Q_m$ , mean bankfull channel depth is estimated by using the equation:

$$d_b = 0.6M^{0.34}Q_m^{0.29} \quad (5)$$

(where  $d_b$  is mean bankfull channel depth in meter) (Schumm, 1969). Using  $d_b$ , bankfull channel width is calculated by:

$$w_b = 8.9d_b^{1.40} \quad (6)$$

(where  $w_b$  is the bankfull channel width in meter) (Leeder, 1973).

This allows for a recalculation of  $Q_m$  (average daily discharge) and making comparison of results with those obtained from equation 5, with the help of following equation:

$$Q_m = 0.027w_b^{1.71} \quad (7)$$

(Osterkamp and Hedman, 1982)

Using  $Q_m$  value palaeoslope (S) is estimated by the equations:

$$S = 60M^{-0.38}Q_m^{-0.32} \quad (8)$$

(Schumm, 1968) and by

$$S = 30 (F^{0.95} / w^{0.98}) \quad (9)$$

(Schumm, 1972)

Assuming that  $Q_m$  is estimated only from equation 7 (which is likely to be more accurate than that derived from equation 4), two estimates of palaeoslope can be obtained from equations 8 and 9, and an approximate range of palaeoslope can be derived. Using the two values of palaeoslope from equations 8 and 9, two estimations of bankfull water discharge ( $Q_b$ ) can be done:

$$Q_b = 4.0A_b^{1.21}S^{0.28} \quad (10)$$

(where  $A_b = d_b \times w_b$ ) (Williams, 1978).

Also, the drainage (catchment) area ( $A_d$  in  $\text{km}^2$ ) of a river system and principle stream length (L in km, from source to depositional site) can be approximated by:

$$Q_b = A_d^{0.75} \quad (11)$$

$$L = 1.4A_d^{0.6} \quad (12)$$

(Leopold *et al.*, 1964).

Substituting the two different values of  $Q_b$  from equation 10 into equations 11 and 12 ( $A$  encompasses  $Q_b$ ) two separate values for drainage area and stream length can be calculated (Eriksson *et al.*, 2006).

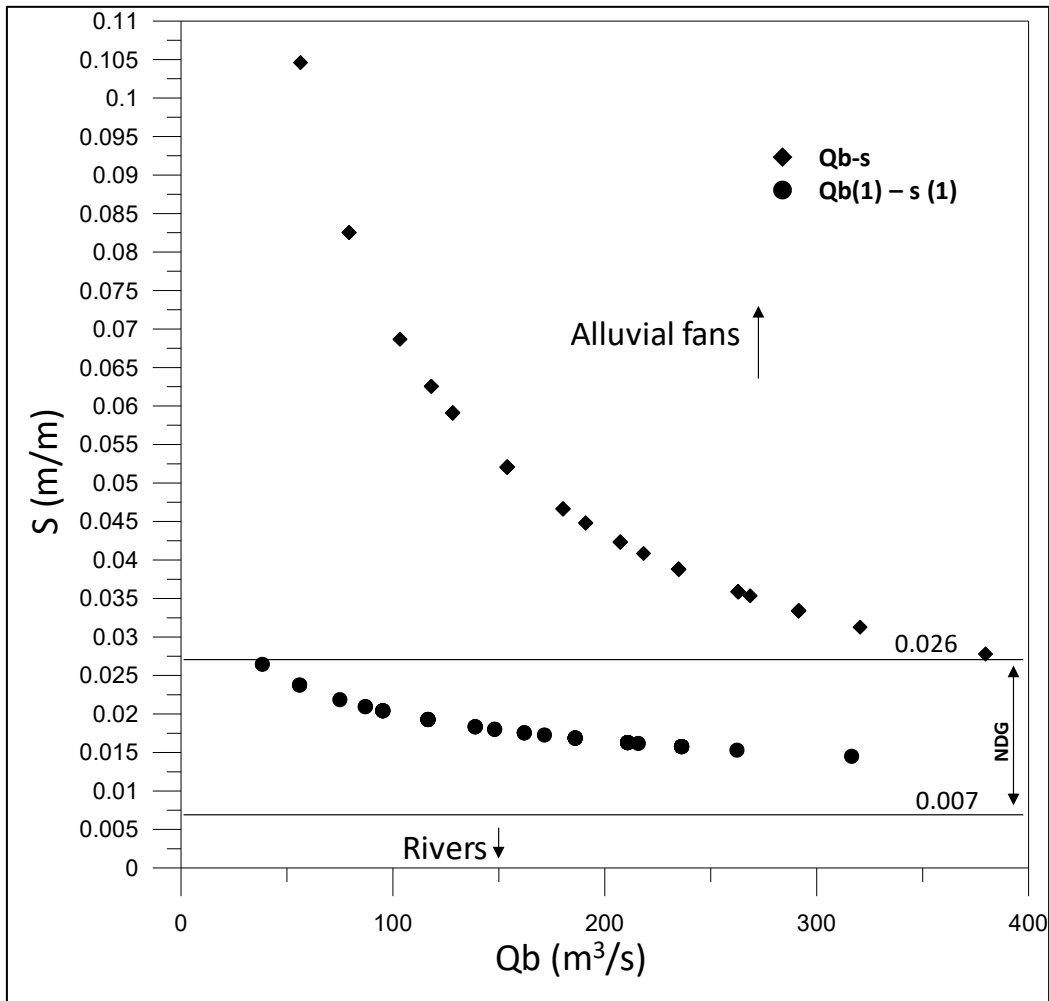


Figure 6.1 Binary plot paleoslope ( $S$ ) and mean annual bankful discharge values ( $q_b$ ) calculated for the Lanjabanda section. The two values of  $S$  (Eq. (8) and Eq. (9) ( $S_1$ )) enables two estimations of  $Q_b$ . Maximum gradient for rivers (0.007 m/m) and minimum gradient for the alluvial fan (0.026 m/m) are shown after Blair and MacPherson (1994). Note paleoslope values from the Lanjabanda section dominantly fall within natural depositional gap (NDG).

Table 6.1 Palaeohydraulic data estimated for the Gulcheru Formation based on set thickness of trough cross-beds, Lanjabanda area

S.No.	h(m)	dm(m)	W(m)	Qm(m <sup>3</sup> /s)	db(m)	Wb(m)	Qm <sub>1</sub> (m <sup>3</sup> /s)	S(m/m)	S <sub>1</sub> (m/m)	Qb(m <sup>3</sup> /s)	Ab(m <sup>2</sup> )	Qb <sub>1</sub> (m <sup>3</sup> /s)	Ad(m <sup>2</sup> )	Ad <sub>1</sub> (m <sup>2</sup> )	L(km)	L <sub>1</sub> (km)
1	0.061	0.744	29.765	16.612	2.343	29.309	8.708	0.016	0.036	210.757	68.662	262.934	1254.230	1684.464	101.194	120.783
2	0.039	0.509	20.359	7.771	1.880	21.531	5.139	0.019	0.052	116.539	40.467	153.913	569.238	824.834	62.995	78.695
3	0.033	0.447	17.885	5.998	1.743	19.381	4.293	0.020	0.059	95.217	33.790	128.220	434.795	646.559	53.592	67.997
4	0.050	0.629	25.146	11.856	2.124	25.558	6.890	0.018	0.042	162.010	54.297	207.296	883.195	1226.837	81.990	99.862
5	0.017	0.250	9.989	1.871	1.244	12.077	1.912	0.026	0.105	38.380	15.020	56.402	129.463	216.301	25.907	35.250
6	0.066	0.801	32.023	19.227	2.444	31.102	9.639	0.016	0.033	236.221	76.019	291.486	1460.239	1932.670	110.862	131.166
7	0.044	0.569	22.776	9.727	2.006	23.585	6.006	0.018	0.047	138.832	47.308	180.295	718.873	1018.542	72.464	89.313
8	0.031	0.422	16.878	5.341	1.686	18.490	3.961	0.021	0.063	86.983	31.170	118.156	385.403	579.794	49.851	63.693
9	0.046	0.593	23.730	10.558	2.054	24.383	6.357	0.018	0.045	148.001	50.087	191.025	782.865	1100.152	76.268	93.540
10	0.044	0.569	22.776	9.727	2.006	23.585	6.006	0.018	0.047	138.832	47.308	180.295	718.873	1018.542	72.464	89.313
11	0.033	0.447	17.885	5.998	1.743	19.381	4.293	0.020	0.059	95.217	33.790	128.220	434.795	646.559	53.592	67.997
12	0.039	0.509	20.359	7.771	1.880	21.531	5.139	0.019	0.052	116.539	40.467	153.913	569.238	824.834	62.995	78.695
13	0.033	0.447	17.885	5.998	1.743	19.381	4.293	0.020	0.059	95.217	33.790	128.220	434.795	646.559	53.592	67.997
14	0.046	0.593	23.730	10.558	2.054	24.383	6.357	0.018	0.045	148.001	50.087	191.025	782.865	1100.152	76.268	93.540
15	0.061	0.744	29.765	16.612	2.343	29.309	8.708	0.016	0.036	210.757	68.662	262.934	1254.230	1684.464	101.194	120.783
16	0.028	0.384	15.345	4.415	1.595	17.114	3.470	0.022	0.069	74.975	27.300	103.310	316.149	484.755	44.265	57.206
17	0.033	0.447	17.885	5.998	1.743	19.381	4.293	0.020	0.059	95.217	33.790	128.220	434.795	646.559	53.592	67.997
18	0.022	0.318	12.721	3.034	1.431	14.697	2.675	0.024	0.083	55.961	21.029	79.309	214.049	340.745	35.030	46.300
19	0.055	0.687	27.474	14.153	2.236	27.463	7.792	0.017	0.039	186.005	61.418	234.857	1061.772	1449.012	91.569	110.350
20	0.061	0.744	29.765	16.612	2.343	29.309	8.708	0.016	0.036	210.757	68.662	262.934	1254.230	1684.464	101.194	120.783
21	0.066	0.801	32.023	19.227	2.444	31.102	9.639	0.016	0.033	236.221	76.019	291.486	1460.239	1932.670	110.862	131.166
22	0.022	0.318	12.721	3.034	1.431	14.697	2.675	0.024	0.083	55.961	21.029	79.309	214.049	340.745	35.030	46.300
23	0.055	0.687	27.474	14.153	2.236	27.463	7.792	0.017	0.039	186.005	61.418	234.857	1061.772	1449.012	91.569	110.350
24	0.039	0.509	20.359	7.771	1.880	21.531	5.139	0.019	0.052	116.539	40.467	153.913	569.238	824.834	62.995	78.695
25	0.055	0.687	27.474	14.153	2.236	27.463	7.792	0.017	0.039	186.005	61.418	234.857	1061.772	1449.012	91.569	110.350
26	0.066	0.801	32.023	19.227	2.444	31.102	9.639	0.016	0.033	236.221	76.019	291.486	1460.239	1932.670	110.862	131.166
27	0.066	0.801	32.023	19.227	2.444	31.102	9.639	0.016	0.033	236.221	76.019	291.486	1460.239	1932.670	110.862	131.166
28	0.061	0.744	29.765	16.612	2.343	29.309	8.708	0.016	0.036	210.757	68.662	262.934	1254.230	1684.464	101.194	120.783

29	0.039	0.509	20.359	7.771	1.880	21.531	5.139	0.019	0.052	116.539	40.467	153.913	569.238	824.834	62.995	78.695
30	0.061	0.744	29.765	16.612	2.343	29.309	8.708	0.016	0.036	210.757	68.662	262.934	1254.230	1684.464	101.194	120.783
31	0.066	0.801	32.023	19.227	2.444	31.102	9.639	0.016	0.033	236.221	76.019	291.486	1460.239	1932.670	110.862	131.166
32	0.072	0.856	34.251	21.996	2.541	32.848	10.582	0.015	0.031	262.353	83.480	320.483	1679.504	2193.173	120.569	141.505
33	0.055	0.687	27.474	14.153	2.236	27.463	7.792	0.017	0.039	186.005	61.418	234.857	1061.772	1449.012	91.569	110.350
34	0.083	0.966	38.627	27.977	2.725	36.217	12.505	0.015	0.028	316.484	98.692	379.698	2156.766	2749.481	140.091	162.061
35	0.039	0.509	20.359	7.771	1.880	21.531	5.139	0.019	0.052	116.539	40.467	153.913	569.238	824.834	62.995	78.695
36	0.044	0.569	22.776	9.727	2.006	23.585	6.006	0.018	0.047	138.832	47.308	180.295	718.873	1018.542	72.464	89.313
37	0.055	0.687	27.474	14.153	2.236	27.463	7.792	0.017	0.039	186.005	61.418	234.857	1061.772	1449.012	91.569	110.350
38	0.039	0.509	20.359	7.771	1.880	21.531	5.139	0.019	0.052	116.539	40.467	153.913	569.238	824.834	62.995	78.695
39	0.050	0.629	25.146	11.856	2.124	25.558	6.890	0.018	0.042	162.010	54.297	207.296	883.195	1226.837	81.990	99.862
40	0.055	0.687	27.474	14.153	2.236	27.463	7.792	0.017	0.039	186.005	61.418	234.857	1061.772	1449.012	91.569	110.350
41	0.061	0.744	29.765	16.612	2.343	29.309	8.708	0.016	0.036	210.757	68.662	262.934	1254.230	1684.464	101.194	120.783
42	0.066	0.801	32.023	19.227	2.444	31.102	9.639	0.016	0.033	236.221	76.019	291.486	1460.239	1932.670	110.862	131.166
43	0.061	0.744	29.765	16.612	2.343	29.309	8.708	0.016	0.036	210.757	68.662	262.934	1254.230	1684.464	101.194	120.783
44	0.050	0.629	25.146	11.856	2.124	25.558	6.890	0.018	0.042	162.010	54.297	207.296	883.195	1226.837	81.990	99.862
45	0.031	0.422	16.878	5.341	1.686	18.490	3.961	0.021	0.063	86.983	31.170	118.156	385.403	579.794	49.851	63.693
46	0.033	0.447	17.885	5.998	1.743	19.381	4.293	0.020	0.059	95.217	33.790	128.220	434.795	646.559	53.592	67.997
47	0.062	0.755	30.219	17.122	2.363	29.671	8.893	0.016	0.035	215.795	70.125	268.607	1294.358	1733.100	103.124	122.863
48	0.052	0.652	26.082	12.755	2.170	26.328	7.249	0.017	0.041	171.513	57.130	218.256	952.937	1314.077	85.816	104.064
49	0.066	0.801	32.023	19.227	2.444	31.102	9.639	0.016	0.033	236.221	76.019	291.486	1460.239	1932.670	110.862	131.166
50	0.039	0.509	20.359	7.771	1.880	21.531	5.139	0.019	0.052	116.539	40.467	153.913	569.238	824.834	62.995	78.695
Average	<b>0.049</b>	<b>0.621</b>	<b>24.845</b>	<b>12.179</b>	<b>2.083</b>	<b>25.042</b>	<b>6.838</b>	<b>0.018</b>	<b>0.047</b>	<b>162.013</b>	<b>53.893</b>	<b>205.902</b>	<b>912.612</b>	<b>1249.781</b>	<b>80.963</b>	<b>98.283</b>

## Results of palaeohydraulic estimation

Estimated hydraulic parameters for the Gulcheru formation (Lanjabannda section) are presented in Table 6.1. Binary plots involving bankfull water discharge (for the two values of  $Q_b$  in  $m^3/s$ ) and palaeoslope (for the two values of  $S$  in  $m/m$ ) the bankfull river discharge varies between 38.380 and 379.698  $m^3/s$ , whereas, slope values range between 0.015 and 0.105  $m/m$ . It is worth noticing that the values are consistently higher than the 0.007 $m/m$ , earmarked for the modern braided river system (Figure 6.1). In the backdrop of maximum gradient of rivers (0.007  $m/m$ ) and minimum gradient for alluvial fans (0.026  $m/m$ ), following Blair and McPherson (1994), it is noteworthy that despite variations in palaeoslope values obtained by the use of Eqs. (8) and (9), none of the values, irrespective of the equation used, fall below the gradient of 0.007  $m/m$ . When plotted by equation 9 all plots fall in alluvial fan field but when derived with the use of Eq. (8) except of one or two values those fall above the slope value of 0.026  $m/m$  within the alluvial fan field, most of the values fall within the ‘natural depositional gap’, demarcated by Blair and McPherson (1994) from their studies in modern rivers and alluvial fans.

Hydraulic studies carried out on paleoproterozoic to Neoproterozoic fluvial deposits however shows remarkable consistency in estimated value/s irrespective of measured section viz. Wilgerivier Formation (van der Nuet and Eriksson, 1999) Heddersvatnet Formation (Koykka, 2011a), Svinsaga Formation (Koykka, 2011b), Sonia Sandstone Formation (Sarkar, et al., 2012) and Ramdurg Formation, Muchkundi quartzite Member, Cave temple arenite Member, Rewa Formation (Mukhopaddhay et al., 2014). Although it is appreciated by workers that the values obtained through such palaeohydraulic analyses should not be considered as absolute, yet it is believed that similar results obtained by researchers from different Palaeo- and Meso-proterozoic successions (2–1.9 Ga Waterberg Group, South Africa; Van derNuet and Eriksson, 1999; Eriksson et al., 2006, 2008; and many others) cannot be a coincidence and hence, interpreted as a signature for comparatively high-gradient for braided fluvial systems, unique for the Proterozoic time period. The present data from

the Gulcheru formation (Lanjabanda section) match well with paleohydraulic data generated from Proterozoic river systems in other parts of the World and in the process strengthen the view that Proterozoic river systems, in general, had steep channel gradients, higher than the upper limit of modern river systems. The present values thus reiterate the view of several Precambrian sedimentologists that the segmentation of alluvial fan and river field as is done by Blair and McPherson does not hold good in Precambrian system when Earth was without any land plant and atmosphere was dominated by Greenhouse gases. Possibly the topographic condition and aggressive weathering regime were deterrent for segmental behavior of alluvial fan and river system.

## **6.2 Pebble morphometric studies**

### **Introduction**

Pebble morphometry is an empirical approach where the sedimentary environment of the processes modifying the pebble shape is believed to be known. Morphometric studies have been used for palaeoenvironmental reconstruction (Okon et al. 2018). They have also been successfully utilized to discriminate between beach and river gravels (Stratten 1974). The basic assumption in these studies is that each sediment is a response to a definite set of environmental conditions and that the properties of the sediments reflect these conditions which are used to reconstruct their environment of deposition.

The fundamental properties of sedimentary particles are size, shape, roundness, mineralogical composition, surface texture and orientation. Of these shape and roundness are most important. Shape is determined from the long, intermediate and short diameters of the particles and roundness is measured by rapid visual estimation. Shape and roundness behave differently during abrasion and selective transport and are important in evaluating the effects of these processes during the formation of the deposit.

The sedimentary history and the hydrodynamic context can be derived from the shape of particles. Particle shape will depend on many factors: particle size, mode and duration of transport, energy of the transporting medium, and nature and extent of post-depositional weathering, history of sediment transport, and deposition (Bluck 1967).

### **Methodology for sampling and measurement**

A total of sixty pebbles were collected from Gulcheru Formation of same composition (Quartz Clast) from Lanjabanda area (Figure 6.2a). Pebbles were selected according to their perfection, while broken pebbles were eliminated. The collected pebbles were washed and numbered serially. The three perpendicular axes i.e. the long (L), intermediate (I) and short (S) axes were measured with the help of Vernier caliper (Figure 6.3). Three-dimensional analyses of individual irregularly shaped particles generally involve measuring the principal axes of a triaxial ellipsoid to approximate particle shape the longest axis (L) is presented by (a), intermediate axis (I) presented by (b), and shortest axis(S) presented by (c). The elongation ratio, flatness index, maximum projection sphericity and oblate-prolate index were calculated to decipher the depositional environment (Table 6.2).

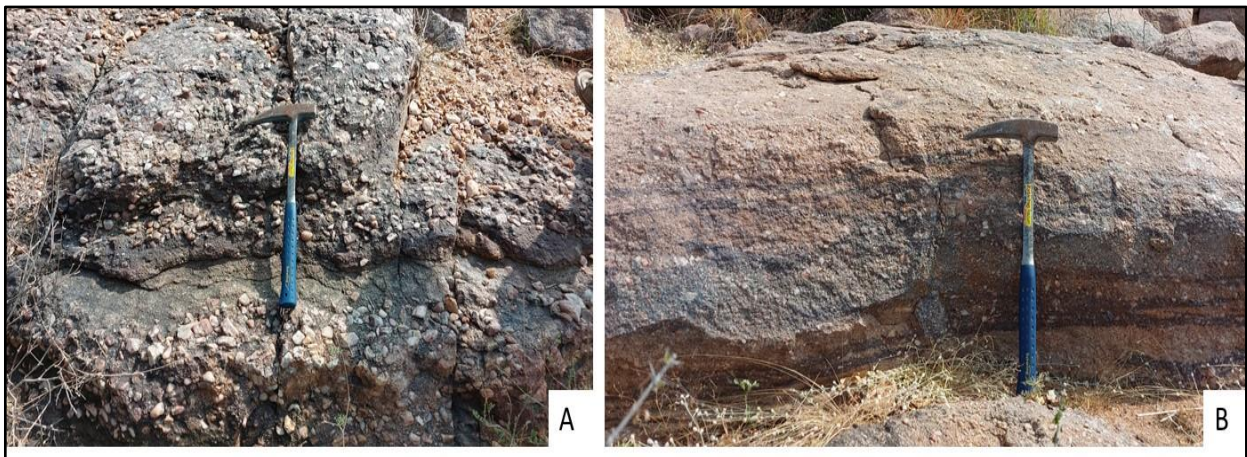


Figure 6.2 a) Fractured oligomictic Gulcheru conglomerate, Lanjabanda area b) Trough cross-stratified quartzite

Table 6.2 Morphometric indices with their formulae used during calculations

Morphometric indices	Formulae	Reference
Flatness index	$(S/L) * 100$	Luttig 1962
Elongation ratio	$I/L$	Luttig 1962
Maximum projection sphericity index	$(S^2/LI)^{1/3}$	Sneed and Folk 1958
Oblate-prolate index	$10[(L-I)/(L-S)-0.5]/(S/L)$	Dobkins and Folk 1970
Roundness	Visual estimation	Sames 1966

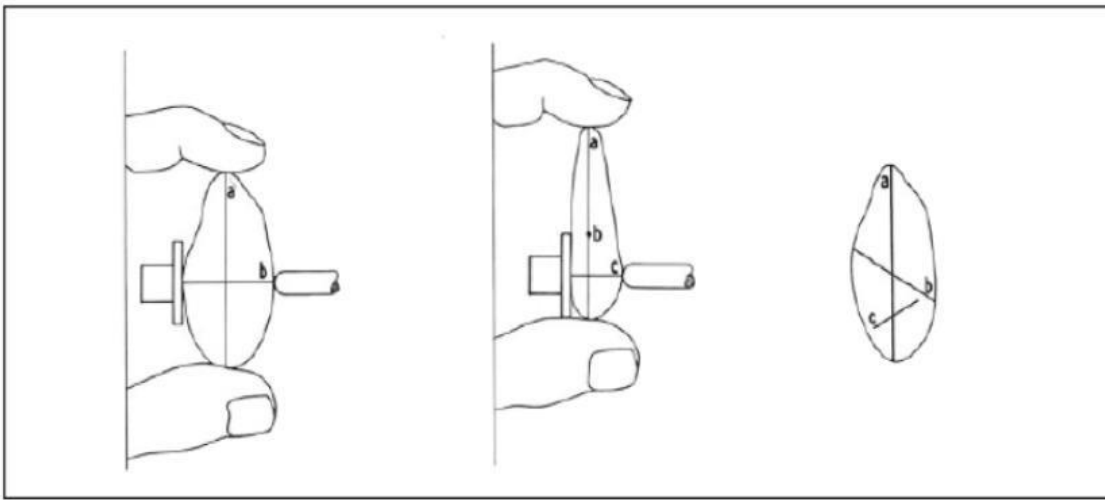


Figure 6.3 Concept and measurement of pebble diameter (adapted from Krumbein 1941).  
 Left: b-axis in position, center: c-axis in position, right: pebble in perspective.

Table 6.3 Morphometric indices of Gulcheru sediments from study area

Pebble no.	L(mm)	I(mm)	S(mm)	Mean size	Flatness (S/L)	Elongation (I/L)	Flatness index	MPSI	OP index
1	59.2	47.5	43.7	50.13	0.74	0.80	73.82	0.88	3.45
2	41.5	33.5	27	34.00	0.65	0.81	65.06	0.81	0.80
3	58.4	26	24.4	36.27	0.42	0.45	41.78	0.73	10.84
4	40	32.5	24	32.17	0.60	0.81	60.00	0.76	-0.52
5	44	31.5	26.5	34.00	0.60	0.72	60.23	0.80	3.56
6	27	24.6	20	23.87	0.74	0.91	74.07	0.84	-2.12
7	44.8	34	31.5	36.77	0.70	0.76	70.31	0.87	4.44
8	67	35	25.5	42.50	0.38	0.52	38.06	0.65	7.12
9	37.5	24.2	23.9	28.53	0.64	0.65	63.73	0.86	7.50
10	62.5	35.5	26.5	41.50	0.42	0.57	42.40	0.68	5.90
11	45	35.5	23.5	34.67	0.52	0.79	52.22	0.70	-1.11
12	34	33.5	28.7	32.07	0.84	0.99	84.41	0.90	-4.81
13	40	33.5	21.9	31.80	0.55	0.84	54.75	0.71	-2.57
14	62	44.3	28	44.77	0.45	0.71	45.16	0.66	0.46
15	52.3	39	31	40.77	0.59	0.75	59.27	0.78	2.10
16	62.5	35.1	28	41.87	0.45	0.56	44.80	0.71	6.57
17	57.5	43.5	35	45.33	0.61	0.76	60.87	0.79	2.01
18	70	61.5	41.5	57.67	0.59	0.88	59.29	0.74	-3.40
19	46.5	32.5	25	34.67	0.54	0.70	53.76	0.75	2.81
20	72	49	35.5	52.17	0.49	0.68	49.31	0.71	2.64
21	43.9	32.5	28.5	34.97	0.65	0.74	64.92	0.83	3.70
22	41.4	40	22	34.47	0.53	0.97	53.14	0.66	-8.05
23	47	39	23.5	36.50	0.50	0.83	50.00	0.67	-3.19
24	59.5	38.5	21.5	39.83	0.36	0.65	36.13	0.59	1.46
25	35	31.5	27.3	31.27	0.78	0.90	78.00	0.88	-0.58
26	61.1	51.5	31	47.87	0.51	0.84	50.74	0.67	-3.57
27	65.5	46.5	32.1	48.03	0.49	0.71	49.01	0.70	1.41
28	44.5	41.5	32.3	39.43	0.73	0.93	72.58	0.83	-3.50
29	48	47	22	39.00	0.46	0.98	45.83	0.60	-10.07
30	81.3	45.5	29.5	52.10	0.36	0.56	36.29	0.62	5.27
31	57.5	37.5	37	44.00	0.64	0.65	64.35	0.86	7.39
32	66.5	45	21.4	44.30	0.32	0.68	32.18	0.53	-0.72
33	52.5	33.3	28.5	38.10	0.54	0.63	54.29	0.77	5.53
34	43.5	37.5	24.5	35.17	0.56	0.86	56.32	0.72	-3.27
35	57.5	35.6	25	39.37	0.43	0.62	43.48	0.67	4.00
36	51.6	44	21.8	39.13	0.42	0.85	42.25	0.59	-5.80
37	54.1	33	28	38.37	0.52	0.61	51.76	0.76	5.96
38	47	41.5	29.5	39.33	0.63	0.88	62.77	0.76	-2.96
39	42	38	21.5	33.83	0.51	0.90	51.19	0.66	-5.96
40	42.3	33.5	28	34.60	0.66	0.79	66.19	0.82	1.74
41	43	39	28	36.67	0.65	0.91	65.12	0.78	-3.58
42	44	29	27	33.33	0.61	0.66	61.36	0.83	6.23

43	55.5	36	22.5	38.00	0.41	0.65	40.54	0.63	2.24
44	47.5	40	23	36.83	0.48	0.84	48.42	0.65	-4.00
45	43.2	31.5	21.1	31.93	0.49	0.73	48.84	0.69	0.60
46	41.9	41	25.5	36.13	0.61	0.98	60.86	0.72	-7.31
47	36.5	29.4	25	30.30	0.68	0.81	68.49	0.84	1.71
48	33.3	29.4	22.2	28.30	0.67	0.88	66.67	0.80	-2.23
49	37.4	31.4	22.5	30.43	0.60	0.84	60.16	0.76	-1.62
50	42	38.5	26.6	35.70	0.63	0.92	63.33	0.76	-4.31
51	57.3	27.7	19.6	34.87	0.34	0.48	34.21	0.62	8.34
52	49.7	31.1	26.4	35.73	0.53	0.63	53.12	0.77	5.62
53	45	37	21.4	34.47	0.48	0.82	47.56	0.65	-3.39
54	46	37.4	23	35.47	0.50	0.81	50.00	0.67	-2.52
55	44.5	36.4	21	33.97	0.47	0.82	47.19	0.65	-3.29
56	37.5	36.4	24.1	32.67	0.64	0.97	64.27	0.75	-6.50
57	39.5	31	20	30.17	0.51	0.78	50.63	0.69	-1.27
58	38.3	31	22.3	30.53	0.58	0.81	58.22	0.75	-0.75
59	48.5	37	20	35.17	0.41	0.76	41.24	0.61	-2.34
60	40	36	23	33.00	0.58	0.90	57.50	0.72	-4.60
<b>Min</b>	27	24.2	19.6	23.87	0.32	0.45	32.18	0.53	-10.07
<b>Max</b>	81.3	61.5	43.7	57.67	0.84	0.99	84.41	0.90	10.84
<b>Average</b>	48.93	36.84	26.17	37.31	0.55	0.77	55.04	0.73	0.19

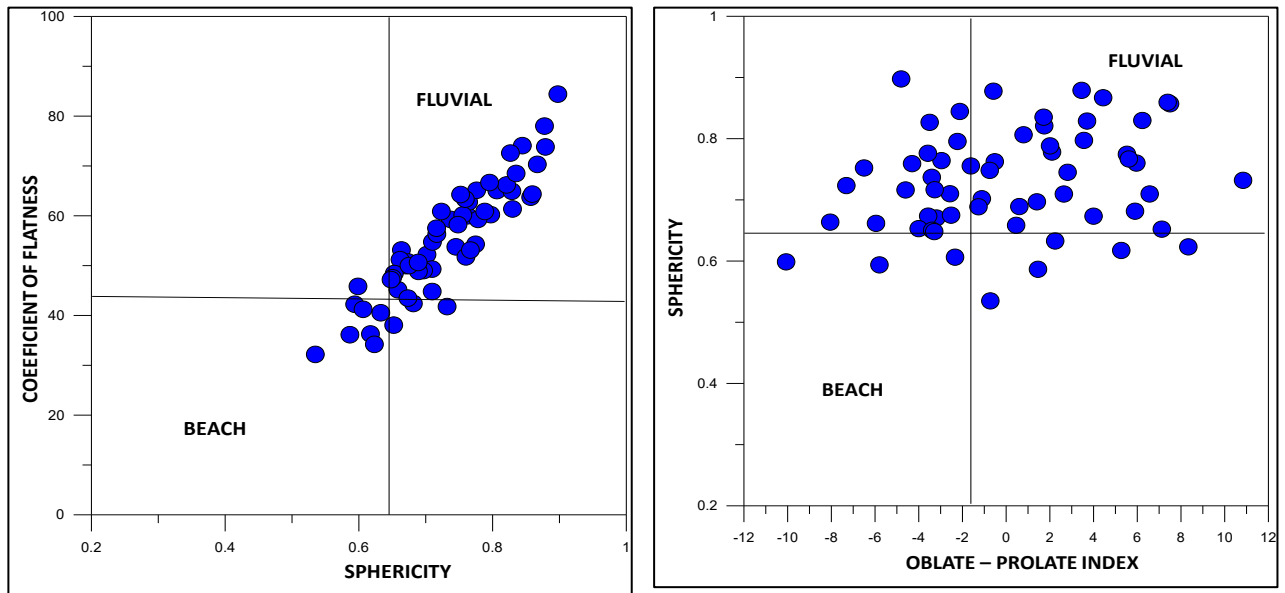


Figure 6.4 a) Coefficient of Flatness vs. Sphericity plot b) Sphericity vs. Oblate-Prolate Index

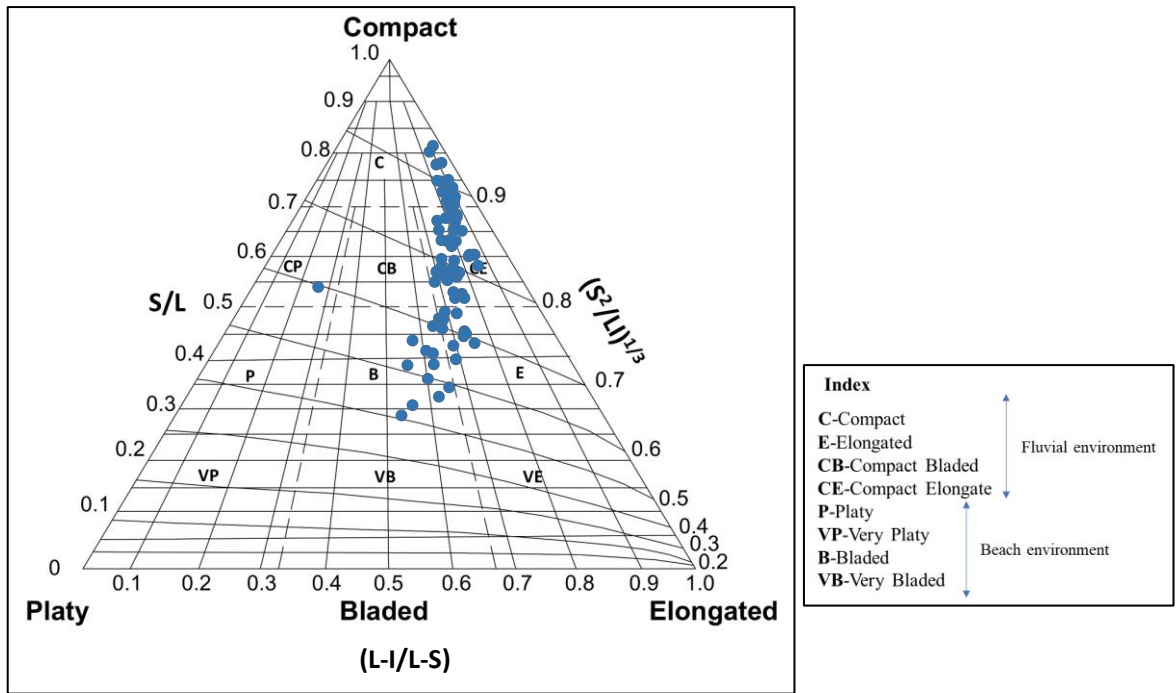


Figure 6.5 Classification of pebble shapes (after Sneed and Folk, 1958).

Table 6.4 Summary of pebble morphometric analysis

Morphometric indices	Range	Average	Environment indications
Length(l)mm	27-81.3	48.93	Fluvial
Width(I)mm	24.2-61.5	36.83	Fluvial
Thickness(S)mm	19.6-43.7	26.17	Fluvial
Mean size	23.87-57.67	37.31	Fluvial
Elongation ratio	0.445-0.985	0.770	0.60 to 0.90 Fluvial
Flatness ratio	0.322-0.844	0.550	>0.45 Fluvial, <0.45 Beach
Maximum projection Sphericity	0.535-0.897	0.731	>0.65 Fluvial, <0.45 Beach
OP index	-10.07-10.84	0.19	>-1.5 Fluvial, <-1.5 Beach
Plot of flatness ratio (FR) versus maximum projection sphericity	83% fluvial and 17% beach		Fluvial
Plot of MPS against OP	67% fluvial and 33% beach		Fluvial
Dominant pebble forms	Compact bladed to compact elongated		Fluvial

## Results and Discussion

In pebble morphometric interpretation, the dominant indices were obtained from the available data. The values of these indices such as elongation ratio, flatness index, maximum projection sphericity and oblate-prolate index ranges from Gulcheru Formation is 0.445 to 0.985, 32.2 to 84.4, 0.535 to 0.897, -10.07 to 10.84 respectively (Table 6.4).

According to Hubert (1968), the elongation ratio values for the fluvial environment ranges from 0.6 to 0.9. About 83 % of the pebbles are falling in fluvial condition from Govardhanagiri-L.Banda area. According to Stratten (1974), the flatness index values for fluvial environment in  $>45$  where as for the beach environment the values is  $<45$ . 83% flatness index values are coming in fluvial environment from Lanjabanda area.

Maximum projection sphericity of pebbles is generally higher for fluvial environment (river) than for beaches (Dobkins and Folk, 1970; Hubert, 1968). An imaginary line distinguishes pebble shape produced by surf processes from those produced by fluvial transport. The range of the value of the magic line is from 0.65 to 0.66 (Dobkins and Folk, 1970). Pebbles whose value fall above 0.65 indicate river environment and whose values fall below 0.65 denote beach environment (Inyang, 2001). From the results of maximum projection sphericity 80% values fall above 0.65. An O.P. Index value  $> -1.5$  generally signifies fluvial conditions and it constitutes 80% of the total value.

The bivariate scatter plot between sphericity against oblate- prolate index and coefficient of flatness against sphericity shows that 80% pebble plots are within fluvial environment (Figure 6.4).

Sneed and Folk (1958) used two somewhat different shape indices to construct a triangular diagram (Figure. 6.5), in which  $D_s/D_L$  is plotted against  $D_L-D_I/D_L-D_S$  to create ten form

fields (e.g. compact, C; platy, P; bladed, B; elongate, E). Lines of maximum projection sphericity drawn across the field again illustrate the disparity between mathematical sphericity and actual form. According to Sneed and Folk (1958), Dobkins and Folk (1970) and Gale (1990), Compact (C), Elongation (E), Compact Bladed (CB) and Compact Elongate (CE) are most favoured by fluvial action whereas Platy (P), Very Platy, Bladed (B) and Very Bladed (VB) are indicative of beach setting. The 80% pebbles favourable for fluvial environment respectively.

The integration of pebble morphometric parameters and bivariate plots are good indicator in distinguishing paleo-depositional environment. The quartzite proves to be deposited in strongly fluvial conditions.

## CHAPTER 7

### PETROGRAPHY

#### 7.1 Petrographic studies

##### Introduction

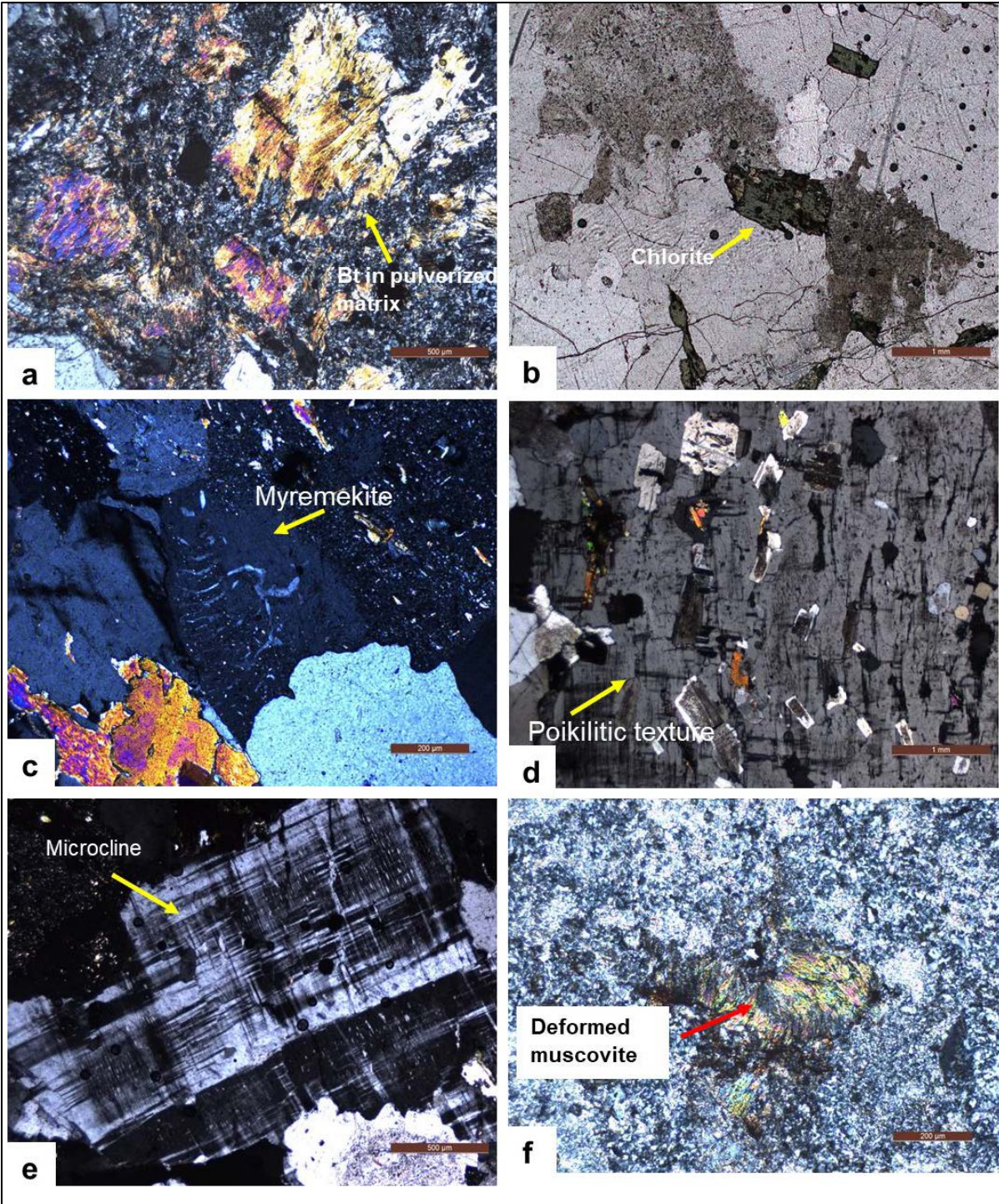
In the present work detailed petrographic, and ore microscopic studies have been carried out. 46 fresh representative rock samples have been collected from the study area. After performing chromogram test, their polished thin sections were prepared and subjected to both reflected light (RL) and transmitted light (TL) microscopy. In addition to that these polished thin sections were exposed to alpha particle sensitive cellulose nitrate film for autoradiography. The alpha track records have been used to differentiate among radioactive and non-radioactive minerals and their respective track density combining with optical properties have been used for identification of radioactive minerals. Mineral identification of rock forming as well as ore forming minerals their textural analysis and alteration studies have been carried out.

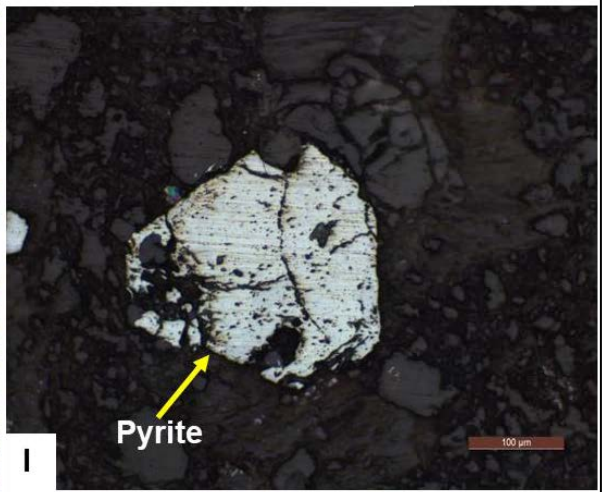
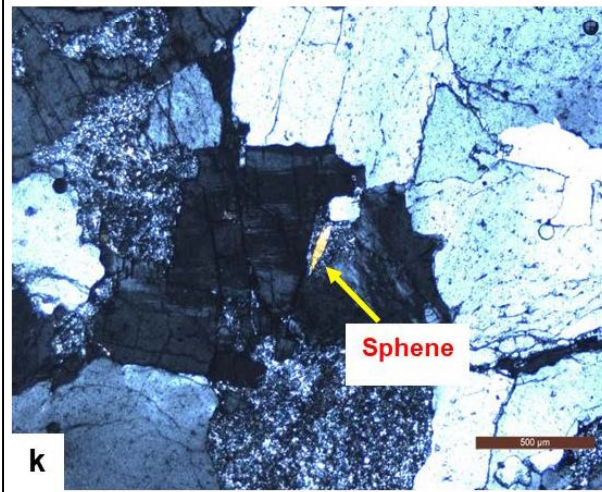
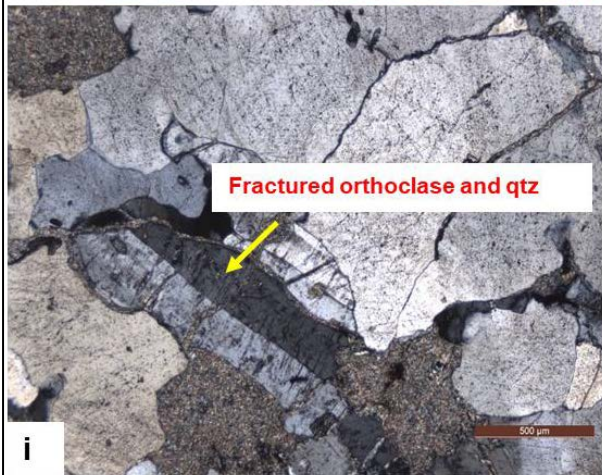
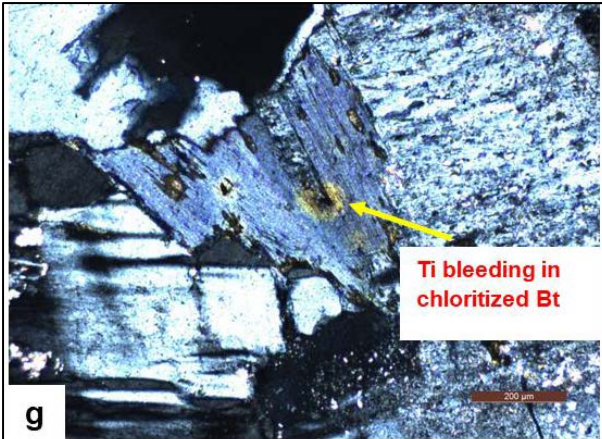
**7.2 Petro-mineralogy of Govardhanagiri-Lanjabanda granites:** Petro-mineralogical studies of basement granites(n=14) was carried out for the present study.

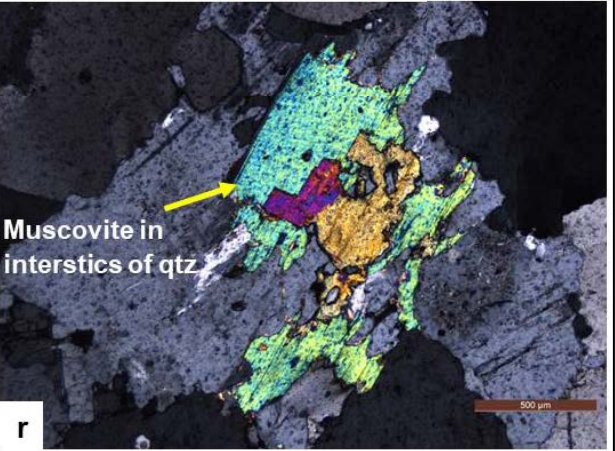
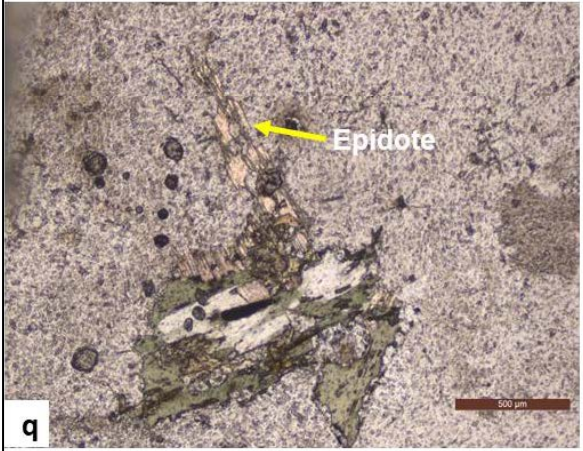
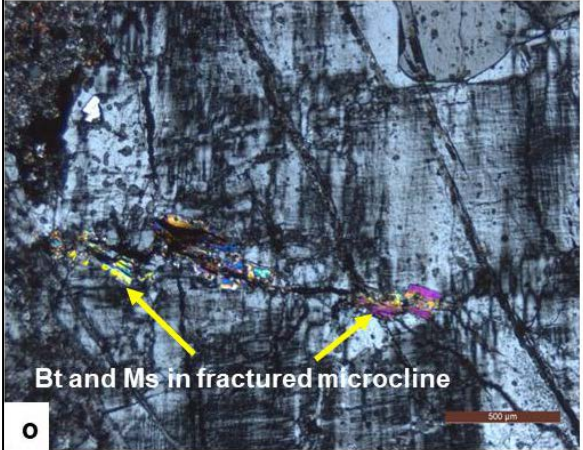
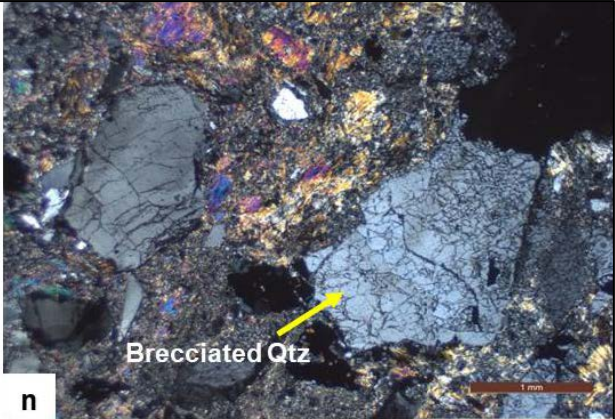
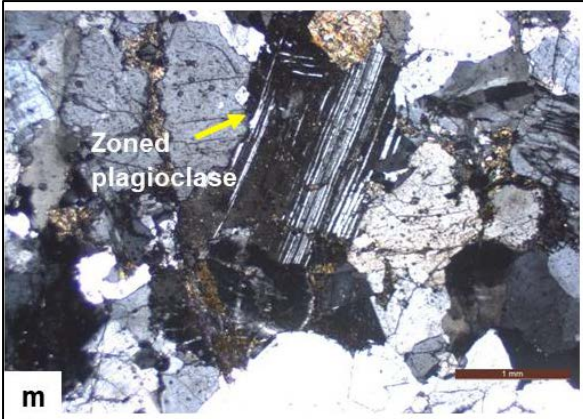
**Megascopic observations:** Megascopically, the granites are hard and compact, grey and pink varieties, leucocratic, medium-coarse grained, fractured with quartz and tourmaline veins as fracture fillings.

**Microscopic observations:** Under the microscope, granites are medium grained and exhibits hypidiomorphic granular texture. Quartz, K-feldspar(microcline>orthoclase) and plagioclase forms the essential minerals while biotite, muscovite and chlorite occur as minor minerals. Accessory minerals include apatite, sphene (Figure 7.1k) and opaques. Opaques are mainly represented by magnetite and pyrite (Figure7.11). K-feldspar is represented by orthoclase, microcline and micropertthite (Figure 7.1 e, i&p). Microcline occurs as sub-rectangular laths with minor sericitisation. Both K-feldspars and plagioclase feldspars exhibit moderate

alteration to sericite in the studied samples (Figure 7.1j). The plagioclase is euhedral to subhedral and its composition is oligoclase (10-30% An). It shows albite and Carlsbad-albite twins with a zonal texture (Figure 7.1m). The core of the plagioclase is partly altered while the rim part is unaltered. Plagioclase feldspars are affected more by alteration to sericite which is of intense degree (Figure 7.1h). Blebs of fine grained quartz are noticed in microperthite (Figure 7.1p). Quartz and feldspars show signs of deformation evidenced by fractured and brecciated nature (Figure 7.1n). Myrmekitic texture observed in albitic plagioclase signifies the intergrowth of quartz and feldspar (Figure 7.1c). Alkali feldspar phenocrysts are mainly perthitic microcline and show poikilitic texture in which muscovite, biotite, plagioclase and quartz are enclosed (Figure 7.1d). The completely enclosed grains are subhedral to anhedral and randomly oriented. This feature is related to the nucleation and growth rates of minerals. The growth rate of alkali feldspar is much higher than quartz and plagioclase thereby forming larger crystals than the enclosed grains. Biotite occurs as subhedral to anhedral grains intergrown with or parallel to muscovite or as an interstitial phase with muscovite (Figure 7.1o, r). Some biotite also shows kink bands because of deformation. Some biotites are altered to chlorite and excess Ti released is evidenced in the form of dark spots (Ti bleeding) (Figure 7.1g). Muscovite occurs as intergrowth with biotite filling the interstices, as a subhedral crystal within K-feldspar (microcline) and as fracture filling in the microcline (Figure 7.1f, o, r). Presence of both primary and secondary muscovite as well as biotite in granite suggests them to be of peraluminous nature (Figure 7.1f, o, r). Epidote is noticed as fine sized aggregates in these samples (Figure 7.1q).







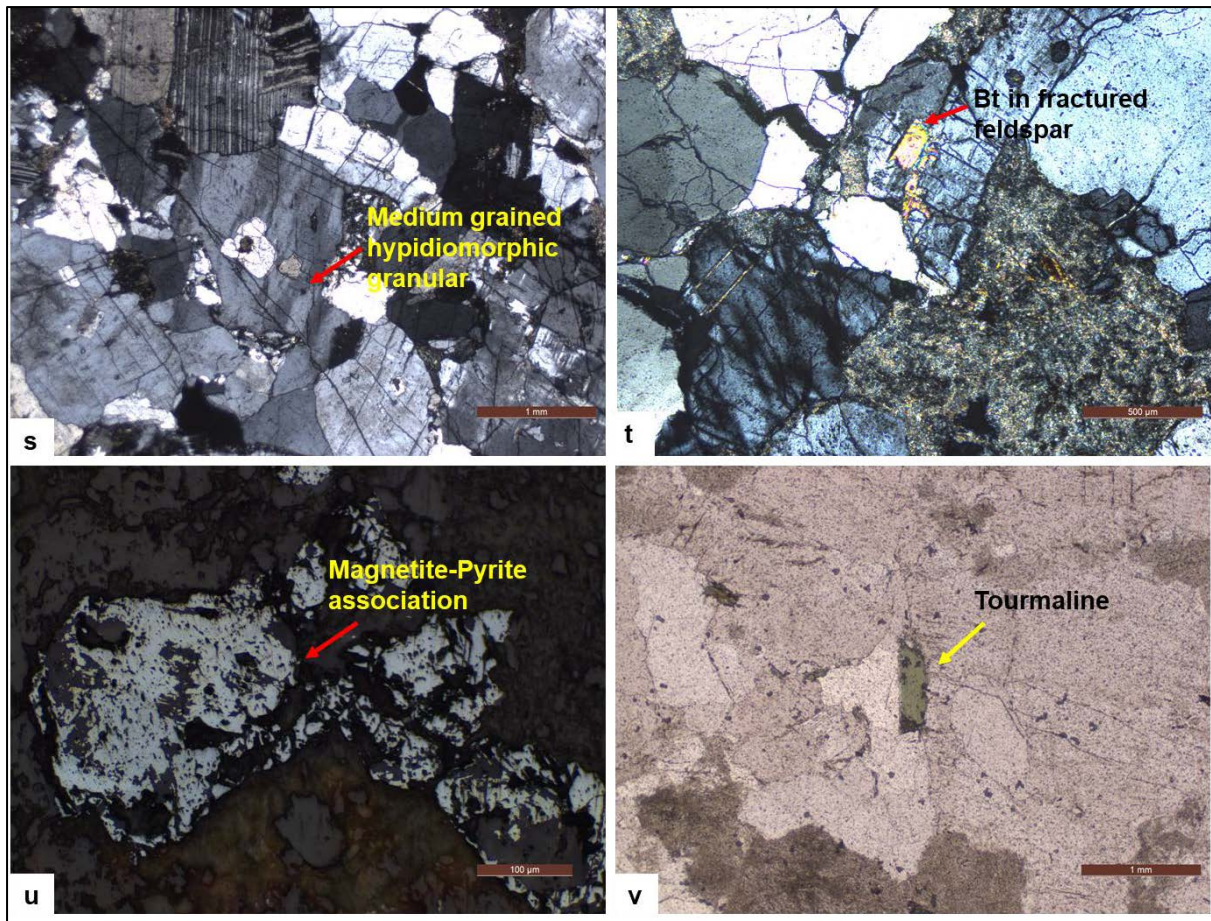


Figure 7.1 Photomicrographs of Govardhanagiri-Lanjabanda granites showing a) Biotite in pulverised matrix b) Chlorite in altered granite c) Myremekitic texture d) Pokilitic texture e) Coarse microcline crystal f) Bent secondary muscovite in sericitized matrix g) Titanium bleeding in chloritized biotite h) Sericitized plagioclase i) Fracture orthoclase and quartz j) Sericitization along quartz vein k) Accessory sphene as inclusion l) Pyrite crystal m) Altered zoned plagioclase n) Brecciated quartz in sericitized matrix o) Biotite and muscovite in fractured microcline p) Microperthite q) Epidote as fine size aggregate r) Primary muscovite intergrown with quartz s) Medium grained hypidiomorphic granular texture t) Biotite in fractured feldspar u) Magnetite-pyrite association in granite v) Tourmaline bearing granite

## Discussion

**Significance of two mica granites and textural criteria to identify primary and secondary muscovite:** Muscovite coexisting with biotite is the most common mineralogical indicator of highly peraluminous composition of plutonic rock. The identification of primary muscovite is important because it is commonly a good indicator of both magma composition and the depth of crystallization. The most important textural criteria for recognizing primary muscovites are

as follows: (1) primary muscovites have relatively coarse, comparable to the other primary phases and they should occur as a major phase comparable to biotite 2) they must be clearly terminated, ideally with subhedral or euhedral form 3) they should not be enclosed by other minerals 4) they should have no reaction texture with other minerals.

**7.3 Petro-mineralogy of basic dyke:** The basic dyke is identified as dolerite. The sampled dolerite is principally composed of medium to coarse grained calcic plagioclase and clinopyroxene. The main accessories include biotite, amphibole and uraltite. Rarer accessories include olivine, orthopyroxene and anhedral quartz. Euhedral to subhedral opaque oxide minerals were noticed. Unaltered dolerite shows ophitic to sub-ophitic and intergranular texture (Figure 7.2 a,b). Effects of later hydrothermal activity is evident in the form of quartz vein (Figure 7.2c). Some samples also show alteration effects in which intense chloritization was

observed (Figure 7.2e). Large size actinolite crystals occurring in vicinity of dyke can also be observed here (Figure 7.2d).

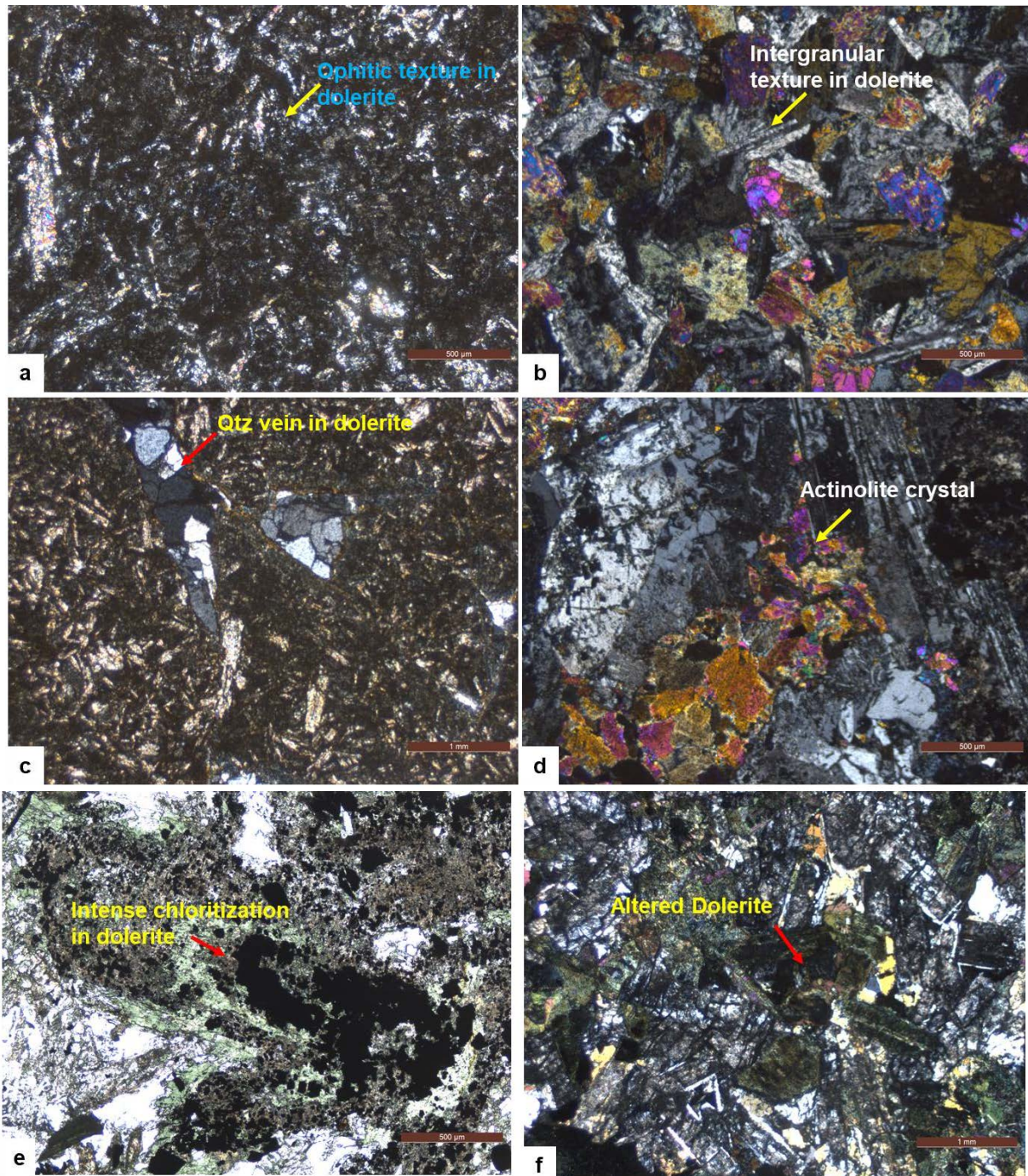


Figure 7.2 a) Ophitic texture in dolerite b) Intergranular texture in dolerite c) Quartz vein in dolerite d) Large actinolite crystal e) Intense chloritization in dolerite f) Altered dolerite

**7.4 Petro-mineralogy of Govardhanagiri-L.Banda Quartzites:** Petro-mineralogical studies of thin sections of Gulcheru Quartzite (n=18) was carried for the present study.

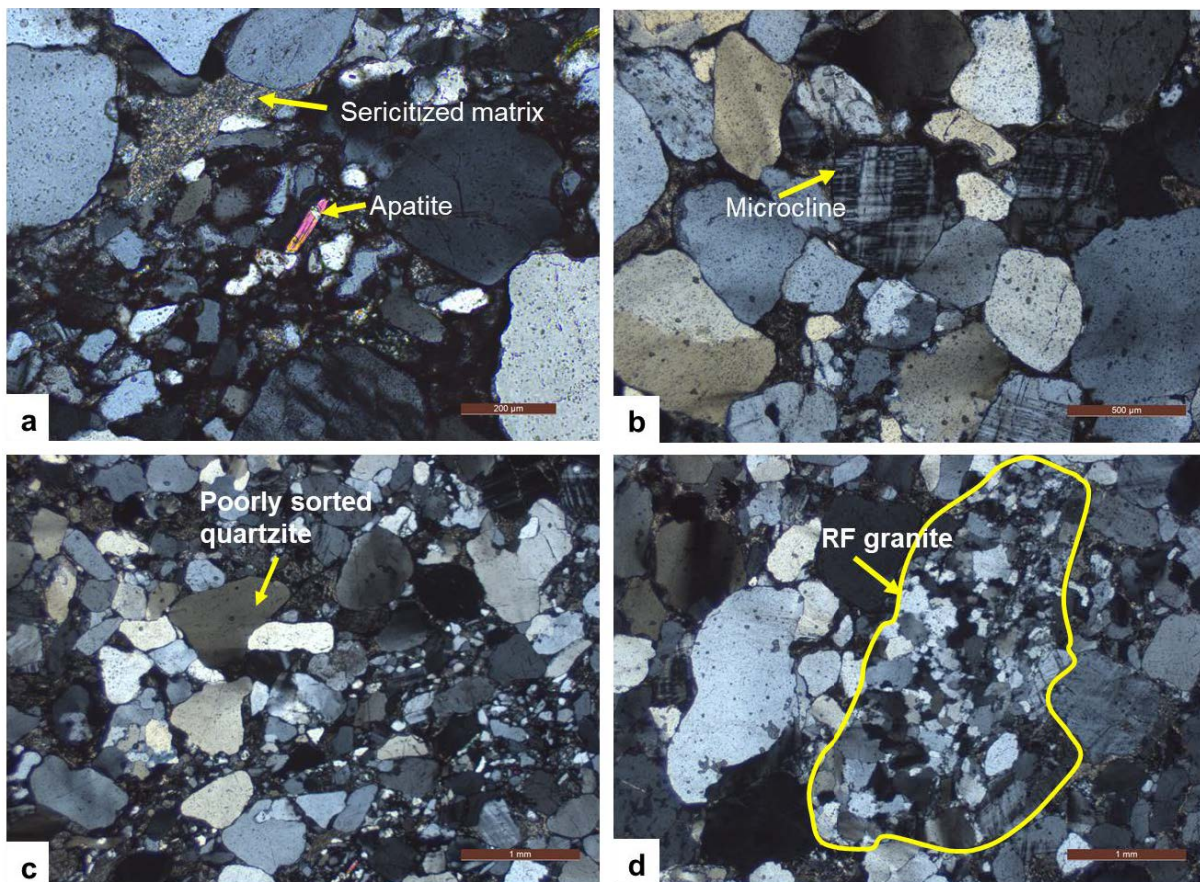
The quartzites of the Gulcheru Formation in the Govardhanagiri-L.Banda area primarily composed of quartz, minor feldspars, rock fragments and accessory heavy minerals and show low variability of framework mineralogy.

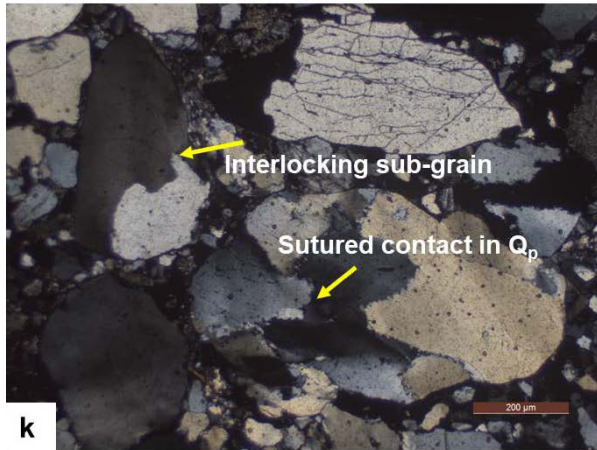
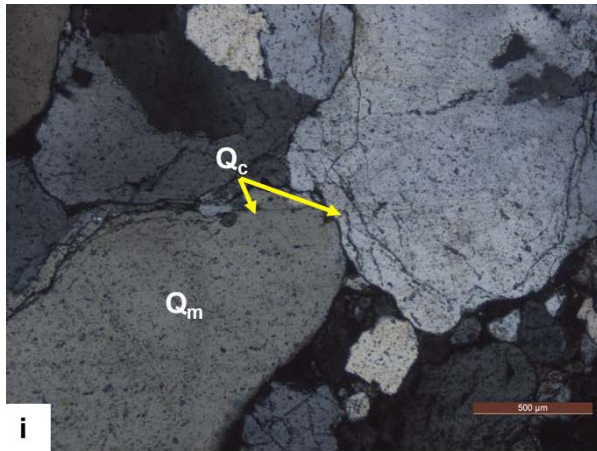
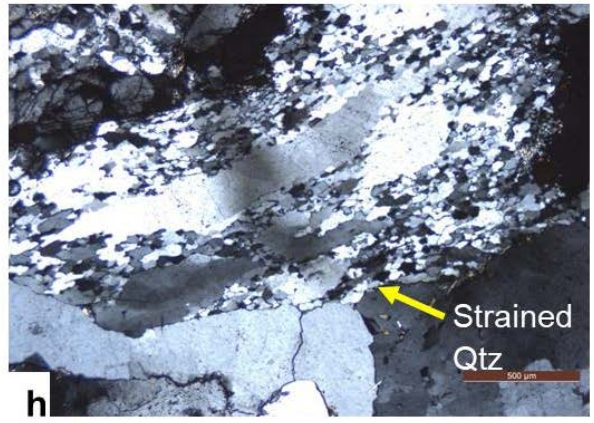
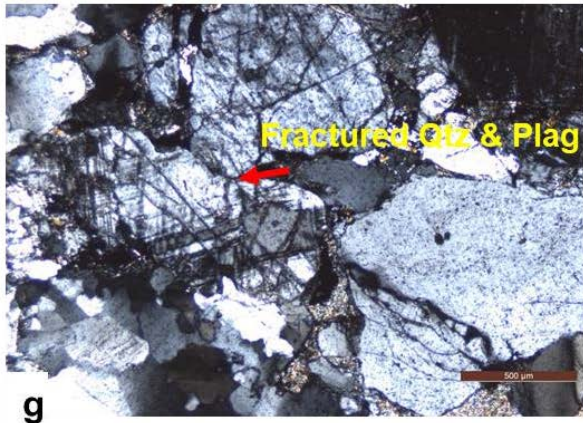
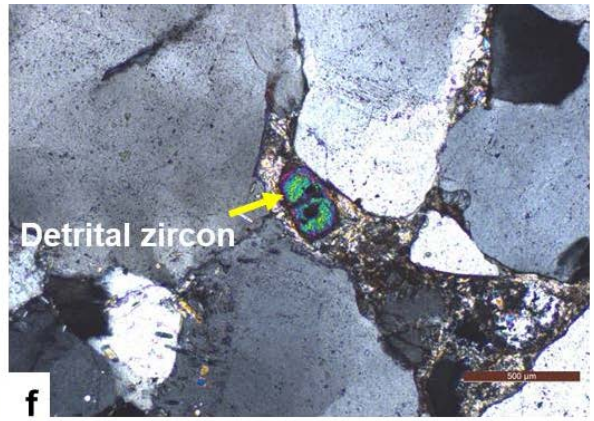
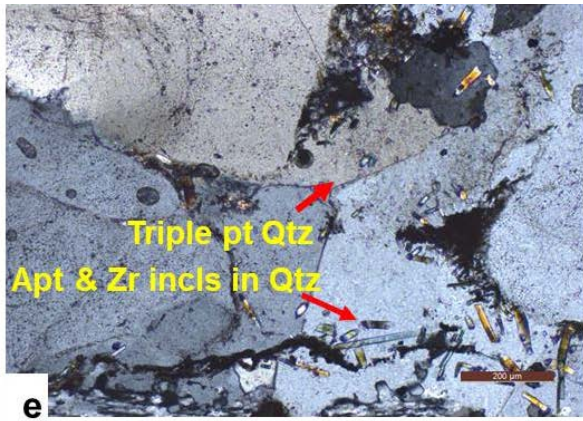
The quartzose fraction comprises dominantly monocrystalline quartz (>45%) and subordinate polycrystalline varieties (5-10%). The monocrystalline quartz grains show two different types of extinction (i) straight(non-undulose) and (ii) undulose and may therefore be unstrained and strained (Figure 7.3c). Non-undulose (unstrained) monocrystalline quartz grains predominates in general. In some samples, monocrystalline quartz contains inclusions of accessory heavy minerals like zircon, apatite and rutile (Figure 7.3 e and m). Polycrystalline quartz grains are also of two distinct types: i) grains with 2-3 interlocking subgrains, and ii) grains with more than 3 subgrains. Quartz subgrains in the second type shows sutured subgrain boundaries (Figure 7.3k). Straight and concavo-convex grain contacts are numerous with minor point contacts (Figure 7.3l). Intensely fractured and granulated quartz was also present (Figure 7.3g). Well-rounded monocrystalline quartz grains with thin relict rims of syntaxial quartz cement have been observed (Figure 7.3i).

Feldspars are mainly K-feldspar(microcline>orthoclase) with minor plagioclase (Figure 7.3b). The feldspars are fresh and only locally feebly altered which they are replaced to sericite mostly in the fractured sandstone. Lithic fragments are minor but some granite clasts were observed in some samples (Figure 7.3d). Chert grains which show sub-rounded shape occur in traces (Figure 7.3n). Zircon is the most common heavy mineral phase present in both detrital form (in matrix) and as inclusions in quartz grains (Figure 7.3e and 7.3f). Other heavy minerals are apatite, rutile, monazite and xenotime which occurs mainly as tiny elongated

needle shaped inclusions in monocristalline quartz (Figure 7.3 e, m, r and s). Matrix content in these quartzites ranges from 10-12% (<15%) with sericite most dominant. It occupies the intergranular pore spaces among the competent framework grains and sometimes completely replaces the detrital feldspar grains and occurs as patches squeezed between framework grains (Figure7.3j). Siliceous cement is the dominant in these sandstones and ferruginous cement is limited to small number of samples with no carbonate cementation in any of the samples.

Sandstones are texturally and mineralogically sub-mature to immature because of the presence of clayey matrix, moderate to poorly sorted nature and degree of roundness (sub-angular to sub-rounded) and presence of fresh K-feldspar grains (Figure 7.3 a, b &c). The sandstones have been classified as sub-arkosic to arkosic arenite.





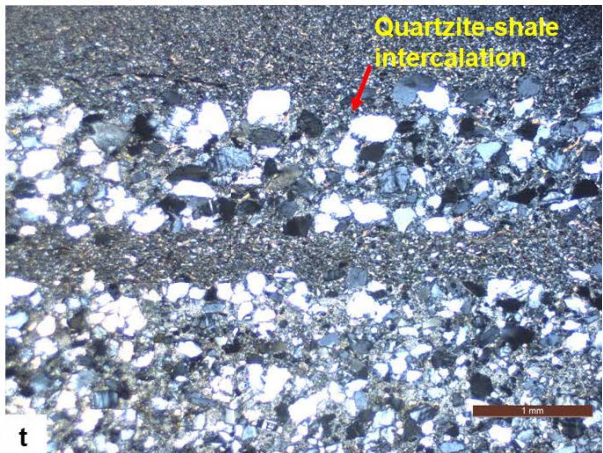
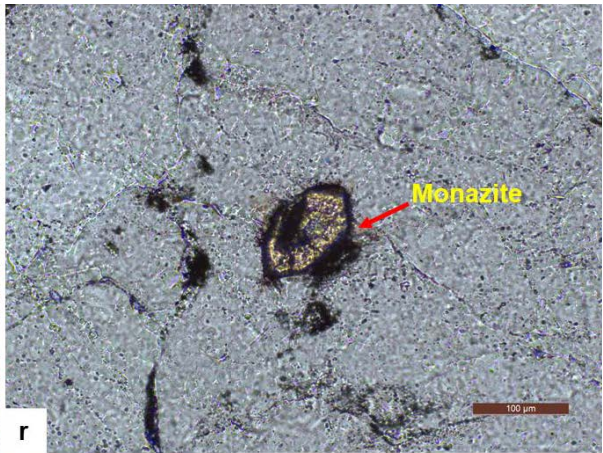
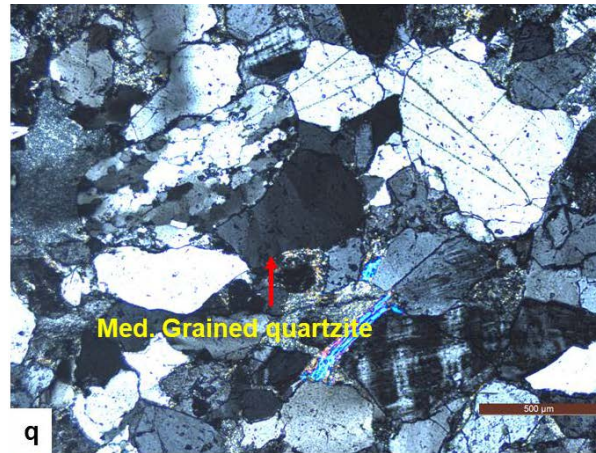
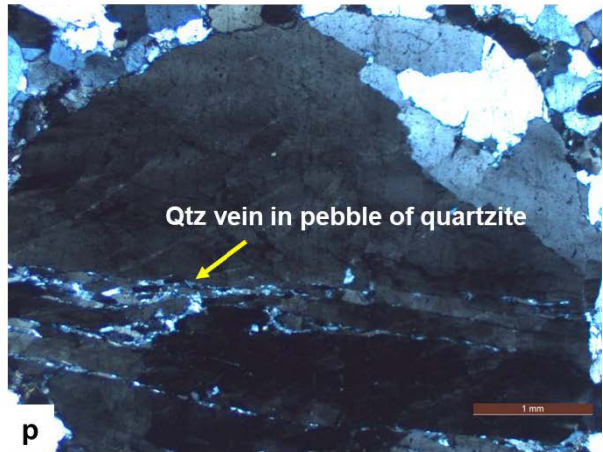
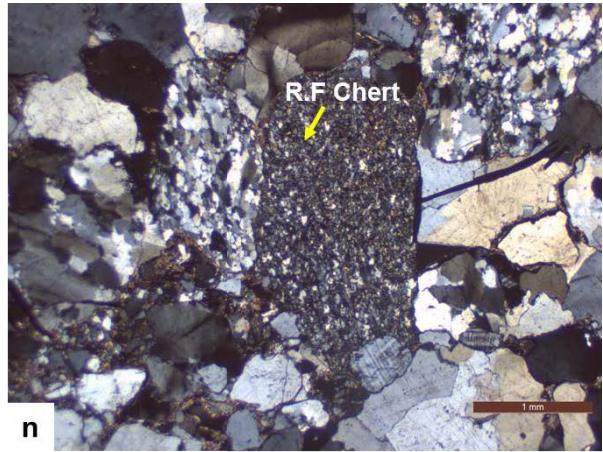
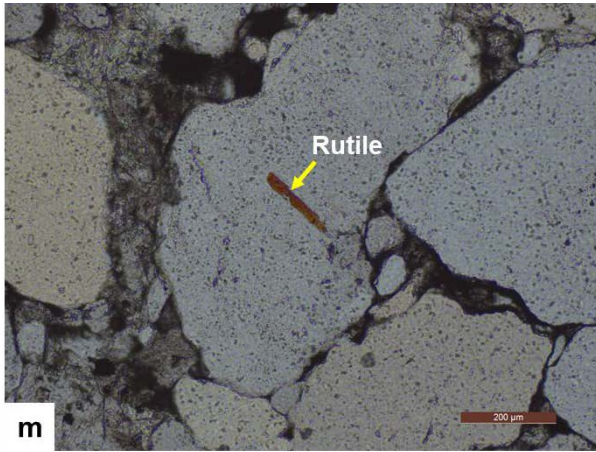


Figure 7.3 Photo- micrographs of quartzites of Gulcheru Formation showing (a) Poorly sorted quartzite with sericite matrix (b) Fresh K-feldspar (microcline) dominance over plagioclase (c) Textural immaturity shown by sub-angular to sub-rounded grains (d) Rock fragment of granite in quartzite (e) Accessory heavy minerals (Apatite and zircon) as inclusions in quartz (f) Detrital zircon in matrix of quartzite (g) Intensely fractured quartz and feldspar (h) Strained quartz as indicator of source rock deformation (i) Authigenic silica as cement forming quartz overgrowth (j) Floating texture in fine grained sericite matrix and altered muscovite (k) Two distinct types of Polycrystalline quartz (l) Straight and concavo-convex contact in quartzite (m) Rutile occurring as needle shaped inclusion in monocrystalline quartz (n) Rock fragment of chert (o) Intensely sericitized K-feldspar (p) Qtz vein in pebble of conglomerate (q) Medium grained quartzite (r) Monazite as a inclusion in quartz (s) Xenotime in quartzite (t) Quartzite-shale intercalation.

**Inferences on Provenance based on petro-mineralogical studies:** Detrital light and heavy minerals as well as rock fragments in sandstone are important in the study of provenance. Rock fragments are the most informative as they carry their own provenance signature (Pettijohn et al., 1987). Source rock for the sandstones of the Gulcheru Formation were recognized based on characteristics of quartz and feldspar as well as accessory heavy mineral phases which retain the characteristics of original source rock and can be used as provenance indicator. The degree of undulosity of monocrystalline quartz and the number of subgrains are useful discriminant of different kinds of source rocks (Basu et al., 1975; Basu 1985). The sandstones of the Gulcheru formation in the Govardhanagiri-L.Banda area contains both strained(undulose) and unstrained(non-undulose) quartz. Such straining of quartz grains could have taken place during post depositional deformation. However, the presence of both undulose and non-undulose quartz indicates strain inheritance from the source area (metamorphic/ plutonic affiliations) (Young, 1976). Predominance of non-undulose monocrystalline quartz suggests derivation of sediments from a granitic source (Blatt, 1967; Basu et al., 1975; Suttner et al., 1981; Tortosa et al., 1991). Presence of accessory heavy minerals like zircon (both detrital as well as incusions in quartz), apatite and rutile further confirm plutonic source rock (Pettijohn et al., 1987). Also,

lithic fragments of granite were seen in some samples. The presence of fresh K-feldspar, moderate-poorly sorted nature, low degree of roundness and presence of clayey matrix indicates that Gulcheru sediments are texturally and mineralogically sub-mature to immature and deposited as first cycle sediments near to the source with low to moderate degree of chemical weathering of the source and less transportation in semi-arid to arid climatic conditions.

### 7.5 U mineralization

Five radioactive core samples of Gulcheru Quartzite of Kappatralla area (B.H. No. KPT-11 and KPT-12) were taken for thin section preparation and study to understand the nature of U mineralization and their controls as a comparative study to that of Gulcheru Quartzite in Govardhanagiri- Lanjabanda area. The details of thin section studies of these samples are mentioned below.

#### KPT-11 and KPT-12:

**Chromogram test:** Chromogram test has indicated positive spots and fine discontinuous streaks in brown colour from four samples viz. (KPT-11/64A, KPT-11/64B, KPT-12/57A, KPT-12/57B) indicative of presence of uranium phases (Figure 7.4).

#### Pictures of chromogram test



Figure 7.4 Positive spots indicated in the form of brown colour in these samples.

**C.N. film studies:** C.N. film exposure of 72 hours has indicated the radioactive phases which contribute to radioactivity in these sub-feldspathic quartzite core samples.

**Megascope description:** In hand specimen, the samples are hard and compact somewhat ferruginized having grey to brownish grey appearance.

**Microscopic description:** Under the microscope, the samples are comprised of framework constituent mineral quartz which forms nearly 85% of the total rock volume followed by feldspars (Both K-feldspars represented by orthoclase and microcline) and plagioclase forming nearly 10% of the total rock volume. Muscovite and heavy minerals such as zircon occur as accessory phases (Figure 7.5d and 7.7c). Quartz grains are dominantly monocrystalline, sub-angular to sub-rounded clasts (Figure 7.7d and g) with size range between 0.25mm to 1mm. Majority of grains showing low degree of angle of undulose extinction. Polycrystalline grains of quartz composed of aggregates of two or more quartz grains are also identified (Figure 7.7g). Among K- feldspars, orthoclase and microcline are identified which occur as sub-rounded grains and altered to variable degrees to sericite both along grain boundaries and through fractures (Figure 7.5a and c). Plagioclase feldspar is identified as albite which are unaltered (Figure 7.5b). Matrix content in these quartzites ranges from 7-8% (<15%) with sericite most dominant. Siliceous cement is dominant in these sandstones and ferruginous cement is limited to small number of samples with no carbonate cementation in any of the samples (Figure 7.7d). The ore minerals identified in these samples are haematite, goethite and pyrite. Haematite forms fine sized grains which shows partial to complete goethitisation. Amongst the sulphide ore minerals, pyrite forms very small sized grains, fine to ultrafine aggregates (Figure 7.6i).

**Deformation:** The constituent mineral grains in these sub-feldspathic quartzite samples manifest effects of brittle deformation mainly as microfracturing of moderate degree and granulation around grain boundaries (Figure 7.5a).

## 7.6 Radioactive Minerals

**Coffinite:** Moderate density alpha tracks (Figure 7.6g) emanate from discrete grains of coffinite occurring in vein. Coffinite is brownish grey in colour with a lower reflectivity than pitchblende. Coffinite grains are closely associated with fine to ultrafine aggregates of pyrite (Figure 7.6i) which are of later origin.

**Uranium adsorbed on goethite:** Highly disseminated alpha tracks are correlatable to uranium adsorbed on irregular patches of goethite showing typical brown colour which are occurring in interstices (Figure 7.7i and j)

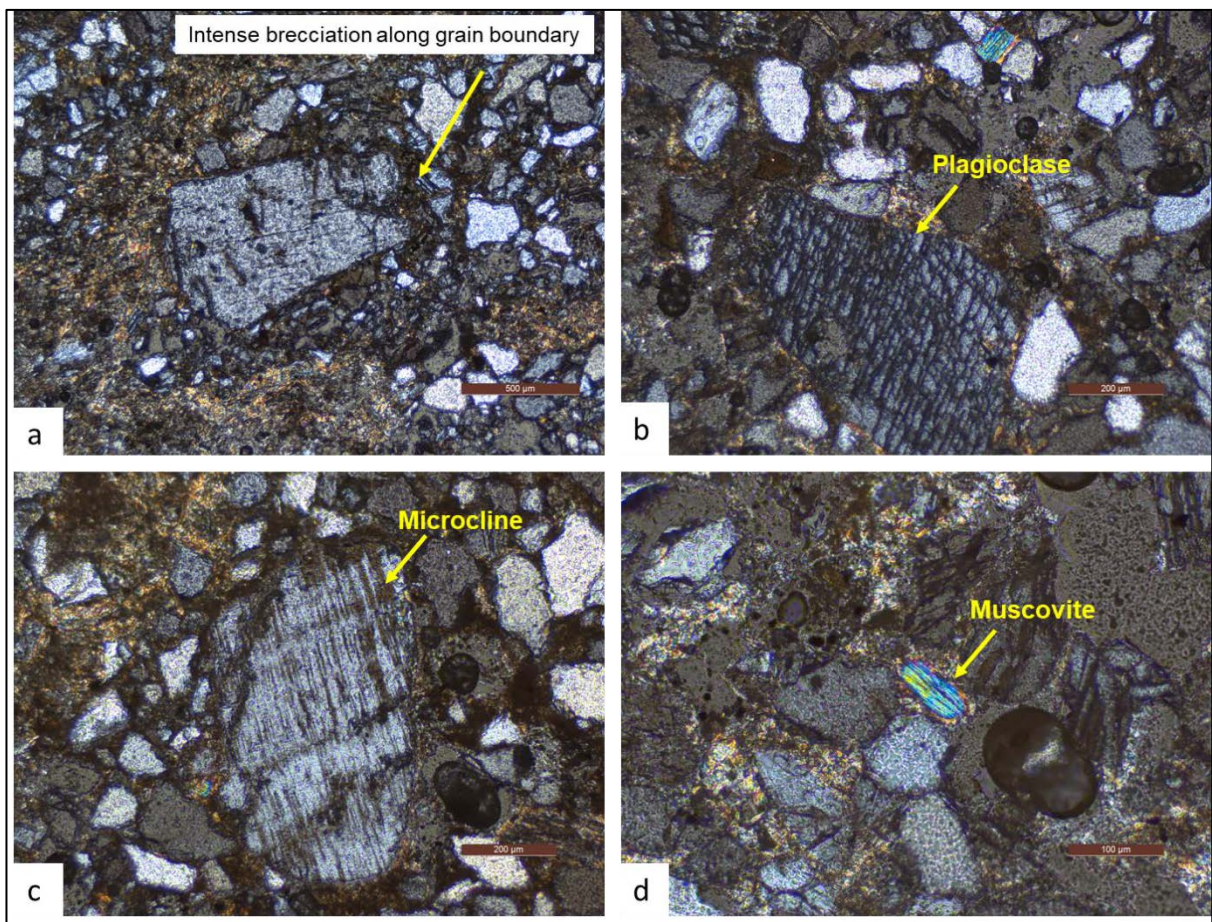


Figure 7.5 a) Intense brecciation around grain boundary b) Plagioclase identified as albite  
c) Microcline showing cross-hatched twinning d) Muscovite in intergranular space in quartzite

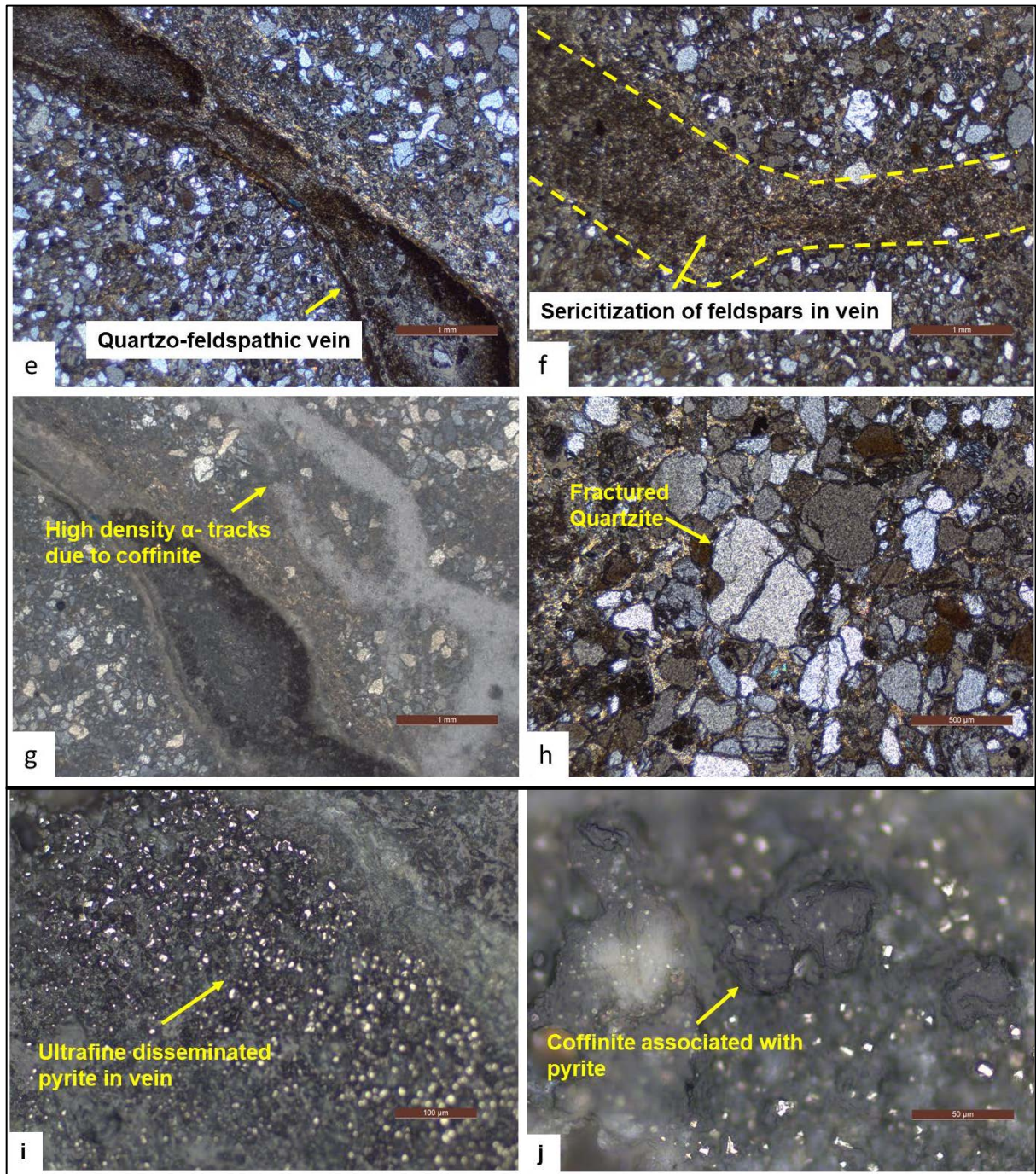


Figure 7.6 e) Quartzo-feldspathic vein in quartzite f) Sericitization of feldspars in vein g) High density  $\alpha$ -tracks due to coffinite h) Fractured quartzite i) Ultrafine disseminated pyrite in quartz vein j) Coffinite associated with pyrite

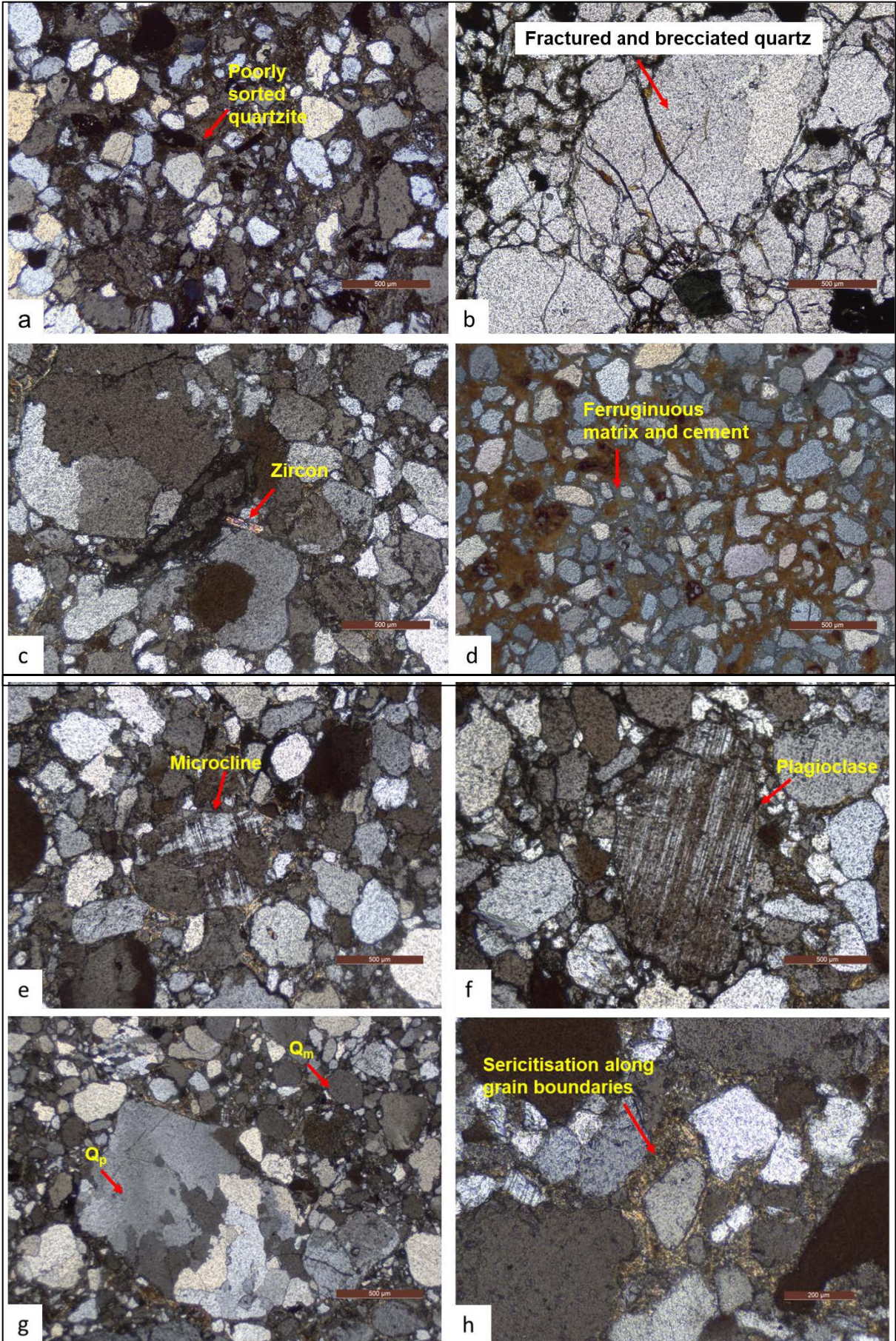




Figure 7.7 a) Poorly sorted quartzite b) Fractured and brecciated quartz c) Detrital zircon in quartzite d) Ferruginous matrix and cement e) Microcline f) Plagioclase g) Monocrystalline and polycrystalline qtz h) Sericitization along grain boundaries i) Goethitisation along fractures j) U adsorbed on goethite

## 7.7 Hydrothermal Alterations

### Chloritization

Chlorite may be present alone or with quartz and tourmaline in very simple assemblage. Chloritization of biotite in granite is well present (Figure 7.1b and g). This alteration is present along the periphery of biotite flakes with shows gradation towards the core. Presence of mafic minerals or introduction of iron and magnesium by some secondary process may boost chloritization. Light green colour of altered product is suspected as Mg rich variety of chlorite.

### Silicification

Silicification involves an increase in the proportion of quartz or cryptocrystalline silica (i.e. cherty or opaline silica). This silica may be introduced by hydrothermal solutions or it may be by product of the alteration of feldspar or other minerals as mentioned in sericitization. Both cherty quartz and vein filling quartz (Figure 7.1h) are present in granite. Small clusters of very fine grain chert have been investigated during petrographic studies (Figure 7.3p).

## Sericitization

Sericitization of K feldspar and plagioclase is well developed. Fine specks of sericite are embedded through-out the plagioclase laths (Figure 7.3o). During sericite alteration hydrogen ions are consumed by K feldspar and potassium ions are released (Evans, 2009). During the sericitization of granitic rocks the feldspar or micas may transform in sericite with secondary quartz as a reaction by product but primary quartz may be largely unaffected. Silica is released in this reaction which may be precipitated as secondary quartz, which can be observed by occurrence of cherty nodules in petrographic studies. The process of sericitization can be given by this general equation.



## 7.8 XRD analysis

Two samples (n=2), one radioactive sample of granite and one non-radioactive sample of quartzite from Govardhanagiri-L.Banda area was sent for X-ray diffraction studies at XRD laboratory, AMD, Hyderabad for radioactive phase determination and clay mineral studies. Granite is pink coloured medium-coarse grained equigranular in nature. Quartzite is hard and compact, grey coloured, massive and sub-feldspathic in nature.

Table 7.1 XRD result of samples from Govardhanagiri- L. Banda area

S.No.	Sample No. and Rock type	Locality	Atomic minerals identified	Other ore minerals	Rock forming minerals
1.	GVD-4 (Granite)	Govardhanagiri-L.Banda area	Rutile, xenotime and zircon	Anatase, haematite and goethite	Biotite, muscovite, quartz, microcline and fluoroapatite
2.	LNJB/GRP/1 (Quartzite)		Thorite, rutile and zircon	Magnetite, haematite and goethite	Quartz, microcline, biotite, muscovite, illite and fluoroapatite

**Ore mineral:** In the Govardhanagiri-Lanjabanda areas the associated ore minerals are anatase, haematite and goethite in granite and magnetite, haematite and goethite in quartzite (Table 7.1).

**Rock forming mineral:** The minerals identified are biotite, muscovite, quartz, microcline, fluorapatite and illite forms by the alteration of biotite and K-feldspar (Table 7.1).

**Rare-Earth Bearing Minerals:** - The observed yttrium and heavy-rare earth element bearing phase are limited, and are represented by Xenotime. Thorium and light REE bearing phase are represented by thorite and zircon (Table 7.1).

### **7.9 Mineral Paragenesis**

The time sequential mineral deposition is known as paragenesis. Studies of mineral sequences are practically based on microscope, because micro-textures and microstructures are used to decide which formed first though relationship between mineralized veins that cut across one another also provide valuable indications for mineral paragenesis. Rock consist a number of different minerals. In an igneous rock, various minerals crystallized from a slowly cooling magmatic melt whereas some are forming from metamorphism of these rocks on attaining particular P-T conditions, constitute an equilibrium assemblage. Such an assemblage is called a mineral paragenesis. Mineral identification and textural characterization are two major objectives in ore microscopy in order to determine formation of associated minerals in time succession, or paragenesis, and the estimation of the conditions under which the minerals have formed or have re-equilibrated.

In general, all the minerals that are detectable within a single thin section belong to the mineral paragenesis that is helpful in characterizing an igneous rock derived from a homogenous melt. However metamorphic rocks derived from sediments the composition may vary over a small volume of thin section, and possibly the mineral observed in a single thin section may not belong to a single metamorphic paragenesis.

There is no standard method for carrying out paragenetic studies, because each deposit is unique. However, as the goal of all such studies is to decipher the sequence of mineral formation, certain general principles are followed.

Table 7.2 Paragenetic sequence for different rock forming and ore minerals

Mineral \ Stage	Pre-Ore Stage	Ore Stage	Post ore stage
Plagioclase	—————		
Biotite	—————		
Orthoclase	—————		
Quartz	—————		—————
Zircon	—————		
Sphene	—————		
Apatite	—————		
Monazite	—————		
Tourmaline	—————		
Pyrite	—————	—————	—————
Magnetite	—————		
Muscovite	—————		
Sericite			—————
Goethite			—————
Coffinite		—————	

In the present study, most of the non-ore forming minerals comprising both major and accessories phases (heavy minerals) are identified as of pre ore stage origin. This identification is based on their textural relationship between individual grains, cross-cutting relationship and twinning. Major phases comprising plagioclase, biotite, orthoclase, muscovite is crystallized earlier while in the accessory heavy minerals zircon, sphene, apatite, monazite, tourmaline is included. Ore stage minerals shows association of U bearing phases(coffinite) with sulphide phase(pyrite) (Table 7.2). Post ore stage mineralisation is associated with U adsorbed on goethite as well as hydrothermal alterations like sericitization and silicification (Table 7.2).

## CHAPTER 8

# GEOCHEMISTRY

### Geochemical Studies

#### 8.1 Introduction

Geochemistry is a very important tool for characterization of lithounits, their nomenclature, identifying chemical variations, intra-elemental abundance and inter-elemental relationship with special reference to mineralized rocks, and petrogenetic processes. These signatures play a significant role in highlighting the origin, nature of possible source and tectonic environment of emplacement.

Geochemical characterization of basement rocks comprising of Govardhanagiri-L.Banda granites and younger basic intrusives as well Gulcheru Quartzite in the study area is one of an important component of this work. Major and trace element analyses of granites(n=11), basic intrusives(n=9), Gulcheru Quartzite(n=7) and Shale(n=7) have been carried out for the complete geochemical picture. In addition to these, 08 samples of granites and 6 samples of quartzite have been analysed for REE. Present chapter incorporates geochemistry showing chemical classification and tectono-magmatic history with the help of established variation and discrimination diagrams.

#### 8.2 Geochemistry of granite

##### Major Elements

The granites are high in SiO<sub>2</sub> (66.07-83.45%; Avg.74.92%), Al<sub>2</sub>O<sub>3</sub> (4.64-16.48%; Avg. 12.46%), K<sub>2</sub>O (1.75 -7.79%; Avg. 4.91%), Na<sub>2</sub>O (0.23-4.09%; Avg.1.026%). Here, K<sub>2</sub>O is mostly dominating over Na<sub>2</sub>O and K<sub>2</sub>O/Na<sub>2</sub>O ratio (1.12 to19.48; Avg. 10.35). While they are depleted in MgO (0.12-1.77%; Avg. 0.68%), CaO (0.005- 5.83%; Avg. 0.973%) and TiO<sub>2</sub> (0.05 -0.37%; Avg. 0.16). The variation in FeO<sub>t</sub> content ranges from 0.89 to 4.21(avg. 2.06%), MnO

ranges from (0.005-0.02%; Avg. 0.007%) and P<sub>2</sub>O<sub>5</sub> ranges from (0.005-3.87%; Avg. 0.686%) (Table 8.1). The variation in agpaite index ranges from 0.47 to 0.92, which is indicating oversaturated to saturated nature with respect to Al<sub>2</sub>O<sub>3</sub>.

Table 8.1 Major oxide (wt%) data of granites(n=11) in study area

Sample Id	LNJB 1/Gr	LNJB- 2/Gr	LNJB /Gr/4	GVD /Gr/1	GVD /Gr/2	LNJB /Gr/1	LNJB /Gr/2	LNJB /Gr/3	LNJV /Gr/1	LNJB /GRP/1	LNJB /UC/1
SiO <sub>2</sub>	79.36	76.38	66.07	70.8	72.03	69.46	82.39	82.43	72.22	69.61	83.45
TiO <sub>2</sub>	0.18	0.1	0.16	0.22	0.12	0.37	0.05	0.08	0.13	0.15	0.22
Al <sub>2</sub> O <sub>3</sub>	11.93	13.18	16.48	14.59	14	14.57	11.53	4.64	14.11	14.96	7.08
Fe <sub>2</sub> O <sub>3</sub> (t)	1.74	1.23	2.73	1.78	2.01	2.81	0.89	1.39	1.64	2.26	4.21
MgO	0.12	0.64	0.43	1.7	0.53	1.77	0.83	0.2	0.29	0.74	0.24
MnO	0.005	0.005	0.005	0.01	0.005	0.01	0.005	0.005	0.02	0.005	0.005
CaO	0.04	0.11	5.83	0.09	0.33	0.3	0.01	3.22	0.65	0.12	0.005
Na <sub>2</sub> O	0.42	0.43	0.39	3.57	0.6	0.35	0.55	0.23	4.09	0.4	0.26
K <sub>2</sub> O	5.85	5.22	4.93	5.4	6.03	6.65	3	1.75	4.59	7.79	2.84
P <sub>2</sub> O <sub>5</sub>	0.04	0.11	3.87	0.03	0.33	0.22	0.005	2.82	0.005	0.12	0.005
Total	99.685	97.405	100.895	98.19	95.985	96.51	99.26	96.765	97.745	96.155	98.315
K <sub>2</sub> O/Na <sub>2</sub> O	13.929	12.140	12.641	1.513	10.050	19.000	5.455	7.609	1.122	19.475	10.923
Molar A/NK	1.903	2.333	3.098	1.627	2.112	2.081	3.248	2.343	1.626	1.827	2.284
Molar A/CNK	1.891	2.288	1.478	1.610	2.011	1.996	3.239	0.892	1.512	1.800	2.280
Agpaite index	0.818	0.667	0.502	0.923	0.735	0.749	0.475	0.661	0.916	0.854	0.680
Diff. Index	95.672	97.919	100.166	102.413	104.66	106.907	109.154	111.401	113.648	115.895	118.142
(%) Norm Corundum	4.834	6.622	0	2.708	5.886	6.25	7.36	0	1.231	5.652	3.569

Table 8.2 CIPW Norms of the granites (n=11) of study area

Sample Id	LNJB -1/Gr	LNJB -2/Gr	LNJB /Gr/4	GVD /Gr/1	GVD /Gr/2	LNJB /Gr/1	LNJB /Gr/2	LNJB /Gr/3	LNJV /Gr/1	LNJB /GRP/1	LNJB /UC/1
Q	54.263	52.711	31.857	26.64	43.964	38.691	66.45	69.251	29.038	36.109	70.7
C	4.834	6.622	0	2.708	5.886	6.25	7.36	0	1.231	5.652	3.569
Or	34.572	30.849	29.135	31.912	35.635	39.299	17.729	10.342	27.125	46.036	16.784
Ab	3.554	3.639	3.3	30.208	5.077	2.962	4.654	1.946	34.608	3.385	2.2
An	0.198	0.546	28.656	0.447	1.637	1.488	0.05	6.46	3.225	0.595	0.025
Di	0	0	0	0	0	0	0	1.075	0	0	0
Wo	0	0	0	0	0	0	0	3.288	0	0	0
Hy	0.299	1.594	1.071	4.234	1.32	4.409	2.067	0	0.722	1.843	0.598
Il	0.011	0.011	0.011	0.021	0.011	0.021	0.011	0.011	0.043	0.011	0.011
Tn	0	0	0.189	0	0	0	0	0.183	0	0	0
Ru	0.174	0.094	0.077	0.209	0.114	0.359	0.044	0	0.108	0.144	0.214
Sum	97.905	96.065	94.295	96.38	93.645	93.48	98.365	92.555	96.1	93.775	94.1

CIPW norm calculations (Table 8.2) indicated that the major normative mineral constituents of these granites are quartz (26.64-70.7, avg.47.24), orthoclase (10.34-46.03, avg.29.04), albite (1.95-34.61, avg. 8.68) and anorthite (0.025-28.65, avg. 3.94). Normative ferromagnesian

minerals, diopside (0-1.07, avg.0.097) and hypersthene (0-4.41, avg. 1.65) are also uncommonly observed along with accessory minerals like ilmenite (0.011-0.043, avg. 0.016), titanite (0-0.189, avg. 0.034) and rutile (0-0.36, avg. 0.14).

Table 8.3 Pearson correlation coefficients of major elements in Govardhanagiri granites

	SiO <sub>2</sub>	TiO <sub>2</sub>	Al <sub>2</sub> O <sub>3</sub>	FeOt	MgO	MnO	CaO	Na <sub>2</sub> O	K <sub>2</sub> O	P <sub>2</sub> O <sub>5</sub>
SiO <sub>2</sub>	1									
TiO <sub>2</sub>	-0.36	1								
Al <sub>2</sub> O <sub>3</sub>	-0.85	0.16	1							
FeOt	-0.15	0.65	-0.11	1						
MgO	-0.46	0.48	0.45	0.03	1					
MnO	-0.30	0.26	0.22	-0.03	0.13	1				
CaO	-0.27	-0.06	-0.03	0.14	-0.29	-0.10	1			
Na <sub>2</sub> O	-0.27	0.13	0.22	-0.12	0.16	0.85	-0.10	1		
K <sub>2</sub> O	-0.63	0.14	0.75	-0.05	0.45	-0.05	-0.33	-0.12	1	
P <sub>2</sub> O <sub>5</sub>	-0.18	-0.10	-0.14	0.11	-0.29	-0.21	0.98	-0.20	-0.36	1

The correlation matrix (Table 8.3) of major element compositions show very good correlation of SiO<sub>2</sub> with MgO, Al<sub>2</sub>O<sub>3</sub> and K<sub>2</sub>O (>0.5) whereas good correlation with TiO<sub>2</sub>, MnO, CaO, Na<sub>2</sub>O and least correlation with P<sub>2</sub>O<sub>5</sub> and FeO<sub>(t)</sub>. Among K<sub>2</sub>O and Na<sub>2</sub>O, correlation with K<sub>2</sub>O is higher than Na<sub>2</sub>O and between CaO and FeO<sub>t</sub>, CaO is higher. All these observations suggest moderate differentiation within the magma which gave rise to the granites (Haruna et al., 2013). MnO is negative with SiO<sub>2</sub> but positive with TiO<sub>2</sub>, Al<sub>2</sub>O<sub>3</sub> and Na<sub>2</sub>O. FeO follows TiO<sub>2</sub> as ilmenite is among an important accessory mineral in the granites. FeO also follows MgO, K<sub>2</sub>O and CaO. K<sub>2</sub>O is positive with Al<sub>2</sub>O<sub>3</sub>, TiO<sub>2</sub> and MgO. MgO follows TiO<sub>2</sub>, CaO and SiO<sub>2</sub> whereas CaO follows SiO<sub>2</sub> and TiO<sub>2</sub>.

In Harker variation diagrams (Figure 8.1) the overall decreasing trends of MgO, FeO<sub>t</sub>, CaO, TiO<sub>2</sub> and P<sub>2</sub>O<sub>5</sub> with progressive increase of SiO<sub>2</sub> have been observed which probably indicates the early fractionation of plagioclase (due to decrease of CaO), amphiboles (due to decrease of

CaO, FeO<sub>t</sub>, MgO, TiO<sub>2</sub>) and resistants such as apatite, zircon, rutile, ilmenite etc (Haruna et al., 2013).

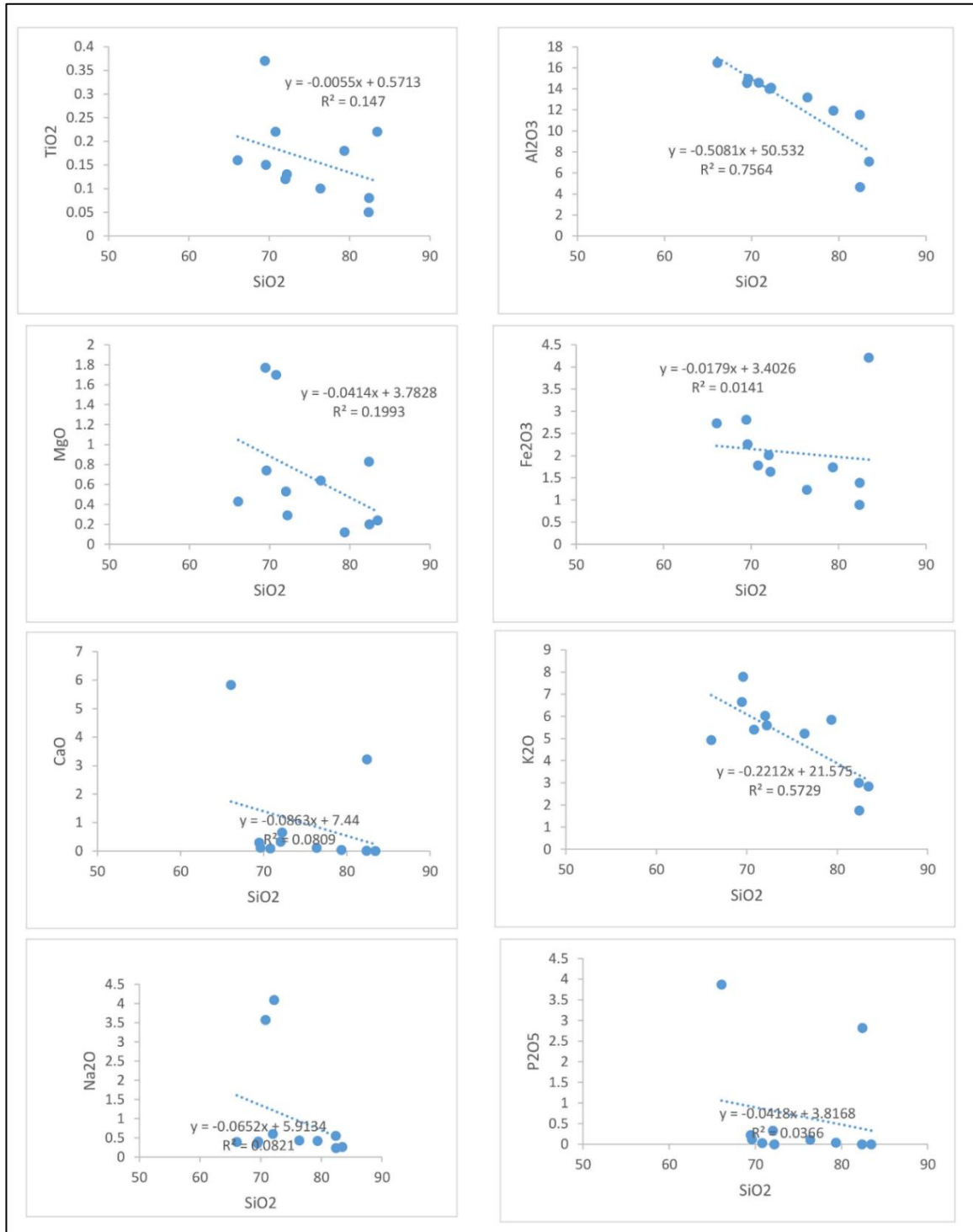


Figure 8.1 Harker variation diagrams of major oxides w.r.t SiO<sub>2</sub> of granites of study area.

## Classification, nomenclature and magmatic affinity

The nomenclature and classification of these granites has been attempted using various parameters based on elemental abundance, ratios and interrelations using major oxides. They typically exhibit their distribution in the granite field in total-alkali silica (TAS) diagram (Figure 8.2a) defined by Middlemost (1985). They distinctly show calc-alkaline nature in AFM [(Na<sub>2</sub>O+K<sub>2</sub>O)-FeO<sup>t</sup>-MgO] diagram (Irvine and Baragar, 1971) (Figure 8.2b) and cluster in the extreme sub-alkaline acidic granitic field in TAS diagram defined by Cox et al. (1979) (Figure 8.3a).

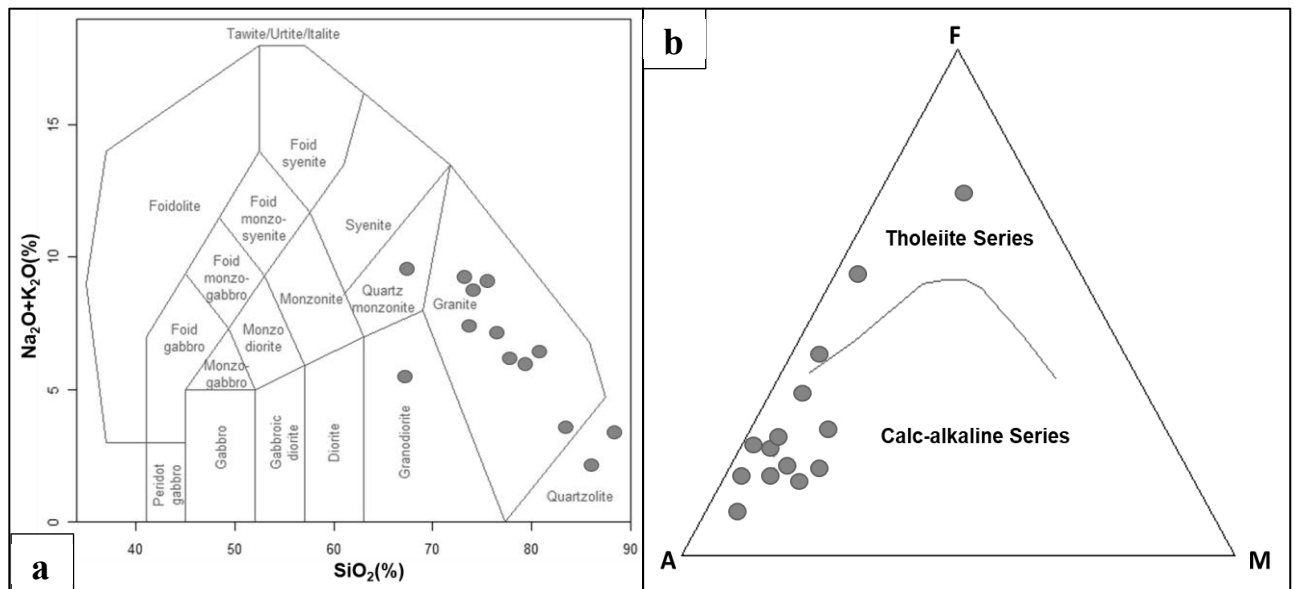


Figure 8.2: a) Total alkali vs. silica classification of granites of study area (after Middlemost, 1985)  
b) AFM ternary plot for granites of the study area (after Irvine and Baragar, 1971).

Similar observation has also been made in K<sub>2</sub>O-Na<sub>2</sub>O diagram after Harpum (1963) where these granites are plotted in granitic-ademellite field (Figure 8.4). The studied granites have K<sub>2</sub>O/Na<sub>2</sub>O ratio ranging from 1.12-19.4 indicating its typical post Archean potassic nature which is substantiated by the predominance of alkali feldspar over Na-plagioclases. These calc-alkaline differentiation trends signify the enrichment of alkalis with progressive crystallization in regard to decrease in oxygen fugacity regime during fractional crystallization (Nocklods and

Allen, 1953 and Thornton and Tuttle, 1969). A similar observation has also been made in normative Ab-An-Or diagram (Baraker, 1979 and O'Conner 1965) (Figure 8.3b) wherein the samples are clustered in granite field.

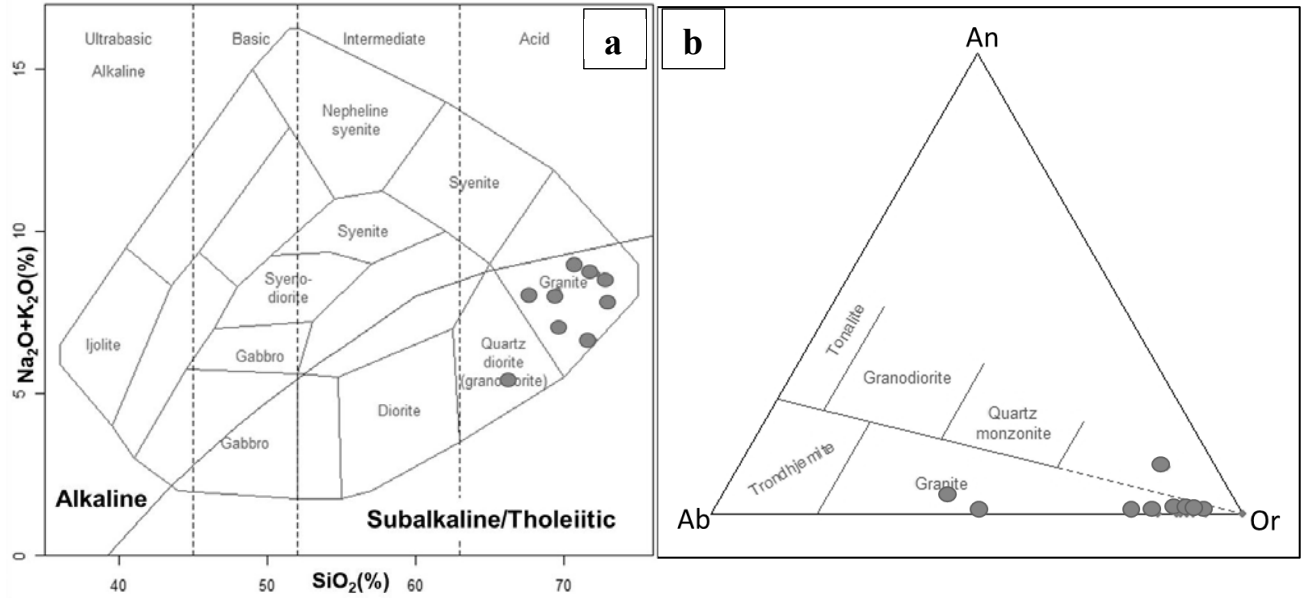


Figure 8.3 a) TAS classification of granites of study area (after Cox et al., 1979) b) Ab-An-Or diagram (Baraker, 1979 and O'Conner 1965)

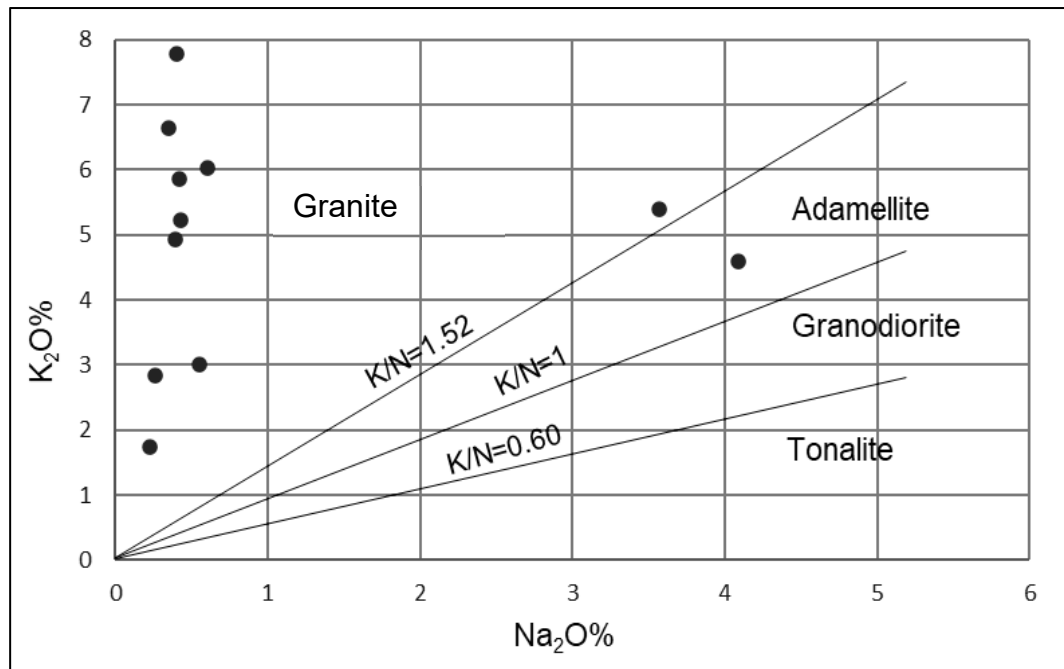


Figure 8.4 K<sub>2</sub>O-Na<sub>2</sub>O binary plot for granites of study area (after Harpum 1963).

On the SiO<sub>2</sub> vs. K<sub>2</sub>O diagram (after Peccerillo and Taylor, 1976) the studied granites show high K calc-alkaline to shoshonitic characters. This is concordant with the high average alumina (12.46%) content and higher proportion of potassic feldspars (Figure 8.5a). In the Modified alkali-lime index (MALI) vs. SiO<sub>2</sub> diagram (Frost et al., 2001) (Figure 8.5b), these granites predominantly fall in calc-alkalic to alkali-calcic field.

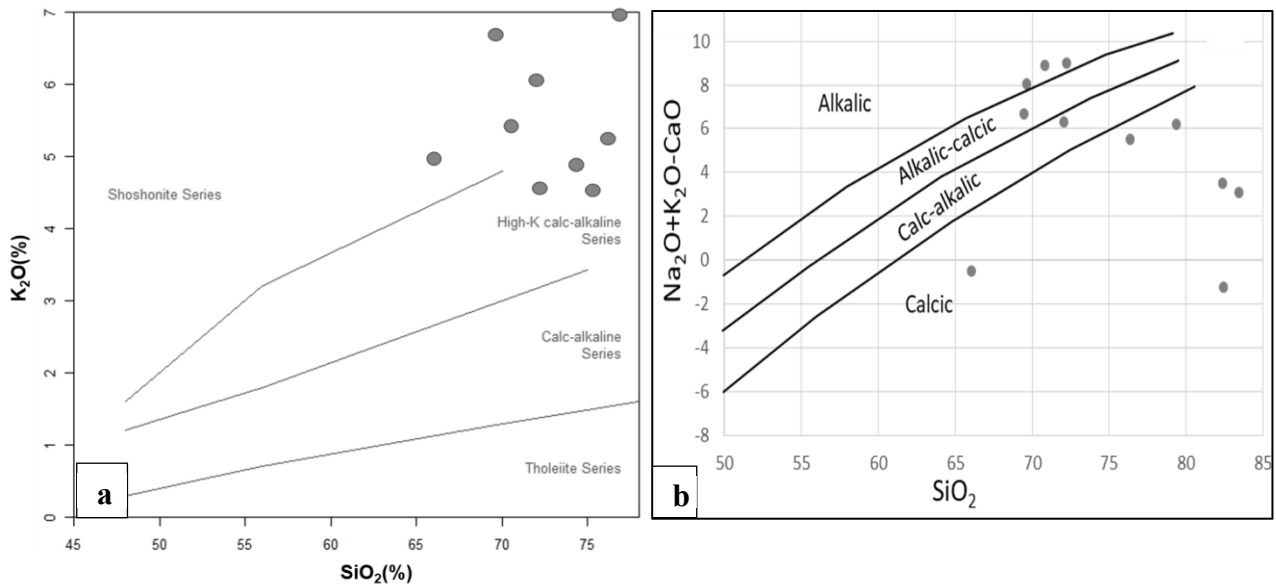


Figure 8.5 a) K<sub>2</sub>O-SiO<sub>2</sub> binary plot for granites of study area (after Peccerillo and Taylor, 1976) b) MALI vs. SiO<sub>2</sub> plot for granites of study area (after Frost et al., 2001).

These granites show agpaite index (molar Na+K/Al) well below 0.95 (0.47-0.92, avg. 0.72) which further supports its calc-alkaline affinity. Lower agpaite index also indicate predominance of peraluminous character (Liegouis et al., 1998). The alumina saturated nature of these granites is apparent from the A/CNK [molar Al<sub>2</sub>O<sub>3</sub>/(CaO+Na<sub>2</sub>O+K<sub>2</sub>O); Clarke, 1981] values ranging from 0.89 to 3.24 (avg.1.91). The dominant peraluminous behaviour of these granites is ascertained by the presence of normative corundum in all samples except the two metaluminous samples with volume percentage ranging from 0%-7.36(avg. 4%). This behaviour is further confirmed by sample plots in alumina saturation diagram (A/CNK vs. A/NK; Shand, 1943) (Figure 8.6). Most of the studied granites show felsic to strongly peraluminous nature in B-A plot (Debon and Le Fort, 1983 and Villaseca et al., 1998) (Figure

8.7a). Most of them plots on the muscovite>biotite field (Debon and Le Fort, 1983) (Figure 8.7b). This has been corroborated with the petrographic observation.

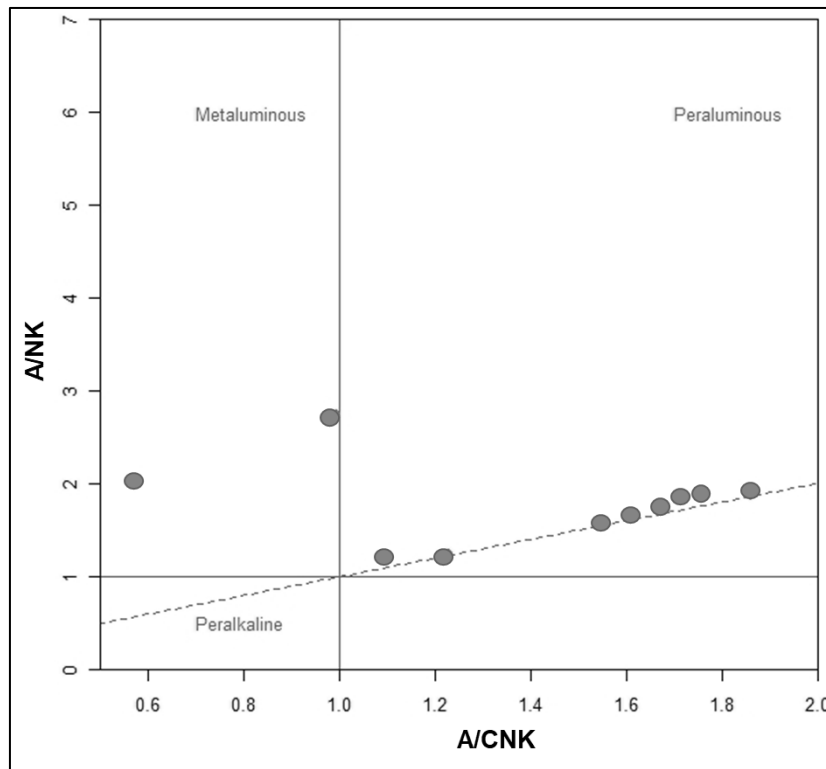


Figure 8.6 A/NK vs. A/CNK plot for granites of study area (after Shand, 1943).

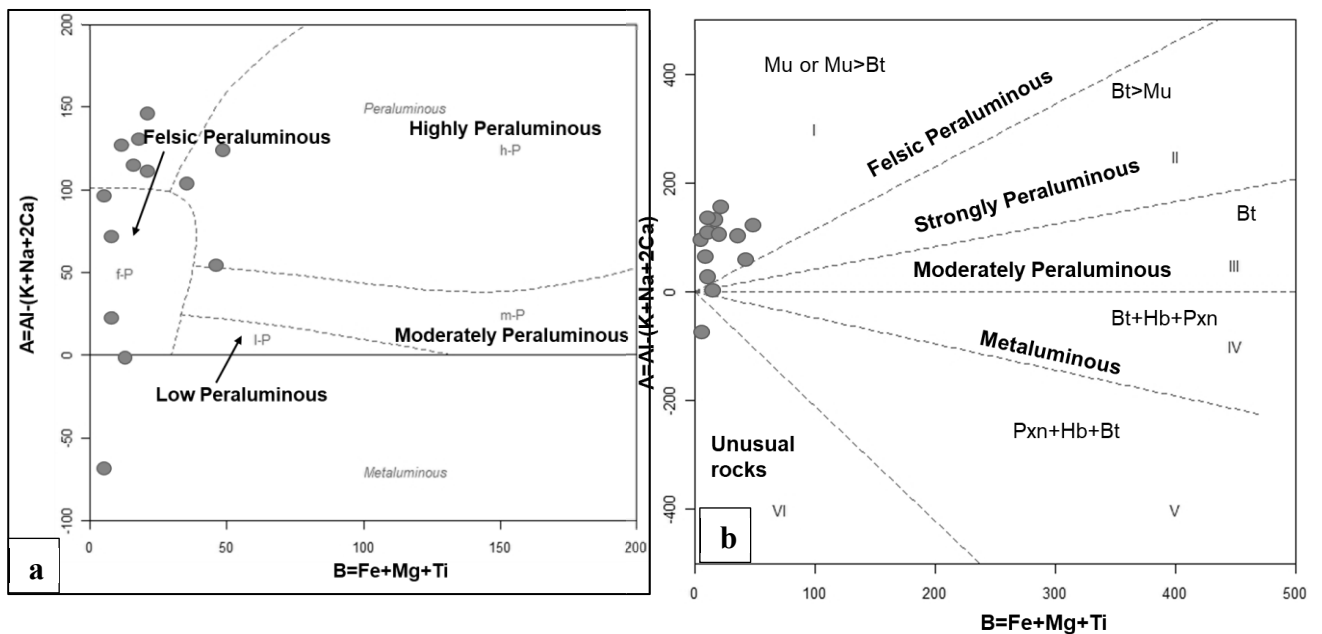


Figure 8.7 a) B-A binary plot for granites of study area (modified after Villaseca et al., 1998)

b) B-A binary plot for granites of study area (after Debon and Le Fort, 1983).

## Trace elements

The trace element composition shows that the concentration of Ni, Cu and Cr are less as compared to normal granites and ranges from 5 to 35ppm (avg. 10.9ppm), (avg. 5ppm), 32 to 83ppm (avg. 51.27ppm) respectively and Zn ranges from 5 to 39 ppm (avg. 10.81 ppm) with moderately high Rb and Ba contents 106-375 ppm (avg. 269 ppm) and 183-769 ppm (avg. 364ppm) respectively (Table 8.4).

The granites from the study area also contain Ga (5 to 16 ppm; avg. 12ppm), Y (5 to 69 ppm; avg. 41.5 ppm), Zr (38 to 216 ppm; avg. 136.27 ppm), Nb (5 to 29 ppm; avg. 13.5 ppm), Pb (5 to 80 ppm; avg. 32.25 ppm), Th (5 to 185 ppm; avg. 54.2 ppm) and U (5 to 405 ppm; avg. 61.2ppm). Uranium content is much higher than normal granites (3.5–5 ppm). Thus, the studied granitoids are characterized by distinct uranium and thorium enrichment. Critical examination of Th/U ratios (ranging from 0.46 to 8) indicates a relatively mixed mineralization in granite samples.

Study of highly incompatible LILE i.e., Rb, Ba and Sr, in granites is also useful to identify the differentiation trends exhibited by magma. Rb is always admitted into K minerals and in micas as it has larger radius than K. Since K is the only major element that Rb can replace, Rb concentration in the melt increases with differentiation. Sr, on the other hand, can replace two major elements: Ca and K. Sr can be admitted to Ca minerals (on account of its higher radius) or captured by K minerals (on account of its higher charge) (Haruna et al., 2013). The composition of studied samples has shown that admittance in place of Ca is the dominant process of removal of Sr from the magma. Hence, with progressive crystallization, Sr is systematically depleted in the melt. Ba cannot replace Ca or Na because of its large radius (1.34Å). The only major element of comparable ionic size is K, and so, on account of its (Ba) higher charge, Ba is captured by K compounds (Haruna et al., 2013). Therefore, it appears in

biotite and potash feldspar. On the other hand, Zr is a classical incompatible element, not readily substituting major mantle phases.

Table 8.4 Trace element data(ppm) of the granites of study area.

Sample Id	LNJB -1/Gr	LNJB -2/Gr	LNJB /Gr/4	GVD /Gr/1	GVD /Gr/2	LNJB /Gr/1	LNJB /Gr/2	LNJB /Gr/3	LNJV /Gr/1	LNJB /GRP/1	LNJB/ UC/1
Cr	54	64	37	34	53	45	72	48	42	32	83
Ni	5	5	5	5	5	5	5	11	35	16	23
Cu	5	5	5	5	5	5	5	5	5	5	5
Zn	10	10	10	5	5	5	5	5	39	13	12
Ga	10	12	13	13	12	14	12	5	16	15	10
Rb	334	308	278	282	276	347	169	106	375	356	125
Sr	79	26	61	88	113	138	45	40	114	147	24
Y	65	38	62	69	36	65	5	11	58	43	5
Zr	152	94	148	216	207	50	70	38	160	174	190
Nb	29	16	21	13	5	25	5	5	20	5	5
Ba	362	189	227	350	537	682	271	183	202	769	233
Ce	29	36	54	120	471	74	69	111	64	74	71
Pb	22	30	57	80	22	25	13	31	50	22	5
Th	49	32	185	88	40	5	21	27	47	35	68
U	13	51	405	39	5	5	11	56	64	5	20
K/Rb	0.0145	0.0141	0.0147	0.0159	0.0181	0.0159	0.0147	0.0137	0.0102	0.0182	0.0189
Rb/Sr	4.228	11.846	4.557	3.205	2.442	2.514	3.756	2.650	3.289	2.422	5.208
Ba/Rb	1.084	0.614	0.817	1.241	1.946	1.965	1.604	1.726	0.539	2.160	1.864
Ba/Sr	4.582	7.269	3.721	3.977	4.752	4.942	6.022	4.575	1.772	5.231	9.708

Table 8.5 Pearson correlation coefficients of trace elements in Govardhanagiri-L.Banda granites

	Cr	Ni	Zn	Ga	Rb	Sr	Y	Zr	Nb	Pb	Ba	Ce	Th	U
Cr	1													
Ni	0.07	1.00												
Zn	-0.13	0.82	1.00											
Ga	-0.40	0.23	0.47	1.00										
Rb	-0.59	0.07	0.35	0.75	1.00									
Sr	-0.63	0.15	0.12	0.57	0.75	1.00								
Y	-0.61	-0.09	0.22	0.50	0.71	0.45	1.00							
Zr	-0.04	0.28	0.22	0.28	0.15	0.14	0.36	1.00						
Nb	-0.18	-0.09	0.27	0.24	0.47	0.06	0.80	0.04	1.00					
Pb	-0.65	-0.04	0.19	0.28	0.27	0.08	0.64	0.28	0.32	1.00				
Ba	-0.40	-0.13	-0.28	0.33	0.52	0.81	0.05	-0.11	-0.25	-0.23	1.00			
Ce	0.04	-0.15	-0.18	-0.07	-0.14	0.13	-0.02	0.43	-0.25	-0.03	-0.02	1.00		
Th	-0.18	-0.02	0.06	0.07	-0.05	-0.21	0.37	0.49	0.27	0.54	-0.35	-0.02	1.00	
U	-0.25	-0.10	0.09	0.06	-0.04	-0.25	0.30	0.10	0.33	0.47	-0.38	-0.12	0.88	1

The trace element correlation data (Table 8.5) shows that Nb is having positive correlation with Rb, Y, U, Th and Zr. U is having positive correlation with Y and Nb. Ba is having positive correlation with Ga, Rb and Sr suggesting its substitution in feldspar. The predominance of Rb over Sr (avg. Rb/Sr ratio-4.19), relatively low CaO and Sr, high K<sub>2</sub>O, Al<sub>2</sub>O<sub>3</sub> and Rb and high average differentiation index (106.9) indicate their S-type signature. This is corroborated by the normal to strongly differentiated trend shown by granitoids in Rb-Ba-Sr diagram which is in accordance with high Rb/Sr ratio (Figure 8.8). The K/Rb ratio in the studied granites vary from 101.5-188.5 with average 153.5 can be correlated with that of S and Felsic S-type (Chappell, 1999) implicating the S type nature. The binary plots of Na<sub>2</sub>O vs. K<sub>2</sub>O (Figure 8.9a) and CaO vs FeOt (Figure 8.9b) (Chappell and White, 2001) also shows S-type nature of these granites.

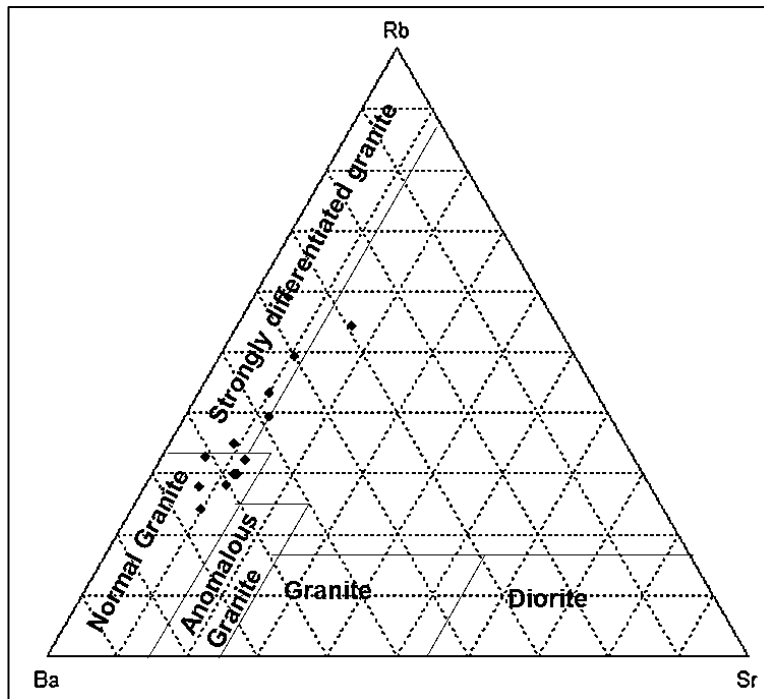


Figure 8.8 Rb-Ba-Sr ternary plot for granites of study area

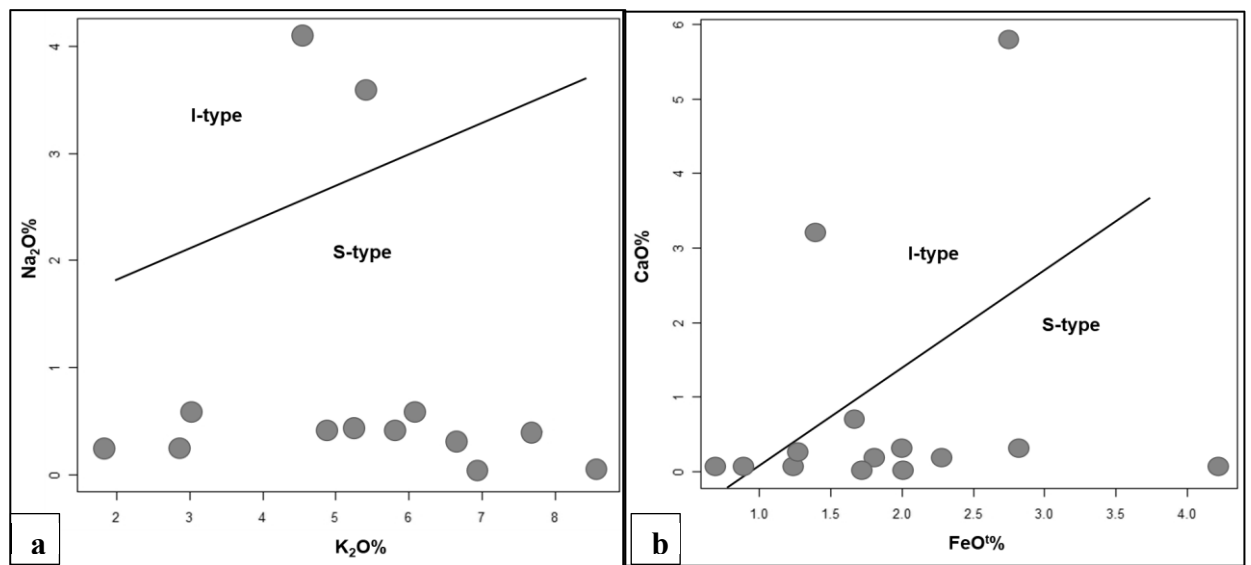


Figure 8.9 a)  $\text{Na}_2\text{O}$ - $\text{K}_2\text{O}$  binary plot for granites of study area (after Chappell and White, 2001)  
 b)  $\text{CaO}$ - $\text{FeO}_t$  binary plot for granites of study area (after Chappell and White, 2001)

The studied granite samples have indicated generation of its parent magma dominantly by partial melting of greywacke source with subordinate contribution from shale in modified Rb/Sr vs. Rb/Ba diagram (Figure 8.10a) (Sylvester, 1998, Dahlquist et al., 2007 and GaO et al., 2011). The magma genesis at greater depths (>30 Km) as indicated by Rb-Sr diagram (Condie, 1986) of these granite accounts a deeper zone for partial melting for rock may be associated with a collisional tectonic setting (Figure 8.10b).

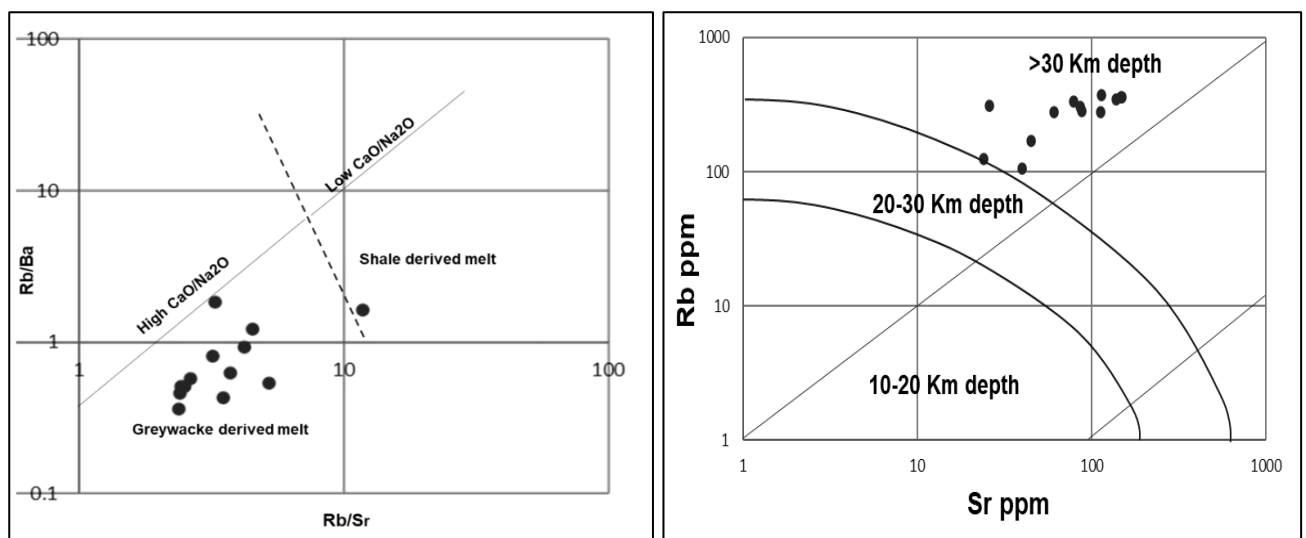


Figure 8.10 a) Discrimination diagram for partial melt source for granites of study area (after Sylvester 1998) b) Rb-Sr plot for depth of generation for granites of study area (after Condie, 1986).

### Tectonic and Geodynamic implications

The granitoids of the study area dominantly plots in the field of syn-collision (syn-COLG) in the geo-tectonic discrimination diagram based on the multi cationic  $R_1$ - $R_2$  factors such as  $R_1=4Si-11(Na+K)-2(Fe+Ti)$  and  $R_2= 6Ca+2Mg+Al$ ; proposed by De la Roche et al.(1980) and modified by Batchelor and Bowden (1985)(Figure 8.11).

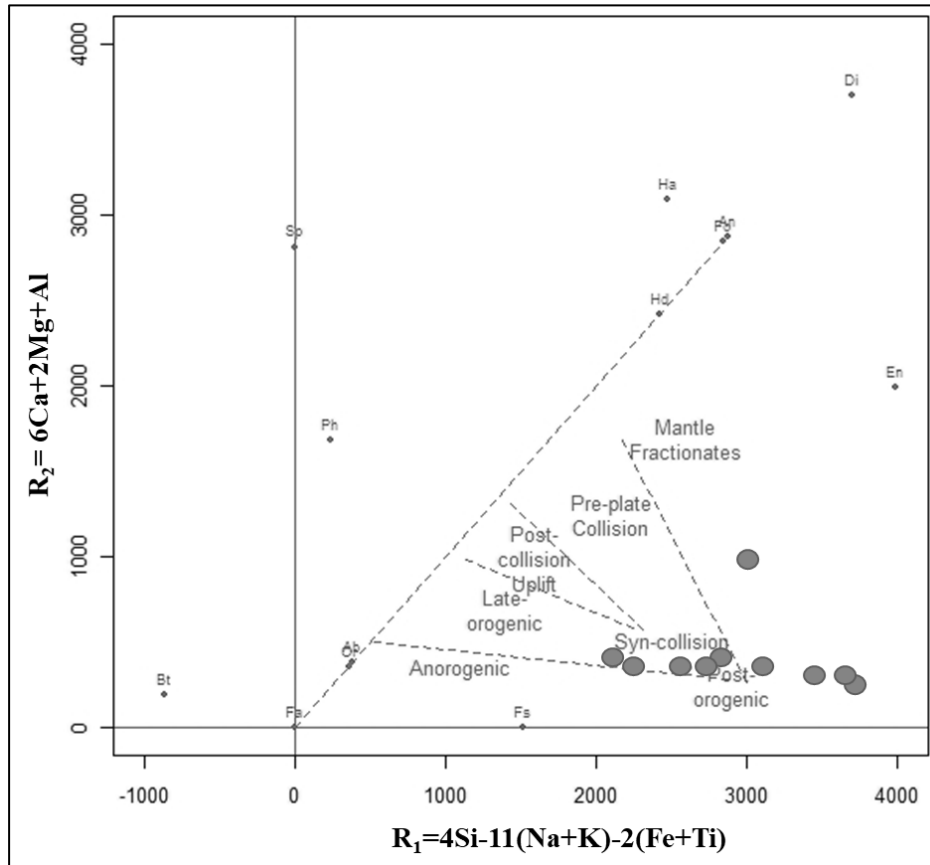


Figure 8.11 Geo-tectonic discrimination diagram for granites of study area (after Batchelor and Bowden, 1985).

## Rare Earth Element distribution in Govardhanagiri-L.Banda granites

The REE data of selected samples (n=8) have been studied to understand the distribution and pattern of REE abundance and their petrogenetic significance. These granites show moderate abundance and distribution pattern of REE ( $\Sigma$ REE 91-238.05 ppm) where the total abundance of REE is more than Clarke's value (189.80ppm) (Clarke, 1924) for average abundance in granite. The representative REEs (n=8) (Table 8.6) shows that the granites are more enriched in LREEs than HREEs. The  $\Sigma$ LREE content in all the samples ranges from 48 to 176 (avg. 122.13) whereas  $\Sigma$ HREEs varies from 29.15 to 61.55 (avg. 46.34). The high level of enrichment of LREE relative to HREE suggests high order of fractionation. Such enrichment is commonly recorded in Precambrian Basement Complexes (Odewumi et al., 2013). The chondrite normalized REE pattern of the granites of study area is presented as Figure 8.12. The ratio of  $(La/Yb)_N$  quantifies the inclination of the curves as it is greater than or equal to 1, the curves of LREE inclines to right side and it means that samples are rich in LREE and low in HREE.

	La	Ce	Pr	Nd	Sm	Eu	Gd	Tb	Dy	Ho
<b>Min</b>	14	20	2.5	9	2.5	0.25	3	1.5	3	1.5
<b>Max</b>	49	81	9	34	8	0.7	9	1.5	7	1.5
<b>Avg.</b>	33.75	53.75	5.68	23.75	5.18	0.39	5.87	1.5	4.62	1.5
	Er	Tm	Yb	Lu	Y	$\Sigma$ REE	$\Sigma$ LREE	$\Sigma$ HREE	$(\Sigma$ LREE / $\Sigma$ HREE)	$(\Sigma$ LREE / $\Sigma$ HREE) <sub>N</sub>
<b>Min</b>	1.5	1.5	0.9	0.25	14	91	48	29.15	1.12	0.67
<b>Max</b>	3	1.5	2.9	0.7	36	238.05	176	61.55	5.97	2.56
<b>Avg.</b>	2.25	1.5	1.79	0.306	27	168.86	122.13	46.34	2.75	1.50
	$(La/Yb)_N$	$(La/Sm)_N$	$(La/Lu)_N$	$(Ce/Yb)_N$	$(Ce/Sm)_N$	$(Eu/Yb)_N$	$(Gd/Lu)_N$	$(Gd/Yb)_N$	$(Eu/Eu^*)_N$	$(Ce/Ce^*)_N$
<b>Min</b>	6.04	3.06	4.57	3.22	1.64	0.30	1.49	1.69	0.10	0.70
<b>Max</b>	34.51	5.51	19.60	20.15	3.00	2.34	4.71	4.70	0.32	0.87
<b>Avg.</b>	13.89	3.91	12.47	8.23	2.29	0.77	2.74	2.95	0.23	0.80

The normalized  $(LREE/HREE)_N$  ratio ranges from 0.67 to 2.56(avg.1.50).The ratios of  $(La/Yb)_N$  and  $(Gd/Yb)_N$  are used to measure the degree of LREE and HREE fractionation respectively. The degree of LREE fractionation,  $(La/Yb)_N$  of 13.89, is slightly higher than that

of HREE fractionation,  $(Gd/Yb)_N$  of 2.95. This is also evident by the presence of significant amount of monazite in these granites.

Large negative Eu anomalies ( $Eu/Eu^* < 0.60$ ; i.e. 0.10-0.32) are recorded in the granites of the study area (Table 8.6 and Figure 8.12). Besides, feebly negative to positive Ce anomalies ( $Ce/Ce^*=0.70-0.87$ ) indicate enrichment of LREE and points toward the presence of Ce-rich monazite in the residual phase. The depletion or enrichment of Ce and Eu usually occurs in the natural environment, which may be linked to their oxidation state and mobility under different oxidation-reduction conditions (Semhi et al., 2009).  $Ce^{3+}$  is more easily oxidized to  $Ce^{4+}$  with higher oxygen fugacity and is much less mobile resulting in positive Ce anomaly ( $\delta Ce > 1$ ). Eu is an incompatible element in the trivalent form ( $Eu^{3+}$ ) in an oxidizing magma, but is preferentially incorporated into plagioclase in its divalent form ( $Eu^{2+}$ ) in a reducing magma. This ion-exchange process is the basis of the negative Eu anomaly ( $\delta Eu < 1$ ). The Eu anomalies are chiefly controlled by plagioclase. Thus, removal of plagioclase from a felsic melt by crystal fractionation or partial melting of a rock in which plagioclase is retained in the source will give way to negative Eu anomaly.

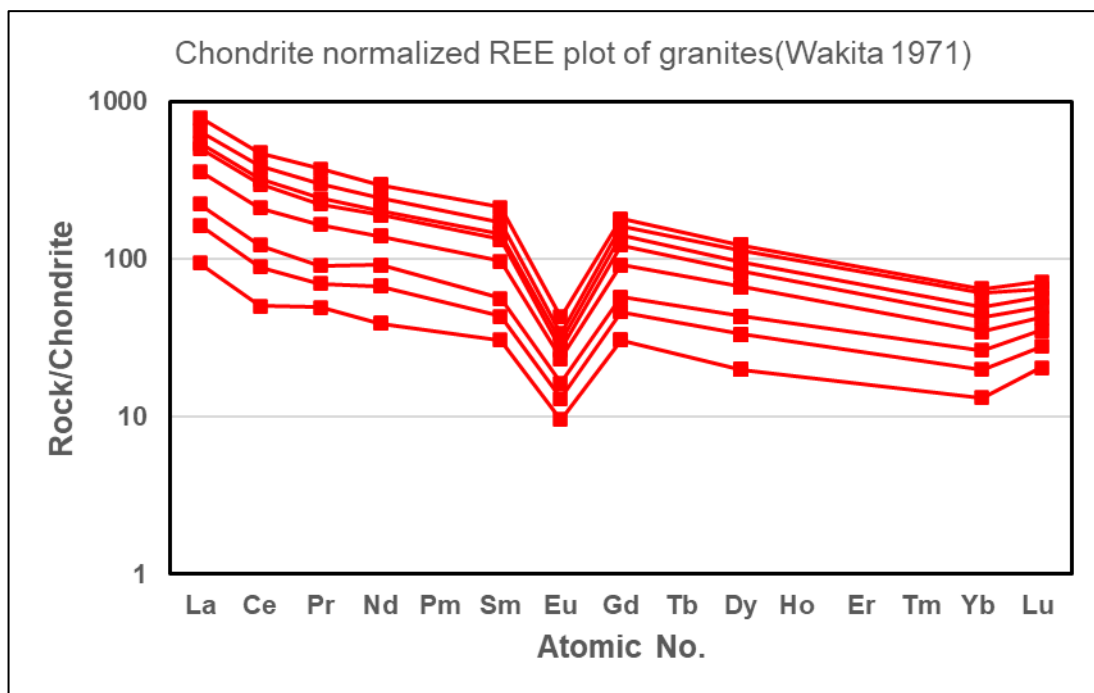


Figure 8.12 Chondrite normalized REE plot of Govardhanagiri-L.Banda granites.

### 8.3 Geochemistry of Dolerite dykes from Govardhanagiri area

Prior to any interpretation of representative geochemical data, it is necessary to identify the effect of post-emplacement alteration processes on the whole-rock chemistry. To elucidate the nature and the extent of migration of these alkali elements, samples were plotted in  $\text{CaO}/\text{Al}_2\text{O}_3$ – $\text{MgO}/10$ – $\text{SiO}_2/100$  ternary diagram (Figure 8.13) of Schweitzer and Kroner (1985). It is evident from these plots that five dolerite dyke samples fall mainly in “not altered” field and four samples fall in altered field. Large ion lithophile elements (LILE) such as Ba, Rb, Sr etc. except Th generally show mobile nature during secondary alteration effects (Cann 1970; Pearce and Cann 1973; Condie and Sinha 1996). The Rb/Sr ratio, a good indicator of secondary alteration, increases from 0.007 in the least altered samples to 8 in highly altered samples (Lafleche et al. 1992).

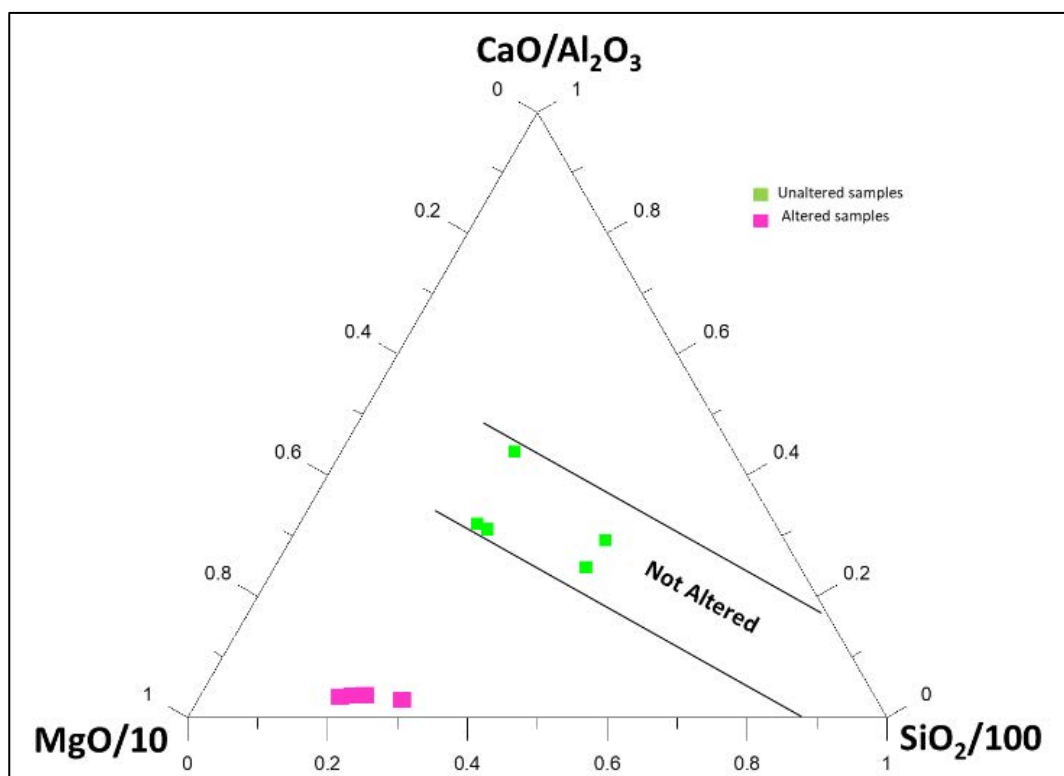


Figure 8.13  $\text{CaO}/\text{Al}_2\text{O}_3$ – $\text{MgO}/10$ – $\text{SiO}_2/100$  ternary diagram (Schweitzer and Kroner 1985).

The present studied five basic samples have lower ratios of Rb/Sr (0.03–0.22) thus indicates that the secondary processes have not altered primary concentrations of LILEs whereas, in four samples the value of Sr is <10 ppm, indicating towards altered nature.

### **Alteration Index**

The alteration index of Hashiguchi et al. (1983):

$$\text{A.I.} = [\text{MgO} + \text{K}_2\text{O} / \text{MgO} + \text{K}_2\text{O} + \text{Na}_2\text{O} + \text{CaO}] \times 100$$

The Hashiguchi index is reliable for most mafic volcanic rocks. For example, the A.I. obtained from compiled data from fresh MORB and arc related mafic volcanic rocks give respectively  $36 \pm 8$  and  $34 \pm 10$ . Chloritization and/or sericitization produce higher A.I. values ( $> 50$ ) whereas A.I. values are much lower than 30 in albitized samples (Lafleche et.al., 1992). The five samples showing low to moderate AI ranging from 34.01 to 47.95 reflect the characteristics of pristine (MORB) and arc related volcanic rocks. Whereas, four samples AI values ranges from 89.25 to 95.16 suggesting intense chloritization, which is also seen in petrographic study.

Table 8.7 Major oxide compositions of the basic rock of Govardhanagiri area (values in wt.%)

Sample Id	GVD/B1/1	GVD/B1/2	LNJB/BD/1A	LNJB/BI/1	LNJB/BD/1	LNJB/BD/2	LNJB/BD/3	LNJB/BD/4	LNJB/BD/5
SiO <sub>2</sub>	47.89	50.08	47.83	55.17	46.84	43.86	46.17	58.3	48.67
TiO <sub>2</sub>	0.91	0.98	1.69	1.41	1.41	1.53	1.26	1.07	0.94
Al <sub>2</sub> O <sub>3</sub>	12.68	12.05	15.47	14.03	13.44	14.38	13.83	12.07	11.91
Fe <sub>2</sub> O <sub>3</sub>	17.28	15.02	13.18	13.64	13.28	14.23	11.36	12.69	16.02
MgO	7.28	6.34	11.15	3.79	14.83	15.6	17	3.31	8.17
MnO	0.22	0.19	0.01	0.11	0.07	0.07	0.09	0.12	0.21
CaO	6.9	10.74	0.67	4.31	1.08	1.13	1.13	4.57	7.31
Na <sub>2</sub> O	3.08	1.93	0.005	2.63	0.9	0.77	0.005	3.31	2.2
K <sub>2</sub> O	0.38	0.19	2.11	1.18	1.61	1.64	1.51	1.37	0.59
P <sub>2</sub> O <sub>5</sub>	0.13	0.16	0.15	0.36	0.67	0.6	0.67	0.85	0.6
LOI	3.21		8.69	3.45	6.9	7.59	6.51	2.08	2.76
Total	99.96	97.68	100.955	100.08	101.03	101.4	99.535	99.74	99.38
Al	43.42	34.01	95.16	41.73	89.25	90.07	94.22	37.26	47.95
Cr	70	133	154	82	124	154	83	48	170
Ni	101	91	71	101	74	86	58	20	102
Cu	147	775	<10	147	<10	<10	<10	77	145
Zn	60	51	24	60	26	43	53	38	87
Ga	15	13	30	14	25	26	21	19	14
Rb	15	12	101	32	84	88	85	36	33
Sr	128	365	<10	182	<10	<10	<10	193	151
Y	24	26	54	62	41	44	41	70	27
Zr	57	81	147	241	128	125	113	298	70
Nb	<10	<10	10	21	<10	<10	<10	25	<10
Pb	11	<10	13	12	15	14	15	11	<10
Ba	72	56	45	427	268	274	682	529	198
Ce	61	<10	76	75	45	43	134	67	15
Th	<10	<10	16	<10	0	0	0	0	0
U	<10	<10	<10	<10	<10	<10	<10	<10	<10
Rb/Sr	0.12	0.03		0.18				0.19	0.22

The CIPW norms of the studied samples, obtained using the standard GCD Kit Software are presented in Table. Rocks anomalous in normative minerals (i.e. corundum) were considered altered (Lafleche et.al., 1992).

Table 8.8 CIPW norm obtained by standard GCD kit software.

	GVD/ B1/1	GVD/ B1/2	LNJB/ BD/1A	LNJB/ BI/1	LNJB/ BD/1	LNJB/ BD/2	LNJB/ BD/3	LNJB/ BD/4	LNJB/ BD/5
Q	6.22	12.29	22.09	21.49	12.91	9.12	14.49	22.15	9.94
C	0.00	0.00	12.32	1.45	9.86	10.72	11.74	0.00	0.00
Or	2.25	1.12	12.47	6.97	9.52	9.69	8.92	8.10	3.49
Ab	26.06	16.33	0.04	22.25	7.62	6.52	0.04	28.01	18.62
An	19.65	23.66	2.34	19.03	0.98	1.69	1.23	14.03	20.88
Di	8.89	20.17	0.00	0.00	0.00	0.00	0.00	0.00	7.02
Hy	14.01	6.44	27.78	9.44	36.94	38.86	42.35	8.25	17.10
Il	0.47	0.41	0.02	0.24	0.15	0.15	0.19	0.26	0.45
Hm	17.28	15.02	13.18	13.64	13.28	14.23	11.36	12.69	16.02
Tn	1.63	1.88	0.00	0.00	0.00	0.00	0.00	2.18	1.73
Ru	0.00	0.00	1.68	1.29	1.33	1.45	1.16	0.05	0.00
Ap	0.31	0.38	0.36	0.85	1.59	1.42	1.59	2.01	1.42
Sum	96.77	97.70	92.28	96.66	94.18	93.85	93.07	97.71	96.66

### Geochemical Characteristics

The studied basic rocks have restricted range of SiO<sub>2</sub> (43.86 - 58.30 wt%). The concentration of other major elements such as; CaO, Na<sub>2</sub>O, K<sub>2</sub>O, Al<sub>2</sub>O<sub>3</sub>, Fe<sub>2</sub>O<sub>3</sub>, MgO, TiO<sub>2</sub>, P<sub>2</sub>O<sub>5</sub> and MnO ranges from (0.67 – 10.74 wt%), (<0.01 - 3.31wt%), (0.19 – 2.11wt%), (11.91 – 15.47wt%), (11.36 – 17.28wt%), (3.31 – 17wt%), (0.91 – 1.69 wt%), (0.13–0.85 wt%) and (0.01–0.22 wt%) respectively.

The triangular TAS diagram (Le Bas et.al., 1986), (Figure 8.14) indicates that the rocks are basaltic and andesitic in nature. In YTC (Y=Y + Zr, Ti=TiO<sub>2</sub> wt%×100, C=Cr) ternary diagram (Davies et al. (1979), most of the studied samples plot along and above the tholeiitic trend (Figure 8.15). The rocks are identified as of being tholeiitic type based on the AFM diagram (Irvine and Baragar, 1971) (Figure 8.16).

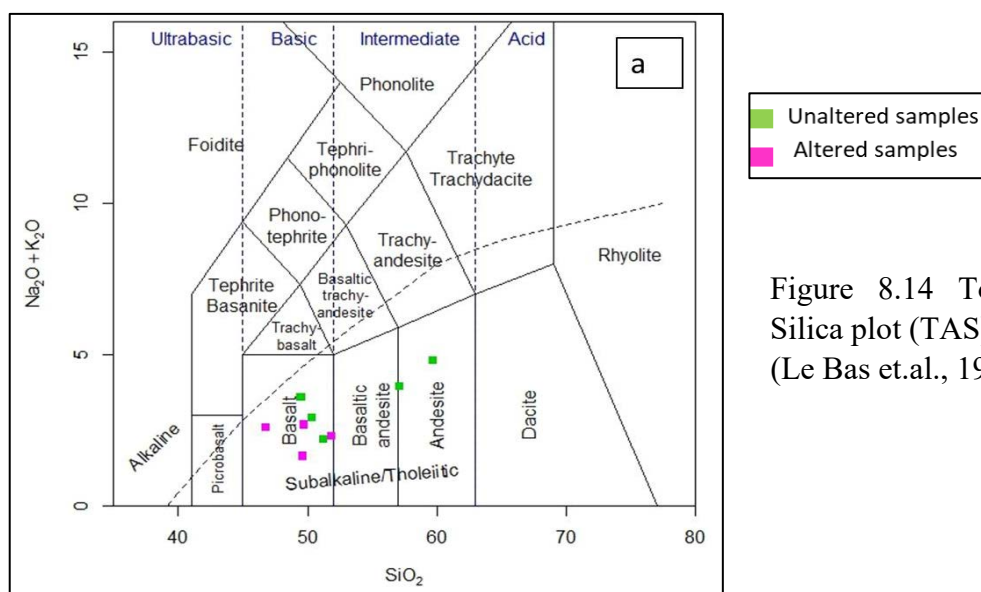


Figure 8.14 Total alkali Silica plot (TAS) (Le Bas et.al., 1986)

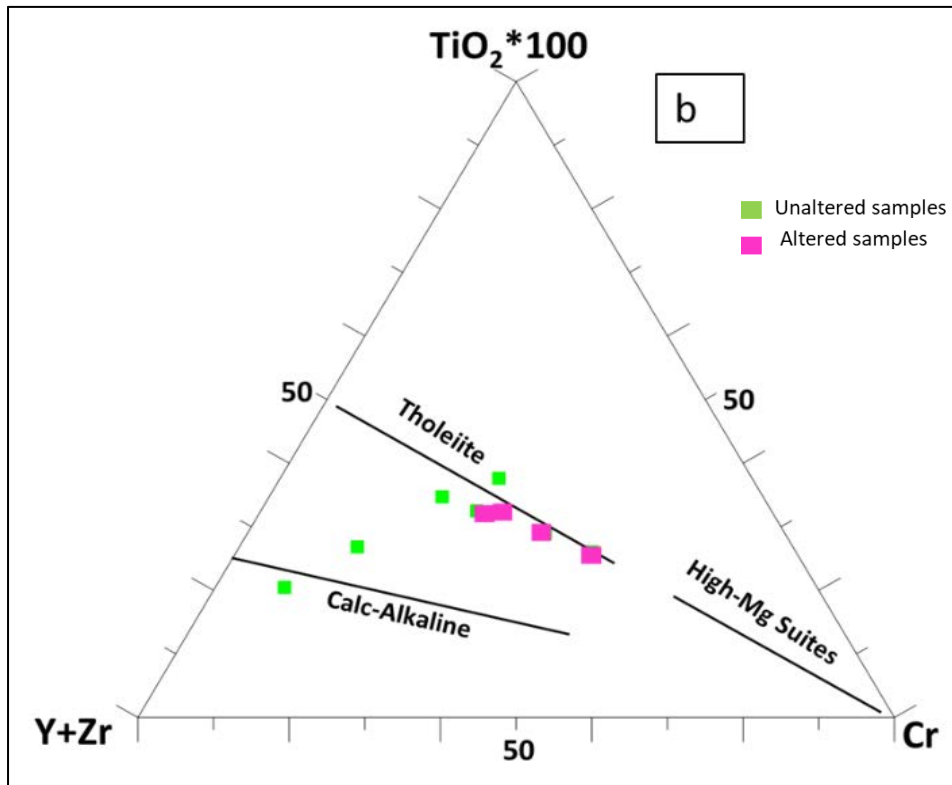


Figure 8.15 Y (Zr + Y) – T (TiO<sub>2</sub> × 100) – C (Cr) ternary plot (after Davis et al. 1979).

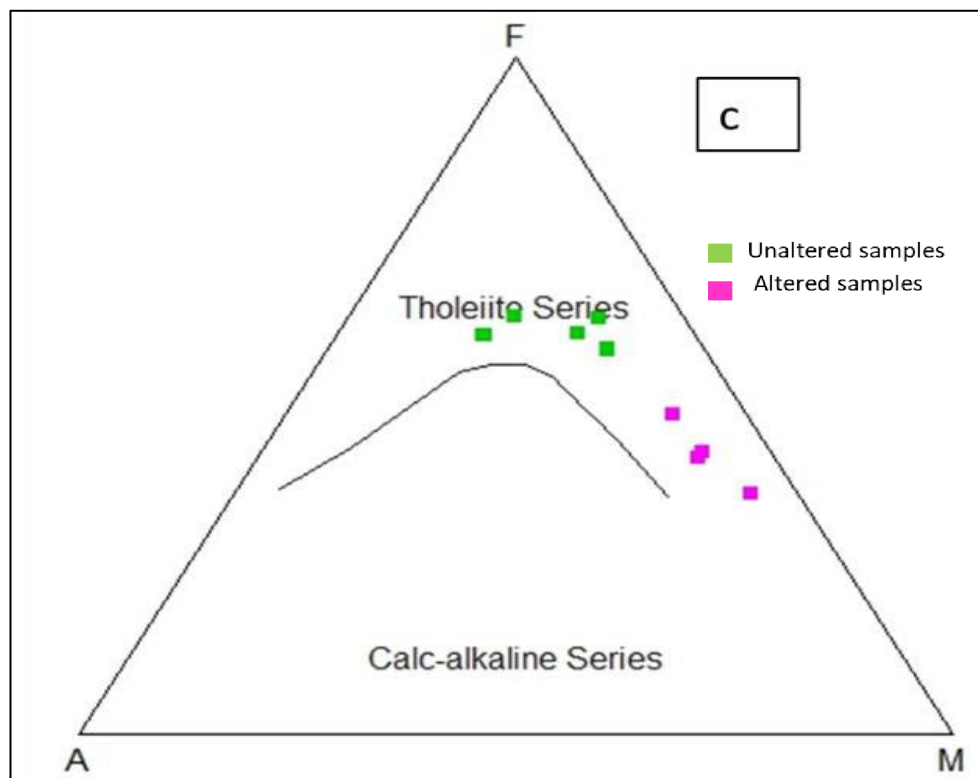


Figure 8.16 AFM classification Scheme (Irvine and Baragar, 1971).

## 8.4 Geochemistry of Gulcheru Quartzite

The quartzite of Gulcheru Formation (n=7) are characterized by high and a relatively narrow range of SiO<sub>2</sub> (76.52–82.61 wt%), dominantly high Al<sub>2</sub>O<sub>3</sub> (11.38 – 12.23 wt%), K<sub>2</sub>O (2.57 – 4.95 wt%), CaO (<0.01 – 0.1 wt%) and moderate Fe<sub>2</sub>O<sub>3</sub>(t) (0.98 – 3.66 wt%). MgO content is generally low (0.2 – 1.2 wt%), TiO<sub>2</sub> content is (0.17 – 0.29 wt%) and P<sub>2</sub>O<sub>5</sub> content is (<0.01 – 0.12 wt%).

Megascopically Gulcheru quartzite grade texturally and compositionally from sub feldspathic arenite to quartz arenite. Geochemical data reflect mineralogically mature nature. High degree of mineralogical maturity is indicated by high SiO<sub>2</sub>, dominantly moderate SiO<sub>2</sub>/Al<sub>2</sub>O<sub>3</sub>, and K<sub>2</sub>O/Na<sub>2</sub>O ratios. Relatively high MgO, Fe<sub>2</sub>O<sub>3</sub>(t) and Al<sub>2</sub>O<sub>3</sub> coupled with low CaO indicate presence of chlorite matrix/cement. The relatively high content of TiO<sub>2</sub> and Zr indicates hydraulic sorting of heavy minerals (anatase/rutile and zircon respectively) during recycling/reworking.

Table 8.9 Major element oxide data (%) of Gulcheru quartzite samples.

Sample Id	LNJB-3/GQ	GVD/GQ/1	GVD/GQ/2	GVD/GQ/3	LNJB/GQ/1	LNJB/GQ/2	LNJB/RUC/2
SiO <sub>2</sub>	76.52	79.52	82.28	78.51	82.61	79.05	78.44
TiO <sub>2</sub>	0.29	0.18	0.17	0.22	0.17	0.23	0.19
Al <sub>2</sub> O <sub>3</sub>	12.22	11.8	11.65	12.23	11.38	11.44	12.1
Fe <sub>2</sub> O <sub>3</sub>	2.77	2.48	0.98	1.36	2.24	3.66	1.87
MgO	0.55	0.2	1.1	1.32	0.6	0.62	0.62
MnO	<0.01	0.01	<0.01	<0.01	<0.01	<0.01	<0.01
CaO	0.1	0.02	0.03	0.07	<0.01	<0.01	<0.01
Na <sub>2</sub> O	0.38	0.61	0.64	0.6	0.54	0.34	0.4
K <sub>2</sub> O	3.97	4.06	2.69	4.92	2.57	4.24	4.95
P <sub>2</sub> O <sub>5</sub>	0.12	<0.01	<0.01	0.05	<0.01	<0.01	0.01
Total	96.92	98.88	99.54	99.28	100.11	99.58	98.58
CIA	71.73	68.52	74.41	65.93	75.63	68.97	66.85
CIW	93.81	91.90	91.32	91.65	92.69	95.27	94.77
PIA	90.76	87.69	88.75	86.10	90.55	92.34	91.00
ICV	0.71	0.66	0.66	0.89	0.60	0.82	0.75

Table 8.10 Trace element (ppm) data of Gulcheru quartzite samples.

Sample Id	LNJB-3/GQ	GVD/GQ/1	GVD/GQ/2	GVD/GQ/3	LNJB/GQ/1	LNJB/GQ/2	LNJB/RUC/2
Cr	54	71	62	40	88	61	55
Ni	5	10	5	11	44	16	25
Cu	<10	<10	<10	<10	<10	<10	<10
Zn	<10	<10	<10	<10	14	<10	22
Ga	<10	<10	<10	<10	10	10	11
Rb	124	96	101	150	113	144	223
Sr	49	52	73	54	31	49	57
Y	<10	<10	<10	<10	15	11	18
Zr	230	90	102	201	124	212	159
Nb	12	<10	<10	<10	<10	<10	<10
Ba	758	958	462	838	372	668	668
Ce	28	38	99	183	34	53	16
Pb	13	22	21	16	10	18	18
Th	16	23	17	15	43	16	17
U	10	<10	<10	<10	<10	<10	11

Table 8.11 Correlation coefficient of major oxides and selective trace elements.

	SiO <sub>2</sub>	TiO <sub>2</sub>	Al <sub>2</sub> O <sub>3</sub>	Fe <sub>2</sub> O <sub>3</sub>	MgO	CaO	Na <sub>2</sub> O	K <sub>2</sub> O	P <sub>2</sub> O <sub>5</sub>	Cr	Ni	Rb	Sr	Zr	Ba	Ce	Pb	Th
SiO <sub>2</sub>	1																	
TiO <sub>2</sub>	-0.83	1.00																
Al <sub>2</sub> O <sub>3</sub>	-0.76	0.51	1.00															
Fe <sub>2</sub> O <sub>3</sub>	-0.38	0.48	-0.30	1.00														
MgO	0.15	-0.03	0.23	-0.66	1.00													
CaO	-0.59	0.76	0.72	-0.13	0.30	1.00												
Na <sub>2</sub> O	0.58	-0.62	-0.07	-0.73	0.35	0.00	1.00											
K <sub>2</sub> O	-0.80	0.39	0.68	0.16	0.04	0.20	-0.38	1.00										
P <sub>2</sub> O <sub>5</sub>	-0.71	0.88	0.68	0.12	0.08	0.93	-0.31	0.23	1.00									
Cr	0.69	-0.53	-0.78	0.23	-0.56	0.58	0.15	0.74	-0.48	1.00								
Ni	0.46	-0.44	-0.48	0.10	-0.21	0.59	-0.11	0.27	-0.42	0.65	1.00							
Rb	-0.43	0.10	0.42	-0.02	0.11	0.17	-0.53	0.70	-0.03	0.46	0.23	1.00						
Sr	-0.02	-0.12	0.29	-0.54	0.43	0.12	0.28	0.12	-0.08	0.53	0.72	0.07	1.00					
Zr	-0.74	0.88	0.43	0.44	0.21	0.55	-0.71	0.53	0.68	0.61	0.20	0.39	0.18	1.00				
Ba	-0.72	0.38	0.60	0.21	-0.23	0.38	-0.02	0.74	0.32	0.52	0.56	0.07	0.13	0.23	1.00			
Ce	0.06	-0.02	0.26	-0.54	0.86	0.36	0.54	0.17	0.06	0.57	0.35	0.11	0.34	0.14	0.15	1.00		
Pb	0.02	-0.33	0.02	-0.18	-0.04	0.25	0.30	0.22	-0.43	0.24	0.59	0.05	0.76	-0.42	0.42	0.12	1.00	
Th	0.64	-0.48	-0.59	0.05	-0.31	0.41	0.23	0.63	-0.33	0.88	0.83	0.33	0.73	-0.46	-0.53	-0.32	-0.56	1.00

### **Provenance and depositional environment**

Chemical composition of Gulcheru quartzite is mostly controlled by the source rock from which the erosion, deposition and diagenetic processes lead to development of this sedimentary rocks. Provenance erosion is controlled by tectonics and finally deposited and preserved portions of the detritus can give insight into the provenance setting. Apart from the major elements it is often observed that trace element content increases in clayed portions compared to the quartz rich arenite portions. Therefore, trace elements concentration can give ideas on paleo weathering and erosion time span, topography and distance between the source and deposition area, styles and agents of transportation etc. In this context inter elemental relationship (Table 8.11) can give significant information on depositional processes due to the geochemical association of some elements with similar properties as well as markedly different characteristics with opposite behaviors of some elements.

Since different tectonic condition have their own characteristic provenance set up with typical sedimentation processes, geochemical signatures of sedimentary rocks will be different from back arc, fore arc, inter arc basins, active and passive margins collisional or rift settings.

After plotting the data in the  $Al_2O_3$  versus  $TiO_2$  (Figure 8.17a) bivariate discrimination diagram (McLennan SM et al.,1990) the samples plot in the alkali granite- granite field. Another bivariate  $TiO_2$  versus Ni (ppm) diagram (Figure 8.17b) to evaluate source rock composition (Floyd PA et al., 1989) indicate this mature sandstone are derived from acidic igneous rocks. The bivariate plot (after Bhatia, 1983) is also used to make out about the possible tectonic settings. The bivariate plot (Figure 8.17c) represents passive margin setting.

$TiO_2$  and Zr concentrations in siliciclastic rocks are good indicators of source rock. Hayashi et al. (1997) have devised a scheme for discriminating the source of sedimentary rocks on the basis of  $TiO_2$  /Zr weight ratios. As per that scheme of discrimination, the  $TiO_2$  /Zr weight ratios

in the studied quartzite samples indicate their derivation dominantly from felsic igneous rocks (Figure 8.17d).

The influence of climatic conditions on the chemical maturity of sandstone can be studied, and thereby the prevalent palaeoclimatic conditions during provenance weathering can be deciphered, using  $\text{SiO}_2$  vs.  $(\text{Al}_2\text{O}_3 + \text{K}_2\text{O} + \text{Na}_2\text{O})$  bivariate plot (Suttner and Dutta, 1986). The plots of quartzites in  $\text{SiO}_2$  vs.  $(\text{Al}_2\text{O}_3 + \text{K}_2\text{O} + \text{Na}_2\text{O})$  (Figure 8.18) binary space apparently (ignoring the effect of reworking/recycling) indicate derivation of the precursor sediments dominantly under a semi-arid palaeoclimatic condition.

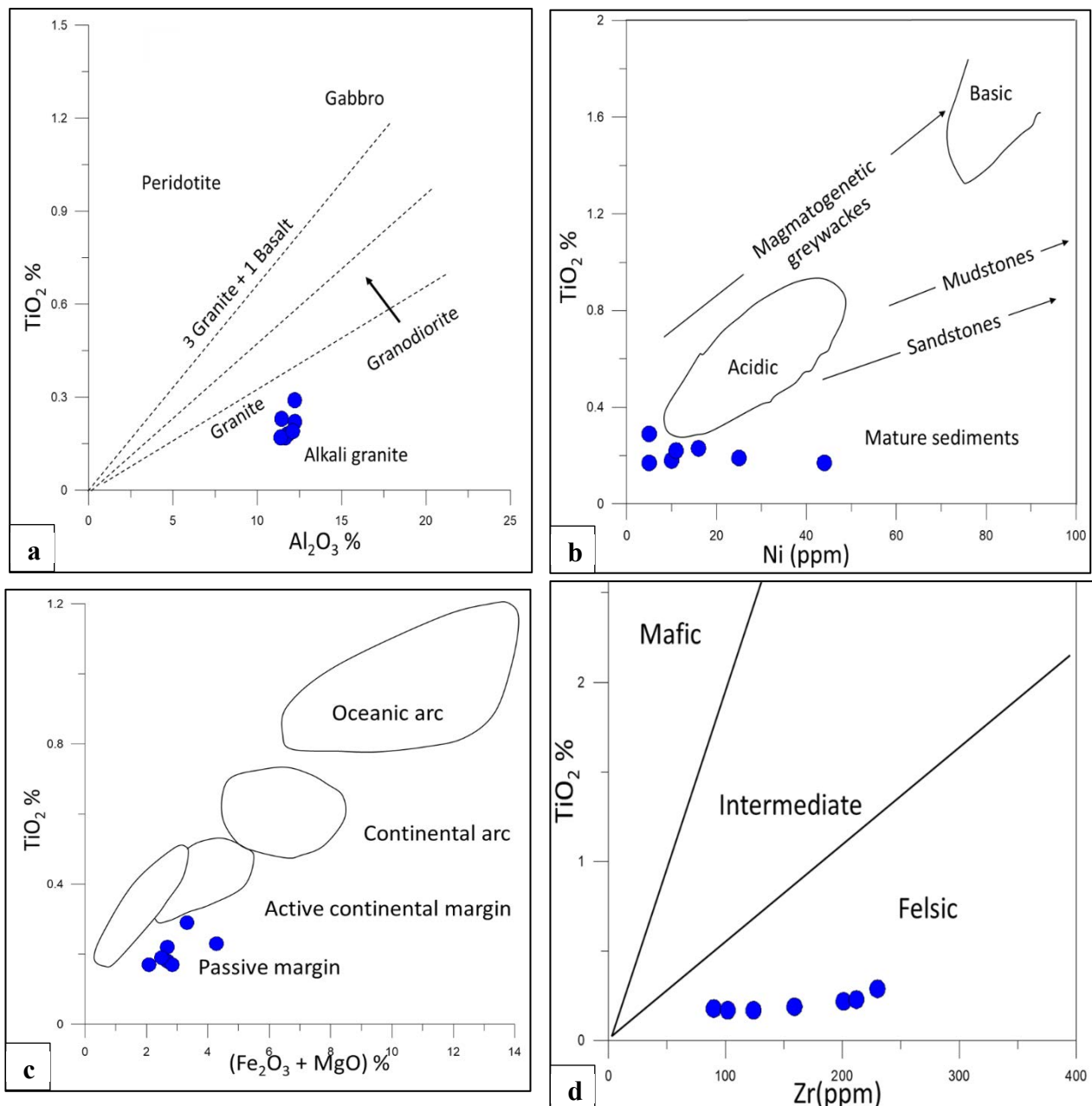


Figure 8.17: a)  $\text{Al}_2\text{O}_3$  versus  $\text{TiO}_2$  bivariate discrimination diagram (McLennan SM et al., 1990) b)  $\text{TiO}_2$  versus Ni (ppm) bivariate diagram (Floyd PA et al.,1989) c)  $\text{TiO}_2$  versus  $(\text{Fe}_2\text{O}_3+\text{MgO})$  diagram (after Bhatia, 1983) d) Zr vs.  $\text{TiO}_2$  plot (after Hayashi et al., 1997)

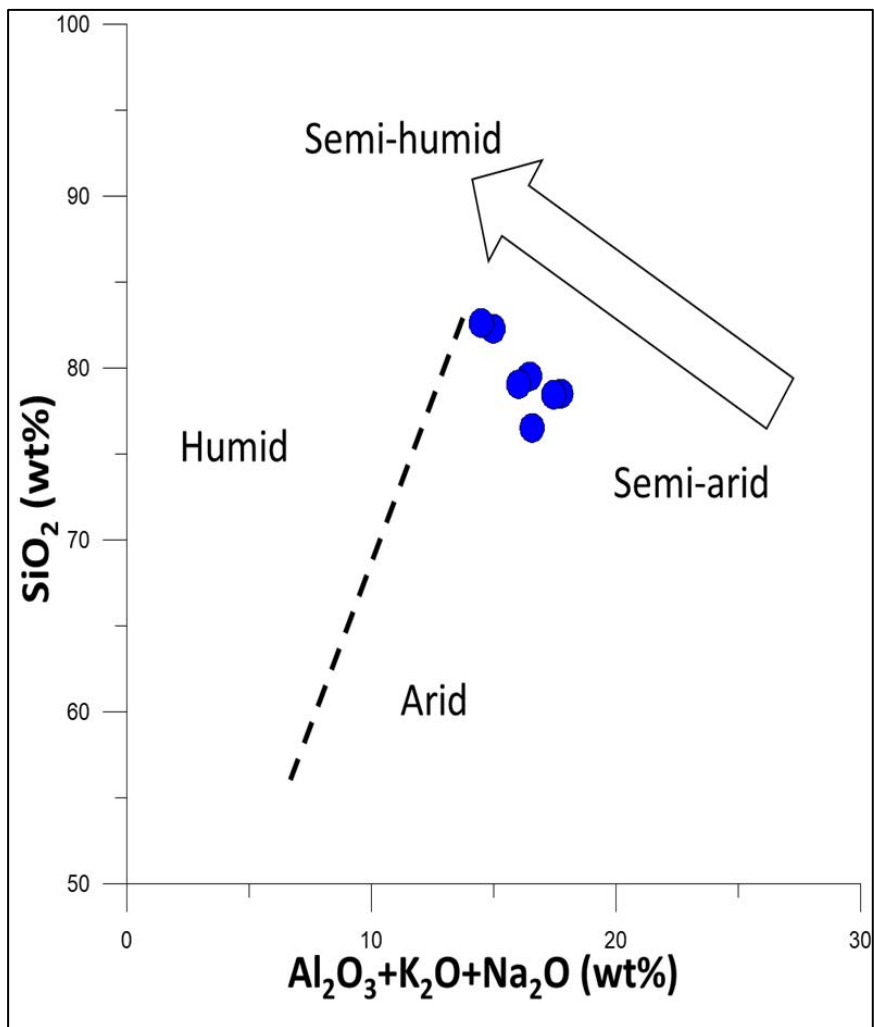


Figure 8.18  $\text{SiO}_2$  and  $(\text{Al}_2\text{O}_3 +\text{K}_2\text{O}+\text{Na}_2\text{O})$  (after Suttner and Dutta, 1986).

## Source area weathering

The intensity and period of weathering in clastic sedimentary rocks can be estimated by examining the association between alkali and alkaline elements. Nesbitt and Young (1982), defined the Chemical Index of Alteration (CIA) formulae to calculate the amount of chemical weathering

$$\text{CIA} = [\text{Al}_2\text{O}_3 / (\text{Al}_2\text{O}_3 + \text{CaO} + \text{Na}_2\text{O} + \text{K}_2\text{O})] \times 100. \quad (1)$$

Oxides are in molar proportions and CaO represents the Ca in silicate fractions only. CIA values are of ~50 for unweathered igneous rocks to near 100 for residual clays (initial 50–60, intermediate 60–80 and extreme >80; Nesbitt and Young 1982; Fedo et al. 1995). The CIA values in the Gulcheru Quartzite range from 65.93 – 75.63 (avg. 70.29) (Table 8.9), suggestive moderate chemical weathering in the source area.

The CIA values are also plotted in  $\text{Al}_2\text{O}_3$ –(CaO+Na<sub>2</sub>O)–K<sub>2</sub>O triangular plot (Nesbitt and Young 1984; Fedo et al. 1995; commonly referred as the ‘A–CN–K’ diagram) to categorize the provenance composition and weathering trends. The concept behind the use of this diagram is to understand the rate of weathering of plagioclase (Ca–Na feldspar) and K-feldspar. Thus, during weathering, CaO and Na<sub>2</sub>O are preferentially leached relative to K<sub>2</sub>O due to which the weathering trend moves parallel to the A–CN join. Intense weathering of a rock removes CaO, Na<sub>2</sub>O and K<sub>2</sub>O, making the trend parallel to the A–K join.

The studied samples of Gulcheru Quartzite are plotted in the A–CN–K ternary diagram (Figure 8.19c) in which majority of the samples are plotted above the feldspar tie line and samples at right of the five trend line towards K-feldspar, which suggest that these samples might have suffered minor amount of K-metasomatism. To ascertain the presence or absence of post-depositional K-metasomatism, we have carried out petrographic and geochemical assessment.

The higher content of K<sub>2</sub>O and Rb and sericitization of plagioclase is also suggestive of post-depositional K-metasomatism (Figure 8.19c). On the basis of weathering trends of the studied samples, it has been suggested that samples have undergone moderate chemical weathering, which could be due to either differential weathering conditions or that the least weathered samples are representative of source rock.

Harnois (1988) emphasized that K should not be used as an index of weathering since it shows no consistent behavior during weathering, being either enriched in the weakly weathered residue or depleted under more intense weathering conditions, and could also be re-enriched by forming K-minerals (e.g., illite) during post-depositional, K-metasomatic diagenesis (Maynard, 1992). Chemical Index of Weathering (CIW) of Harnois (1988) is also used to assess intensity of chemical weathering. It is considered as a better index than CIA because it does not include K<sub>2</sub>O content and thus eliminate the possibility of K-metasomatism. It is calculated as:

$$\text{CIW} = [\text{Al}_2\text{O}_3/\text{Al}_2\text{O}_3 + \text{CaO}^* + \text{Na}_2\text{O}] \times 100$$

CIW values of the Gulcheru Quartzite range from 91.32 – 95.27 (avg. 93.06). CIW indices are higher than CIA values for some analysed samples due to exclusion of K<sub>2</sub>O from the index. On the basis of CIW, the studied sediments show intense weathering.

Fedo et al. (1995) suggested a correction to CIW calculations based on the Al content in K-feldspar, otherwise fresh K-rich rocks will have misleadingly high CIW values, and this is referred to as PIA (plagioclase index of alteration). In this, all oxides are expressed in molecular proportions

$$\text{PIA} = [(\text{Al}_2\text{O}_3 - \text{K}_2\text{O})/(\text{Al}_2\text{O}_3 + \text{CaO} + \text{Na}_2\text{O} - \text{K}_2\text{O})] \times 100 \quad (3)$$

PIA values of ~50 for fresh rocks and values similar to 100 designate considerable productions of secondary aluminous clay minerals (Fedo et al. 1997). The PIA value of Gulcheru Quartzite

is 86.10 – 92.34 (avg. 89.60). Like CIA, A–CN–K ternary diagram and CIW, the range of PIA values of all these quartzites also suggest intense chemical weathering.

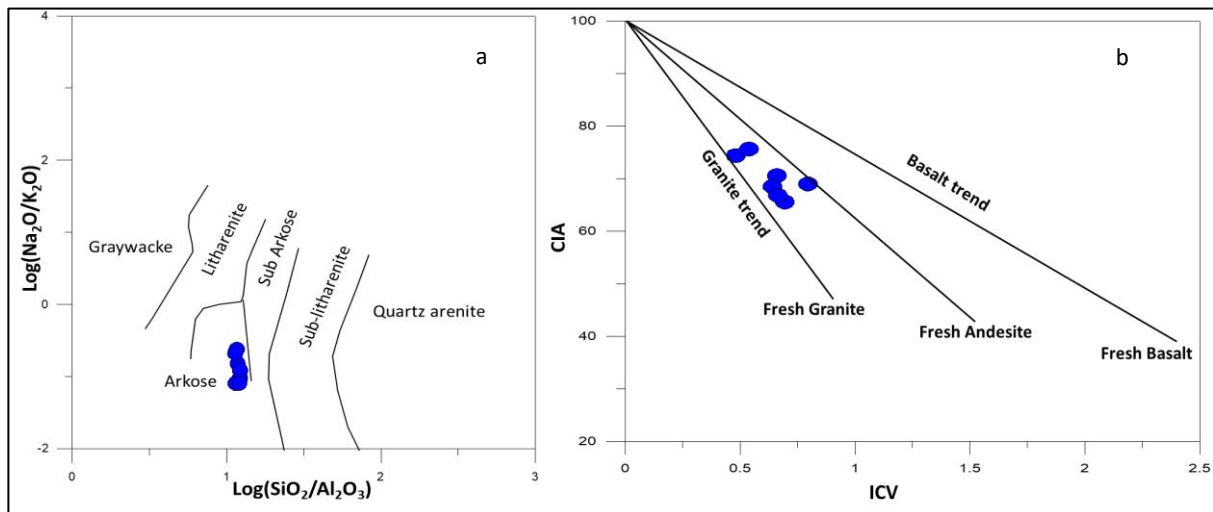
The Index of Chemical Variability (ICV) can also be useful as an index for recycling and compositional maturity in sedimentary rocks (Cox et al. 1995; Armstrong-Altrin 2015)

$$\text{ICV} = (\text{Fe}_2\text{O}_3 + \text{K}_2\text{O} + \text{Na}_2\text{O} + \text{CaO} + \text{MgO} + \text{MnO} + \text{TiO}_2) / \text{Al}_2\text{O}_3 \quad (4)$$

ICV values of Gulcheru Quartzite range from 0.60 to 0.89 (avg. 0.73) reflect the high mature sediments recycled. The high ICV value (~1) reflects that the sediments were deposited as first cycle deposits in tectonically active continental margins. The samples with ICV >1 are indicating that these are first cycle of sediments and immature nature.

Similarly, the ICV vs. CIA plot (Figure 8.19b), suggest that the source of the studied sediments is from predominantly granitoid source rocks.

The Gulcheru sediments of study area are classified on the chemical data (major oxides) after Herron (1988) into Arkose (Figure 8.19a). The observation has also been confirmed by the Petrographic study.



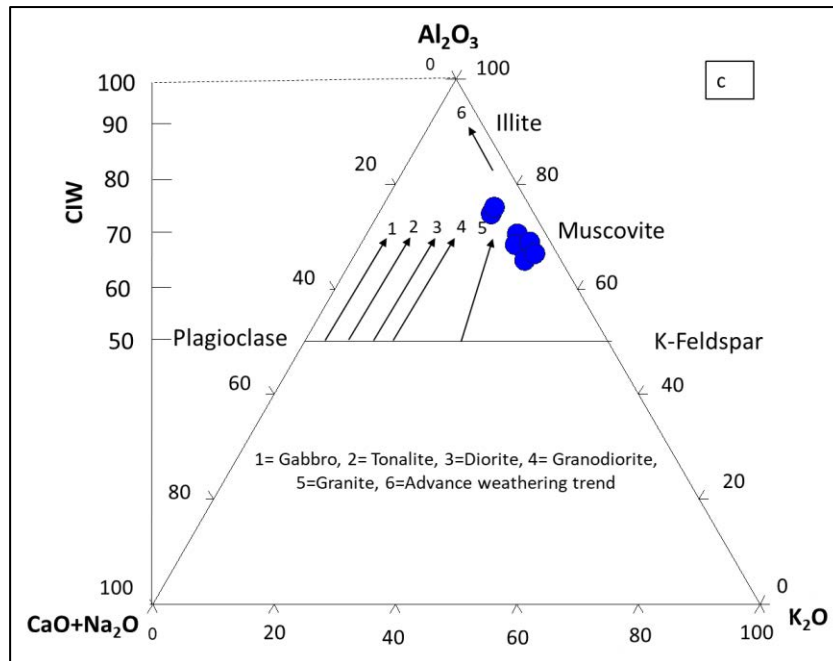


Figure 8.19 (a) Sandstone classification diagram using  $\log(\text{Na}_2\text{O}/\text{K}_2\text{O})$  vs.  $\log(\text{SiO}_2/\text{Al}_2\text{O}_3)$  (after Pettijohn et al. 1987), (b) Two weathering indicators, Index of Chemical Variation (ICV) vs. Chemical Index of Alteration (CIA; fields after Potter et al. 2005), (c) A–CN–K ternary diagram of molecular proportions of  $\text{Al}_2\text{O}_3$ – $(\text{CaO}+\text{Na}_2\text{O})$ – $\text{K}_2\text{O}$  for Gulcheru Quartzite (after Nesbitt and Young 1984).

#### 8.4 Geochemistry of Gulcheru Shale

Geochemistry of Gulcheru shale ( $n=7$ ) has been carried out and the diagrams shown in following study incorporates samples of Gulcheru Quartzite.

Table 8.12 Major elements (in wt%) and trace elements (in ppm) concentrations in the Gulcheru shale.

Sample Id	LNJB/Sh/1	LNJB/Sh/2	LNJB/Sh/3	LNJB/Sh/4	LNJB/Sh/5	LNJB/Sh/6	LNJB/GQS/2
<b>SiO2</b>	58.38	59.3	57.97	58.96	58.28	56.41	55.33
<b>TiO2</b>	0.55	0.65	0.7	0.61	0.68	0.68	0.68
<b>Al2O3</b>	25.41	23.6	24.33	23.62	24.46	24	25.2
<b>Fe2O3(t)</b>	1.36	1.48	1.59	1.86	2.04	2.28	2.07
<b>MgO</b>	2.3	2.3	2.61	2.81	2.53	3.69	2.55
<b>MnO</b>	0.01	0.01	0.01	0.02	0.01	0.01	0.01
<b>CaO</b>	<0.01	<0.01	<0.01	<0.01	<0.01	<0.01	<0.01
<b>Na2O</b>	<0.01	<0.01	0.48	<0.01	<0.01	<0.01	0.14
<b>K2O</b>	8.44	8.9	8.96	8.25	8.83	8.34	8.67
<b>P2O5</b>	0.09	0.09	0.1	0.09	0.09	0.1	0.1
<b>Total</b>	96.54	96.33	96.75	96.22	96.92	95.51	94.75
<b>CIA</b>	73.98	71.44	70.34	73.01	72.33	73.16	72.87
<b>CIW</b>	99.93	99.93	96.82	99.93	99.93	99.93	99.06
<b>PIA</b>	99.89	99.88	94.82	99.88	99.88	99.88	98.51
<b>ICV</b>	0.65	0.73	0.78	0.76	0.74	0.86	0.73
<b>K2O/Al2O3</b>	0.33	0.38	0.37	0.35	0.36	0.35	0.34
<b>Al2O3/TiO2</b>	46.2	36.31	34.76	38.72	35.97	35.29	37.06
<b>Cr</b>	90	95	108	103	105	110	117
<b>Ni</b>	31	31	33	32	30	43	36
<b>Cu</b>	132	69	99	140	144	427	373
<b>Zn</b>	10	10	13	13	<10	12	11
<b>Ga</b>	18	19	19	20	21	20	20
<b>Rb</b>	307	359	345	338	346	355	337
<b>Sr</b>	51	54	49	45	44	35	41
<b>Y</b>	30	41	39	36	41	41	42
<b>Zr</b>	203	304	274	228	247	200	180
<b>Nb</b>	14	17	19	19	20	19	22
<b>Ba</b>	628	632	587	549	540	474	574
<b>Pb</b>	19	20	20	16	38	17	46
<b>Ce</b>	80	108	99	80	108	80	99
<b>Pb</b>	19	20	20	16	38	17	46
<b>Th</b>	26	12	27	26	22	25	25
<b>U</b>	<10	<10	<10	<10	43	<10	130

Table 8.13 Pearson correlation coefficient for major oxides in shale.

Cr	Ni	Cu	Zn	Ga	Rb	Sr	Y	Zr	Nb
Cr	-0.79	0.77	0.04	0.79	0.48	-0.05	0.37	0.06	0.79
Ni	-0.72	0.38	-0.07	0.68	0.89	-0.17	-0.01	-0.41	0.75
Cu	-0.90	0.32	0.22	0.80	0.72	-0.18	-0.15	-0.43	0.67
Zn	-0.16	-0.03	-0.23	-0.08	0.35	0.39	0.41	-0.36	0.48
Ga	-0.28	0.58	-0.28	0.84	0.38	0.19	-0.20	-0.02	0.09
Rb	-0.02	0.77	-0.75	0.43	0.40	-0.08	0.07	0.36	0.26
Sr	0.74	-0.42	-0.02	-0.95	-0.84	-0.04	0.15	0.47	-0.57
Y	-0.41	0.91	-0.37	0.62	0.29	-0.27	0.15	0.45	0.46
Zr	0.72	0.22	-0.60	-0.50	-0.38	-0.06	0.25	0.67	-0.33

Table 8.14 Pearson correlation coefficient for trace elements in shale.

	Cr	Ni	Cu	Zn	Ga	Rb	Sr	Y	Zr	Nb	Ba	Ce	Pb	Th	U
Cr	1														
Ni	0.58	1.00													
Cu	0.69	0.89	1.00												
Zn	0.19	0.43	0.18	1.00											
Ga	0.64	0.19	0.37	-0.39	1.00										
Rb	0.40	0.32	0.13	0.01	0.51	1.00									
Sr	-0.74	-0.81	-0.90	-0.09	-0.65	-0.24	1.00								
Y	0.70	0.36	0.38	-0.15	0.67	0.86	-0.41	1.00							
Zr	-0.38	-0.51	-0.76	-0.11	-0.14	0.51	0.67	0.20	1.00						
Nb	0.93	0.32	0.50	-0.01	0.80	0.50	-0.61	0.79	-0.20	1.00					
Ba	-0.61	-0.72	-0.69	-0.05	-0.71	-0.40	0.92	-0.41	0.41	-0.53	1.00				
Ce	0.14	-0.42	-0.33	-0.54	0.28	0.48	0.34	0.62	0.60	0.35	0.32	1.00			
Pb	0.55	-0.08	0.32	-0.52	0.51	-0.01	-0.26	0.48	-0.32	0.65	-0.02	0.55	1.00		
Th	0.37	0.29	0.34	0.36	0.03	-0.52	-0.46	-0.37	-0.66	0.16	-0.38	-0.61	0.01	1.00	
U	0.65	0.11	0.50	-0.20	0.39	-0.06	-0.35	0.43	-0.50	0.68	-0.03	0.34	0.93	0.11	1.00

Table 8.12 Represents the major oxides data of the shale samples (n=7). Gulcheru shales from the Lanjabanda area fall in the field of shale and wacke of the bivariate plot of  $\log (\text{SiO}_2 / \text{Al}_2\text{O}_3)$  versus  $\log (\text{Fe}_2\text{O}_3 / \text{K}_2\text{O})$  (Figure 8.20, Herron 1988).

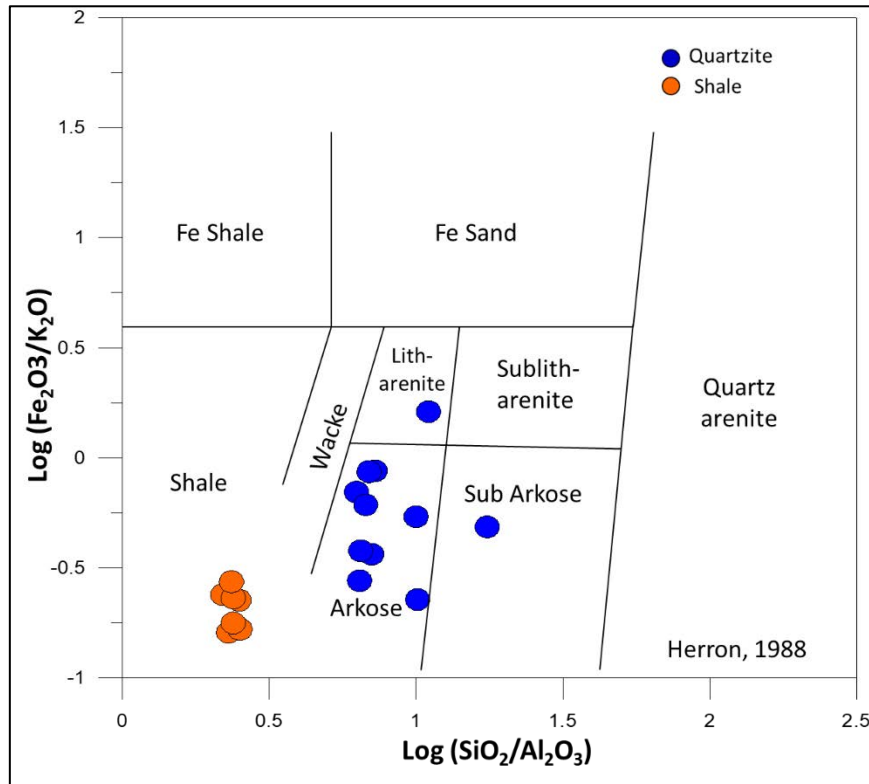


Figure 8.20 Geochemical classification of Gulcheru shale using the major element composition.

The ternary plot of  $\text{Fe}_2\text{O}_3\text{-K}_2\text{O-Al}_2\text{O}_3$  (Figure 8.21) shows that most of the shale samples are plotted near  $\text{Al}_2\text{O}_3$  apex. This indicates their enrichment in  $\text{Al}_2\text{O}_3$ , which further implies that element abundance is predominantly controlled by clay minerals (Wronkiewicz and condie 1987). The  $\text{K}_2\text{O}/\text{Al}_2\text{O}_3$  ratio of the sediment is used as the index of initial composition of ancient sediments; for example, for clay minerals and feldspar it is 0.0 to 0.3 and 0.3 to 0.9, respectively (Cox et.al., 1995). For the Gulcheru shale samples, the  $\text{K}_2\text{O}/\text{Al}_2\text{O}_3$  ratio shows a variation from 0.33 to 0.37 with an average of 0.35 (Table 8.12). As the

$K_2O/Al_2O_3$  ratio in some shale samples is near the upper limit of clay mineral, illite is considered to be the dominant clay mineral (Chakrabarti et al. 2009).

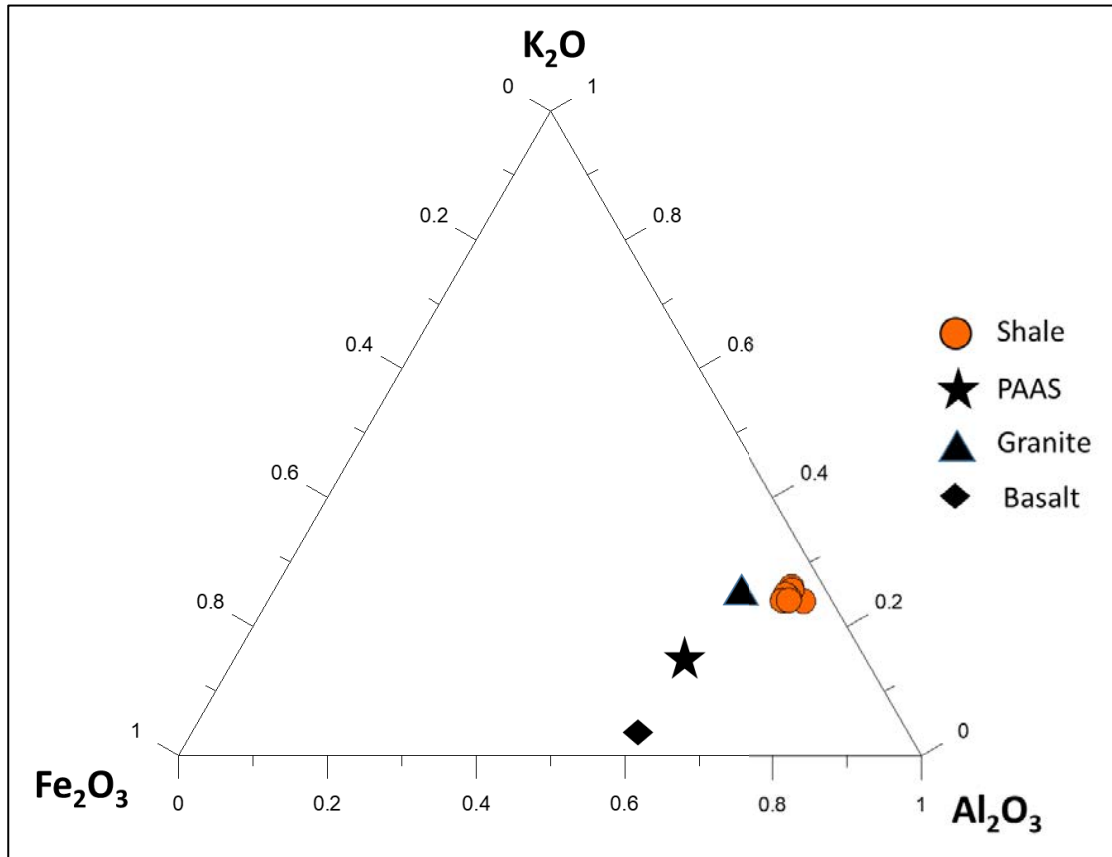


Figure 8.21 Major element distribution in the Gulcheru shales in  $Fe_2O_3$ –  $K_2O$ – $Al_2O_3$  compositional space. The data on granite, basalt and PAAS are defined from Condie (1993) and Taylor and McLennan (1985) respectively.

### Trace Elements

Table 8.12 also represents the trace elements data with the elemental ratios of the shale samples. PAAS normalized trace elements are plotted in a multielement diagram, which shows depletion of Ni, Zn, Sr, and moderate to slight enrichment of Cu, Rb, and Nb (Figure 8.22).

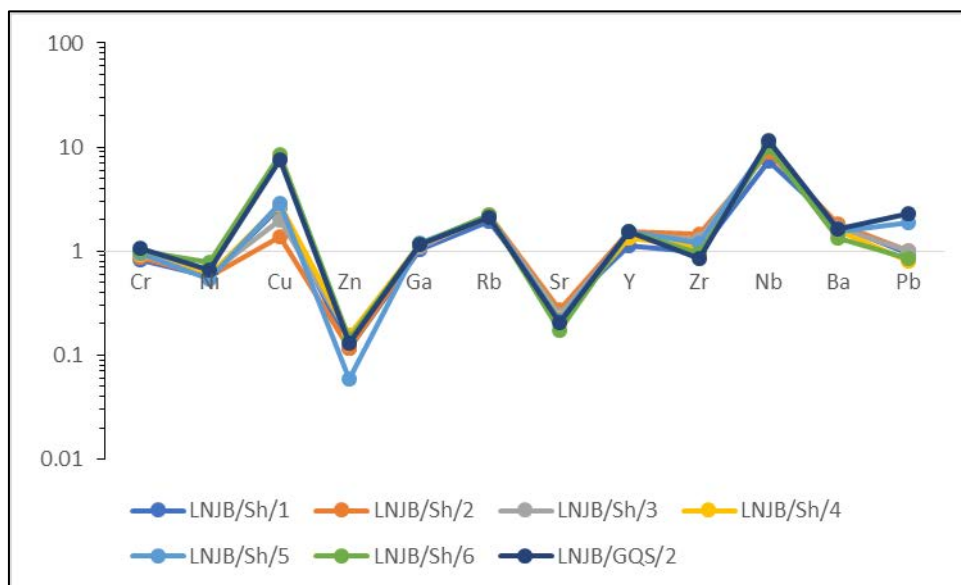


Figure 8.22 Distribution of PAAS normalized trace elements of Gulcheru shale.

### Paleo weathering

Numerous geochemical parameters are frequently used to determine the weathering intensity of source rock. Within these parameters, the Chemical Index of Alteration (CIA) and A–CN–K diagram are the most important. CIA is considered as the ratio of primary mineral and clay mineral and is formulated as  $[Al_2O_3 / (Al_2O_3 + CaO^* + K_2O + Na_2O)] \times 100$  (Nesbitt and Young 1982, 1984). The value is expressed in molar proportion, and CaO\* represents CaO present in silicate mineral. In unweathered igneous rock the CIA value is around 50, and for intensely weathered rock (mainly composed of kaolinite, gibbsite), the value is near 100 (Nesbitt and Young 1984). The CIA computed for Gulcheru shale samples have values ranging from 70.34 to 73.98 with an average 72.45 (Table 8.12), which indicates intermediate weathering of the source rock. In  $Al_2O_3 - (CaO^* + Na_2O) - K_2O$  (A–CN–K) diagram (Figure 8.23) the sample plotted close to the  $Al_2O_3 - K_2O$  line, which indicates intense weathering of the source rock (Hessler and Lowe 2006). The direction advanced near to the muscovite composition (Fedo et al. 1995). The CIA value may be decreased due to K-metasomatism and therefore the Plagioclase Index of Alteration (PIA) and Chemical Index of Weathering (CIW)

values are considered to better estimate the weathering of source rock. PIA and CIW are formulated as  $[(Al_2O_3 - K_2O)/(Al_2O_3 + CaO^* + K_2O + Na_2O)] \times 100$  and  $[Al_2O_3/(Al_2O_3 + CaO^* + Na_2O)] \times 100$ , respectively (Fedo et al. 1995; Harnois 1988). Higher average values of PIA and CIW (98.96 and 99.36 respectively, Table 8.12) of Gulcheru shales also indicate that the source rock has suffered intense weathering. The Index of Compositional variability (ICV) also indicates the original composition of fine clastic rock and is formulated as  $(Fe_2O_3 + K_2O + Na_2O + CaO + MgO + TiO_2)/Al_2O_3$ . Compared to the clay minerals, non-clayey minerals (pyroxene, feldspar) show higher ICV values ( $>1$ ) (Cullers and Podkovyrov 2000). Therefore, shale with high ICV values indicates the presence of higher amounts of non-clayey minerals and is considered to be immature (Cox et al. 1995). All of the Gulcheru shale have ICV value less than 1 and therefore are considered to be mature.

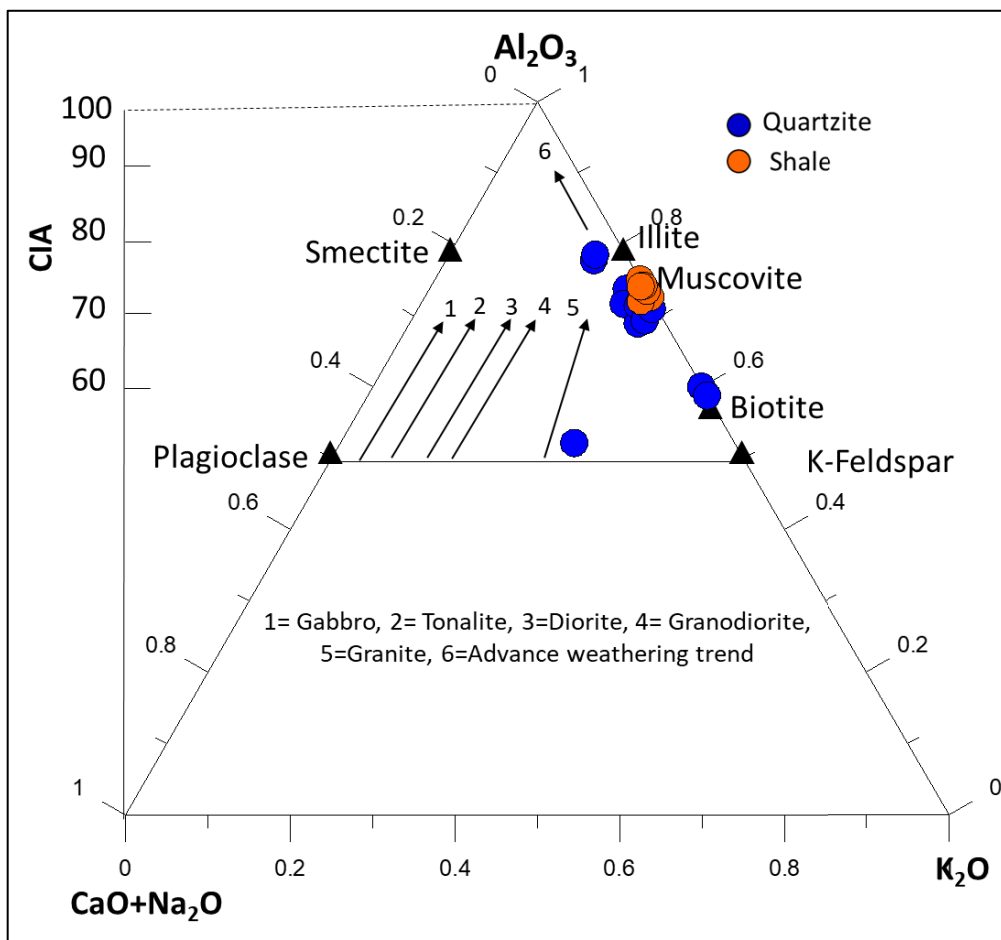


Figure 8.23 A-CN-K diagram for the Gulcheru shales.

## Provenance

The geochemical characteristics of shale have been widely used to depict the provenance nature.  $\text{Al}_2\text{O}_3/\text{TiO}_2$  ratio distinctly varies from mafic (3–8) to intermediate (8–21) as well as in felsic rocks (21–70) (Hayashi et al. 1997). Therefore  $\text{Al}_2\text{O}_3/\text{TiO}_2$  ratio of the sediments, derived from those igneous rocks can be used as a proxy of source rock composition (Armstrong-Altrin 2009). In Gulcheru shale samples,  $\text{Al}_2\text{O}_3/\text{TiO}_2$  varies between 34.75 and 46.20 with the average of 37.76. This suggests that felsic granitoid to granite rocks are the probable source rocks.

Plotting of the Gulcheru shale samples in the binary  $\text{Al}_2\text{O}_3$  versus  $\text{TiO}_2$  diagram (Figure 8.24a) demonstrates all the shales are in the field of granite, which indicates their derivation from a felsic source rock. Ni versus  $\text{TiO}_2$  bivariate plot (Figure 8.24b.; Floyd et al. 1989) demonstrates the derivation of Gulcheru shale from a felsic rock.

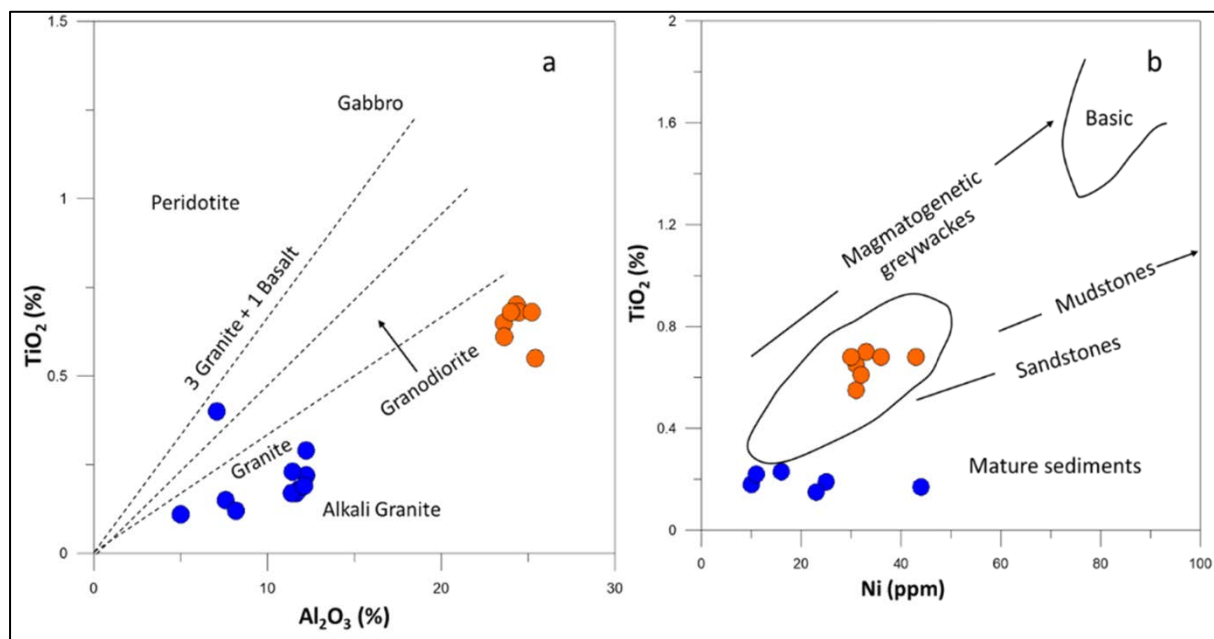


Figure 8.24 Scatter plots of a)  $\text{Al}_2\text{O}_3$  versus  $\text{TiO}_2$  b) Ni versus  $\text{TiO}_2$

The bivariate plot  $\text{SiO}_2$  versus  $(\text{Al}_2\text{O}_3 + \text{Na}_2\text{O} + \text{K}_2\text{O})$  (Figure 8.25, Suttner and Dutta 1986) is applied to depict the climatic situation during Gulcheru clastic sedimentation. Most of the Gulcheru shale samples are well fitted in the area of arid climate, suggesting their deposition principally in arid condition.

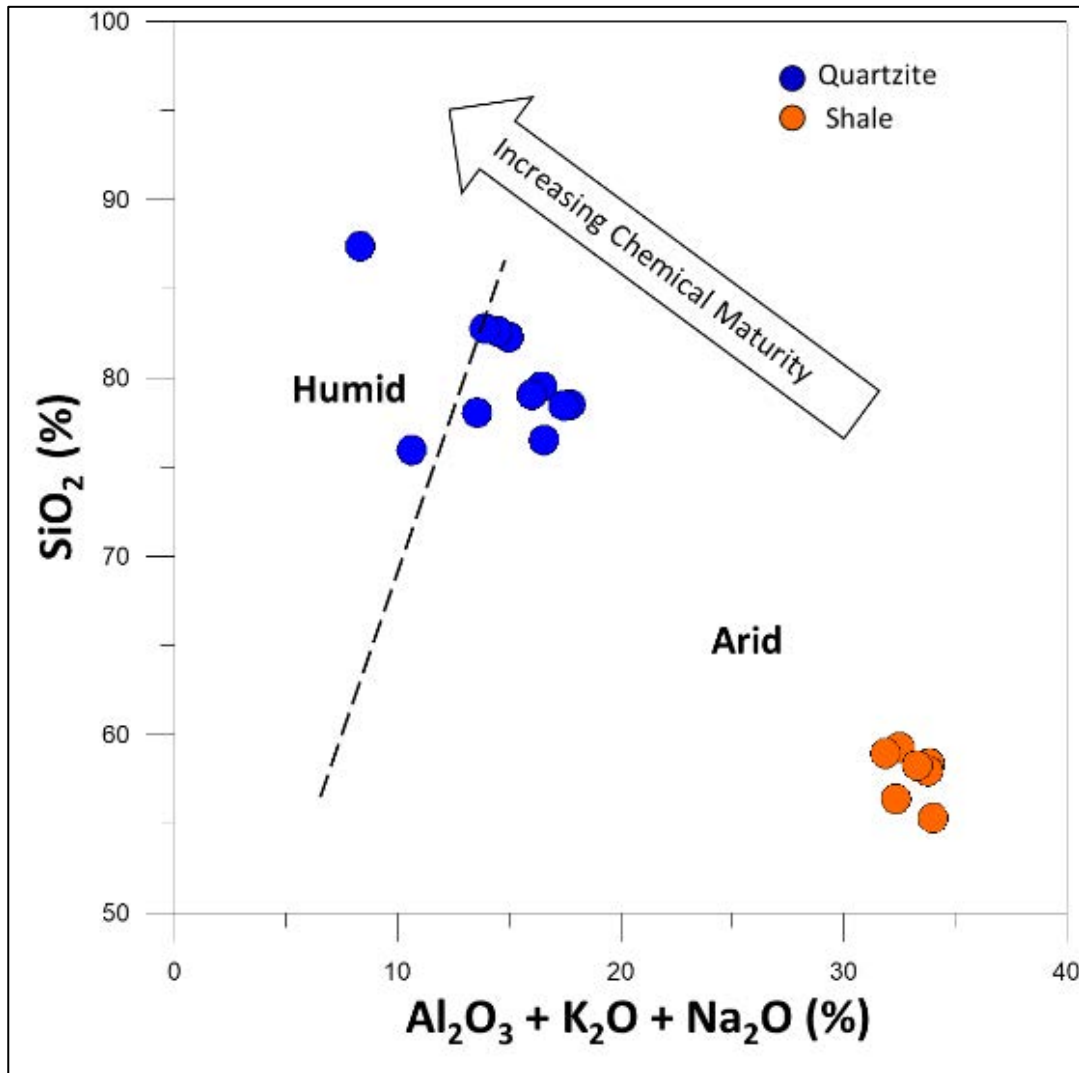


Figure 8.25 Binary plot of  $\text{SiO}_2$  versus  $(\text{Al}_2\text{O}_3 + \text{Na}_2\text{O} + \text{K}_2\text{O})$ .

## REE distribution and pattern in Gulcheru quartzites

Distribution patterns of the sediments normalized to chondrite values are plotted (Figure 8.26) following Bonyton et al. (1974). REE analysis was carried out to understand the evolution and genesis of the sediments. The representative REEs (n=6) (Table 8.15) shows that the sandstones are more enriched in LREEs than HREEs.

	La	Ce	Pr	Nd	Sm	Eu	Gd	Tb	Dy	Ho
<b>Min</b>	103	209	23	91	16	1.4	13	1.5	5	1.5
<b>Max</b>	428	805	95	348	64	4.6	36	5	13	1.5
<b>Avg.</b>	234.8	451.16	50.33	196.16	35.5	2.63	22.83	3.08	8.83	1.5
	Er	Tm	Yb	Lu	Y	ΣREE	ΣLREE	ΣHREE	(ΣLREE/ΣHREE)	(ΣLEE/ΣHREE) <sub>N</sub>
<b>Min</b>	1.5	1.5	1.4	0.25	26	472.15	442	25.65	15.42	11.04
<b>Max</b>	5	1.5	3	0.5	53	1810.1	1740	65.5	26.56	19.42
<b>Avg.</b>	3.08	1.5	2.15	0.375	38.83	1013.9	968	43.35	21.17	15.42
	(La/Yb) <sub>N</sub>	(La/Sm) <sub>N</sub>	(La/Lu) <sub>N</sub>	(Ce/Yb) <sub>N</sub>	(Ce/Sm) <sub>N</sub>	(Eu/Yb) <sub>N</sub>	(Gd/Lu) <sub>N</sub>	(Gd/Yb) <sub>N</sub>	(Eu/Eu*) <sub>N</sub>	(Ce/Ce*) <sub>N</sub>
<b>Min</b>	49.60	3.90	42.79	38.61	2.95	2.84	6.46	7.06	0.25	0.92
<b>Max</b>	96.18	4.31	88.91	69.41	3.16	4.36	8.95	9.68	0.28	1
<b>Avg.</b>	68.90	4.15	61.39	50.90	3.07	3.33	7.46	8.41	0.27	0.96

The ΣLREE content in all the samples ranges from 442 to 1740 (avg. 968) whereas ΣHREEs varies from 25.65 to 65.5 (avg. 43.35). The high level of enrichment of LREE relative to HREE suggests high order of fractionation of source rock. The chondrite normalized REE pattern of the sandstones of study area is presented in Figure 8.26. The ratio of (La/Yb)<sub>N</sub> quantifies the inclination of the curves as it is greater than or equal to 1, the curves of LREE inclines to right side and it means that samples are rich in LREE and low in HREE. The normalized (LREE/HREE)<sub>N</sub> ratio ranges from 11.04 to 19.42 (avg. 15.42). The ratios of (La/Yb)<sub>N</sub> and (Gd/Yb)<sub>N</sub> are used to measure the degree of LREE and HREE fractionation respectively. The degree of LREE fractionation, (La/Yb)<sub>N</sub> of 68.90, is slightly higher than that of HREE fractionation, (Gd/Yb)<sub>N</sub> of 8.41. This is also evident by the presence of significant amount of monazite and xenotime in these sandstones.

Large negative Eu anomalies (Eu/Eu\* < 0.27; i.e. 0.25-0.28) are recorded in the sandstones of the study area (Table 8.15 and Figure 8.26). Besides, feebly negative to positive Ce anomalies (Ce/Ce\*=0.92–1) indicate enrichment of LREE and points toward the presence of Ce-rich

monazite in the residual phase.  $Ce^{3+}$  is more easily oxidized to  $Ce^{4+}$  with higher oxygen fugacity and is much less mobile resulting in positive Ce anomaly ( $\delta Ce > 1$ ). Eu is an incompatible element in the trivalent form ( $Eu^{3+}$ ) in an oxidizing magma, but is preferentially incorporated into plagioclase in its divalent form ( $Eu^{2+}$ ) in a reducing magma. This ion-exchange process is the basis of the negative Eu anomaly ( $\delta Eu < 1$ ). The Eu anomalies are chiefly controlled by plagioclase. Thus, removal of plagioclase from a felsic melt by crystal fractionation or partial melting of a rock in which plagioclase is retained in the source will give way to negative Eu anomaly.

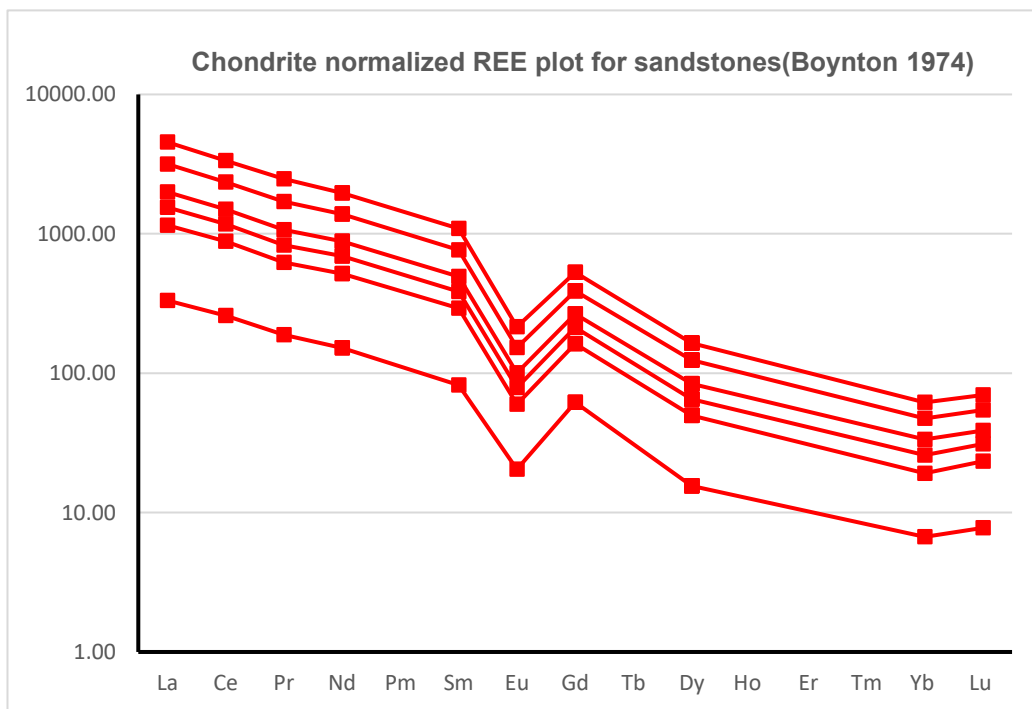


Figure 8.26 Chondrite normalized REE plot of Gulcheru sandstones, Govardhanagiri-L.Banda area.

## CHAPTER 9

### INTEGRATED GEOPHYSICAL AND GEOLOGICAL STUDIES

#### 9.1 Integration of airborne geophysical and geological data

All detectable gamma radiation from earth materials come from the natural decay products of only three elements, i.e. uranium, thorium, and potassium because they produce gamma rays of sufficient energy and intensity to be measured by gamma ray spectrometry because of their abundance in the natural environment (Table 9.1).

Airborne gamma ray spectrometry can be very helpful in mapping surface geology. This provides estimates of the apparent surface concentrations of the most common naturally occurring radioactive elements, such as potassium(K), equivalent uranium(eU) and equivalent thorium(eTh). This is based on the assumption that the absolute and relative concentrations of these radioelements vary measurably and significantly with lithology. The composite image technique is used to display simultaneously three parameters of the three radioelement concentrations and their three binary ratios on one image. The technique offers much in terms of lithological discrimination, based on colour differences and showed efficiency in defining areas, where different lithofacies occur within areas mapped as one continuous lithology. The integration between surface geological information and geophysical data led to detailing the surface geology and the contacts between different rock units. Significant locations or favourable areas for uranium exploration are defined, where the measurements exceed  $(X+2S)$ , taking  $X$  as the arithmetic mean of eU, eU/eTh and eU/K measurements and  $S$  as the standard deviation corresponding to each variable.

Table 9.1 Radioelemental concentration in different classes of rocks and soil  
(average value in brackets) (after Dickson and Scott, 1997).

Rock type	Rock			Soil		
	K(%)	U(ppm)	Th(ppm)	K%	U(ppm)	Th(ppm)
<b>Intrusives</b>						
Granitoids	0.3-4.5 (2.4)	0.4-7.8 (3.3)	2.3-45 (16)	0.4-3.9 (2.1)	0.5-7.8 (2.7)	2-37 (13)
Gneissic rock	2.4-3.8 (2.4)	2.1-3.6 (2.5)	18-55 (15)	0.7-1.9 (1.3)	1.6-3.8 (2.2)	6-19 (12)
Pegmatite	2.6-5.5 (3.7)	0.3-1 (0.7)	0.3-9.6 (2)			
Aplites	0.6-4 (2.4)	1-8 (3.3)	3-20 (7)			
Quartz-feldspar porphyry	1-5 (2.9)	1.3-2.9 (1.7)	6-14 (13)			
Intermediate intrusives	0.7-5.6(2.7)	0.1-1.2 (0.8)	0.8-6.1 (2.4)	0.7-3.4 (1.6)	1.5-2.3 (1.9)	2.9-8.4 (5.6)
Mafic intrusives	0.1-0.8 (0.4)	0.0-1.1 (0.3)	0.0-3.1 (1.2)			
<b>Extrusives</b>						
Felsic volcanics	2.0-4.4 (3.7)	1.4-13 (2.4)	13-28 (17)	1.8-3.2 (2.4)	1.3-2.4 (2.1)	10-18 (13)
Intermediate volcanics	1.8-4.1 (2.7)	0.9-5.6 (2.3)	1.5-15 (9)	1.0-2.7 (1.9)	1.2-3.6 (2.1)	4-17 (10)
Low-K andesites	0.7-0.9 (0.8)	1.0-2.5 (1.6)	3-8 (5)	0.8-1.5 (1.1)	1.2-1.5 (1.3)	4-6 (5)
Mafic volcanics	0.3-1.3 (0.9)	0.3-1.3 (0.7)	2.0-5.0 (3.0)	0.2-1.4 (0.7)	0.6-2.5 (1.6)	3.3-13 (7.9)
Ultramafic volcanics	0.2-0.9 (0.4)	0.3-0.9 (0.6)	0.0-4.0 (1.2)	0.6	2.0	6
<b>Sedimentary rocks</b>						
Archean shales	0.4-1.6 (0.9)	0.3-1.3 (0.9)	1-5 (2.7)	0.8	1.2	3
Other shales	0.1-4.0 (2.6)	1.6-3.8 (2.6)	10-55 (19)	0.7-3.0 (1.5)	1.2-5 (2.3)	6-19 (13)
Arenites	0.0-5.5 (1.8)	0.7-5.1 (2.3)	4-22 (12)	0.1-2.4 (1.3)	1.2-4.4 (2.1)	7-18 (11)
Carbonates	0.0-0.5 (0.2)	0.4-2.9 (1.6)	0-2.9 (1.4)			

## 9.2 Ratio Radioelemental Maps

A ternary radioelement map is a color composite image generated by modulating the red, green and blue phosphors of the display device. The use of red, green and blue for K, Th and U respectively is standard for displaying gamma ray spectrometric data. Blue is used to display the U channel, since this is the noisiest channel and the human eye is least sensitive to variations in blue intensity.

## 9.3 Airborne Gamma Ray Spectrometric Survey

The study area was included in the systematic airborne geophysical survey conducted by ASRS Group, AMD, Hyderabad, in 1984. It was conducted along parallel flight lines at 1.5Km line spacing approx. and 120m ground clearance.

## 9.4 Qualitative interpretation

Gamma ray spectrometric maps (Figure 9.2, 9.5, 9.6) emphasize the nature of the three radioelement distributions and thus are better suited to the recognition of geological features. These maps show a general relationship to various rock units and structural trends. Careful inspection of the four radioelements countour maps (TC, K, eU and eTh), as well as ratio maps (eU/eTh and eU/K) were performed and then interpreted qualitatively. Examination of the aeroradiospectrometric maps reveals the existence of a wide range of their levels, which reflect the fact that, the area under study is covered by rocks of various compositions. It is evident, from regional correlation between different rock units and recorded levels of gamma radiation, that the pattern of aeroradioactivity is closely connected with surface geology of the area. Brief descriptions of qualitative interpretation of the aeroradiospectrometric maps is given below.

### Geological map of Kurnool-Dhone Block, Andhra Pradesh

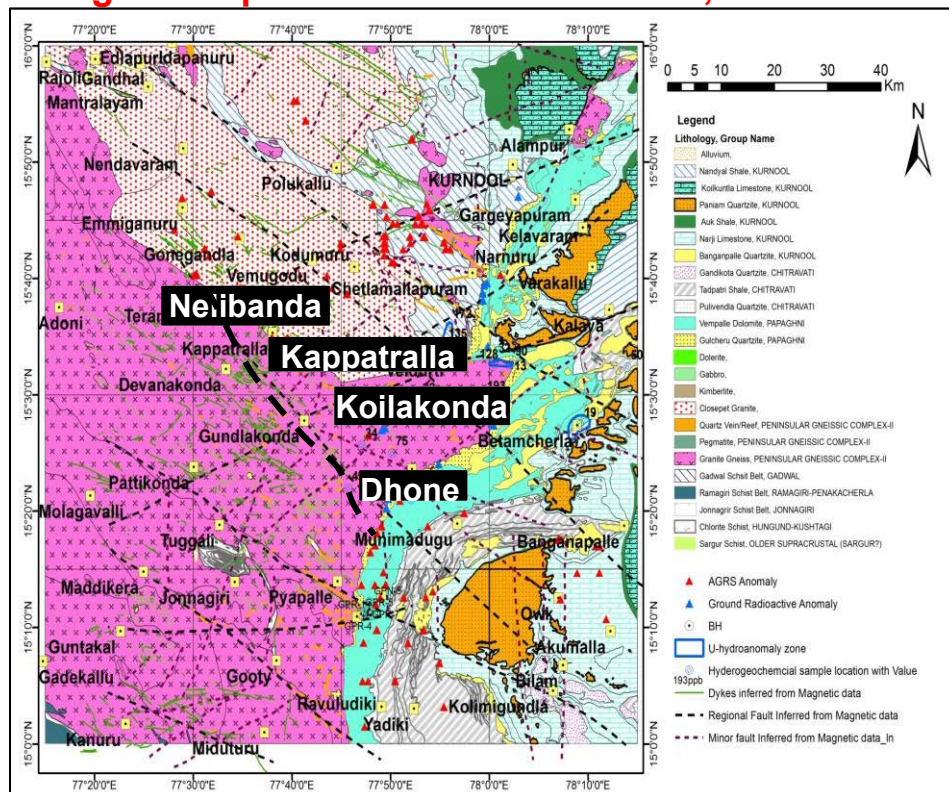


Figure 9.1 Geological map (1:50,000) of Kurnool- Dhone Block (Bhukosh) with ASRS anomalies and major lineaments.

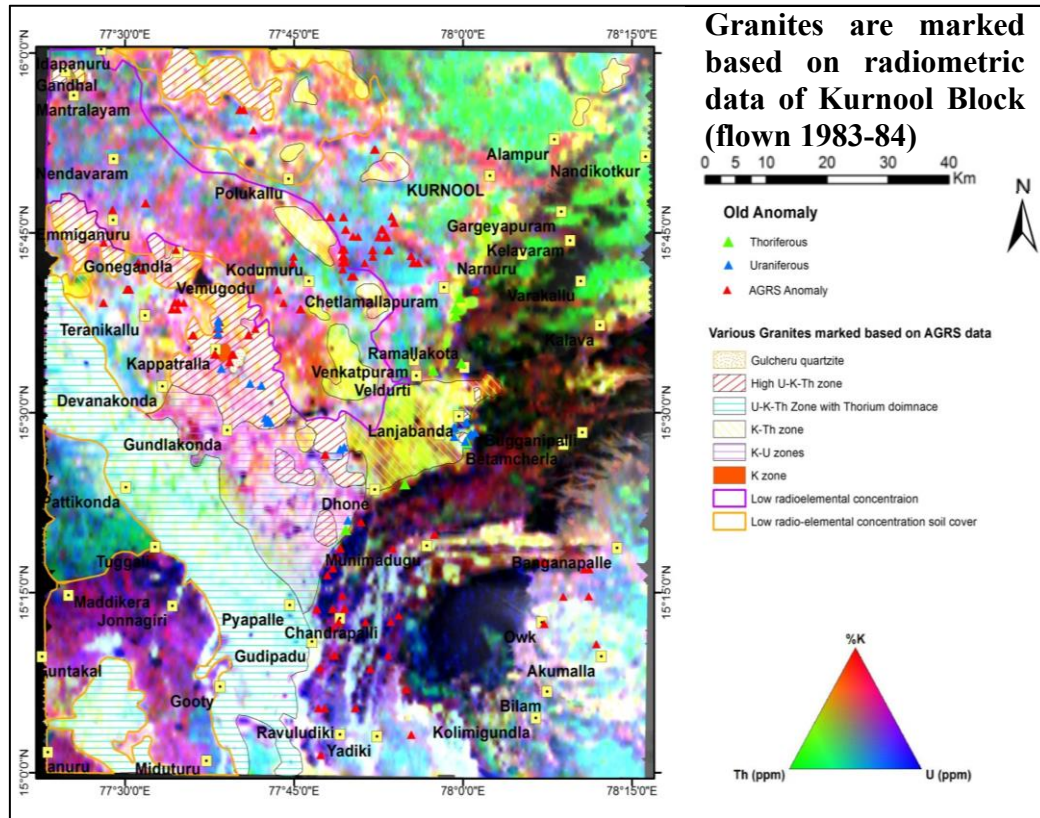


Figure 9.2 Ternary radiometric map of Kurnool-Dhone block showing different radioelement concentration zones.

Ternary radiometric map of the Kurnool block shows the high concentration of U, Th and K in fresh granite (white to violet) and in the granitic soil where clay layers are close to or exposed at the surface (yellow, pink and white). In the given map, different zones within granite have been marked on the basis of their radioelemental concentration. High U-Th-K zone corresponds to the NW-SE trending Kappatralla-Nelibanda granites where several uraniferous and thoriferous anomalies were recorded. Govardhanagiri-L.Banda area is characterized by low radioelemental concentration (yellow) having mixed K-Th zone. In the Gulcheru Quartzite along the western margin of Cuddapah basin from Dhone to Yadiki is characterized by uraniferous zone. The high K fertile granites of the Kappatralla-Nelibanda area shows continuity towards basin margin below Gulcheru sediments thus forming suitable loci for unconformity proximal U mineralisation.

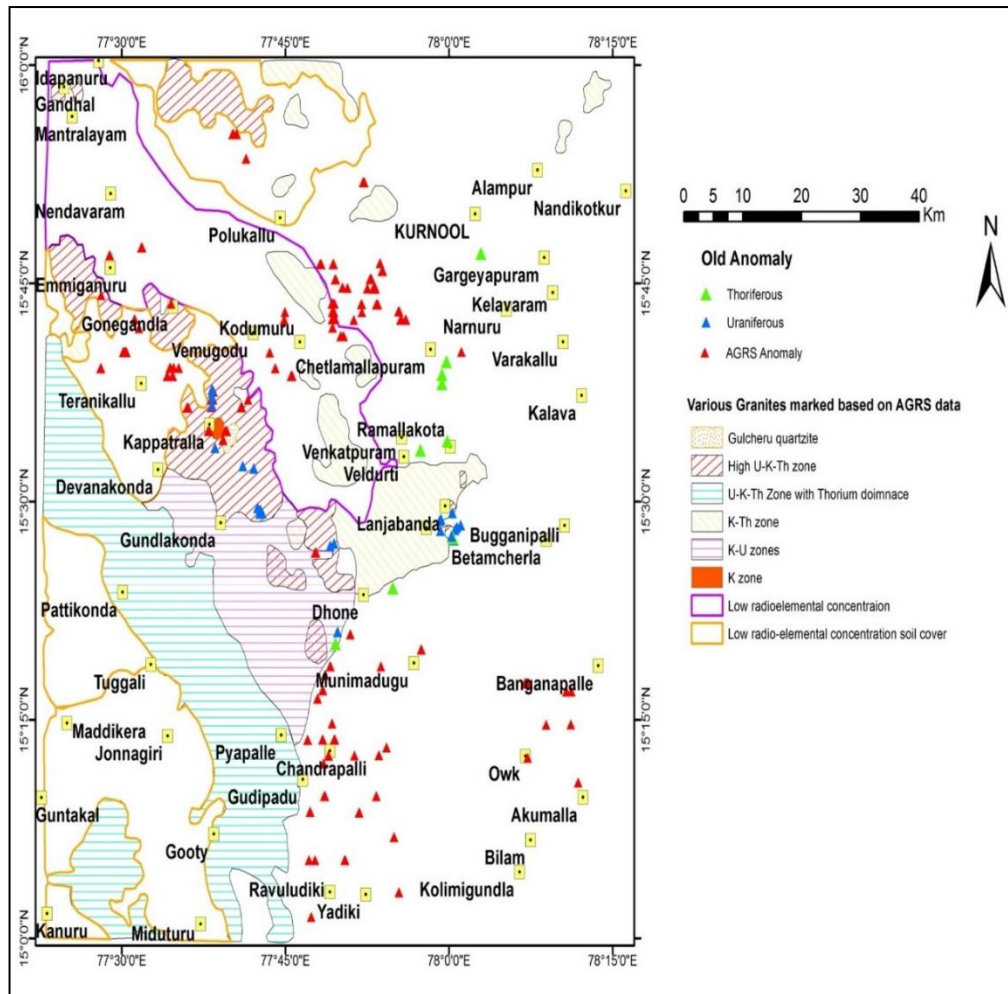
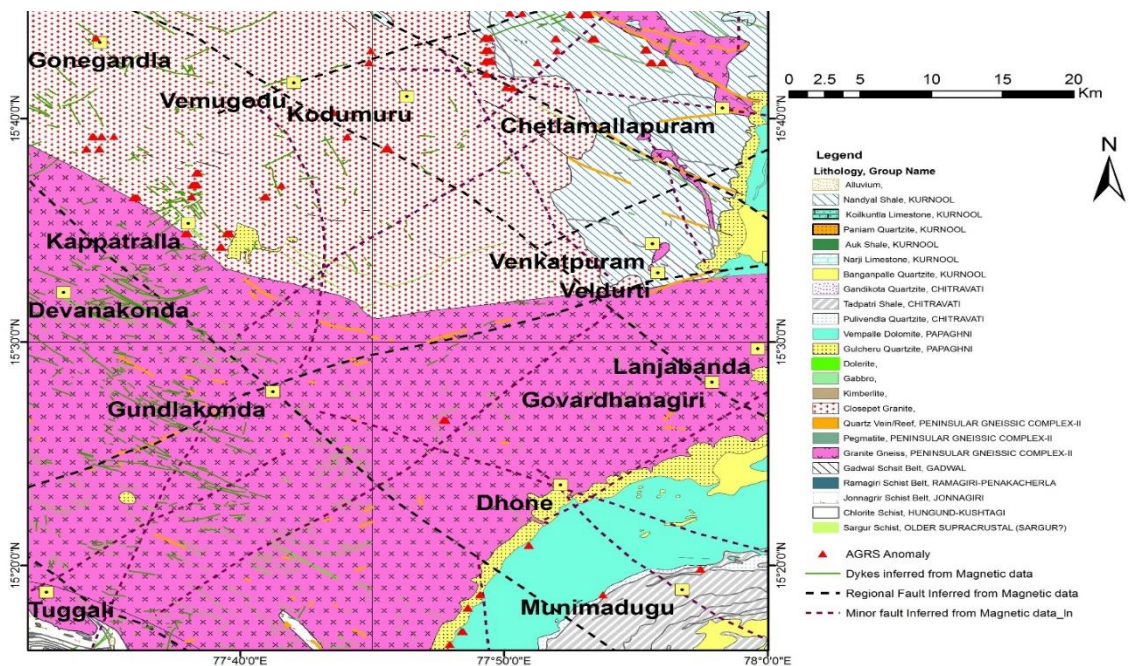


Figure 9.3 Pseudo geological map prepared on the basis of different radioelemental zones.



Base

Figure 9.4 Geological map as a base map for geophysical interpretation.

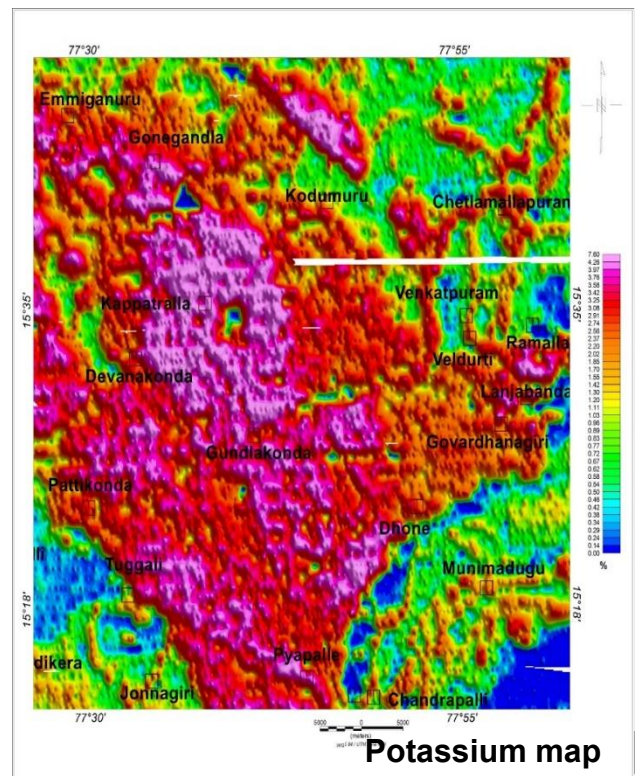
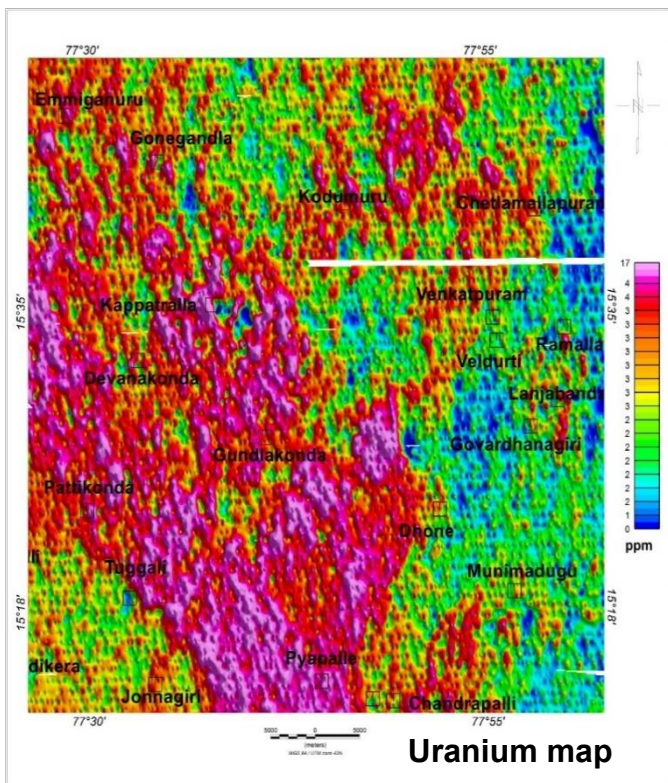
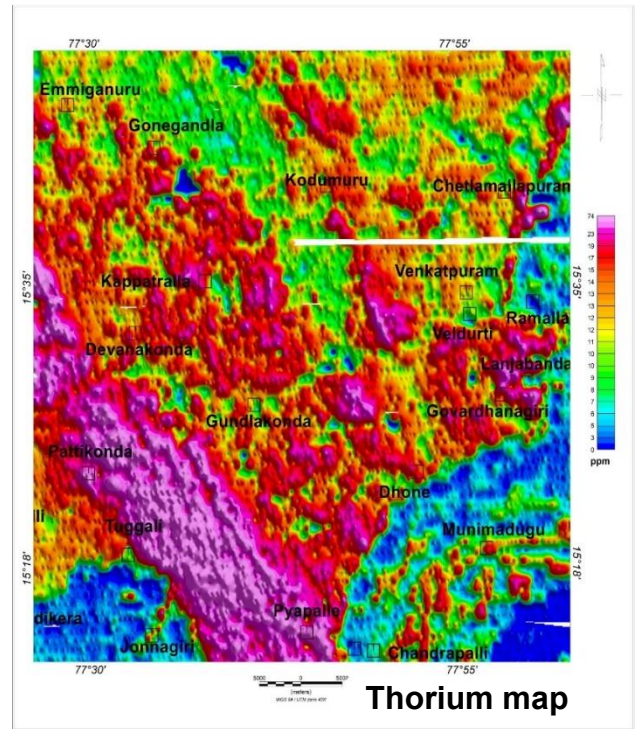
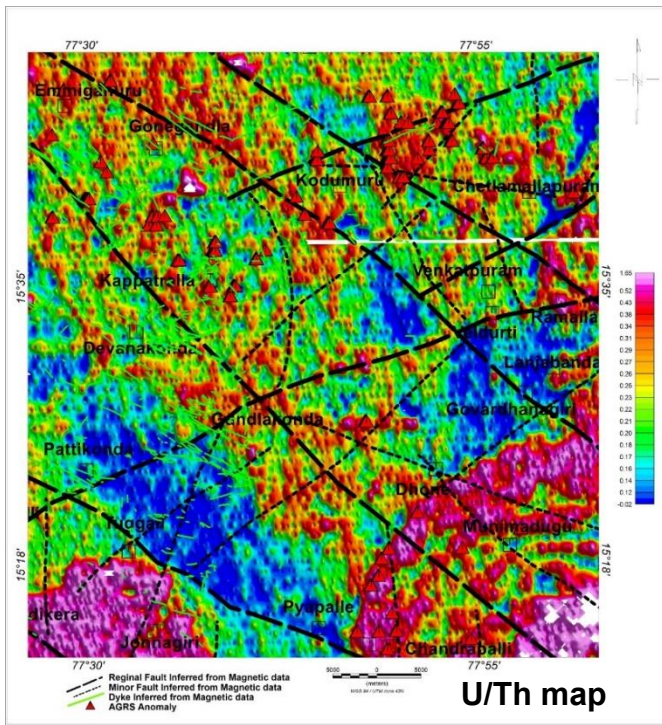


Figure 9.5 a) U/Th map of the area b) Thorium map c) Uranium map d) Potassium map

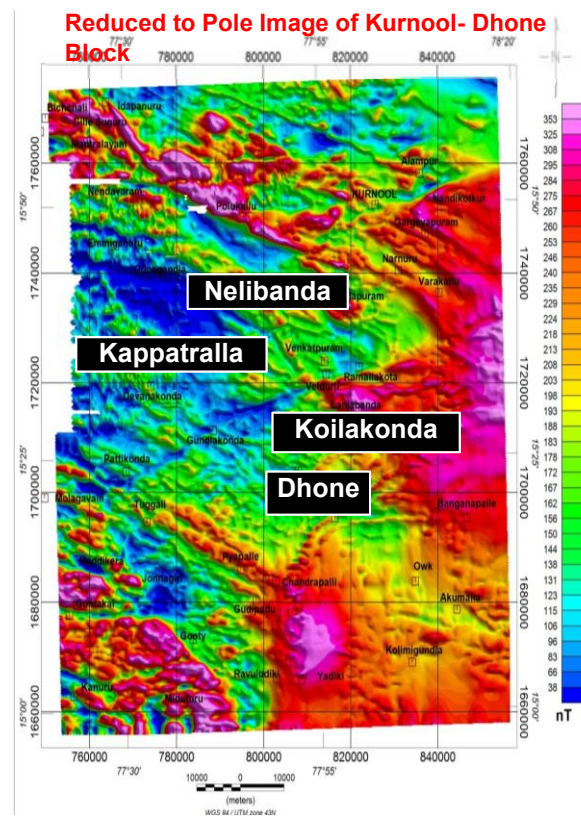
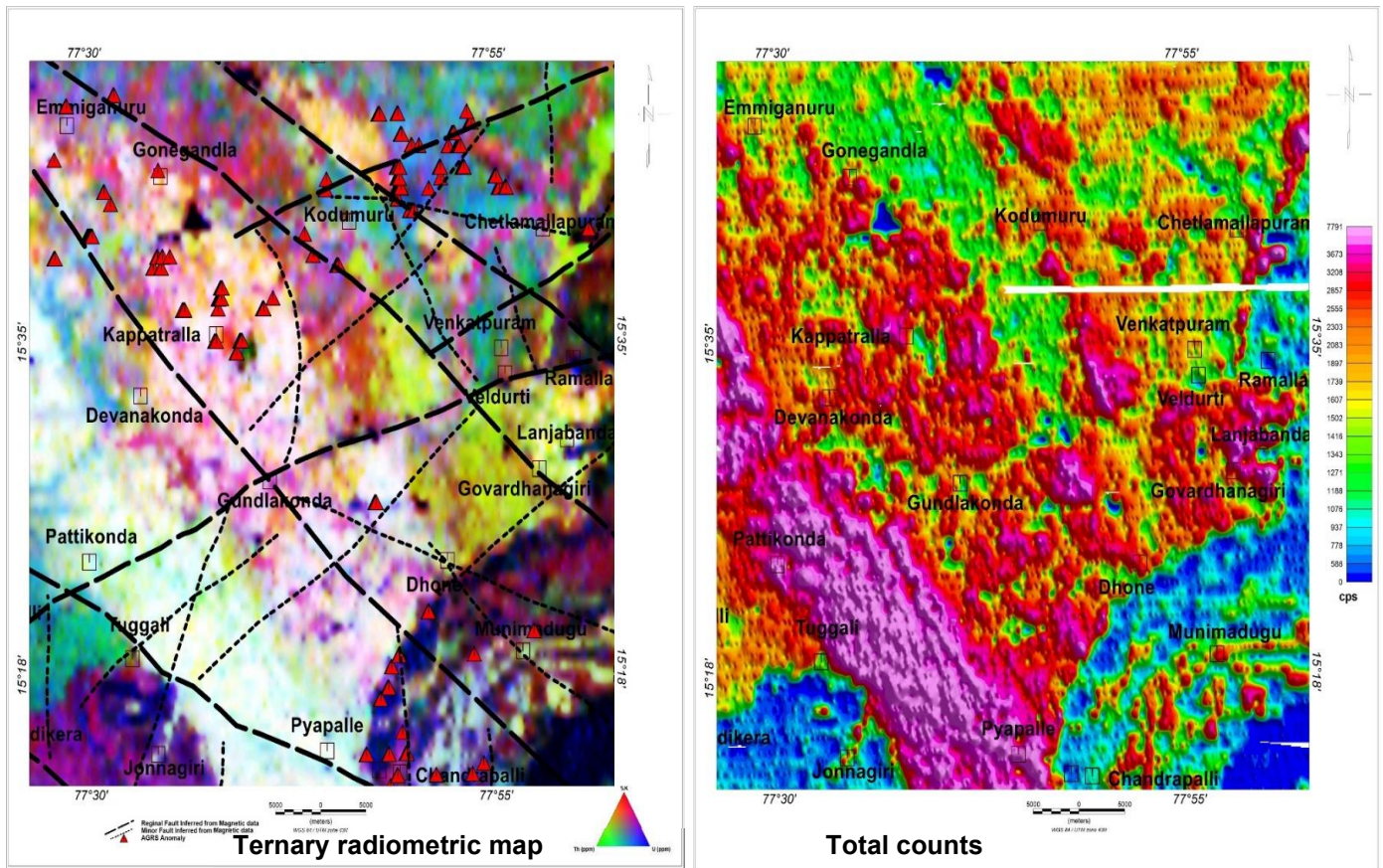


Figure 9.6 a) Ternary radiometric map b) Total counts c) RTP map of the area

## 9.5 Comparative geochemical studies of Kappatralla and Lanjabanda basement granites

Comparative geochemical study between Kappatralla(n=70) and Lanjabanda(n=13) basement granites has been carried out to understand the nature of granite and to validate the airborne radiometric data which shows the continuity of the younger K-rich Bt granite in Kappatralla area towards basin margin along NW-SE trend(Figure 9.2).

### Geochemical characterization

XRF analysis of basement granite samples (n=70) (Table 9.2) from Kappatralla-Nelibanda-Gundlakonda and Lanjabanda (n=13) (Table 9.3) areas have been compiled, processed and interpreted. These granitoids represents the younger phases of felsic magmatism in the area include medium to coarse grained grey biotite granite with occasional pink feldspars at many places and subordinate porphyritic variants. These granitoids forms the basement for overlying Gulcheru Quartzite.

	Min.	Max.	Avg.		Min.	Max.	Avg.
<b>SiO<sub>2</sub></b>	70.06	78.95	72.69	<b>Cr</b>	16.00	128.00	47.44
<b>TiO<sub>2</sub></b>	0.02	0.31	0.14	<b>Ni</b>	4.00	23.00	8.06
<b>Al<sub>2</sub>O<sub>3</sub></b>	12.47	15.99	14.58	<b>Cu</b>	5.00	36.00	6.91
<b>FeO<sup>t</sup></b>	0.46	2.67	1.53	<b>Zn</b>	5.00	42.00	20.41
<b>MgO</b>	0.01	1.81	0.28	<b>Ga</b>	10.00	31.00	14.21
<b>MnO</b>	0.01	0.03	0.02	<b>Rb</b>	100.00	350.00	215.27
<b>CaO</b>	0.15	1.23	0.67	<b>Sr</b>	59.00	233.00	107.50
<b>Na<sub>2</sub>O</b>	3.10	6.48	4.12	<b>Y</b>	5.00	222.00	38.34
<b>K<sub>2</sub>O</b>	3.45	7.36	5.17	<b>Zr</b>	19.00	1432.00	203.99
<b>P<sub>2</sub>O<sub>5</sub></b>	0.01	0.52	0.06	<b>Nb</b>	5.00	43.00	10.84
<b>Total</b>	97.70	100.96	99.26	<b>Pb</b>	27.00	406.00	68.04
<b>K<sub>2</sub>O/Na<sub>2</sub>O</b>	0.65	2.25	1.29	<b>Ba</b>	100	697.00	277.76
<b>K<sub>2</sub>O+Na<sub>2</sub>O</b>	7.25	11.59	9.29	<b>Ce</b>	5.00	351.00	82.25
<b>Molar A/NK</b>	0.97	1.41	1.19	<b>Th</b>	5.00	253.00	50.13
<b>Molar A/CNK</b>	0.88	1.29	1.08	<b>U</b>	5.00	770.00	79.83
<b>Agpiatic Index</b>	0.71	1.03	0.85	<b>K/Rb</b>	1.56	4.96	2.53
<b>Diff. Index</b>	85.73	97.29	92.74	<b>Rb/Sr</b>	0.99	3.47	2.09
<b>Alkali Index</b>	0.00	0.04	0.02	<b>Ba/Rb</b>	0.46	3.56	1.33
<b>ASI</b>	0.88	1.30	1.08	<b>Ba/Sr</b>	0.89	5.20	2.63
<b>(%) Norm Corundum</b>	0.00	3.35	1.27	<b>(%) Norm Diopside</b>	0.00	2.85	0.12

	<b>Min.</b>	<b>Max.</b>	<b>Avg.</b>		<b>Min.</b>	<b>Max.</b>	<b>Avg.</b>
<b>SiO<sub>2</sub></b>	66.07	83.45	74.902	<b>Cr</b>	32	83	49.92
<b>TiO<sub>2</sub></b>	0.05	0.37	0.149	<b>Ni</b>	5	35	10.69
<b>Al<sub>2</sub>O<sub>3</sub></b>	4.64	16.48	12.738	<b>Cu</b>	5	5	5
<b>FeO<sup>t</sup></b>	0.73	4.21	1.955	<b>Zn</b>	5	39	10.307
<b>MgO</b>	0.12	1.77	0.716	<b>Ga</b>	5	16	12.076
<b>MnO</b>	0.005	0.02	0.007	<b>Rb</b>	106	375	278.15
<b>CaO</b>	0.005	5.83	0.824	<b>Sr</b>	24	150	85.46
<b>Na<sub>2</sub>O</b>	0.005	4.09	0.869	<b>Y</b>	5	69	39.07
<b>K<sub>2</sub>O</b>	1.75	8.59	5.352	<b>Zr</b>	37	216	126.76
<b>P<sub>2</sub>O<sub>5</sub></b>	0.005	3.87	0.596	<b>Nb</b>	5	29	12.23
<b>Total</b>	95.98	100.89	98.11	<b>Pb</b>	5	80	31.538
<b>K<sub>2</sub>O/Na<sub>2</sub>O</b>	1.12	1718	247.68	<b>Ba</b>	183	981	437.92
<b>K<sub>2</sub>O+Na<sub>2</sub>O</b>	1.98	8.97	6.22	<b>Ce</b>	5	471	91
<b>Molar A/NK</b>	1.206	2.77	1.89	<b>Th</b>	5	185	49.53
<b>Molar A/CNK</b>	1.096	3.36	1.96	<b>U</b>	5	405	52.61
<b>Agpatic Index</b>	0.475	0.928	0.75	<b>K/Rb</b>	0.010	0.02	0.016
				<b>Rb/Sr</b>	2.38	11.846	4
				<b>Ba/Rb</b>	0.54	2.75	1.59
				<b>Ba/Sr</b>	1.77	9.708	5.486

### Classification and Magmatic affinity

The granitoids of the study area characteristically plots in granite field in total alkali-silica diagram (TAS Middlemost, 1994) (Figure 9.7a) with few samples plotted near marginal zone with the quartz-monzonite field. They distinctly show calc-alkaline trend nature in AFM (Na<sub>2</sub>O+K<sub>2</sub>O-FeO<sup>t</sup>-MgO) diagram (Irvine and Baragar, 1971) (Figure 9.7b) with clustering more towards the alkali vertex. Similar observation has noted in TAS diagram defined by Cox et al., 1979 where the samples spread across alkaline-sub alkaline boundary in acidic granite field. These granites show Ferroan nature where Fe\* is >0.5 (Fe\*=FeO<sup>t</sup>/FeO<sup>t</sup>+MgO) (Frost et al., 2001). The Fe\* varies from 0.56-0.99 (n=70) indicating silica enrichment with only minimal enrichment of FeO<sup>t</sup> relative to MgO; suggesting their differentiated nature

(Nockolds & Allen, 1956) (Figure 9.8c). These samples also exhibit mostly alkali-calcic nature in MALI vs. SiO<sub>2</sub> diagram (Frost et al., 2001) (Figure 9.8d).

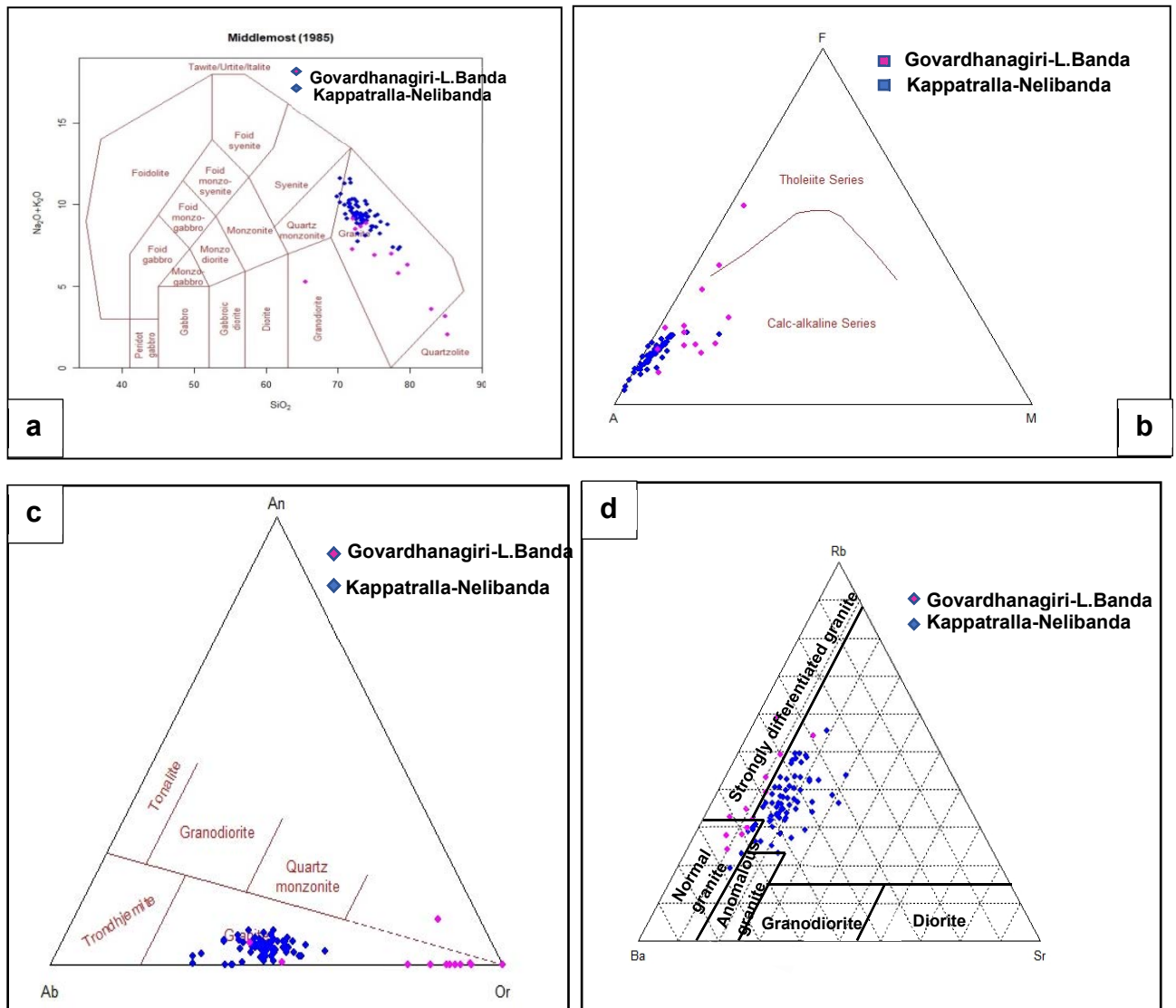


Figure 9.7 a) Total alkali-silica diagram (Middlemost, 1994) b) AFM (Na<sub>2</sub>O+K<sub>2</sub>O-FeO<sup>t</sup>-MgO) diagram (Irvine and Baragar, 1971) c) Ab-An-Or diagram (Barker, 1979 and O'Conner 1965) d) Ba-Rb-Sr ternary plot

The studied granites have  $K_2O/Na_2O$  ratio ranging from 1.01- 2.25 (n=60) indicating its typical post-Archean potassic nature which is substantiated by the predominance of K-feldspars. These calc-alkaline differentiation trends signify the enrichment of alkalis with progressive crystallization in regard to decrease in oxygen fugacity regime during fractional crystallization (Nocklods and Allen, 1953 and Thornton and Tuttle, 1969). A similar observation has also made in normative Ab-An-Or diagram (Barker, 1979 and O'Conner 1965) (Figure 9.7c) wherein the samples are clustered in granite field. The alumina saturated nature of these granites is apparent from the A/CNK [molar  $Al_2O_3 / (CaO+Na_2O +K_2O)$ ; Clarke, 1981] values ranging from 0.88 to 1.29 (avg. 1.08). The dominant peraluminous behaviour of these granites is ascertained by the presence of normative corundum in most of the samples. The alumina saturation index (ASI:  $Al / [(Ca-1.67P) +Na+K]$ ; Zen, 1986) has widely used as a tool for discriminating I-type granite and S-type granites (Chappell and White, (1974 and 1992) and Chappell,1999). The ASI of the studied granite varies from 0.88-1.30 with average 1.08 indicating an overall S-type nature (I type-A/CNK-<1.1 and S type-A/CNK->1.1) (Figure 9.8a). The predominance of Rb over Sr (avg. Rb/Sr ratio-2.09), relatively low CaO and moderate Sr, high  $K_2O$ ,  $Al_2O_3$  and Rb and high average differentiation index (92.74) indicate their S-type signature. The evolved nature of the studied granite is further ascertained by the ternary plot of Ba-Rb-Sr where the samples plot adjacent to the boundary zone of strongly differentiated granite field (Figure 9.7d).

### **Tectonic and Geodynamic Implications**

The granitoids of the study area dominantly plots in the field of syn-collision (syn-COLG) in the geo-tectonic discrimination diagram based on the multi cationic  $R_1$ - $R_2$  factors such as  $R_1$ :

$4Si-11(Na+K)-2(Fe+Ti)$  and  $R_2: 6Ca+2Mg+Al$ ; proposed by De la Roche et al.(1980) and modified by Batchelor and Bowden (1985) (Figure 9.8b).

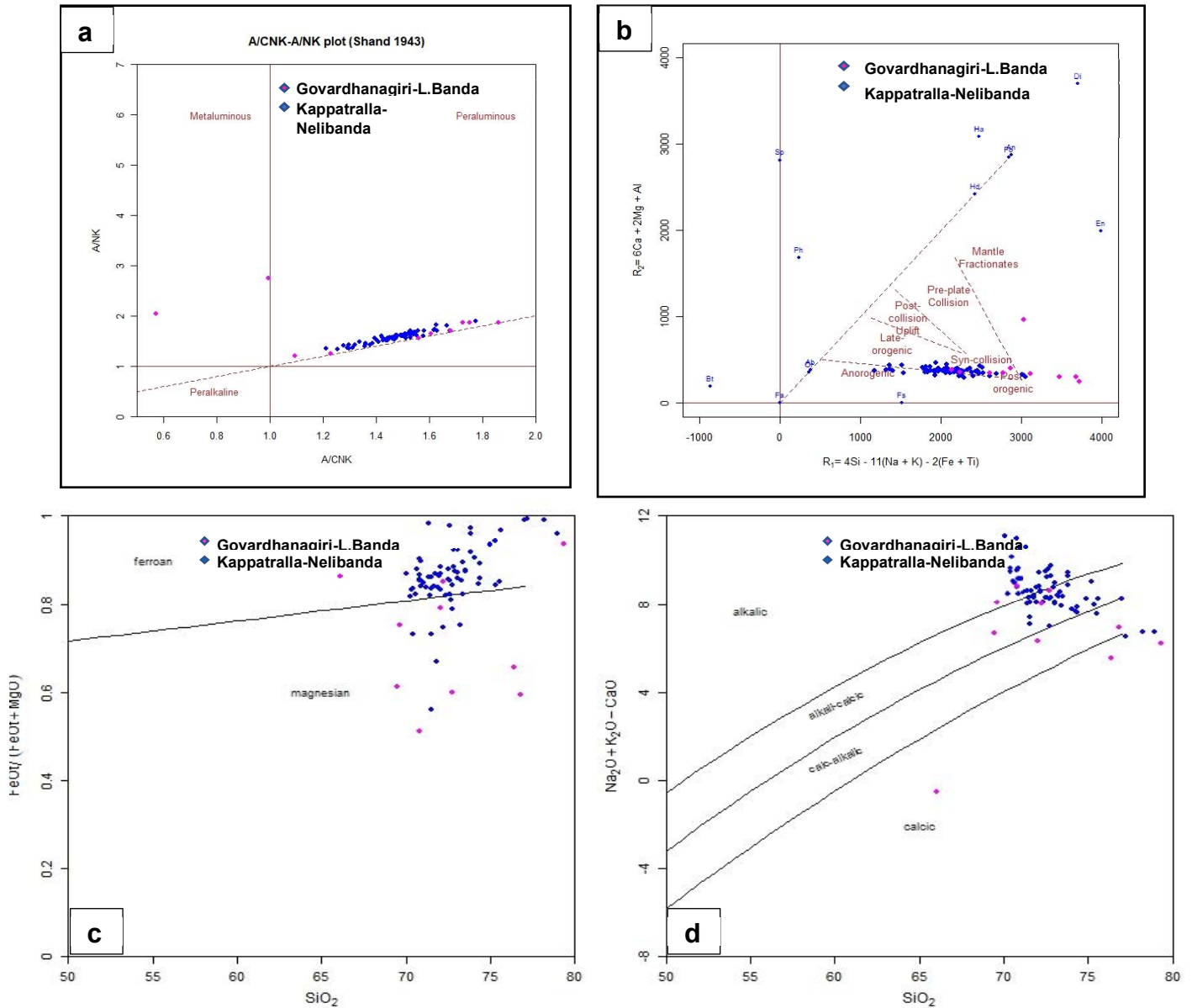


Figure 9.8 a) A/CNK-A/NK plot (Shand 1943) b)  $R_1$ - $R_2$  geo-tectonic discrimination diagram Batchelor and Bowden (1985) c)  $(Fe^*/(FeO^t + MgO))$  vs  $SiO_2$  diagram (Frost et al., 2001) d) MALI vs.  $SiO_2$  diagram (Frost et al., 2001).

## 9.6 Comparison of Gulcheru Quartzite of Govardhanagiri-Lanjabanda area and Kappatralla area

The Gulcheru Quartzite of Govardhanagiri-Lanjabanda area and Kappatralla area are characterized more or less similar major oxide content (Table 9.4). Govardhanagiri-Lanjabanda area has narrow range of SiO<sub>2</sub> (76.52–82.61 wt%), dominantly high Al<sub>2</sub>O<sub>3</sub> (11.38 – 12.23 wt%), K<sub>2</sub>O (2.57 – 4.95 wt%), CaO (<0.01 – 0.1 wt%) and moderate Fe<sub>2</sub>O<sub>3</sub>(t) (0.98 – 3.66 wt%). MgO content is generally low (0.2 – 1.2 wt%), TiO<sub>2</sub> content is (0.17 – 0.29 wt%) and P<sub>2</sub>O<sub>5</sub> content is (<0.01 – 0.12 wt%). Whereas, Kappatralla area has wide range of SiO<sub>2</sub> (63.33–84.41 wt%), dominantly moderate to high Al<sub>2</sub>O<sub>3</sub> (7.55 – 16.38 wt%), K<sub>2</sub>O (1.32 – 5.1 wt%), CaO (0.06 – 0.11 wt%) and moderate Fe<sub>2</sub>O<sub>3</sub>(t) (0.86 – 8.35 wt%). MgO content is generally low (0.17 – 0.57wt%), TiO<sub>2</sub> content is (0.05– 0.45 wt%) and P<sub>2</sub>O<sub>5</sub> content is (0.03 – 0.05 wt%).

Table 9.4 Major oxide (wt%) and trace elements (ppm) data of Gulcheru Quartzite of Govardhanagiri – Lanjabanda and Kappatralla area.

Area	Govardhanagiri – Lanjabanda (n=7)	Kappatralla (n=10)
SiO <sub>2</sub>	75.52 – 82.61 (Av. 79.56)	63.33 – 84.41 (Av. 77.48)
TiO <sub>2</sub>	0.17 – 0.29 (Av. 0.21)	0.05 – 0.45 (Av. 0.23)
Al <sub>2</sub> O <sub>3</sub>	11.38 – 12.23 (Av. 11.83)	7.55 – 16.38 (Av. 12.31)
Fe <sub>2</sub> O <sub>3</sub> (t)	0.98 – 3.66 (Av. 2.19)	0.86 – 8.35 (Av. 3.39)
MgO	0.2 – 1.32 (0.72)	0.17 – 0.57 (Av. 0.35)
MnO	<0.01 – 0.01	0.005 – 0.01 (Av. 0.01)
CaO	<0.01 – 0.1	0.06 – 0.11 (Av. 0.09)
Na <sub>2</sub> O	0.34 – 0.64 (Av. 0.50)	0.04 – 0.52 (Av. 0.14)
K <sub>2</sub> O	2.57 – 4.95 (Av. 3.91)	1.32 – 5.1 (Av. 2.78)
P <sub>2</sub> O <sub>5</sub>	<0.01 – 0.12	0.03 – 0.05 (Av. 0.04)
CIA	65.93 – 75.63 (Av. 70.29)	71.75 – 83.09 (Av. 79.13)
CIW	91.32 – 95.27 (Av.93.06)	94.24 – 98.06 (Av. 96.90)
PIA	86.10 – 92.34 (Av. 89.60)	91.56 – 97.54 (Av. 95.90)
ICV	0.60 – 0.89 (Av. 0.73)	0.38 – 0.97 (Av. 0.56)
Cr	40 – 88	75 – 158
Ni	<10 – 44	17 - 77
Cu	<10	<10 – 86
Zn	<10 - 22	15 – 44
Ga	<10 - 11	12 – 15
Rb	96 – 223	68 - 220
Sr	31 - 73	15 – 46
Y	<10 – 18	<10 - 28
Zr	90 – 230	89 – 312

<b>Nb</b>	<10 – 12	<10
<b>Pb</b>	10 - 22	105 – 264
<b>Ba</b>	372 – 958	19 – 51
<b>Ce</b>	16 - 183	23 - 81

### Geochemical Classification

The Gulcheru Quartzite of Govardhanagiri-Lanjabanda area is classified into arkose and in Kappatralla area, into arkosic to litharenite with few samples into wacke on the basis of chemical data (major oxides) after Pettijohn et. al, (1972) Herron (1988) (Figure 9.9 a &b).

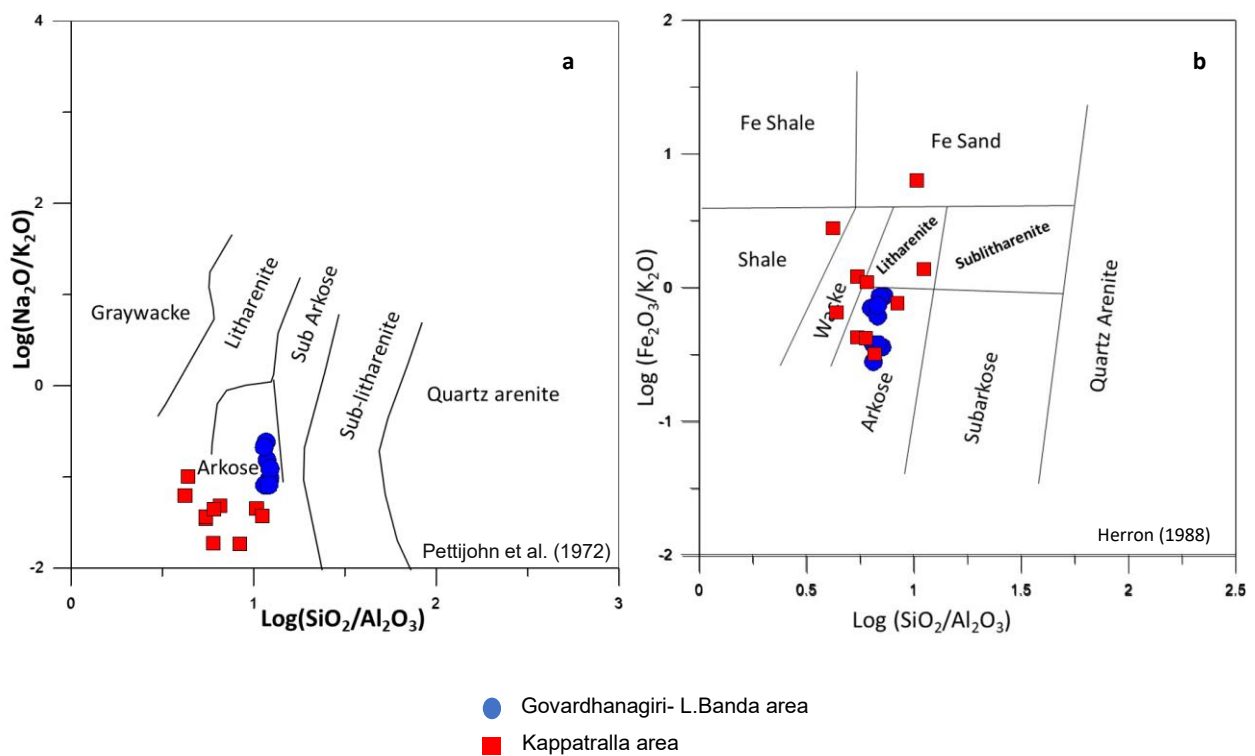
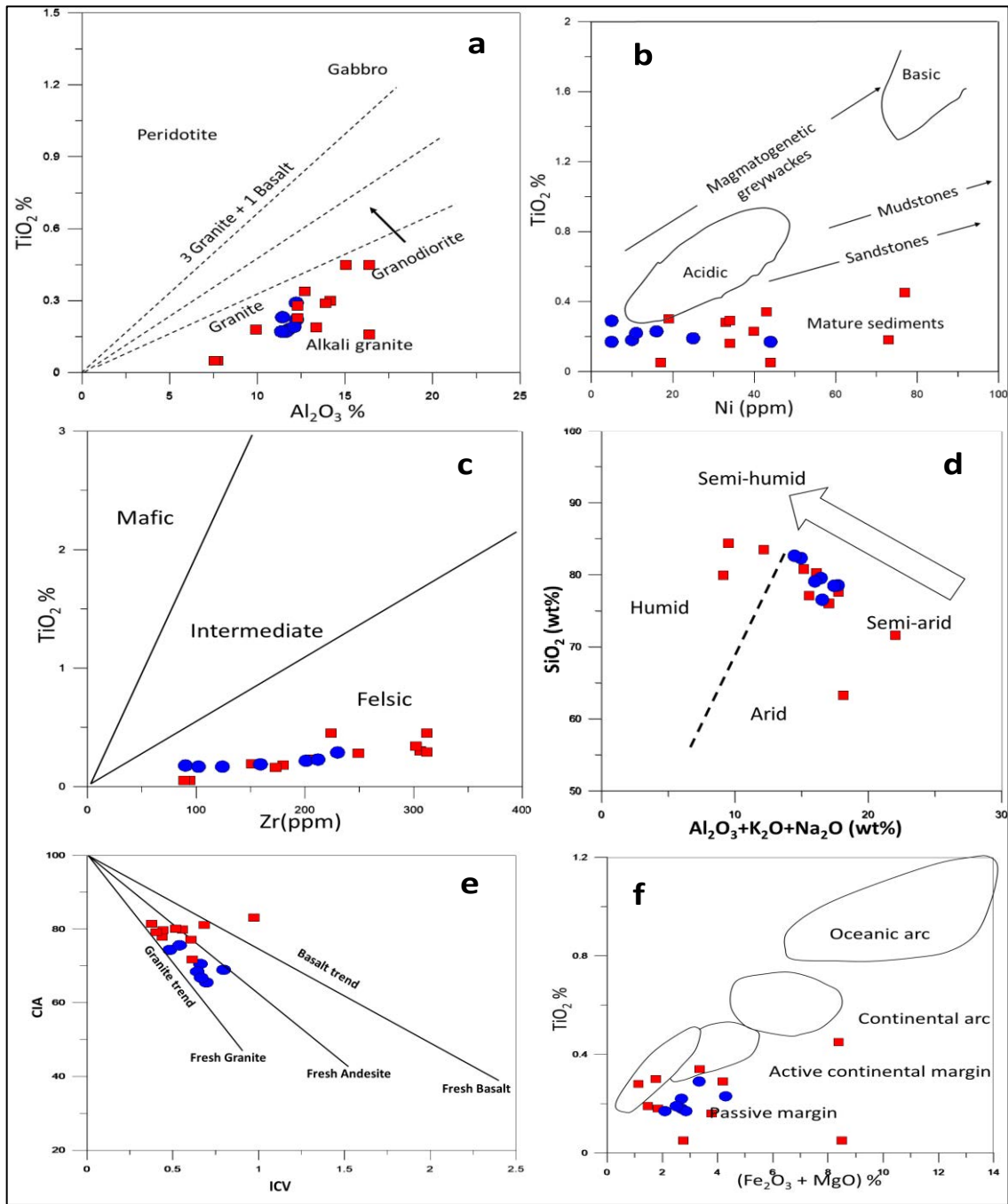


Figure 9.9 Geochemical classification of sandstone. (a) Bivariate plot Log (SiO<sub>2</sub>/Al<sub>2</sub>O<sub>3</sub>) vs. Log (Na<sub>2</sub>O/K<sub>2</sub>O) (b) Bivariate plot Log (SiO<sub>2</sub>/Al<sub>2</sub>O<sub>3</sub>) vs. Log (Fe<sub>2</sub>O<sub>3</sub>/K<sub>2</sub>O).

### Provenance and depositional environment:

After plotting the data in the Al<sub>2</sub>O<sub>3</sub> versus TiO<sub>2</sub> (Figure 9.10a) bivariate discrimination diagram (McLennan SM et al.,1990) samples of both areas plot in the alkali granite- granite field.



● Govardhanaqiri- L.Banda area  
 ■ Kappatralla area

Figure 9.10 Bivariate Plot (a)  $Al_2O_3$  versus  $TiO_2$  plot (McLennan SM et al., 1990) (b) Ni (ppm) versus  $TiO_2$  plot (Floyd PA et al., 1989). (c) Zr vs.  $TiO_2$  plot (after Hayashi et al., 1997) (d)  $(Al_2O_3 + K_2O + Na_2O)$  versus  $SiO_2$  (after Suttner and Dutta, 1986). (e) Index of Chemical Variability (ICV) vs. Chemical Index of Alteration (CIA) plot (after Potter et al. 2005) (f)  $(Fe_2O_3 + MgO)$  versus  $TiO_2$  bivariate diagram (Bhatia MR, 1983).

Another bivariate  $\text{TiO}_2$  versus Ni (ppm) diagram (Figure 9.10b) to evaluate source rock composition (Floyd PA et al., 1989) indicate this mature sandstone are derived from acidic igneous rocks for both the areas the source of sedimentary rocks on the basis of  $\text{TiO}_2/\text{Zr}$  weight ratios. Hayashi et al. (1997) have devised a scheme for discriminating As per that scheme of discrimination, the  $\text{TiO}_2/\text{Zr}$  weight ratios in the studied quartzite samples indicate their derivation dominantly from felsic and to some extent intermediate igneous rocks (Figure 9.10c). Similarly, the ICV vs. CIA plot (Figure 9.10e), also suggest that the source of the studied sediments is from predominantly granitoid source rocks.

The binary plots of  $\text{SiO}_2$  vs.  $(\text{Al}_2\text{O}_3 + \text{K}_2\text{O} + \text{Na}_2\text{O})$  (Suttner and Dutta, 1986) of Gulcheru quartzites indicate derivation of the precursor sediments dominantly under a semi-arid palaeoclimatic condition with some samples falling in semi humid condition of Kappatralla area (Figure 9.10d). The bivariate plot after Bhatia, 1983 is also used to make out about the possible tectonic settings. The bivariate plot (Figure 9.10f) represents passive margin setting.

### **Source area weathering**

The CIA values of Gulcheru Quartzite of Govardhangiri-Lanjabanda area and Kappatralla area range from 65.93 – 75.63 (avg. 70.29) and 71.75 – 83.09 (avg. 79.13) respectively (Table 9.4), suggestive of moderate to high chemical weathering in the source area.

The CIA values are also plotted in  $\text{Al}_2\text{O}_3 - (\text{CaO} + \text{Na}_2\text{O}) - \text{K}_2\text{O}$  triangular plot (Nesbitt and Young 1984; Fedo et al. 1995; commonly referred as the 'A–CN–K' diagram) to categorize the provenance composition and weathering trends. The concept behind the use of this diagram is to understand the rate of weathering of plagioclase (Ca–Na feldspar) and K-feldspar. Thus, during weathering, CaO and  $\text{Na}_2\text{O}$  are preferentially leached relative to  $\text{K}_2\text{O}$  due to which the weathering trend moves parallel to the A–CN join. Intense weathering of a rock removes CaO,  $\text{Na}_2\text{O}$  and  $\text{K}_2\text{O}$ , making the trend parallel to the A–K join.

The studied samples of Gulcheru Quartzite of both the area are plotted in the A–CN–K ternary diagram (Figure 9.11) in which majority of the samples are plotted above the feldspar tie line and samples at right of the five trend line towards K-feldspar, which suggest that these samples might have suffered minor amount of K-metasomatism. The higher content of K<sub>2</sub>O and Rb and sericitization of plagioclase is also suggestive of post-depositional K-metasomatism. On the basis of weathering trends of the studied samples of both areas, the samples have undergone moderate chemical weathering, which could be due to either differential weathering conditions or that the least weathered samples are representative of source rock.

CIW values of Govardhangiri-Lanjabanda area and Kappatralla area range from 91.32 – 95.27 (avg. 93.06) and 94.24 – 98.06 (avg. 96.90) respectively. CIW indices are higher than CIA values for some analysed samples due to exclusion of K<sub>2</sub>O from the index. On the basis of CIW, the studied sediments show intense weathering.

PIA (plagioclase index of alteration) values of ~50 for fresh rocks and values similar to 100 designate considerable productions of secondary aluminous clay minerals (Fedo et al. 1997). The PIA value of Govardhangiri-Lanjabanda area and Kappatralla area ranges from 86.10 – 92.34 (av. 89.60) and 91.56 to 97.54 (av. 95.90) respectively. Like CIA, A–CN–K ternary diagram and CIW, the range of PIA values of all these quartzites also suggest intense chemical weathering. The Index of Chemical Variability (ICV) of Govardhangiri-Lanjabanda area and Kappatralla area range from 0.60 to 0.89 (avg. 0.73) and 0.38 to 0.97 (Av. 0.56) respectively reflect the high mature sediments recycled. The high ICV value (~1) reflects that the sediments were deposited as first cycle deposits in tectonically active continental margins. The samples with ICV >1 is indicating that these are first cycle of sediments and immature nature.

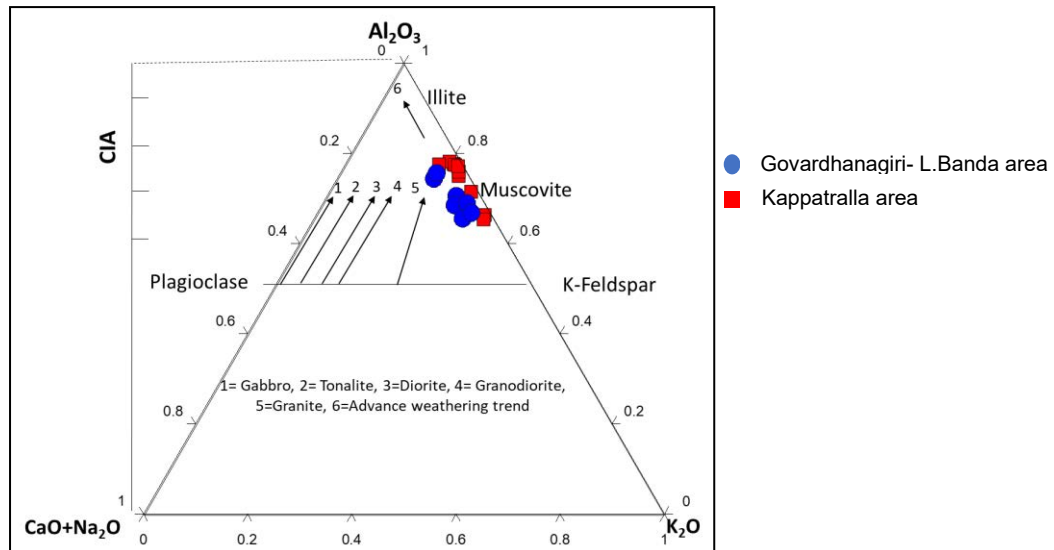


Figure 9.11 A–CN–K ternary diagram of molecular proportions of  $\text{Al}_2\text{O}_3$ –( $\text{CaO}+\text{Na}_2\text{O}$ )– $\text{K}_2\text{O}$  for Gulcheru Quartzite (after Nesbitt and Young 1984).

### K-metasomatism in the quartzites

Conversion of secondary aluminous clay minerals such as kaolinite to illite by K addition results in a CIA value lower than the premetasomatized one. Binary plot of  $\text{MgO}/\text{Al}_2\text{O}_3$  vs.  $\text{K}_2\text{O}/\text{Al}_2\text{O}_3$  (Sopuck et. al., 1983) reveals that illite is the main clay mineral in both the areas (Figure 9.12). Potassium enrichment in the Gulcheru sub-feldspathic quartzite in the form of illitization is substantiated by  $\text{K}_2\text{O}/\text{Al}_2\text{O}_3$  ratios (Govardhanagiri – Lanjabanda area, Av. 0.33 and Kappatralla area, Av. 0.22) and presence of illite (confirmed by XRD Report).

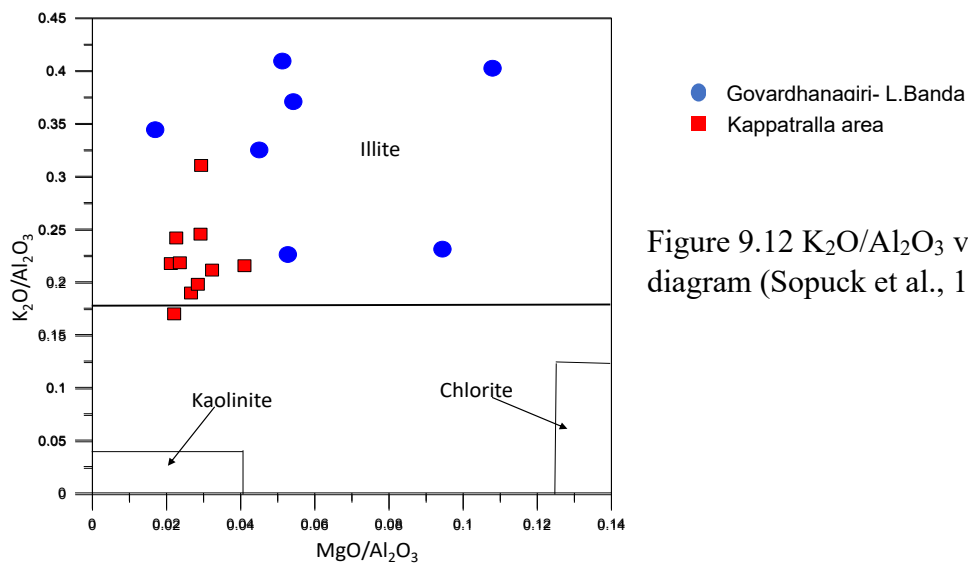


Figure 9.12  $\text{K}_2\text{O}/\text{Al}_2\text{O}_3$  vs  $\text{MgO}/\text{Al}_2\text{O}_3$  diagram (Sopuck et al., 1983).

## **CHAPTER 10**

### **DISCUSSIONS AND CONCLUSIONS**

Detailed geological and litho-structural mapping (1:5000) over 10 sq. km area has been carried out in Govardhanagiri-Lanjabanda area. The area lies in the western margin of Cuddapah basin where Paleo-Mesoproterozoic Papaghni Group comprising of Gulcheru and the Vempalle Formation non-conformably overlies the Archaean basement. The basement crystallines comprises peninsular gneisses, different types of intrusive granites, basic dykes and quartz reefs. The PGC group of rocks are represented by grey/pink alkali feldspar granite gneisses and tonalites which forms the major rock type. The intrusive granite is essentially medium grained pink and grey variety with occasional zones of K-feldspar porphyries and pegmatite variants. The granites are affected by vertical to steeply dipping fractures of E-W, N80°E-S80°W, N60-80°W-S60-80°E and N-S trends. A number of doleritic dykes, pegmatite and quartz veins are intruding in basement granite along ENE-WSW and WNW-ESE trending fracture planes. The basement gneisses and intrusive granite are unconformably overlain by 10-20° easterly and south-easterly dipping basal conglomerate and quartzite sequence of Gulcheru Formation. The unconformity is clearly exposed at many places with occasional thin layer of (about 10-20cm) paleosol between the basement granite and Gulcheru conglomerate. Thus, the litho-structural setup is ideal for hosting unconformity proximal uranium mineralisation akin to Kappatralla uranium deposit.

The Gulcheru Formation mainly comprises of rudaceous and arenaceous sediments. It occurs as narrow linear, gently dipping and frequently offset by a number of mainly ESE-WNW trending diagonal faults. The ESE-WNW and NE-SW faults have affected basement and the overlying sediments. The entire basement-sediment sequence is affected by E-W

trending sinistral Veldurthi-Kalva-Gani (VKG) strike slip fault systems and associated cross faults with prominent E-W displacements. The structural set up comprises of fault/fracture system provides potential conduits for the movement of labile uranium as solution.

Three radioactive anomalies recorded in basement granite in Lanjabanda area assayed 0.020%  $U_3O_8$  (Spotty to 3-1.5m) while anomalies in Gulcheru Quartzite were thoriferous (0.013-0.055%  $ThO_2$ ) in nature. The radioelemental concentration of the granitoid rocks of the study area varies from U (8-62ppm, avg. 32ppm), Th (2.5-53ppm, avg. 16ppm) and K (0.6%-5.7% avg. 2.96%) (n=15) (Table 5.2). The average concentration of these elements in Closepet granite is 3.5ppm of U, 18.2 ppm of Th and 3.8% of K (Rao et al., 1972). The Th/U ratio of granites of the study area with average value of 0.5 (Table 5.2 and Figure 5.3) indicate less evolved felsic magma than Closepet Granite (avg. Th/U ratio 6.4). It is observed that the grey and pink varieties of granite show differential degree of differentiation and the pink varieties appear to be more evolved than corresponding grey varieties. Fracture data collected (n=75) using joints (n=65), dykes (n=4) and veins (n=6) in Lanjabanda area from basement and Gulcheru Quartzite and plotted on rose diagram resulted in delineation of NW-SE and NE-SW as two most prominent trends. ENE-WSW trending fractures are the youngest which are sympathetic to sinistral strike slip Veldurthi-Kalva-Gani (VKG).

Deductive palaeohydraulic reconstructions using cross-bed set thickness (n=40) of Gulcheru quartzite suggests fluvial environment of deposition with steep channel gradient (>0.007m/m) typical of Precambrian fluvial system. Morphometric indices such as elongation ratio, flatness index, maximum projection sphericity and oblate-prolate index ranges from 0.44 – 0.99, 29.05 – 81.12, 0.52 – 0.92 and -8.35 – 11.28 respectively. All these indices signify fluvial condition of deposition. The bivariate plot between sphericity against oblate-prolate index and coefficient of flatness against sphericity also shows cluster of samples in fluvial environment. In the triangular sphericity form diagram, most of the samples falls in

compact, compact elongate, and elongate field, suggesting fluvial nature of deposition of Gulcheru sediments. The porosity and permeability of the basal conglomerate is likely to favour transmission of mineralised solution and the redox interface along the unconformity helps in its precipitation.

Petro-mineralogy and geochemical characterization of Basement Granites from Govardhanagiri-Lanjabanda area suggests it to be classified as two-mica granite with strongly peraluminous nature ( $A/CNK > 1.1$ ), high silica content (avg. 74.92 wt%), low amount of ferromagnesian oxides ( $< 4\%$ ) (avg. 2.73 wt%), high  $K_2O$  with  $K_2O/Na_2O > 1$ , low  $CaO/(Na_2O+K_2O)$  (avg. 0.05 wt%), high  $Al_2O_3/(FeO_t+MgO)$  (avg. 5.34 wt%), high Rb content and presence of normative corundum ( $> 1$  wt%). These mineralogical and geochemical characteristics of the granites suggests crustal origin which are very fertile in terms of uranium concentration as they are derived from partial melting of metasediments. On total alkali vs. silica discrimination plot, and  $R_1-R_2$  plot (Da la Roche 1980) the studied samples occupy the field of granites. Modified alkali lime index (MALI) shows alkali to calcic character (Frost et al 2001). On the basis of  $CaO$  and  $Fe_2O_3$  content, the samples fall in S-type granite (Chappel and White, 2001). Based on  $R_1$  vs.  $R_2$  (Batchelor and Bowden 1985) multiple discrimination diagrams granites were formed in syn-collisional to post orogenic tectonic setting. The  $\Sigma LREE$  content in granite ( $n=8$ ) ranges from 48 to 176 (avg. 122.13) whereas  $\Sigma HREEs$  varies from 29.15 to 61.55 (avg. 46.34). The high level of enrichment of LREE relative to HREE suggests high order of fractionation. The normalized  $(LREE/HREE)_N$  ratio ranges from 0.67 to 2.56 (avg. 1.50). The degree of LREE fractionation,  $(La/Yb)_N$  of 13.89, is slightly higher than that of HREE fractionation,  $(Gd/Yb)_N$  of 2.95. This is also evident by the presence of monazite in these granites.

Petro-mineralogy and geochemical characterization of Gulcheru Quartzite from Govardhanagiri-Lanjabanda area suggests that Gulcheru quartzite grades texturally from sub-

feldspathic arenite to quartz arenite and classified on the chemical data (major oxides) into Arkose (Herron, 1988). Geochemical data reflect mineralogically mature nature. High degree of mineralogical maturity is indicated by high SiO<sub>2</sub>, dominantly moderate SiO<sub>2</sub>/Al<sub>2</sub>O<sub>3</sub>, and K<sub>2</sub>O/Na<sub>2</sub>O ratios. In Al<sub>2</sub>O<sub>3</sub> versus TiO<sub>2</sub> bivariate discrimination diagram (McLennan SM et al., 1990) the samples plot in the alkali granite- granite field. TiO<sub>2</sub> versus Ni (ppm) diagram to evaluate source rock composition (Floyd PA et al., 1989) indicate this mature sandstone are derived from acidic igneous rocks. The bivariate plot (after Bhatia, 1983) represents passive margin setting. TiO<sub>2</sub> and Zr concentrations in siliciclastic rocks are good indicators of source rock. TiO<sub>2</sub> /Zr weight ratios (Hayashi et al, 1997) indicate their derivation dominantly from felsic igneous rocks. SiO<sub>2</sub> vs. (Al<sub>2</sub>O<sub>3</sub> +K<sub>2</sub>O+Na<sub>2</sub>O) (Suttner and Dutta, 1986) binary plot apparently (ignoring the effect of reworking/recycling) indicate derivation of the precursor sediments dominantly under a semi-arid palaeoclimatic condition. The CIA, CIW, PIA and ICV values in the Gulcheru Quartzite range from 65.93 – 75.63 (avg. 70.29), 91.32 – 95.27 (avg. 93.06), 86.10 – 92.34 (avg. 89.60) and 0.60 to 0.89 (avg. 0.73) respectively suggestive moderate to intense chemical weathering in the source area. ICV vs. CIA binary plot suggest Gulcheru Quartzite form predominantly from granitoids source rocks. Conversion of secondary aluminous clay minerals such as kaolinite to illite by K addition results in a CIA value lower than the pre-metasomatized one. The petrographic expression is the presence of illite, both as matrix material between grains, and as alteration of partially weathered plagioclase grains.

The Gulcheru Quartzite of Govardhanagiri-Lanjabanda and Kappatralla area are classified into arkose and arkose to litharenite with few samples fall into wacke field respectively. Conversion of secondary aluminous clay minerals such as kaolinite to illite by K-addition results in a CIA value lower than the premetasomatized one. Binary plot of MgO/Al<sub>2</sub>O<sub>3</sub> Vs. K<sub>2</sub>O/Al<sub>2</sub>O<sub>3</sub> (Sopuck et. al., 1983) reveals that illite is the main clay mineral in both the areas. Potassium metasomatism in the Gulcheru sub-feldspathic quartzite in the form

of illitization is substantiated by  $K_2O/Al_2O_3$  ratios (Govardhanagiri – Lanjabanda area, Av. 0.33 and Kappatralla area, Av. 0.22) and which is confirmed by presence of illite (confirmed by XRD Report). The granitoids of Govardhanagiri-Lanjabanda and Kappatralla area show similarity in chemical behaviour and plots in granite field in total alkali-silica diagram (TAS Middlemost, 1994). The dominant peraluminous behaviour of these granites is ascertained by the presence of normative corundum. The granitoids of the study area dominantly plots in the field of syn-collision (syn-COLG) tectonic settings. Additionally, the ASRS survey over Kurnool-Dhone block during 1983-84 reveals the occurrence of high K bearing younger basement granites and their continuity towards basin margin. These NW-SE trending younger granites are forming the basement for Gulcheru sediments in Kappatralla outlier where unconformity proximal mineralisation has been established by detailed survey and drilling.

**Controls of uranium mineralisation:** The presence of NW-SE and NE-SW cross fractures in both the basement granites and overlying Gulcheru sediments facilitated the movement of ore bearing fluid. The precipitation of uranium from the solution in the host Gulcheru Quartzite is mainly controlled by the presence of sulphide minerals like pyrite and chalcopyrite which provides redox conditions for the change in oxidation state of uranium and hence its precipitation as coffinite.

## REFERENCES

- Acharyulu, A.A.P.S.R., Murty, B.S. and Bhaumik, B.K., (2004). Enrichment characteristics of radioelements in various types of rock from Sambalpur district, Orissa, India. *Journal of Earth System Science*, 113(3), pp.321-352.
- Alexander, J., Bridge, J.S., Cheel, R.J. and Leclair, S.F., (2001). Bedforms and associated sedimentary structures formed under supercritical water flows over aggrading sand beds. *Sedimentology*, 48(1), pp.133-152.
- Allen, J.R.L., (1968). The nature and origin of bed-form hierarchies. *Sedimentology*, 10(3), pp.161-182.
- Anand, M., Gibson, S.A., Subbarao, K.V., Kelley, S.P. and Dickin, A.P., (2003). Early Proterozoic melt generation processes beneath the intra-cratonic Cuddapah Basin, southern India. *Journal of Petrology*, 44(12), pp.2139-2171.
- Anderson, E.M., (1951). The dynamics of faulting and dyke formation with applications to Britain. Oliver and Boyd.
- Armstrong-Altrin, J.S., (2009). Provenance of sands from Cazonas, Acapulco, and Bahía Kino beaches, Mexico. *Revista Mexicana de Ciencias Geológicas*, 26(3), pp.764-782.
- Barker, F., (1979). Trondhjemite: definition, environment and hypotheses of origin. In *Developments in petrology* (Vol. 6, pp. 1-12). Elsevier.
- Bas, M.L., Maitre, R.L., Streckeisen, A., Zanettin, B. and IUGS Subcommittee on the Systematics of Igneous Rocks, (1986). A chemical classification of volcanic rocks based on the total alkali-silica diagram. *Journal of petrology*, 27(3), pp.745-750.
- Basu, A., (1985). Reading provenance from detrital quartz. In *Provenance of arenites* (pp. 231-247). Springer, Dordrecht.
- Basu, A., Young, S.W., Suttner, L.J., James, W.C. and Mack, G.H., (1975). Re-evaluation of the use of undulatory extinction and polycrystallinity in detrital quartz for provenance interpretation. *Journal of Sedimentary Research*, 45(4), pp.873-882.
- Batchelor, R.A. and Bowden, P., (1985). Petrogenetic interpretation of granitoid rock series using multicationic parameters. *Chemical geology*, 48(1-4), pp.43-55.
- Bhaskar Rao Y J, Pantulu G V C, Damodara Reddy V and Gopalan K (1995) Time of early sedimentation and volcanism in the Proterozoic Cuddapah basin, south India: evidence from the Rb-Sr age of Pulivendla mafic sill; *Mem. Geol. Soc. India* 33 329–338.
- Bhatia, M.R., (1983). Plate tectonics and geochemical composition of sandstones. *The Journal of Geology*, 91(6), pp.611-627.

- Bhaumik, B.K., Bhattacharya, T., Acharyulu, A.A.P.S.R., Srinivas, D. and Sandilya, M.K., (2004). Principles of radiometry in radioactive metal exploration.
- Bisht, B.S., Rajasekaran, P. and Sinha, R.M., (2001). Fluid inclusion characteristics of unconformity-related uranium mineralisation, Lambapur-Peddagattu area, Andhra Pradesh. *Journal of the Geological Society of India*, 58(1), pp.45-51.
- Blair, T.C. and McPherson, J.G., (1994). Alluvial fans and their natural distinction from rivers based on morphology, hydraulic processes, sedimentary processes, and facies assemblages. *Journal of sedimentary research*, 64(3).
- Blatt, H., (1967). Provenance determinations and recycling of sediments. *Journal of Sedimentary Research*, 37(4), pp.1031-1044.
- Bluck, B.J., (1967). Sedimentation of beach gravels; examples from South Wales. *Journal of Sedimentary Research*, 37(1), pp.128-156.
- Bose, P.K., Eriksson, P.G., Sarkar, S., Wright, D.T., Samanta, P., Mukhopadhyay, S., Mandal, S., Banerjee, S. and Altermann, W., (2012). Sedimentation patterns during the Precambrian: a unique record? *Marine and Petroleum Geology*, 33(1), pp.34-68.
- Boynton, W.V., (1984). Cosmochemistry of the rare earth elements: meteorite studies. In *Developments in geochemistry* (Vol. 2, pp. 63-114). Elsevier.
- Chakrabarti, G., Shome, D., Bauluz, B. and Sinha, S., (2009). Provenance and weathering history of Mesoproterozoic clastic sedimentary rocks from the basal Gulcheru Formation, Cuddapah Basin. *Journal of the Geological Society of India*, 74(1), pp.119-130.
- Chappell, B.W. and White, A.J., (2001). Two contrasting granite types: 25 years later. *Australian journal of earth sciences*, 48(4), pp.489-499.
- Chappell, B.W., (1999). Aluminium saturation in I- and S-type granites and the characterization of fractionated haplogranites. *Lithos*, 46(3), pp.535-551.
- Chaudhuri, A.K., Saha, D., Deb, G.K., Deb, S.P., Mukherjee, M.K., Ghosh, G., (2002). The Purana basins of southern cratonic province of India—a case for Mesoproterozoic fossil rifts. *Gondwana Res.* 5, 22–33.
- Clarke, D.B., (1981). The mineralogy of peraluminous granites; a review. *The Canadian Mineralogist*, 19(1), pp.3-17.

- Clarke, F.W. and Washington, H.S., (1924). The composition of the earth's crust (Vol. 127). US Government Printing Office.
- Condie, K.C. and Sinha, A.K., (1996). Rare earth and other trace element mobility during mylonitization: a comparison of the Brevard and Hope Valley shear zones in the Appalachian Mountains, USA. *Journal of Metamorphic Geology*, 14(2), pp.213-226.
- Condie, K.C., (1986). Origin and early growth rate of continents. *Precambrian Research*, 32(4), pp.261-278.
- Condie, K.C., (1993). Chemical composition and evolution of the upper continental crust: contrasting results from surface samples and shales. *Chemical geology*, 104(1-4), pp.1-37.
- Coulson A L (1933-44) *Mere. Geol Surv. India* 64 182
- Cox R, Lowe D R and Cullers R L (1995) The influence of sediment recycling and basement composition on evolution of mudrock chemistry in the southwestern United States; *Geochim. Cosmochim. Acta* 9(14) 2919–2940.
- Cox, K.G., Bell, J.D. and Pankhurst, R.J., (1979). *The Interpretation of Igneous Rocks*. George Allen & Unwin, London, 450 pp.
- Cullers, R.L. and Podkovyrov, V.N., (2000). Geochemistry of the Mesoproterozoic Lakhanda shales in southeastern Yakutia, Russia: implications for mineralogical and provenance control, and recycling. *Precambrian Research*, 104(1-2), pp.77-93.
- Cuney, M., (2014). Felsic magmatism and uranium deposits. *Bulletin de la Société Géologique de France*, 185(2), pp.75-92.
- Dahlquist, J.A., Galindo, C., Pankhurst, R.J., Rapela, C.W., Alasino, P.H., Saavedra, J. and Fanning, C.M., (2007). Magmatic evolution of the Peñón Rosado granite: petrogenesis of garnet-bearing granitoids. *Lithos*, 95(3-4), pp.177-207.
- Darnley, A. G., and Ford, K. L., (1989), Regional airborne gamma-ray survey: A review; in “Proceedings of Exploration 87: Third Decennial International Conference on Geophysical and Geochemical Exploration for Minerals and Ground Water”, *Geol. Surv. of Canada, Special Vol. 3*, 960 p.
- De La Roche, D.H., Leterrier, J.T., Grandclaude, P. and Marchal, M., (1980). A classification of volcanic and plutonic rocks using R1R2-diagram and major-element analyses—its relationships with current nomenclature. *Chemical geology*, 29(1-4), pp.183-210.

- Debon, F. and Le Fort, P., (1983). A chemical–mineralogical classification of common plutonic rocks and associations. *Earth and Environmental Science Transactions of the Royal Society of Edinburgh*, 73(3), pp.135-149.
- Dhana Raju, R., Umamaheswar, K., Tripathi, B.K., Rai, A.K., Zakauilla, S., Thirupathi, P.V. and Nanda, L.K. (2002). Structurally controlled and crystalline rock-hosted uranium mineralisation in the southern environs of Cuddapah basin, Andhra Pradesh, India. *Expl. Res. At. Miner.*, v.14, p.95–108.
- Dickson, B.L. and Scott, K.M., (1997). Interpretation of aerial gamma-ray surveys-adding the geochemical factors. *AGSO Journal of Australian Geology and Geophysics*, 17, pp.187-200.
- Divakara Rao, V., Aswathanarayana, U. and Qureshy, M.N., (1972). Trace element geochemistry of parts of the closepet granite, Mysore State, India. *Mineralogical Magazine*, 38, pp.678-686.
- Dobkins, J.E. and Folk, R.L., (1970). Shape development on Tahiti-nui. *Journal of Sedimentary Research*, 40(4), pp.1167-1203.
- Dutt, N.V.B.S. (1962). Geology of the Kurnool System of rocks in Cuddapah and the southeastern part of the Kumool district. *Andhra Pradesh. Rec. Geol. Surv. India*.v. 87, pp. 540-604.
- Dwivedi, A.K., Hegde, G.N. and Umamaheswar, K., (2006). Uranium Mineralisation in the Gulcheru Quartzite of Cuddapah Basin, in the Tipparajupalle and Cheruvula Bodu Area, Cuddapah District, Andhra Pradesh. *CLJ*, 76, p.30.
- Eriksson, P., Long, D., Bumby, A., Eriksson, K., Simpson, E., Catuneanu, O., Claassen, M., Mtinkulu, M., Mudziri, K., Brümer, J. and van der Neut, M., (2008). Paleohydrological data from the c. 2.0 to 1.8 Ga Waterberg Group, South Africa: discussion of a possibly unique Palaeoproterozoic fluvial style. *South African Journal of Geology*, 111(2-3), pp.281-304.
- Fedo, C.M., Nesbitt, H.W., Young, G.M., (1995). Unraveling the effects of K-metasomatism in sedimentary rocks and paleosols, with implications for paleoweathering conditions and provenance. *Geology* 23, p. 921-924.
- Floyd, P.A., Winchester, J.A. and Park, R.G., (1989). Geochemistry and tectonic setting of Lewisian clastic metasediments from the Early Proterozoic Loch Maree Group of Gairloch, NW Scotland. *Precambrian Research*, 45(1-3), pp.203-214.

- French, B.M., Heaman, L.M., Chacko, T., Srivastava, R.K., (2008). 1891–1883 Ma Southern Bastar–Cuddapah mafic igneous events, India: a newly recognized large igneous province. *Precambrian Research* 160, 308–322.
- Frost, B.R., Barnes, C.G., Collins, W.J., Arculus, R.J., Ellis, D.J. and Frost, C.D., (2001). A geochemical classification for granitic rocks. *Journal of petrology*, 42(11), pp.2033-2048.
- Galbraith, J.H. and Saunders, D.F., 1983. Rock classification by characteristics of aerial gamma-ray measurements. *Journal of Geochemical Exploration*, 18(1), pp.49-73.
- Gangadharan, G.R., Achar, K.K., Umamaheshwar, K. and Mary K. Kumar (2000) A note on uraniferous leucogranite along the Idupulapaya fault zone, Cuddapah district, A.P. *Jour. Geol. Soc. India*, v.56, pp.223-225.
- Gao, J., Klemd, R., Qian, Q., Zhang, X., Li, J., Jiang, T. and Yang, Y., (2011). The collision between the Yili and Tarim blocks of the Southwestern Altaids: geochemical and age constraints of a leucogranite dike crosscutting the HP–LT metamorphic belt in the Chinese Tianshan Orogen. *Tectonophysics*, 499(1-4), pp.118-131.
- Gnojek, I. and Přichystal, A., (1985). A new zinc mineralization detected by airborne gamma-ray spectrometry in northern Moravia (Czechoslovakia). *Geoexploration*, 23(4), pp.491-502.
- Grasty, R.L. and Shives, R.B.K., (1997). Applications of gamma ray spectrometry to mineral exploration and geological mapping. In *Workshop presented at Exploration (Vol. 97)*.
- Harnois, L., (1988). The CIW index: A new chemical index of weathering. *Sediment. Geol.*, 55: 319-322.
- Harpum, J.R., (1963). Petrographic classification of granitic rocks by partial chemical analysis. *Tanganyika Geol. Surv. Rep*, 10, pp.80-86.
- Hashiguchi H, Yamada R and Inone T (1983) Practical application of low Na<sub>2</sub>O anomalies in footwall acid lava for delimiting promising areas around the Kosaka and Fukagawa Kuroko deposits, Aketa Prefectural, Japan; *Econ. Geol.* 387-394
- Hayashi, K.I., Fujisawa, H., Holland, H.D. and Ohmoto, H., (1997). Geochemistry of ~ 1.9 Ga sedimentary rocks from northeastern Labrador, Canada. *Geochimica et Cosmochimica Acta*, 61(19), pp.4115-4137.
- Herron, M.M., (1988). Geochemical classification of terrigenous sands and shales from core or log data. *Journal of Sedimentary Research*, 58(5), pp.820-829.

- Hessler, A.M. and Lowe, D.R., (2006). Weathering and sediment generation in the Archean: an integrated study of the evolution of siliciclastic sedimentary rocks of the 3.2 Ga Moodies Group, Barberton Greenstone Belt, South Africa. *Precambrian Research*, 151(3-4), pp.185-210.
- Irvine, T.N.J. and Baragar, W.R.A., (1971). A guide to the chemical classification of the common volcanic rocks. *Canadian journal of earth sciences*, 8(5), pp.523-548.
- Itam, A. E., and Inyang, D.O., (2015). Granulometry and pebble morphometry of Awi sandstones, Calabar Flank, Nigeria., *Int. Jour. of Engg. and Applied Sci.*, vol.6 No.4, p. 15-27.
- Ito, Y. and Obara, K., (2006). Very low frequency earthquakes within accretionary prisms are very low stress-drop earthquakes. *Geophysical Research Letters*, 33(9).
- Jeyagopal, A.V., Deshpande, M.S.M., Gupta, S., Ramesh Babu, P.V., Umamaheswar, K. and Maithani, P.B., (2011). Uranium mineralization and association of carbonaceous matter in Koppunuru Area, Palnad sub-basin, Cuddapah basin, Andhra Pradesh. *Ind. Mineral*, 45(1), pp.100-111.
- Jhanwar, M.L. Rajurkar, S.T. and Phadtere, P.N., (1964). Stratigraphy of the Vempalle formation of Cuddapah basin. *J. Indian Geosc. Ass.*, 4: 43--62.
- King, W. (1872). Kudapah and Karnul Formations in the Madras Presidency. *Geological Survey of India, Memoir*, 8, 346.
- Krumbein, W.C., (1941). Measurement and geological significance of shape and roundness of sedimentary particles. *Journal of Sedimentary Research*, 11(2), pp.64-72.
- Laflèche, M.R., Dupuy, C. and Bougault, H., (1992). Geochemistry and petrogenesis of Archean mafic volcanic rocks of the southern Abitibi Belt, Québec. *Precambrian Research*, 57(3-4), pp.207-241.
- Leeder, M.R., (1973). Fluvial fining-upwards cycles and the magnitude of palaeochannels. *Geological Magazine*, 110(3), pp.265-276.
- Leopold, L.B., Wolman, M.G., Miller, J.P. and Wohl, E., (2020). *Fluvial processes in geomorphology*. Courier Dover Publications.
- Liegeois, J.P., Navez, J., Hertogen, J. and Black, R., (1998). Contrasting origin of post-collisional high-K calc-alkaline and shoshonitic versus alkaline and peralkaline granitoids. The use of sliding normalization. *Lithos*, 45(1-4), pp.1-28.

- Lorenz, J.C., Heinze, D.M., Clark, J.A. and Searls, C.A., (1985). Determination of widths of meander-belt sandstone reservoirs from vertical downhole data, Mesaverde Group, Piceance Creek Basin, Colorado. *AAPG bulletin*, 69(5), pp.710-721.
- Luttig, G. (1962). The shape of pebbles in the continental, fluvial and marine facies. *Int. Assoc. Science Hydro. Publ.* 59,253 – 258.
- Matin, A. and Guha, J., (1996). Structural geometry of the rocks of the southern part of the Nallamalai Fold Belt, Cuddapah Basin, Andhra Pradesh. *Journal of the Geological Society of India*, 47(5), pp.535-545.
- McLennan, S.M., Taylor, S.R., McCulloch, M.T. and Maynard, J.B., (1990). Geochemical and Nd–Sr isotopic composition of deep-sea turbidites: crustal evolution and plate tectonic associations. *Geochimica et Cosmochimica Acta*, 54(7), pp.2015-2050.
- Meijerink, A.M.J., Rao, D.P. and Rupke, J., (1984). Stratigraphic and structural development of the Precambrian Cuddapah Basin, SE India. *Precambrian Research*, 26(1), pp.57-104.
- Miall, A.D., (1976). Palaeocurrent and palaeohydrologic analysis of some vertical profiles through a Cretaceous braided stream deposit, Banks Island, Arctic Canada. *Sedimentology*, 23(4), pp.459-483.
- Miall, A.D., (2010). Architectural-element analysis: a new method of facies analysis applied to fluvial deposits. *Recognition of fluvial depositional systems and their resource potential*, 1(1), p.33.
- Middlemost, E.A., Magmas, K. and Rocks, M., (1985). An introduction to igneous petrology. *Magma and magmatic Rocks*. Longmans.
- Milani, E.J. and Davison, I., (1988). Basement control and transfer tectonics in the Recôncavo-Tucano-Jatobá rift, Northeast Brazil. *Tectonophysics*, 154(1-2), pp.41-70.
- Nagaraja Rao, B.K., Rajurkar, S.T., Ramalinga Swamy, G. and Ravindar Babu, B., *Mem. Geol. Soc.India*, (1987), 6, Stratigraphy, Structure and evolution of Cuddapah basin p.33–86
- Narayanaswami, S., (1966). Tectonics of the Cuddapah basin. *Geological Society of India*, 7, pp.33-50.
- Nesbitt H W and Young G M (1984) Prediction of some weathering trends of plutonic and volcanic rocks based on thermodynamic and kinetic considerations; *Geochim. Cosmochim. Acta* 48(7) 1523–1534.

- Nesbitt, H.W., Young, G.M., (1982). Early Proterozoic climates and plate motions inferred from major elements of lutites. *Nature*, 299, p. 715-717.
- Nockolds, S.R. and Allen, R., (1953). The geochemistry of some igneous rock series. *Geochimica et Cosmochimica Acta*, 4(3), pp.105-142.
- O'connor, J.T., (1965). A classification for quartz-rich igneous rocks. Geological Survey Professional Paper, 525, p.79.
- Ogundele, F.O., Odewumi, S.G. and Ganniy, B., (2013). Morphometric Description of Gullies Developing on Coastal Plain Formations around Yewa South and Ipokia in Ogun State South-West Nigeria. *Journal of Geography and Geology*, 5(1), p.126.
- Okon, E.E., Asi, M.O. and Ojong, R.A., (2018). Morphometric studies of pebbles from Ewen area, Calabar flank, southeastern Nigeria: implications for Paleoenvironmental reconstruction. *Physical Science International Journal*, pp.1-12.
- Osterkamp, W.R., Hedman, E.R. and Wiseman, A.G., (1982). Geometry, basin-characteristics, discharge, and particle-size data from gaged stream-channel sites, Western United States (No. 82-93). US Geological Survey.
- Patranabis-Deb, S., Saha, D. and Tripathy, V., (2012). Basin stratigraphy, sea-level fluctuations and their global tectonic connections—evidence from the Proterozoic Cuddapah Basin. *Geological Journal*, 47(2-3), pp.263-283.
- Pearce, J.A. and Cann, J.R., (1973). Tectonic setting of basic volcanic rocks determined using trace element analyses. *Earth and planetary science letters*, 19(2), pp.290-300.
- Peccerillo, A. and Taylor, S.R., (1976). Rare earth elements in East Carpathian volcanic rocks. *Earth and Planetary Science Letters*, 32(2), pp.121-126.
- Pettijohn, F.J., Potter, P.E., Siever, R., (1987). *Sand and Sandstone*. Springer-Verlag, Berlin. 306 pp.
- Potter, P.E., (1978). Petrology and geochemistry of modern Big River sands. *Jour. Geol.* 86, p. 423-449.
- Rai, A.K., Zakaula, S., Jeyagopal, A.V., Rao, M.V., Nagabhushana, J.C. and Varadaraju, H.N. (2002). Uranium mineralisation in the southwestern part of the Cuddapah basin, Andhra Pradesh. *Expl. Res. At. Miner.*, v.14, p.79–94.
- Rajaraman and K.K Tiwari (2018-19) AMD unpublished annual report.

- Rajaraman, H.S., Jain, S.K., Bisht, B.S., Jeyagopal, A.V. and Verma, M.B. (2019) Uranium mineralization in Kappatralla outlier of Gulcheru quartzite formation, Mesoproterozoic Cuddapah Supergroup, Kurnool district, Andhra Pradesh, India. *Current Science*, 116(8), p.1294-1298.
- Ramakrishnan, M. and Vaidyanadhan, R., (2010) *Geology of India (Vol. 1 & 2)*. GSI Publications, 2(1).
- Ramakrishnan, M., Vaidyanathan (2008) *Geology of India; Vol. 1*. Geol. Soc. India, Bangalore.
- Ramam, P.K. and Murty, V.N., (1997) *Geology of Andhra Pradesh: Geological Society of India. Text Book Series, (4)*, pp.1-245.
- Rao, V.D., Aswathanarayana, U. and Qureshy, M.N., (1972) Trace element geochemistry of parts of the Closepet granite, Mysore State, India 1. *Mineralogical Magazine*, 38(298), pp.678-686.
- Rapela, C.W., Pankhurst, R.J., Casquet, C., Fanning, C.M., Baldo, E.G., González-Casado, J.M., Galindo, C. and Dahlquist, J., (2007). The Río de la Plata craton and the assembly of SW Gondwana. *Earth-Science Reviews*, 83(1-2), pp.49-82.
- Roy, M. and Dhana Raju, R. (1997). Petrography and depositional environment of the U-mineralized phosphatic siliceous dolostone of Vempalle Formation, Cuddapah basin, India. *Jour. Geol. Soc. India*, v.50, p.577-585.
- Roy, M., Dhana Raju, R., Vasudeva Rao, M. and Vasudeva, S.G. (1990). Stromatolitic uraniferous dolostone of the Vempalle Formation, Cuddapah Supergroup, Andhra Pradesh, India: nature and bearing of stromatolites on uranium mineralisation. *Expl. Res. At. Miner.*, v.3, p.103–113.
- Saha, D. and Tripathy, V., (2012) Palaeoproterozoic sedimentation in the Cuddapah Basin, south India and regional tectonics: a review. *Geological Society, London, Special Publications*, 365(1), pp.161-184.
- Saha, D. and Tripathy, V., (2012) Tuff beds in Kurnool subbasin, southern India and implications for felsic volcanism in Proterozoic intracratonic basins. *Geoscience Frontiers*, 3(4), pp.429-444.

- Saha, D., (2002) Multi-stage deformation in the Nallamalai Fold Belt, Cuddapah basin, South India-Implications for Mesoproterozoic tectonism along southeastern margin of India. *Gondwana Research*, 5(3), pp.701-719.
- Saha, D., Chakraborti, S. and Tripathy, V., (2010) Intracontinental thrusts and inclined transpression along eastern margin of the East Dharwar Craton, India. *Journal of the Geological Society of India*, 75(1), pp.323-337.
- Sames, C.W., (1966) Morphometric data of some recent pebble associations and their application to ancient deposits. *Journal of Sedimentary Research*, 36(1), pp.126-142.
- Schumm, S. A. (1972) "Fluvial paleochannels."
- Schumm, S.A., (1968) Speculations concerning paleohydrologic controls of terrestrial sedimentation. *Geological Society of America Bulletin*, 79(11), pp.1573-1588.
- Schumm, S.A., (1969) River metamorphosis. *Journal of the Hydraulics division*, 95(1), pp.255-274.
- Schweitzer, J. and Kröner, A., (1985) Geochemistry and petrogenesis of early Proterozoic intracratonic volcanic rocks of the Ventersdorp Supergroup, South Africa. *Chemical Geology*, 51(3-4), pp.265-288.
- Shand S J (1943) *Eruptive Rocks. Their Genesis, Composition, Classification, and Their Relation to Ore-Deposits with a Chapter on Meteorite* New York: John Wiley & Sons.
- Shives, R.B., Charbonneau, B.W. and Ford, K.L., (2000) The detection of potassic alteration by gamma-ray spectrometry—recognition of alteration related to mineralization. *Geophysics*, 65(6), pp.2001-2011.
- Sinha, R.M., Shrivastava, V.K., Sarma, G.V. and Parthasarathy, T.N., (1995) Geological favourability for unconformity-related uranium deposits in northern parts of the Cuddapah basin: Evidences from Lambapur uranium occurrence, Andhra Pradesh, India. *Exploration and Research for Atomic Minerals*, 8, pp.,111-126.
- Sneed, E.D. and Folk, R.L., (1958) Pebbles in the lower Colorado River, Texas a study in particle morphogenesis. *The Journal of Geology*, 66(2), pp.114-150.
- Srivastava, R.K., Samal, A.K. and Gautam, G.C., (2015) Geochemical characteristics and petrogenesis of four Palaeoproterozoic mafic dike swarms and associated large igneous provinces from the eastern Dharwar craton, India. *International Geology Review*, 57(11-12), pp.1462-1484.

- Srivastava, S.K. and Rajasekharan, P. (2001) Secondary brannerite in fracture-controlled uranium mineralisation from Mulapalle, Cuddapah District, Andhra Pradesh, India; a petro-mineragraphic evidence. *Jour. At. Min. Sci.*, v.7, p.29-32.
- Srivastava, V.K., Parthasarathy, T.N. and Sinha, K.K., (1992) Geochemical studies of uraniferous granitoids from Lambapur area, Nalgonda dist. Andhra Pradesh, India. *Expl. and Res. for Atom. Min*, 5, pp.41-52.
- Stratten, T., (1974) Notes on the application of shape parameters to differentiate between beach and river deposits in southern Africa. *South African Journal of Geology*, 77(3), pp.383-384.
- Stuckless, J. S., and Ferreira, C. P., (1976) Labile uranium in granitic rocks: International Atomic Energy Agency International Symposium on Exploration of Uranium Ore Deposits, Vienna, 1976, Proceedings, p. 717-730.
- Suttner, L.J. and Dutta, P.K., (1986) Alluvial sandstone composition and paleoclimate; I, Framework mineralogy. *Journal of Sedimentary Research*, 56(3), pp.329-345.
- Suttner, L.J., Basu, A. and Mack, G.H., (1981) Climate and the origin of quartz arenites. *Journal of Sedimentary Research*, 51(4), pp.1235-1246.
- Sylvester, P.J., (1998) Post-collisional strongly peraluminous granites. *Lithos*, 45(1-4), pp.29-44.
- T.S Sunil Kumar and others (2003-04) AMD unpublished annual report.
- Taylor, S.R. and McLennan, S.M., (1985) The continental crust: its composition and evolution. Thimmaiah, M., Ramachar, T.R., Veerabhaskar, D. and Jayaram, K.V., 1986. The uraniferous biotite-sericite schist of Kasturi Gattu Hillock, north-east of Somasila, Nellore District, Andhra Pradesh. *Current science (Bangalore)*, 55(7).
- Thornton, C.P. and Tuttle, O.F., (1960) Chemistry of igneous rocks--[Part] 1, Differentiation index. *American Journal of Science*, 258(9), pp.664-684.
- Tortosa, A., Palomares, M. and Arribas, J., (1991) Quartz grain types in Holocene deposits from the Spanish Central System: some problems in provenance analysis. *Geological Society, London, Special Publications*, 57(1), pp.47-54.
- Umamaheswar, K., Basu, H., Patnaik, J.K., Ali, M.A. and Banerjee, D.C. (2001). Uranium mineralisation in the Mesoproterozoic quartzites of Cuddapah Basin in Gandi area,

- Cuddapah District, Andhra Pradesh: a new exploration target for uranium. *Jour. Geol. Soc. India*, v.57, p.405–409.
- Van der Neut, M. and Eriksson, P.G., (2009) Palaeohydrological parameters of a Proterozoic braided fluvial system (Wilgerivier Formation, Waterberg Group, South Africa) compared with a Phanerozoic example. *Fluvial Sedimentology VI*, Blackwell Publishing, Oxford, 28, pp.381-392.
- Veerabhaskar, D., Sarkar, M., Thimmaiah, M., Sharma, M. and Dhana Raju, R., (1991) Uranium mineralization at Kasturigattu, Nellore district, Andhra Pradesh, India: An example of shear-controlled, syngenetic remobilized type in the Proterozoic granite and low-grade metamorphic rocks. *Exploration and Research for Atomic Minerals, AMD, India*, 4, pp.27-37.
- Venkatakrishnan, R. and Dotiwalla, F.E., (1987) The Cuddapah salient: a tectonic model for the Cuddapah basin, India, based on Landsat image interpretation. *Tectonophysics*, 136(3-4), pp.237-253.
- Villaseca, C., Barbero, L. and Rogers, G., (1998) Crustal origin of Hercynian peraluminous granitic batholiths of Central Spain: petrological, geochemical and isotopic (Sr, Nd) constraints. *Lithos*, 43(2), pp.55-79.
- Wedepohl, K.H., (1995). The composition of the continental crust. *Geochimica et cosmochimica Acta*, 59(7), pp.1217-1232.
- Young, S.W., (1976) Petrographic textures of detrital polycrystalline quartz as an aid to interpreting crystalline source rocks. *Journal of Sedimentary Research*, 46(3), pp.595-603.
- Zakoulla, S., Umamaheswar, K., Thirupathi, P.V., Sharma, U.P., Basu, H. and Ali, M.A. (2004) Geological and geochemical appraisal of U bearing Gulcheru Formation of Cuddapah Supergroup, Gandhi area, Cuddapah district, Andhra Pradesh. *Jour. Geol. Soc. India*, v.64, pp.719–730.